

AD-A019 094

DEVELOPMENT OF EMISSIONS MEASUREMENT TECHNIQUES FOR
AFTER BURNING TURBINE ENGINES

T. F. Lyon, et al

General Electric Company

Prepared for:

Air Force Aero Propulsion Laboratory

October 1975

DISTRIBUTED BY:

NTIS

National Technical Information Service
U. S. DEPARTMENT OF COMMERCE

013127
AFAPL-TR-75-52

AD1919094

DEVELOPMENT OF EMISSIONS MEASUREMENT TECHNIQUES FOR AFTERBURNING TURBINE ENGINES

GENERAL ELECTRIC COMPANY
AIRCRAFT ENGINE GROUP
CINCINNATI, OHIO 45215

OCTOBER 1975

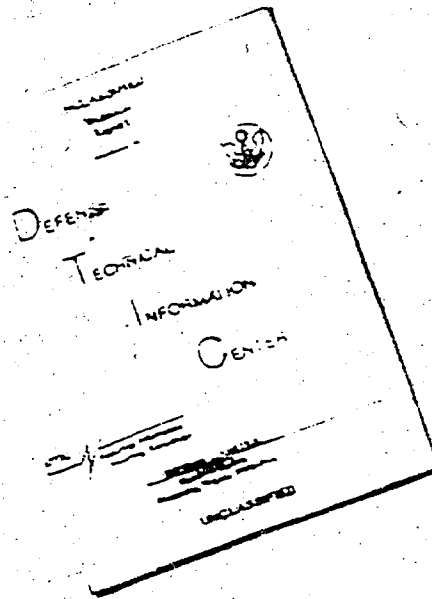
TECHNICAL REPORT AFAPL-TR-75-52
FINAL REPORT FOR PERIOD 1 APRIL 1973 - 31 MARCH 1975

Approved for public release; distribution unlimited

Reproduces in part
NATIONAL TECHNICAL
INFORMATION SERVICE
U.S. Department of Commerce
Springfield, VA 22151

AIR FORCE AERO PROPULSION LABORATORY
Air Force Wright Aeronautical Laboratories
Wright-Patterson Air Force Base, Ohio 45433

DISCLAIMER NOTICE



THIS DOCUMENT IS BEST
QUALITY AVAILABLE. THE COPY
FURNISHED TO DTIC CONTAINED
A SIGNIFICANT NUMBER OF
PAGES WHICH DO NOT
REPRODUCE LEGIBLY.

REPRODUCED FROM
BEST AVAILABLE COPY

UNCLASSIFIED

SECURITY CLASSIFICATION OF THIS PAGE (When Data Entered)

REPORT DOCUMENTATION PAGE		READ INSTRUCTIONS BEFORE COMPLETING FORM
1 REPORT NUMBER AFAPL-TR-75-52	2 GOVT ACCESSION NO.	3 RECIPIENT'S CATALOG NUMBER
4 TITLE (and Subtitle) DEVELOPMENT OF EMISSIONS MEASUREMENT TECHNIQUES FOR AFTERBURNING TURBINE ENGINES		5 TYPE OF REPORT & PERIOD COVERED Final Technical Report 1 Apr 73 - 31 Mar 75
7 AUTHOR(s) T. F. Lyon, W. C. Colley, M. J. Kenworthy, and D. W. Bahr		6 PERFORMING ORG. REPORT NUMBER R75AEG457
9 PERFORMING ORGANIZATION NAME AND ADDRESS General Electric Company Aircraft Engine Group Cincinnati, Ohio 45215		8 CONTRACT OR GRANT NUMBER(s) F33615-73-C-2047
11 CONTROLLING OFFICE NAME AND ADDRESS Air Force Aero Propulsion Laboratory (AFAPL/SFF) Air Force Wright Aeronautical Laboratories Wright-Patterson AFB, Ohio 45433		10 PROGRAM ELEMENT, PROJECT, TASK AREA & WORK UNIT NUMBERS Project 1900
14 MONITORING AGENCY NAME & ADDRESS (if different from Controlling Office)		12 REPORT DATE October 1975
		13. NUMBER OF PAGES 327
		15. SECURITY CLASS. (of this report) Unclassified
		15a. DECLASSIFICATION/DOWNGRADING SCHEDULE
16 DISTRIBUTION STATEMENT (of this Report) Approved for public release; distribution unlimited.		
17. DISTRIBUTION STATEMENT (of the abstract entered in Block 20, if different from Report)		
18 SUPPLEMENTARY NOTES		
19. KEY WORDS (Continue on reverse side if necessary and identify by block number) Afterburner Emissions Exhaust Plumes Combustion Efficiency Gas Sampling Probes Emissions Measurement Turbine Engine Emissions Environmental Pollution		
20 ABSTRACT (Continue on reverse side if necessary and identify by block number) Detailed emissions measurements were made throughout the plumes of J85-5 and J79-15 engines at military power and three afterburning power levels. Calculations of integrated pollutant flow rates at various axial stations showed that hydrocarbons are most reactive in the plume, with significant decreases observed at all afterburning power levels. Carbon monoxide can either increase or decrease with axial distance in the plume, depending on the power level and the hydrocarbon contents. No significant change in total oxides		

UNCLASSIFIED

SECURITY CLASSIFICATION OF THIS PAGE(When Data Entered)

of nitrogen was observed at any power level. Under certain conditions, NO from the mainburner was converted to NO₂ in the afterburner. Since NO₂ is colored, the potential for plume visibility exists for afterburning engines.

A computerized analytical plume model was developed and verified, which considers the simultaneous mixing and chemical reaction processes that can occur in the plumes of afterburning engines. The model enables calculating local concentrations of the various exhaust gases at any axial or radial location from initial values measured at the exhaust plane. In addition, the model permits investigation of the effects of such factors as engine size, ambient conditions, altitude, and flight Mach number.

A procedure for afterburning engine emissions measurements was developed. This procedure describes two different methods. The first, and recommended, procedure requires measurement of emissions at a location far enough removed from the engine that mixing and reactions are complete. A new data reduction approach was developed for use with this method. An alternative method is described which utilizes samples taken at the nozzle exit plane. Due to the reactive nature of the plume, the plume model computer program is used with this method in order to calculate the quantity of contaminants ultimately ejected into the atmosphere.

UNCLASSIFIED

SECURITY CLASSIFICATION OF THIS PAGE(When Data Entered)

PREFACE

This report covers all work accomplished in the "Development of Emission Measurement Techniques for Afterburning Turbine Engines" Program conducted under Contract F33615-73-C-2047 by the General Electric Company, Aircraft Engine Group, Cincinnati, Ohio 45215. The report was submitted by the authors on 19 June 1975.

This program was sponsored by the Air Force Aero Propulsion Laboratory, Air Force Wright Aeronautical Laboratories, Wright-Patterson Air Force Base, Ohio 45433. The Air Force Project Engineer was Dr. W. S. Blazowski (AFAPL/SFF).

The General Electric Program Managers were R. A. Monteferrante and, later, A. L. Meyer; the Technical Program Manager was D. W. Bahr; the Principal Investigator was Dr. T. F. Lyon.

Valuable contributions to this program were made by the following personnel of the General Electric Company, Aircraft Engine Group, Engineering Division. Continuing support and consultation was provided by C. C. Gleason. The plume modeling effort was directed by M. J. Kenworthy with major contributions by W. C. Colley. Additional computer programming support was supplied by D. R. Ferguson and M. A. Smith. Data reduction procedures were programmed by D. W. Rogers and J. Burns; data reduction was performed by V. M. Cecil. R. C. Williamson and B. W. Stowe contributed to the design of the sampling and analysis system with C. M. Stanforth directing this effort. Engine emissions testing was performed at the General Electric Edwards Flight Test Center under the overall direction of C. L. Shumate; engine operation at Edwards was supervised by C. Morgan.

Comprehensive test data acquired in the engine testing phases of this program are contained in a separate volume subtitled "Supplement 1 - Engine Emissions Test Data". Computational routines and operating instructions for the plume model computer program developed in this program are contained in a separate volume subtitled "Supplement 2 - Computer Program User's Manual".

TABLE OF CONTENTS

<u>Section</u>		<u>Page</u>
1.0	INTRODUCTION	1
2.0	SUMMARY	3
3.0	AFTERBURNER EMISSIONS MEASUREMENT SYSTEM DEFINITION	6
	3.1 Afterburner Emissions Characteristics	6
	3.2 Afterburner Plume Characteristics	7
	3.3 Probes for Afterburner Exhaust Measurements	15
	3.3.1 General Considerations	15
	3.3.2 Probe Cooling	16
	3.3.3 Quenching of Gas Sample	18
	3.3.4 High Temperature Probe Design	19
	3.3.5 Low Temperature Probe Design	23
	3.4 Emissions Sampling and Analysis System	23
4.0	ANALYTICAL PLUME MODEL DEVELOPMENT	29
	4.1 Methods of Analysis	30
	4.2 Two-Part Model of Heterogeneous Gas Flow	32
	4.2.1 Sample Fuel-Air Ratio and Emissions Indices	32
	4.2.2 Local Vitiated Air Properties	33
	4.2.3 Proportion and Composition of Each Part of Heterogeneous Gas	36
	4.3 Steady-State Turbulent Gas Jet Mixing	44
	4.3.1 Continuity Equation	17
	4.3.2 Species Continuity Equation	47
	4.3.3 X-Momentum Equation	17
	4.3.4 Energy Equation	17
	4.3.5 Viscosity Model	19
	4.3.6 Turbulent Kinetic Energy	50
	4.3.7 Determination of the Jet Edge and the Core Length	52
	4.3.8 Boundary Conditions	53
	4.3.9 Transformation of Differential Equations	53
	4.3.10 Numerical Solution of Differential Equations	56
	4.3.11 Representation of Jet Properties and Initial Profiles	59

TABLE OF CONTENTS (Continued)

<u>Section</u>	<u>Page</u>
4.1 Conservation of the Heterogeneity Parameter	61
4.5 Mixing and Homogenization of the Heterogeneous Gas	68
4.5.1 Definition of New Computation Tubes	69
4.5.2 Mixing and Homogenization	72
4.6 Chemical Reaction Kinetics	77
4.6.1 General Chemical Kinetics (GCKP)	77
4.6.2 Special Chemical Kinetics Procedure (SCKP)	81
4.6.3 Consumption of Unburned Hydrocarbons (HYCARB)	86
4.7 Summation of Contaminant Flows	88
4.8 Overall Description and Capability of Integrated Model	91
5.0 INITIAL AFTERBURNER EMISSIONS TESTS OF J85-5 and J79-15 ENGINES	93
5.1 Engine Description	93
5.1.1 J85 Engine	93
5.1.2 J79 Engine	94
5.2 Engine Test Facility	99
5.3 Data Reduction Procedures	102
5.3.1 PCM System	102
5.4 J85-5 Afterburner Emissions Tests	106
5.4.1 J85 Engine Setup and Instrumentation	106
5.4.2 J85 Emissions Test Data	109
5.4.3 Adjustment for Plume Symmetry	121
5.4.4 Calculation of Integrated Results for J85	121
5.5 J79-15 Afterburner Emissions Tests	125
5.5.1 J79 Emissions Test Data	125
5.5.2 Calculations of Integrated Results for J79	133
5.6 Interpretation of Data at Downstream Locations	133
5.7 Effect of Afterburning on NO _x Emissions	146

TABLE OF CONTENTS (Continued)

<u>Section</u>		<u>Page</u>
6.0	PLUME MODEL VERIFICATION	153
	6.1 Comparison with J85-5 Test Data	153
	6.2 Comparison with J79-15 Test Data	172
	6.3 Comparison with Altitude Wind Tunnel Data	191
7.0	DEVELOPMENT OF AFTERBURNER EMISSIONS MEASUREMENTS PROCEDURES	191
	7.1 General Considerations	195
	7.2 Far Plume Procedure (Part A)	197
	7.3 Near Plume Procedure (Part B)	199
8.0	FINAL ENGINE EMISSIONS TESTS USING NEAR PLUME AND FAR PLUME PROCEDURES	201
	8.1 Test Setup and Instrumentation	201
	8.2 Final Test Results - J85-5 Engine	202
	8.3 Final Test Results - J79-15 Engine	204
	8.4 Comparison of Phase II and Phase III Measurements	225
	8.5 Comparison with Plume Model	233
9.0	CONCLUSIONS AND RECOMMENDATIONS	242
	9.1 Conclusions	242
	9.2 Recommendations	243
10.0	REFERENCES	245
APPENDIX A	DERIVATION OF MATHEMATICAL RELATIONS USED IN PLUME MODEL DEVELOPMENT	249
	Part 1. Computation of Sample Fuel-Air Ratio and Emissions Indices from Gas Analysis	250
	Part 2. Efficient Calculation of Equilibrium and Pseudo-Equilibrium Composition of Combustion Gases	253
	Part 3. Thermostatic Properties of Combustion Gas Mixtures and Hydrocarbon Fuels.	262
	Part 4. Interaction of Probes with Two-Part Heterogeneous Gas Streams	267

TABLE OF CONTENTS (Concluded)

<u>Section</u>	<u>Page</u>
APPENDIX B PROCEDURE FOR MEASUREMENT OF GASEOUS EMISSIONS FROM AFTERBURNING AIRCRAFT GAS TURBINE ENGINES	277
Part A. Far Plume Method (Measurement Procedure for Sampling at Axial Stations Far Removed from Nozzle Exit Plane)	280
Part B. Near Plume Method (Measurement Procedure for Sampling at Nozzle Exit Plane)	301

LIST OF ILLUSTRATIONS

<u>Figure</u>		<u>Page</u>
1.	Consumption of CO in Equilibrium Stoichiometric Combustion Products Which have been Rapidly Diluted with Air to the Indicated Equivalence Ratio.	12
2.	Presentation of Concentrated Species Mixing from Outer Edge of Engine Exit.	13
3.	Comparison of Trace Species Concentration Profile with Temperature Profile at Two Axial Distances.	14
4.	Results of Probe Coolant Test.	17
5.	High Temperature Probe Assembly.	20
6.	High Temperature Probe Tip Showing Gas Sample and Total Pressure Orifices.	21
7.	High Temperature Probes with Actuators Mounted at Nozzle Exit Plane of J85-3 Engine.	22
8.	Low Temperature Probe System.	24
9.	Low Temperature Probe Tip Showing (Left to Right) Total/Static Pressure Tube, Gas Sample Tip, and Aspirated Thermocouple.	25
10.	Low Temperature Probe System with Pneumatic Damper Added for Improved Stability.	26
11.	Gas Sampling and Analysis System Schematic.	27
12.	Augmented Turbofan Engine Schematic.	31
13.	Subsonic Turbulent Jet.	45
14.	Supersonic Turbulent Jet.	46
15.	Finite Difference Grid Network.	66
16.	J85-3 Diffuser Assembly.	95
17.	J85-3 Afterburner Casing and Variable Exhaust Nozzle Assembly.	96
18.	J79-15 Afterburner and Exhaust Nozzle Assembly.	98

LIST OF ILLUSTRATIONS (Continued)

<u>Figure</u>		<u>Page</u>
19.	GE-Edwards Flight Test Center North Site Control Room Showing Gas Analysis System (Background), Smoke Console (Right), and Engine Run Console (Foreground).	100
20.	J79-15 Engine on Test Stand at GE-Edwards North Site Test Facility.	101
21.	Relation of Probe Angle to Radial Position.	105
22.	Engine Test Data Flow Chart.	107
23.	Effect of Power Level on Radial Distribution of Fuel-Air Ratio at Nozzle Exit, J85-5 Engine, Probe No. 1.	113
24.	Effect of Power Level on Radial Distribution of Fuel-Air Ratio 7.5 feet Aft of Nozzle Exit, J85-5 Engine, Probe No. 1.	114
25.	Effect of Power Level on Radial Distribution of Fuel-Air Ratio 30 feet Aft of Nozzle Exit, J85-5 Engine, Probe No. 1.	115
26.	Effect of Power Level on Radial Distribution of NO_x at Nozzle Exit, J85-5 Engine, Probe No. 1.	116
27.	Effect of Power Level on Radial Distribution of NO_x 7.5 feet Aft of Nozzle Exit, J85-5 Engine, Probe No. 1.	117
28.	Effect of Power Level on Radial Distribution of NO_x 30 feet Aft of Nozzle Exit, J85-5 Engine, Probe No. 1.	118
29.	CO Concentration Profile at Various Axial Distances for J85-5 Engine at Min. A/B Power (Probe No. 1).	119
30.	CO Concentration Profile at Various Axial Distances for J85-5 Engine at Max. A/B Power (Probe No. 1).	120
31.	Radial Fuel-Air Ratio Profiles for J85-5 Engine at Military Power, 15 feet Aft of Nozzle Exit, with and without Symmetry Adjustment.	122
32.	Radial Fuel-Air Ratio Profiles at Nozzle Exit for J79-15 Engine at Various Engine Power Levels.	128

LIST OF ILLUSTRATIONS (Continued)

<u>Figure</u>		<u>Page</u>
33.	Radial Fuel-Air Ratio Profiles for J79-15 Engine at 7.5 feet Alt of Nozzle Exit for Various Power Levels.	129
34.	Radial Fuel-Air Ratio Profiles for J79-15 Engine at 15 feet Alt of Nozzle Exit for Various Power Levels.	130
35.	Radial HC Concentration Profile at Nozzle Exit for J79-15 Engine at Mid. A/B Power.	131
36.	HC Concentration Radial Profile, J79-15 Engine at Mid. A/B Power Level.	132
37.	CO vs. CO ₂ Concentration for J79-15 Engine at Min. A/B Power, 60 feet alt of Exhaust Nozzle.	137
38.	CO vs. CO ₂ Concentration for J79-15 Engine at Military Power, at Each of Five Axial Stations. Emission Index (EI) Calculated from the Slope is given on Each Plot.	138
39.	CO vs. CO ₂ Concentration for J79-15 Engine at Mid. A/B Power, at Each of Five Axial Stations.	139
40.	NO _x vs. CO ₂ Concentration for J79-15 Engine at Max. A/B Power, at Each of Five Axial Stations.	141
41.	HC vs. CO ₂ Concentration for J79-15 Engine at Min. A/B Power, at Each of Five Axial Stations.	142
42.	HC vs. CO ₂ Concentration for J79-15 Engine at Mid. A/B Power, at Each of Five Axial Stations.	143
43.	NO _x and NO Profiles for J85-5 Engine at Military and Min. A/B Power, Samples from Probe No. 1 at Nozzle Exit.	151
44.	NO _x and NO Profiles for J79-15 Engine at Military and Min. A/B Power, Samples from Probe No. 1 at Nozzle Exit.	152
45.	Plume Model Profile Predictions Compared with Phase II Test Data - J85-5 Engine, Min. A/B, X = 0 feet.	154
46.	Plume Model Profile Predictions Compared with Phase II Test Data - J85-5 Engine, Min. A/B, X = 3.75 feet.	155

LIST OF ILLUSTRATIONS (Continued)

<u>Figure</u>		<u>Page</u>
47.	Plume Model Profile Predictions Compared with Phase II Test Data - J85-5 Engine, Min. A/B, X = 7.5 feet.	156
48.	Plume Model Profile Predictions Compared with Phase II Test Data - J85-5 Engine, Min. A/B, X = 15 feet.	157
49.	Plume Model Profile Predictions Compared with Phase II Test Data - J85-5 Engine, Min. A/B, X = 30 feet.	158
50.	Plume Model Predictions of Overall Emissions Indices Compared with Phase II Test Data - J85-5 Engine, Min. A/B.	159
51.	Plume Model Profile Predictions Compared with Phase II Test Data - J85-5 Engine, Mid. A/B, X = 0.	160
52.	Plume Model Profile Predictions Compared with Phase II Test Data - J85-5 Engine, Mid. A/B, X = 3.75 feet.	161
53.	Plume Model Profile Predictions Compared with Phase II Test Data - J85-5 Engine, Mid. A/B, X = 7.5 feet.	162
54.	Plume Model Profile Predictions Compared with Phase II Test Data - J85-5 Engine, Mid. A/B, X = 15 feet.	163
55.	Plume Model Profile Predictions Compared with Phase II Test Data - J85-5 Engine, Mid. A/B, X = 30 feet.	164
56.	Plume Model Predictions of Overall Emissions Indices Compared with Phase II Test Data - J85-5 Engine, Mid. A/B.	165
57.	Plume Model Profile Predictions Compared with Phase II Test Data - J85-5 Engine, Max. A/B, X = 0.	166
58.	Plume Model Profile Predictions Compared with Phase II Test Data - J85-5 Engine, Max. A/B, X = 3.75 feet.	167
59.	Plume Model Profile Predictions Compared with Phase II Test Data - J85-5 Engine, Max. A/B, X = 7.5 feet.	168
60.	Plume Model Profile Predictions Compared with Phase II Test Data - J85-5 Engine, Max. A/B, X = 15 feet.	169

LIST OF ILLUSTRATIONS (Continued)

<u>Figure</u>		<u>Page</u>
61.	Plume Model Profile Predictions Compared with Phase II Test Data - J85-5 Engine, Max. A/B, X = 30 feet.	170
62.	Plume Model Predictions of Overall Emissions Indices Compared with Phase II Test Data - J85-5 Engine, Max. A/B.	171
63.	Plume Model Profile Predictions Compared with Phase II Test Data - J79-15 Engine, Min. A/B, X = 0.	173
64.	Plume Model Profile Predictions Compared with Phase II Test Data - J79-15 Engine, Min. A/B, X = 7.5 feet.	174
65.	Plume Model Profile Predictions Compared with Phase II Test Data - J79-15 Engine, Min. A/B, X = 15 feet.	175
66.	Plume Model Profile Predictions Compared with Phase II Test Data - J79-15 Engine, Min. A/B, X = 30 feet.	176
67.	Plume Model Profile Predictions Compared with Phase II Test Data - J79-15 Engine, Min. A/B, X = 60 feet.	177
68.	Plume Model Predictions of Overall Emissions Indices Compared with Phase II Test Data - J79-15 Engine, Min. A/B.	178
69.	Plume Model Profile Predictions Compared with Phase II Test Data - J79-15 Engine, Mid. A/B, X = 0.	179
70.	Plume Model Profile Predictions Compared with Phase II Test Data - J79-15 Engine, Mid. A/B, X = 7.5 feet.	180
71.	Plume Model Profile Predictions Compared with Phase II Test Data - J79-15 Engine, Mid. A/B, X = 15 feet.	181
72.	Plume Model Profile Predictions Compared with Phase II Test Data - J79-15 Engine, Mid. A/B, X = 30 feet.	182
73.	Plume Model Profile Predictions Compared with Phase II Test Data - J79-14 Engine, Mid. A/B, X = 60 feet.	183
74.	Plume Model Predictions of Overall Emissions Indices Compared with Phase II Test Data - J79-15 Engine, Mid. A/B.	181

LIST OF ILLUSTRATIONS (Continued)

<u>Figure</u>		<u>Page</u>
75.	Plume Model Profile Predictions Compared with Phase II Test Data - J79-15 Engine, Max. A/B, X = 0.	185
76.	Plume Model Profile Predictions Compared with Phase II Test Data - J79-15 Engine, Max. A/B, X = 7.5 feet.	186
77.	Plume Model Profile Predictions Compared with Phase II Test Data - J79-15 Engine, Max. A/B, X = 15 feet.	187
78.	Plume Model Profile Predictions Compared with Phase II Test Data - J79-15 Engine, Max. A/B, X = 30 feet.	188
79.	Plume Model Profile Predictions Compared with Phase II Test Data - J79-15 Engine, Max. A/B, X = 60 feet.	189
80.	Plume Model Predictions of Overall Emissions Indices Compared with Phase II Test Data - J79-15 Engine, Max. A/B.	190
81.	Plume Model Profile Predictions Compared with AEDC Test Data - J85-5 Engine, Mach 1.6/55,000 feet, X = 0.4 feet.	192
82.	Plume Model Profile Predictions Compared with AEDC Test Data - J85-5 Engine, Mach 1.6/55,000 feet, X = 13.9 feet.	193
83.	Plume Model Profile Predictions Compared with AEDC Test Data - J85-5 Engine, Mach 1.6/55,000 feet, X = 29.7 feet.	194
84.	Fuel-Air Ratio Profile for J85-5 Engine at Nozzle Exit for Various Power Levels. Final Data by Near Plume Method.	205
85.	Fuel-Air Ratio Profile for J85-5 Engine 30 feet Aft of Nozzle for Various Power Levels. Final Data by Far Plume Method.	206
86.	CO Radial Profile for J85-5 Engine, 30 feet Aft of Nozzle for Various Power Levels. Final Data by Far Plume Method.	207
87.	Emissions Concentrations Vs. CO ₂ for J85-5 Engine, 30 feet Aft of Exhaust Nozzle, Military Power. Final Data by Far Plume Method.	208

LIST OF ILLUSTRATIONS (Continued)

<u>Figure</u>		<u>Page</u>
88.	Emissions Concentrations Vs. CO ₂ for J85-5 Engine, 30 feet Aft of Exhaust Nozzle, Min. A/B Power. Final Data by Far Plume Method.	209
89.	Emissions Concentrations Vs. CO ₂ for J85-5 Engine, 30 feet Aft of Exhaust Nozzle, at Mid. A/B Power. Final Data by Far Plume Method.	210
90.	Emissions Concentrations Vs. CO ₂ for J85-5 Engine, 30 feet Aft of Exhaust Nozzle, at Max. A/B Power. Final Data by Far Plume Method.	211
91.	Fuel-Air Ratio Radial Profile for J79-15 Engine at 60 feet Aft of Nozzle for Various Power Levels. Final Data by Far Plume Method.	216
92.	CO Radial Profile for J79-15 Engine at 60 feet Aft of Nozzle for Various Power Levels. Final Data by Far Plume Nozzle.	217
93.	HC Radial Profile for J79-15 Engine at 60 feet Aft of Nozzle for Various Power Levels. Final Data by Far Plume Nozzle.	218
94.	NO _x Radial Profile for J79-15 Engine at 60 feet Aft of Nozzle for Various Power Levels. Final Data by Far Plume Method.	219
95.	Emissions Concentrations Vs. CO ₂ for J79-15 Engine, 60 feet Aft of Exhaust Nozzle, at Military Power. Final Data by Far Plume Method.	220
96.	Emissions Concentrations Vs. CO ₂ for J79-15 Engine, 60 feet Aft of Exhaust Nozzle, at Min. A/B Power. Final Data by Far Plume Method.	221
97.	Emissions Concentrations Vs. CO ₂ for J79-15 Engine 60 feet Aft of Exhaust Nozzle, at Mid. A/B Power. Final Data by Far Plume Method.	222
98.	Emissions Concentrations Vs. CO ₂ for J79-15 Engine, 60 feet Aft of Exhaust Nozzle, at Max. A/B Power. Final Data by Far Plume Method.	223

LIST OF ILLUSTRATIONS (Continued)

<u>Figure</u>		<u>Page</u>
99.	CO Emission Index Vs. Axial Distance for J85-5 Engine at Various Power Levels,	227
100.	HC Emission Index Vs. Axial Distance for J85-5 Engine at Various Power Levels,	228
101.	NO _x Emission Index Vs. Axial Distance for J85-5 Engine at Various Power Levels,	229
102.	CO Emission Index Vs. Axial Distance for J79-15 Engine at Various Power Levels,	230
103.	HC Emission Index Vs. Axial Distance for J79-15 Engine at Various Power Levels,	231
104.	NO _x Emission Index Vs. Axial Distance for J79-15 Engine at Various Power Levels,	232
105.	Predicted Fuel-Air Ratio Profile Compared to Final Test Data, J85-5 Engine at Min. A/B and Max. A/B; 30 feet Aft of Exhaust Plane,	234
106.	Plume Model Predictions of Overall Emission Indices Compared with Phase III Test Data - J85-5 Engine, Min. A/B.	236
107.	Plume Model Predictions of Overall Emission Indices Compared with Phase III Test Data - J85-5 Engine, Mid. A/B.	237
108.	Plume Model Predictions of Overall Emission Indices Compared with Phase III Test Data - J85-5 Engine, Max. A/B.	238
109.	Plume Model Predictions of Overall Emission Indices Compared with Phase III Test Data - J79-15 Engine, Min. A/B.	239
110.	Plume Model Predictions of Overall Emission Indices Compared with Phase III Test Data - J79-15 Engine, Mid. A/B.	240
111.	Plume Model Predictions of Overall Emission Indices Compared with Phase III Test Data - J79-15 Engine, Max. A/B.	241

LIST OF ILLUSTRATIONS (Concluded)

<u>Figure</u>		<u>Page</u>
A1.	Gas Sample Probe in Two-Part Heterogeneous Stream.	268
A2.	Total Pressure Probe in Two-Part Heterogeneous Stream.	271
A3.	Aspirated Thermocouple Probe in Two-Part Heterogeneous Stream.	273
A4.	Approximate Relationship Between Thermal Conductivity, Viscosity, and Temperature for Combustion Gases.	276
B1.	Sampling System Schematic.	287
B2.	Sampling System Schematic. Instrument layout is the same as in Figure B1. Major Difference is the Probe Pump.	311
B3.	Impact Pressure Vs. Radial Position at Max. A/B Power Level. R_0 is Outer Radius of Exhaust.	322
B4.	CO_2 and CO Concentrations Vs. Radial Position at Max. A/B Power Level. R_0 is Outer Radius of Exhaust.	323
B5.	HC and NO_x Concentrations Vs. Radial Position at Max. A/B Power Level. R_0 is Outer Radius of Exhaust.	325

LIST OF TABLES

<u>Table</u>		<u>Page</u>
1.	Summary of Previous Afterburner Emissions Test Data.	8
2.	Summary of Plume Conditions - JETMIX Calculations.	10
3.	Chemical Reaction System.	79
4.	Third Body Efficiencies.	80
5.	SCKF Chemical Reaction System.	82
6.	Afterburner Emissions Tests - List of Drawings.	103
7.	Instrumentation list for Afterburner Emissions Tests.	108
8.	J85-5 Engine Data for Phase II Afterburner Emissions Tests - JP-4 Fuel.	110
9.	Analyses of JP-4 Fuel Samples from Phase II Afterburner Emissions Tests.	111
10.	Adjustment of Plume Centerline Required to Shift Origin to Center of Symmetry for J85 Engine.	123
11.	Integrated Results - J85-5 Afterburner Emissions Tests.	124
12.	J79-15 Engine Data for Phase II Afterburner Emissions Tests - JP-4 Fuel.	127
13.	Adjustment of Plume Centerline Required to Shift Origin to the Center of Symmetry for J79.	131
14.	Integrated Results - J79-15 Exhaust Emissions Tests.	133
15.	Typical ABE Computer Program Printout.	145
16.	J79-15 Afterburner Emissions - ABE Program Summary.	147
17.	J85-5 Afterburner Emissions - ABE Program Summary.	148
18.	NO _x Formation in J85 and J79 Afterburners.	149
19.	J85-5 Engine Data for Final Afterburner Emissions Tests (Phase III) - JP-4 Fuel.	203

LIST OF TABLES (Concluded)

<u>Table</u>		<u>Page</u>
20.	Summary of Emissions Data from Final J85-5 Tests.	212
21.	Summary of Statistical Parameters for J85-5 - Far Plume Method - Final Test Data.	213
22.	J79-15 Engine Data for Final Afterburner Emissions Tests (Phase III) - JP-4 Fuel.	215
23.	Summary of Emissions Data from Final J79-15 Tests.	224
24.	Summary of Statistical Parameters for J79-15 - Far Plume Method - Final Test Data.	226
A1.	Polynomial Coefficients for Thermodynamic Properties of Pure Gases.	261
B1.	Input Data to Plume Model Computer Program.	326

NOTICE

When Government drawings, specifications, or other data are used for any purpose other than in connection with a definitely related Government procurement operation, the United States Government thereby incurs no responsibility nor any obligation whatsoever; and the fact that the government may have formulated, furnished, or in any way supplied the said drawings, specifications, or other data, is not to be regarded by implication or otherwise as in any manner licensing the holder or any other person or corporation, or conveying any rights or permission to manufacture, use, or sell any patented invention that may in any way be related thereto.

This final report was submitted by the General Electric Company, Aircraft Engine Group, Cincinnati, Ohio, under Contract F33615-73-C-2047. The effort was sponsored by the Air Force Aero Propulsion Laboratory, Air Force Wright Aeronautical Laboratories, Wright-Patterson Air Force Base, Ohio, under Project 1900, with W.S. Blazowski (AFAPL/SFF) as Project Engineer-in-Charge. D.W. Bahr of the General Electric Company was technically responsible for the work.

This program was funded through the "Control of Noxious Effluents (CONE)" Program, which is administered by the Air Force Weapons Laboratory (AFWL/DEE), Kirtland Air Force Base, New Mexico.

This report has been reviewed by the Information Office, (ASD/OIP) and is releasable to the National Technical Information Service (NTIS). At NTIS, it will be available to the general public, including foreign nations.

This technical report has been reviewed and is approved for publication.

William S. Blazowski

W.S. Blazowski
Project Engineer

FOR THE COMMANDER

Arthur V. Churchill

A.V. Churchill
Chief, Fuels Branch

Copies of this report should not be returned unless return is required by security considerations, contractual obligations, or notice on a specific document.

SECTION 1.0

INTRODUCTION

Up to this time, development of emissions measurement techniques generally has been concerned only with nonafterburning engines. Measurement procedures for such engines were first issued by the Society of Automotive Engineers (ARP 1256, Oct. 1971). Procedures adopted by the EPA as part of the methods for Control of Pollution from Aircraft Engines (Federal Register July 17, 1973) are based on the SAE procedures. These techniques for nonafterburning engines require rather limited sampling at the nozzle exit plane, which is adequate since the exhaust concentrations are fairly uniform across the nozzle diameter except for mixed-flow turbofan engines. In addition, uncooled probes are generally adequate since the exhaust temperatures are moderate.

In contrast, local temperatures at the exhaust plane of afterburning engines can reach 3600° F. These extremely high temperatures can result in continued reactions downstream of the exhaust plane, so that exhaust plane measurements would yield emissions levels which are not representative of the actual contribution to atmospheric pollution. In addition, the high exhaust plane temperatures can cause continued reactions within the sampling probe, necessitating careful design of the probe to quench the reactions at the probe entrance.

Since existing measurement procedures are not applicable to afterburning engines, this program was undertaken to provide the definition, development, and demonstration of emissions measurement techniques for afterburning turbine engines.

A key part of this program has been the development of a computerized analytical model of the simultaneous mixing and chemical reaction processes that can occur in the plumes of afterburning engines. This model was developed so that local concentrations of the various exhaust gases, at any axial station and radial position downstream of the engine exhaust nozzle, may be calculated from the initial exhaust plane values. This highly complex and sophisticated model not only permits calculation of final emissions levels from exhaust plane data, but also permits investigation of the effects of such factors as engine size, ambient conditions, altitude, flight Mach number, etc.

The program was divided into three phases. Phase I, completed in October 1973, was the system definition study. This phase involved development of the analytical model of the exhaust plume and preliminary planning of the emission measurement system to be used on the engine tests. In Phase II, the emissions measurement system was constructed and installed at the General Electric Edwards Flight Test Center at Edwards Air Force Base.

Detailed emissions measurements were made throughout the plumes of two afterburning engines, a J85-5 and a J79-15. The measured emissions levels were compared with the predictions of the analytical studies of Phase I. Phase III consisted of refinement of the measurement system and plume model, and definition of the final emissions measurement procedures in a format similar to that of SAE ARP 1256. Emissions measurements on the same two engines were then made to demonstrate these procedures. Emissions tests on the F101 engine, originally planned as part of this program, were not performed due to unavailability of a test engine.

The finalized measurement procedure, described in a format similar to that used for SAE ARP 1256, is presented as Appendix B of this report.

SECTION 2.0

SUMMARY

This program was undertaken to provide the definition, development, and demonstration of emissions measurement techniques for afterburning turbine engines. The study involved both analytical and experimental investigation of emissions levels at the exhaust plane and subsequent changes of the emissions levels in the exhaust plume.

Analytical procedures were developed and combined with existing procedures to form a model of the exhaust plume of afterburning turbojet or turbofan engines. The model represents those features of the gas flow which influence the consumption of gaseous contaminant emissions in the plume. These features include:

1. Time-average turbulent mixing of each element of the axisymmetric exhaust jet into adjacent elements and the mixing of ambient air into the hot gas
2. Time-varying composition (heterogeneity) of the gas flow past each point in space
3. Generation and decay of gas heterogeneity in the plume
4. Alteration of instantaneous gas composition by mixing with gas from adjacent parts of the flow and by homogenization
5. Consumption of gaseous contaminants by rate-limited chemical reactions.

Input to the model includes data from a probe survey of the engine exhaust stream, together with properties of the fuel and ambient air and parameters of the engine cycle. Based on this input, the model predicts profiles of velocity, fuel, and contaminant concentrations at various axial locations in the plume and overall residual emissions indices derived from integration of these profiles.

The primary use intended for the model is to estimate the true residual emissions released into the atmosphere, based upon emissions measurements made at the afterburner exhaust plane. This procedure is useful in applications where direct sampling of the mixed and cooled exhaust plume is not practical, such as engine tests in enclosed test cells. The model is also capable of accommodating a moving environment, which makes it useful in estimating contaminant consumption in the plume under high-altitude, high-speed flight conditions.

An afterburner emissions measurement system was designed, constructed, and set up at the General Electric Edwards Flight Test Center at Edwards Air Force Base, California. Afterburner emissions measurements were made on J85-5 and J79-15 engines at four power levels from military to maximum afterburning. At each power level, measurements were made at five axial stations: from the nozzle exit to 30 feet aft of the J85 and to 60 feet aft of the J79. At each axial station, measurements were made at approximately 24 radial locations across the plume. Data from these tests indicate that hydrocarbons are most reactive in the plume, with significant consumption observed at all afterburner power settings. At maximum afterburner power setting, all of the hydrocarbons initially in the exhaust are ultimately consumed by the plume reactions. Carbon monoxide is less reactive, with large reductions occurring only at the higher afterburner power settings. No significant change in oxides of nitrogen was observed in the plume at any power setting.

A data reduction procedure was developed which is well suited to evaluation of emissions indices at locations far downstream from the engine where extremely low emissions concentrations are encountered. This method involves plotting the emission concentrations against CO_2 concentration. At axial stations far enough removed from the engine that mixing and plume reactions are complete, this plot becomes a straight line, the slope of which is related to the emission index.

This method gives reliable emission indices under suitable conditions, and provides a graphical display which is amenable to statistical treatment. The procedure has also been found useful at locations where mixing and reactions are not complete. In these cases, the nonlinear curves are interpretable in terms of the degree of mixing and reactions occurring at that location.

An afterburner emissions measurement procedure was formulated and described in a format similar to that used in ARP 1256. The procedure consists of two parts. Part A, the Far Plume Method, describes the procedure for emissions measurements at axial stations far removed from the engine exhaust plane. This is the preferred procedure, and data reduction methods are based on the slope method described above. In case the required test facilities are not available for using this procedure, an alternate procedure, the Near Plume Method, is also described. This method involves measurement of emissions at the nozzle exit plane, along with total pressure measurements to properly mass weight the local values. Data reduction for the Near Plume procedure utilizes the plume model computer program to calculate the quantity of contaminants ultimately ejected into the atmosphere.

A final series of emissions measurements on both the J85 and J79 engines were made to demonstrate these afterburner emissions measurement procedures.

This final test series showed that reliable emissions measurements can be made on afterburning engines by both the Near Plume and the Far Plume test methods. The Far Plume procedure provides more accurate overall results, especially when large changes in emissions levels occur in the plume.

SECTION 3.0

AFTERBURNER EMISSIONS MEASUREMENT SYSTEM DEFINITION

System definition studies were performed in Phase I of the program, which involved assessment of afterburner emissions characteristics and assessment of measurement system selection considerations. The measurement system to be used for the Phase II engine emission tests was also defined in Phase I. Included in system definition was the design of the probes to be used for the engine tests. These activities are described in this section of the report.

3.1 AFTERBURNER EMISSIONS CHARACTERISTICS

Emissions from augmentor combustion systems are generally similar to emissions from main engine combustors in that the primary objectionable pollutants consist of carbon monoxide (CO), hydrocarbons (HC), oxides of nitrogen (NO_x), and particulate emissions. The CO and HC emissions generally are products of inefficient combustion, and, since CO results from partial oxidation of the fuel, CO tends to occur where high HC concentrations exist. However, at high afterburning power levels, where the fuel-air mixture may be stoichiometric or greater, very high levels of equilibrium CO may exist. In these regions, temperatures are too high for HC to persist. The general tendency in afterburners, thus, is that the CO concentrations are highest in regions of highest temperatures, while both CO and HC may exist in low temperature regions.

For most afterburning aircraft engines, the main engine operates at its maximum power conditions as the afterburner power is modulated over its entire range. This maximum power level of the main engine is referred to as military or intermediate rated power. The emissions from the mainburner which enter the afterburner are, thus, the same regardless of afterburner power level. The CO and HC from the main engine tend to be consumed in the afterburner flame when the afterburner is operating. But CO and HC are also formed within the afterburner, which may result in a net increase or decrease in CO and HC when operating with afterburner, depending upon the relative magnitudes of the various changes involved.

As for NO_x emissions, the chemical kinetics of NO formation are reasonably well understood and the dominant parameter in NO production is the maximum flame temperature. Since the flame temperatures are much higher in the mainburner, the NO production rates would be expected to be higher in the mainburner than in the afterburner. However, the kinetics of the NO formation process are such that there can be no significant decrease in total NO_x in the afterburner but only an increase. The basic reason for this is that at the lower temperatures where thermodynamic equilibrium favors a decrease in overall NO level, the kinetics are too slow to permit any appreciable change.

Smoke tends to be generated under very rich, high pressure conditions such as may be found in the primary zone of main engine combustors. The smoke generated in augmentors would be expected to be of minor significance because pressure levels are low, and the fuel-air mixtures are not as rich as in the primary zones of main engine combustors. In fact, it has been shown that main combustor smoke is partially consumed in the afterburner combustion processes.

The general remarks made here concerning afterburner emissions characteristics refer to the formation of objectionable emissions within the main-burner and afterburner, and apply to emissions levels to be found at the nozzle exit plane. The general composition of the exhaust at this station influences the choice of the sampling and analysis equipment to be used for the nozzle exit plane measurements.

Until recently, very little information had been available on emissions from afterburning engines. This was due mainly to the rather specialized probe required for sampling in the high temperature stream. Still less information was available on the extent of reactions in the exhaust plume due to the extensive facilities required to make such measurements. Table 1 is a summary of previously published afterburner emission test data.

3.2 AFTERBURNER PLUME CHARACTERISTICS

The extremely high exhaust plane temperatures produced when operating turbine engines with afterburners can result in continued reactions downstream of the exhaust nozzle. In order to adequately define the emissions measurement system, it was necessary early in the Phase I efforts to determine the approximate extent of mixing and chemical reactions occurring within the plume. These determinations were calculated utilizing the existing JETMIX and GCKP Programs. The JETMIX program provides the rate of mixing in the exhaust plume, while the GCKP program provides the overall chemical reaction rates in the plume. A thorough discussion of both these programs is contained in a later section of this report.

Calculations of radial profiles at various downstream axial stations were made for three engines utilizing the JETMIX computer program. The F101 engine was included in these calculations since the original plans for this program included testing the F101. A summary of the plume conditions at Max A/B power and at each selected axial stations, for these three engines, is given in Table 2. The five axial stations selected are at approximately 0, 3, 6, 12, and 24 nozzle diameters for the J85-5 and J79-15, and at about 0, 2, 4, 8, and 16 nozzle diameters for the F101, as shown in Column 4 of the table. The nozzle diameter (Column 2) for each engine is that corresponding to the ideal A9, which is the area that would be required for an isentropic expansion to ambient pressure.

In Table 2, the fifth through the ninth columns give the static and total temperature, velocity, total pressure, and Mach number at the plume centerline. The second sampling station for each engine is near the end of

Table 1. Summary of Previous Afterburner Emissions Test Data.

<u>Engine</u>	<u>Simulated Mach No.</u>	<u>Simulated Altitude (ft)</u>	<u>Axial Sampling Location (ft)</u>	<u>Test Location</u>	<u>Reference</u>
TF30-P-3	0-1.3	0-40K	0.75	NASA-Lewis	a.
TF30-P-412	0-1.8	0-70K	27	NAPTC	b.
J85-5	0	0	0,4,8,16	AEDC	c.
YJ93-3	0-2.7	0-75K	0	AEDC	d.
J85-13	0-1.5	6.5-42K	0.5	NASA-Lewis	e.
Olympus	0	0	33	SNECMA	f.
J85-5	1.6-2.0	55-65K	0,14,30	AEDC	g.
J58	2.0-2.8	65K	0.2	NASA-Lewis	h.
Various	0	0	Various	NORIS	i.

References to Table 1

- a. Diehl, L.A., "Preliminary Investigation of Gaseous Emissions from Jet Engine Afterburner," NASA TM X-2323 (July 1971).
- b. Palcza, J.L., "Study of Altitude and Mach Number Effects on Exhaust Gas Emissions of an Afterburning Turbofan Engine," FAA-RD-72-31 (December 1971).
- c. Lazolier, G.R. and Gearhart, J.W., "Measurement of Pollutant Emissions from an Afterburning Turbojet Engine at Ground Level-II, Gaseous Emissions," AEDC-TR-72-70 (August 1972).
- d. Davidson, D.L. and Domal, A.F., "Emissions Measurements of a J93 Turbojet Engine," FAA-RD-73-66 (September 1973).

Table 1. Summary of Previous Afterburner Emissions Test Data (concluded).

- e. Diehl, L.A., "Measurement of Gaseous Emissions from an Afterburning Turbojet Engine at Simulated Altitude Conditions," NASA TM X-2726 (March 1973).
- f. Quillévéré, A., et al., "The Concept of Low-Pollution Rate Afterburning from the Viewpoint of Jet Engine Manufacturers," AGARD-CP-125 (September 1973). (Proceedings of AGARD Conference on Atmospheric Pollution by Aircraft Engines, held in London, 9-13 April 1973).
- g. German, R.C., et al., "Measurement of Exhaust Emissions from a J85-GE-5B Engine at Simulated High-Altitude, Supersonic, Free-Stream Flight Conditions," FAA-RD-73-92 (June 1973).
- h. Holdeman, J.D., "Gaseous Exhaust Emissions from a J-58 Engine at Simulated Supersonic Flight Conditions," NASA TM X-71532 (April 1974).
- i. Longley-Cook, E.A. and Krimmel, J.A., "Aircraft Engine Emissions Catalog," AESO 101 (Naval Environmental Protection Support Service, North Island CA) (Rev 3 June 1974).

Table 2. Summary of Plume Conditions - JETMIX Calculations.

MAX. A/B POWER - SEA LEVEL STATIC - STD. DAY

Engine	Dg Nozz. Dia. (in)	L Axial Dist. (ft)	L / Dg	Plume Centerline				Jet Dia. (ft)	Temp at Jet Dia. (°R)	
				TS (°R)	TT (°R)	U (Ft/Sec)	Ptot (psia)			M
J85-5	15.41	0	0	3064	3573	2835	29.83	1.086	1.33	-
		3.75	2.92	3057	3566	2834	29.86	1.097	2.67	720
		7.50	5.84	2399	2742	2198	25.49	0.952	3.74	690
		15.00	11.68	1510	1606	1058	18.14	0.568	5.91	610
		30.00	23.36	1023	1046	500	15.77	0.322	10.28	560
J79-15	30.28	0	0	2783	3303	2839	31.71	1.144	2.61	-
		7.50	2.97	2778	3297	2828	31.74	1.144	5.22	710
		15.00	5.94	2220	2574	2217	26.82	0.996	7.32	670
		30.00	11.89	1421	1521	1071	18.46	0.592	11.70	605
		60.00	23.78	979	1003	508	15.86	0.334	20.43	560
F101	44.74	0	0	3162	3650	2720	27.77	1.036	3.86	-
		7.50	2.01	3152	3650	2720	27.77	1.036	6.82	-
		15.00	4.02	3024	3472	2654	27.69	1.032	8.94	725
		30.00	8.05	1936	2111	1481	20.19	0.709	13.39	645
		60.00	16.09	1259	1303	707	16.47	0.413	21.55	585

the potential core, and the centerline conditions decrease rather rapidly with axial distance after this station. The tenth column gives the jet diameter, which here is defined as that diametral distance at which the local velocity is 2 percent of the centerline velocity.

Preliminary calculations using GCKP were made to determine the regions in the exhaust plume of an afterburning engine where significant chemical reactions take place. Figure 1 shows an example of chemical kinetic calculations made at the conditions of an augmentor exhaust plume. Stoichiometric combustion products at equilibrium conditions were assumed to be instantaneously mixed with ambient air. The initial CO mole fraction, $(X_{CO})_i$, for each mixture is shown in the figure. The progress of the CO consumption was then monitored with the GCKP program. Reaction progress is shown after 0.1, 1.0, and 10 milliseconds. The curves illustrate that the maximum consumption rate occurs near an equivalence ratio of 0.5, with much slower rates at the lower temperatures existing at an equivalence ratio of 0.3. It should be noted that this calculation is merely the kinetic calculation and does not include mixing effects.

From this preliminary calculation, it was concluded that the continuing chemical reactions in the plume beyond the point where the centerline concentrations have mixed below an equivalence ratio of 0.3 would have only a very small effect on the final emission level. From the JETMIX calculations, this condition was expected to occur in the region near 15 jet diameters downstream of the engine exit, for the condition where a stoichiometric mixture exists near the nozzle exit; that is, for the maximum reheat condition. For lower reheat settings, the region of continuing CO oxidation would be close to the nozzle. These initial calculations thus indicated that the originally proposed axial sampling stations appropriately bracketed the region of continuing reactions. These five initially proposed axial sampling locations were at the nozzle exit and at 3, 6, 12, and 24 nozzle diameters downstream.

As part of the early investigations of mixing and reactions in the plume, the JETMIX program was used to provide some special details of the plume mixing field not previously determined. Normally, the JETMIX program is applied to uniform afterburner temperature profiles and to simple radial profiles. In this special case, in the presence of a uniform temperature profile at the nozzle exit plane, a concentrated composition or emissions peak was input and its spreading through the plume was calculated.

An example of the calculated results is presented in Figure 2. The initial composition streak is at the outer edge of the afterburner exit. The figure shows the spread of this emissions streak as it mixes in the plume. In the first three engine diameters aft of the engine, none of the species has yet reached the plume centerline. Figure 3 shows the effect of continued mixing at 8 and 15 diameters. Also shown for comparison in Figure 3 is the simultaneously calculated temperature profile. At the 15-diameter station, the temperature profile and the emissions species profile have almost the same shape. Since the temperature began as a uniform condition at the engine exit, this demonstrates that after 15 diameters, streak effects from the

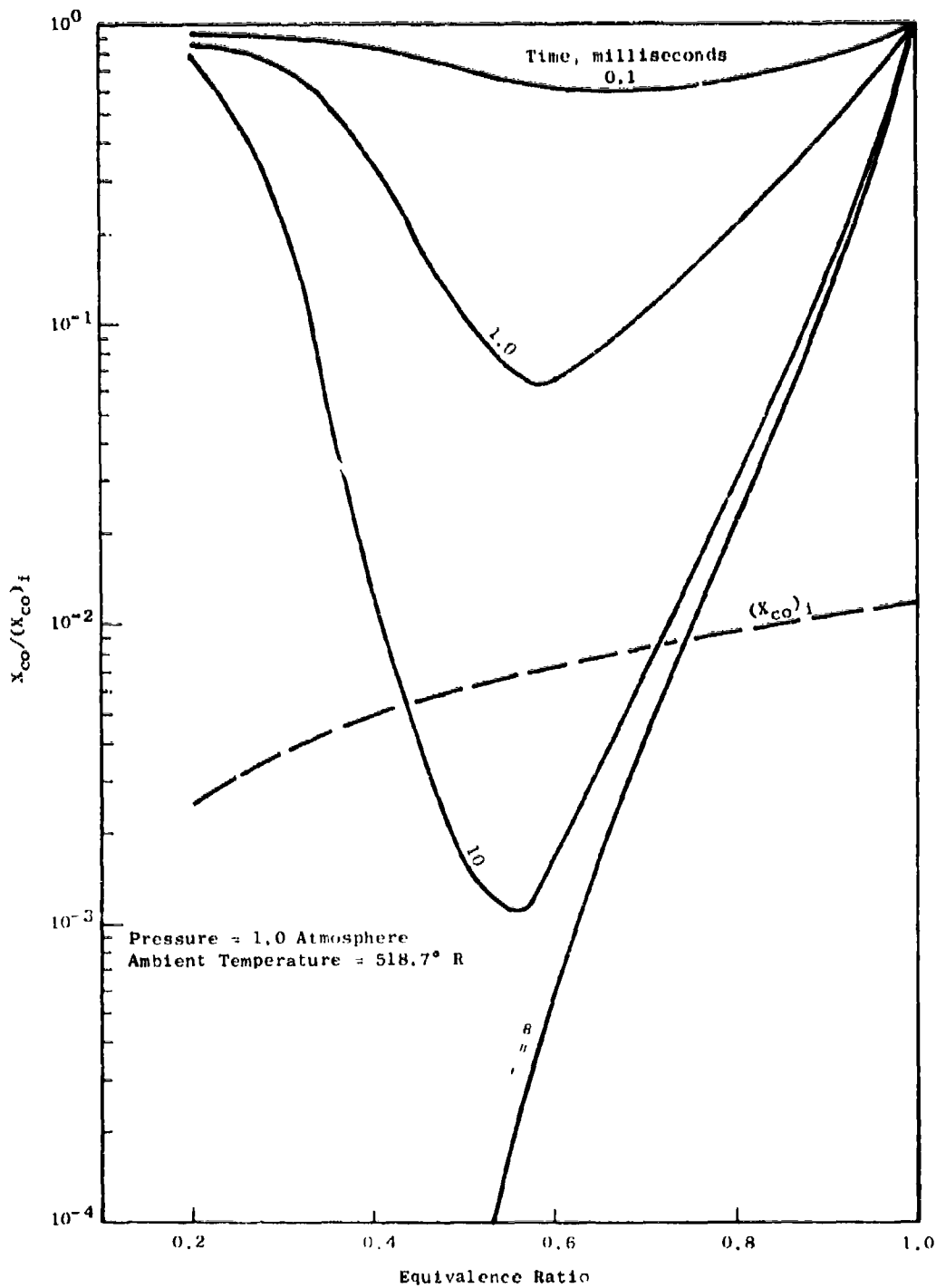


Figure 1. Consumption of CO in Equilibrium Stoichiometric Combustion Products which have been Rapidly Diluted with Air to the Indicated Equivalence Ratio.

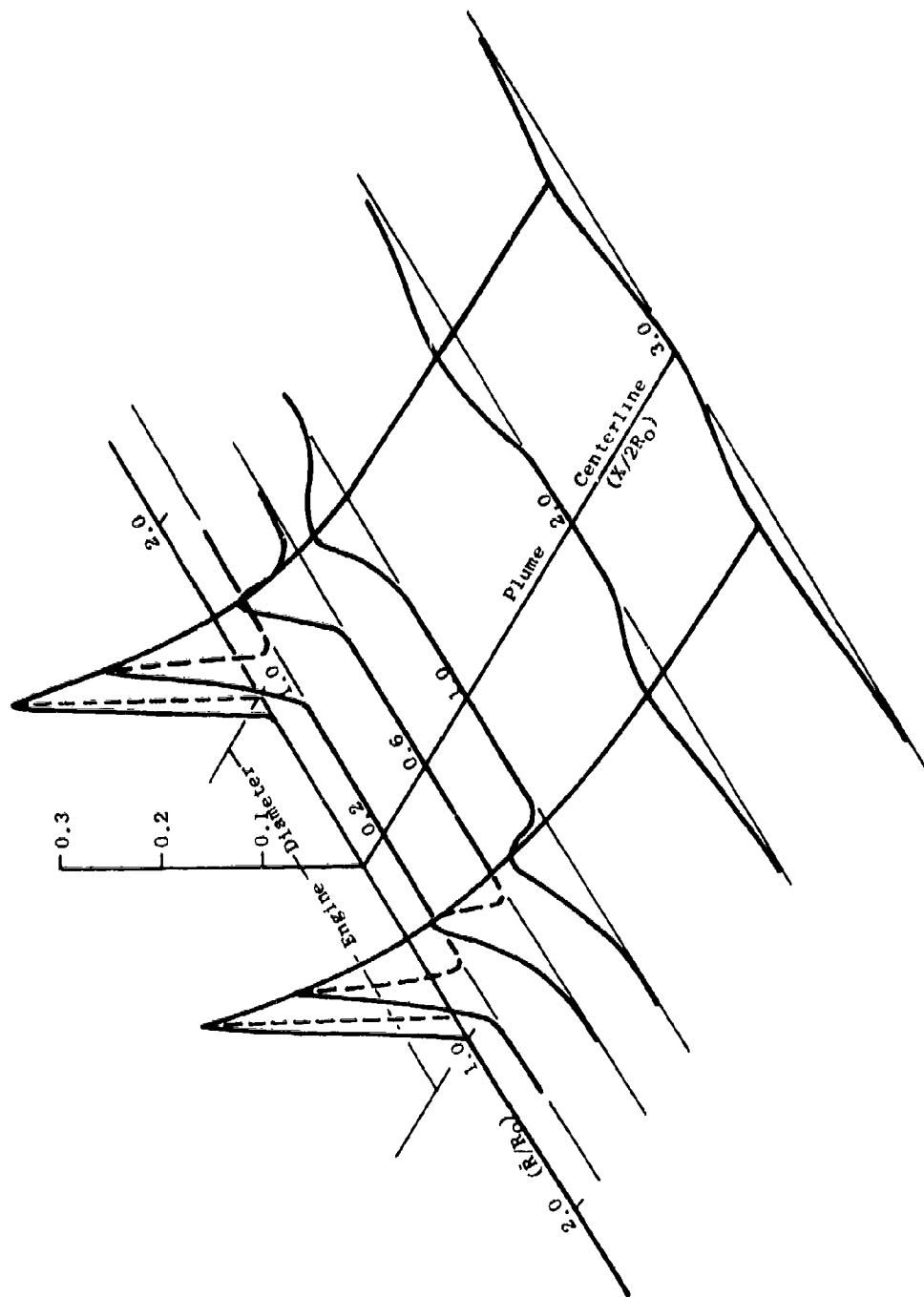


Figure 2. Presentation of Concentrated Species Mixing from Outer Edge of Engine Exit.

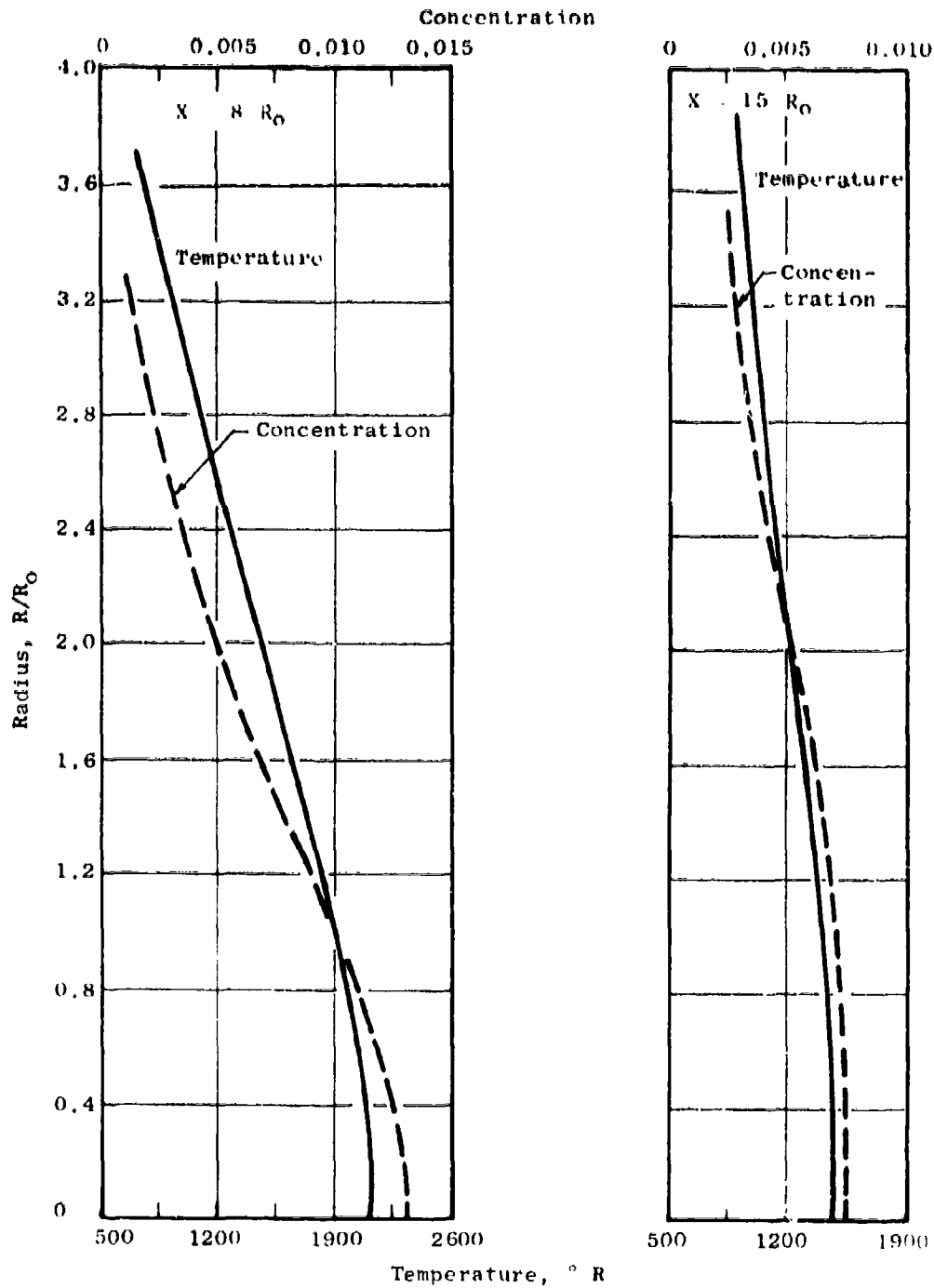


Figure 3. Comparison of Trace Species Concentration Profile with Temperature Profile at Two Axial Distances.

augmentor have essentially mixed to the equivalent of a uniform engine exit emission level. However, since the temperature histories to this station are quite different between the streak and the uniform case, the chemical kinetics may show very significant differences in the actual final calculated emissions levels. At eight engine diameters there is still a significant difference between the temperature profile and the emissions streak profile.

These calculations demonstrated the extremely intense mixing which occurs in the plume outside of the potential core. Due to this intense mixing, the concentration profiles will be similar, at distances far enough removed from the exhaust nozzle, regardless of the initial distribution at the exhaust plane. This concept forms the basis for the "far plume" measurement procedure which was developed in this program.

3.3 PROBES FOR AFTERBURNER EXHAUST MEASUREMENTS

3.3.1 General Considerations

For the afterburner emissions measurements made in Phase II of this program, a complete plume survey was required at several engine power settings up to maximum afterburner power. For an engine at maximum afterburner power in sea level static operation, local total temperatures at the exhaust plane may reach levels as high as 3600° F. This corresponds to nearly equilibrium temperatures at stoichiometric fuel-air ratio. Corresponding local total pressures are typically in the range 30 to 40 psia. Very careful design of the probe is required to withstand such severe environments.

At the other extreme of conditions, near the edge of the plume, temperatures and pressures are near the ambient values. Reliable sampling and subsequent accurate analyses of the exhaust gases over this extremely wide range of conditions was one of the most challenging problems of this program. It was determined that two pairs of probes would be used for the plume surveys. The high temperature probes were used at axial sampling locations where temperatures exceeded 2000° F. The low temperature probes had a much longer span and were used at the downstream sampling stations where temperatures were below 2000° F. The major factor in choosing the movable single-element probes over the fixed-rake array was the much greater adaptability of the movable probes to the various engine sizes and axial sampling stations.

The high temperatures at the exhaust planes required special construction of the probe tip to quench, or freeze, the chemical reactions at the probe entrance. These quick-quench probes were constructed in such a way that reactions were frozen at the probe entrance by rapid expansion of the gas to lower pressure, and by cooling of the sample by conduction to the walls.

Since there could be quite severe and somewhat unpredictable gradients in the exhaust stream, it was necessary to determine the local mass flow so that the individual samples could be properly weighted. Once the local mass flow was determined, along with the gas composition, then the local flux of

all gas species could be evaluated. This method also allowed calculation of total carbon flux in the plume for comparison with the total carbon in the engine fuel flow. This redundant information provided a valuable check on the overall sample consistency.

3.3.2 Probe Cooling

An important consideration in the design of the sampling probe, especially at sample locations near the exhaust nozzle, was the method of cooling the probe. While the probe itself must be cooled sufficiently to maintain structural integrity, a conflicting requirement was that the sample line must be kept hot enough to prevent condensation of hydrocarbons and water. Ideally, the probe would be maintained at about 300° F, the same temperature as required for the sample line. This presented considerable difficulty in the nozzle exit plane where heat fluxes to the probe are extremely high. Several types of cooling media were considered for use in maintaining the probe at 300° F. Among these cooling media were steam, pressurized water, and various types of heat transfer salts. These were all rejected for various reasons.

A second approach to maintaining the probe at 300° F was to use a dual-fluid system where the probe coolant circuit is separate from the sample heating circuit within the probe. This approach was undesirable due to the considerable expense and complexity involved in the construction and operation of such a probe.

Consideration of the various alternatives favored the use of a low pressure, heated water system for probe cooling, if it could be determined that temperatures as low as the range 130° F to 180° F could be tolerated. With this objective, a relatively simple test was performed using an existing small-scale combustion system.

The combustion system was instrumented with two probes. One probe, the one normally used for gas sampling in this system, was cooled with heated water (about 150° F) in the usual way. The other probe was cooled by oil pumped from a special oil reservoir. The temperature of this oil could be varied from 300° F to 95° F. A 50-foot section of sample line connected to the oil-cooled probe was also heated by circulation of the same oil. Samples from each probe were analyzed with a gas chromatograph and flame ionization hydrocarbon analyzer.

The rig was operated with pilot burner only, a total fuel-air ratio of about 0.01, and an air inlet temperature of 340° F. The sample from the water-cooled probe was analyzed to monitor the burner stability, while the coolant temperature of the oil-cooled probe was slowly varied from 300° F to 95° F. As shown in Figure 4, the oil-cooled probe gave a relatively constant level of HC (2800-3000 ppm) over the complete range of coolant temperatures. In Figure 4, the corrected HC concentration is plotted against probe coolant temperatures, where the corrected value is:

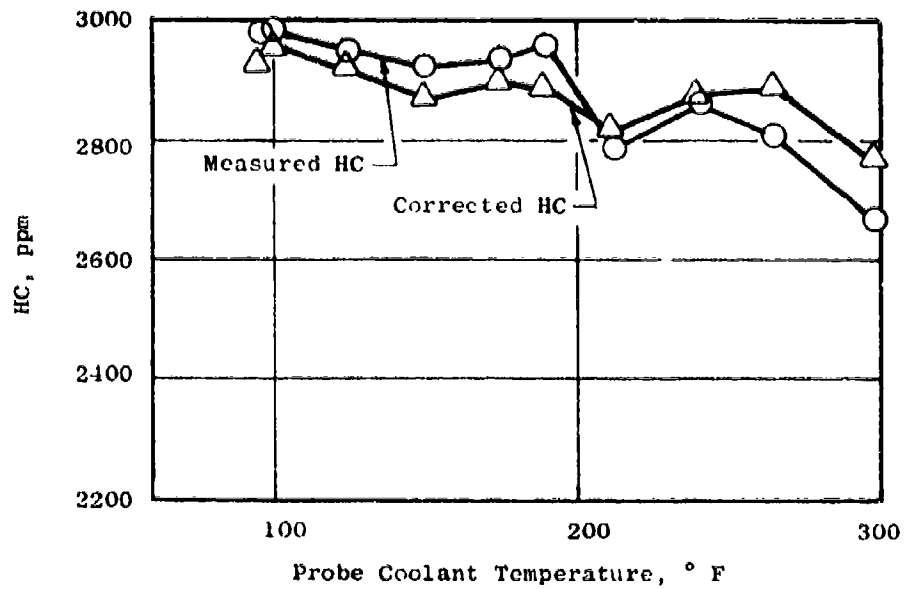


Figure 4. Results of Probe Coolant Test.

$$\text{HC (Corrected)} = \frac{\text{HC (Measured)}}{\text{HC (Reference)}} \times \text{HC (Reference)}_{\text{avg}}$$

The reference value was obtained through the water-cooled probe. Figure 4, thus, shows that a portion of the variation in HC concentration was actually due to variation in the burner itself.

It should be noted that this simple test did not cover the complete range of possible conditions which could be encountered in emissions sampling of afterburning engines. It was, however, a relatively severe test in that not only was the probe coolant temperature varied, but also the temperature of the adjacent 50 feet of sample line.

It had been determined previously that heated-water cooling of the probe was the most attractive of several cooling schemes considered. The results of this test further favored the choice of this method. It was necessary to set a lower limit of about 130° F on the coolant temperature in order to prevent condensation of water in the sample lines.

In a similar test reported recently (Reference 1), no significant difference in HC concentration was noted over sample line temperatures ranging from 150° F to 350° F.

3.3.3 Quenching of Gas Sample

Quenching of the sample gases at the probe orifice was required at the high temperatures to prevent continued chemical reaction within the probe which would give distorted values of the gas composition. In these probes, quenching of the gas sample was accomplished by:

- Water cooling of the probe.
- Providing a diverging passage leading away from the probe tip.
- Reducing the sample line pressure to provide a pressure ratio of 5 to 1, or more, across the probe tip.

The diverging passage in conjunction with the low pressure in the probe created a short supersonic expansion which reduced the static pressure of the gas stream. This action combined with the wall cooling effect provided the necessary quenching of the chemical reactions.

Although expansion of the exhaust gases across the probe orifice coupled with conductive cooling to the interior walls of the probe are effective in quenching reactions within the probe, the processes above are apparently not sufficient to freeze the reactions. A calculation based on reaction kinetics in a homogeneous stream will generally show a large fractional reduction in reactive species within the probe, that is, a lack of quenching. It is known, however, that quenching probes are considerably more effective than

indicated by such calculations. The reason for this is that simplified calculation neglects the axial heterogeneity of the exhaust stream. Consideration of this axial heterogeneity is a key element in the formulation of the plume model, to be described in detail in the next section of this report. Thus, while the effects of gas expansion and cooling can qualitatively be demonstrated by rather straightforward calculations, a thorough analytical treatment of gas compositional changes within the probe would be extremely complex due to the stream heterogeneity and was not attempted on this program.

The required flow through the sample system was determined by the gas sample flow rate required at the analyzers. Once this flow was determined, the probe orifice was sized so as to give critical flow across the orifice. The gas sample pump was then chosen to give the required inlet and outlet pressure with the selected flow rate.

In the design of the quick-quench probes, copper sampling tips were used. This was to provide good heat transfer from the water cooled region out to the end of the tip. Although copper is not generally recommended for use in measuring NO_x , this short length of the copper tip in contact with the gas sample would probably have negligible effect on the NO_x readings.

3.3.4 High Temperature Probe Design

The high temperature probe assembly was 60 inches long from the gas sample orifice to the axis of rotation. The probe assembly consisted of three separable components - the probe, probe support body, and probe support arm. Both the probe and probe support body were separately water-cooled. The probe support arm was uncooled. A sketch of the high temperature probe assembly is shown in Figure 5.

The tips of the high temperature probe contained both total pressure and gas sample orifices, as shown in Figure 6. Since the orifices were separated by only 0.188 inch, very careful design of the sensor tip was required to assure that a continuous sampling flow through one orifice would not interfere with the total pressure measurement at the other orifice. A model of the probe tip was constructed and aerodynamically calibrated to verify the measurement of total pressure during continuous gas sampling.

Each high temperature probe was positioned by a "windshield wiper" type actuator, which consisted of an electric motor and reduction gear train turning the shaft to which the probe assembly was fixed. The probe assembly and actuator mounted behind the J85-5 engine is shown in Figure 7. The actuators were so placed that each probe swept in an arc through the engine centerline. The angular position of the actuator shaft was measured by a calibrated potentiometer affixed to the shaft. This angular position, along with fixed geometrical factors, was used to determine the probe tip radial location with respect to the engine centerline.

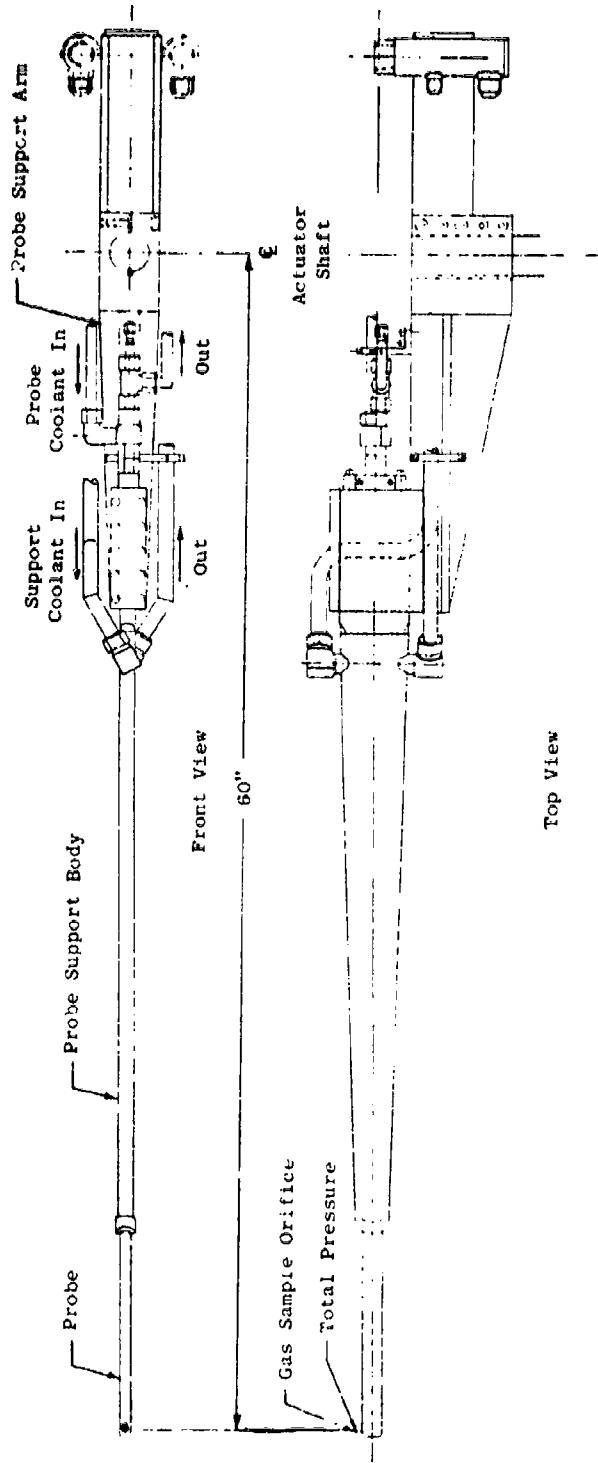


Figure 5. High Temperature Probe Assembly.



Figure 6. High Temperature Probe Tip Showing Gas Sample and Total Pressure Orifices.

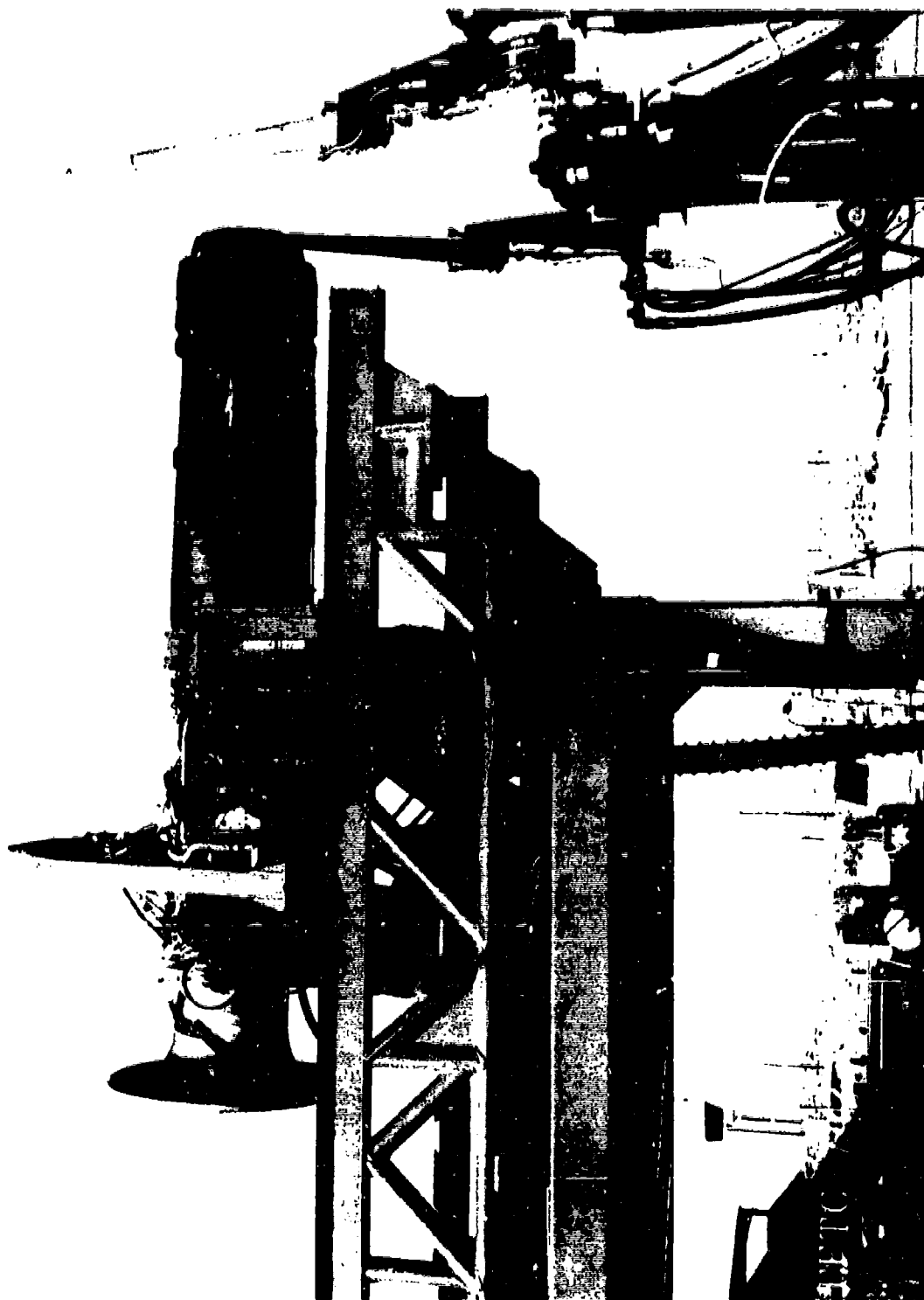


Figure 7. High Temperature Probes with Actuators Mounted at Nozzle Exit Plane of J85-5 Engine.

3.3.5 Low Temperature Probe Design

The low temperature probe was 10 feet long, as measured from the gas sample tip to the axis of rotation, and the axis of rotation was located 4.93 feet from ground level. The low temperature probe system consisted of the probe itself, actuator, and stand, as shown in Figure 8. The end of the probe contained a total and static pressure tube, a gas sample orifice, and a thermocouple. The end of the probe was removable, so that in the event of damage to the elements, the entire end of the probe could be replaced. Figure 9 shows the probe end.

The probe was positioned by a screw-type actuator (Duff-Norton Company "Jactuator" #CM4802-36-B-1) with 36-inch stroke. The actuator system was designed for a total travel of 130 degrees. The angular position of the probe was measured by a calibrated potentiometer similar to that used for the high temperature probes. The support stands for the low temperature probes were anchored directly to the reinforced concrete pad extending behind the engine test stand.

Figure 10 shows the low temperature probe attached to the concrete at the 60-foot axial station. At the time of this photograph, a pneumatic dampener had been added to improve stability of the probe in the extremely turbulent exhaust plume.

3.4 EMISSIONS SAMPLING AND ANALYSIS SYSTEM

The basic elements of the emissions sampling and analysis system used in the Phase II and Phase III tests are shown in Figure 11. Two separate sample lines connected the probes to the gaseous emissions and smoke measurement equipment through a double, three-way valve system. With this arrangement, smoke was sampled from one probe while gaseous emissions were analyzed from the other probe. The pumps immediately downstream of each probe provided the reduced pressure within the probe necessary for rapid quenching of the exhaust sample. These pumps were Contamination Control, Inc., Model 299 four-stage "Diavac" pumps and were sized to maintain a pressure in the probe of about 6 psia.

The sample line connecting the sample pumps to the heated valve box was a steam-traced "Dekoron" tube bundle. The length of the line between the probe pumps and the valve box was approximately 100 feet. The steam generator was an Ebcor electrode boiler, Model 5-240-4, rated at 250 psig, 5 Bhp, 173 lb per hr, 50 KW. All sample lines from the probe exit to the analyzer unit were steam-traced and maintained at a temperature of about 300° F during the tests.

Heated water for probe cooling was circulated from a 500-gallon tank through the probes by a 50 gpm electric pump. Water in the tank was maintained at 160 to 180° F by a thermostatically controlled electric heater.

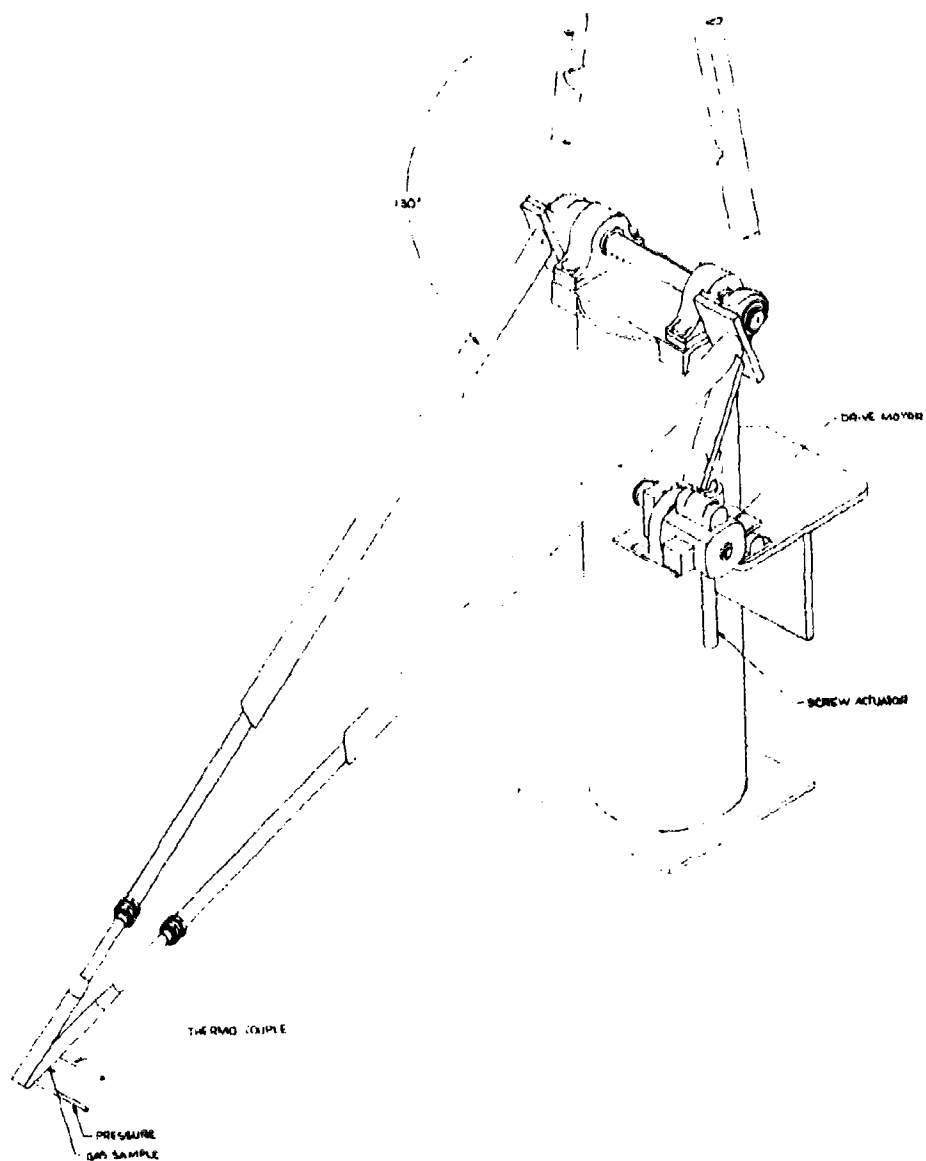


Figure 8. Low Temperature Probe System.

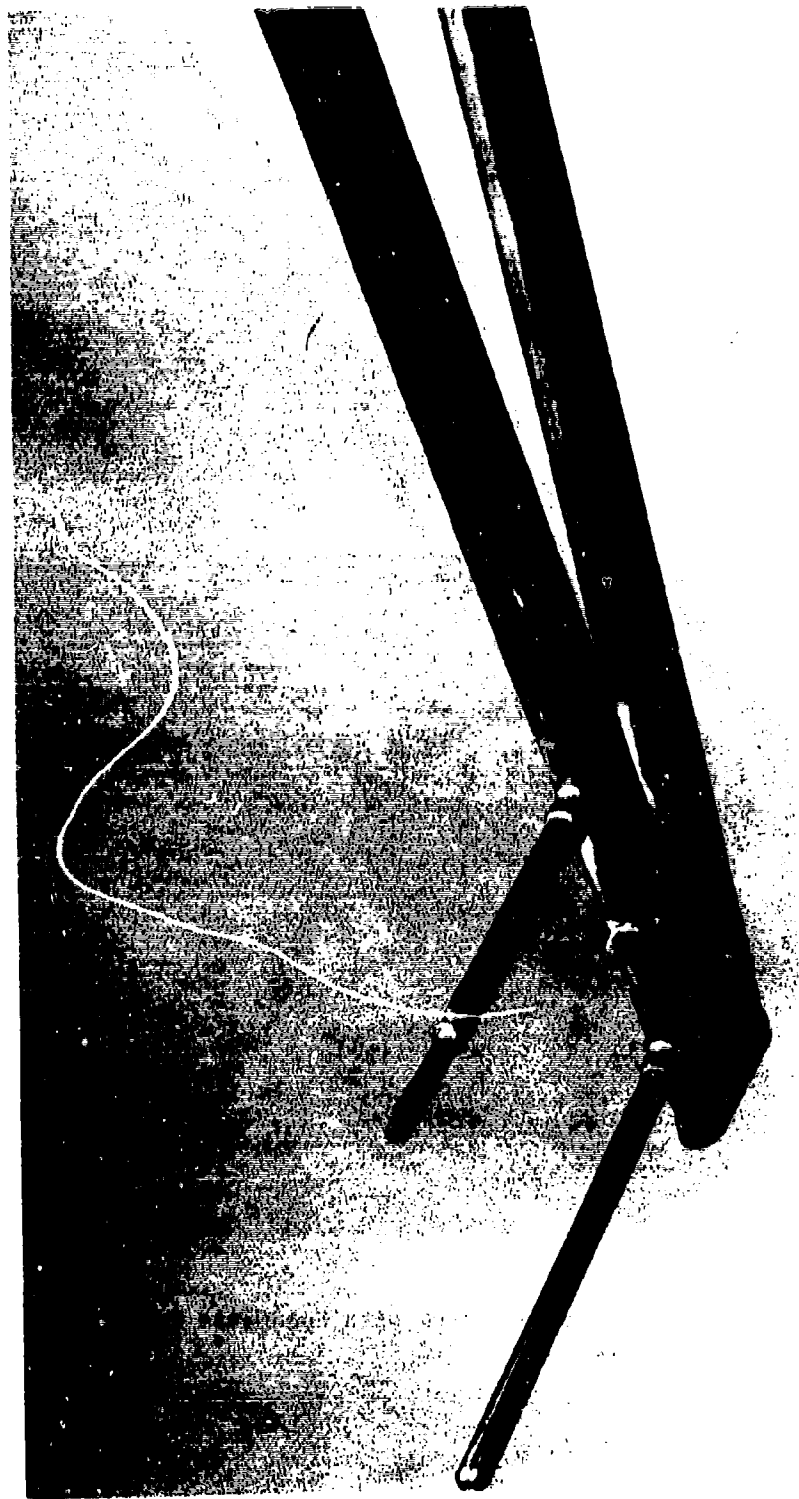


Figure 9. Low Temperature Probe Tip Showing (Left to Right) Total/Static Pressure Tube, Gas Sample Tip, and Aspirated Thermocouple.

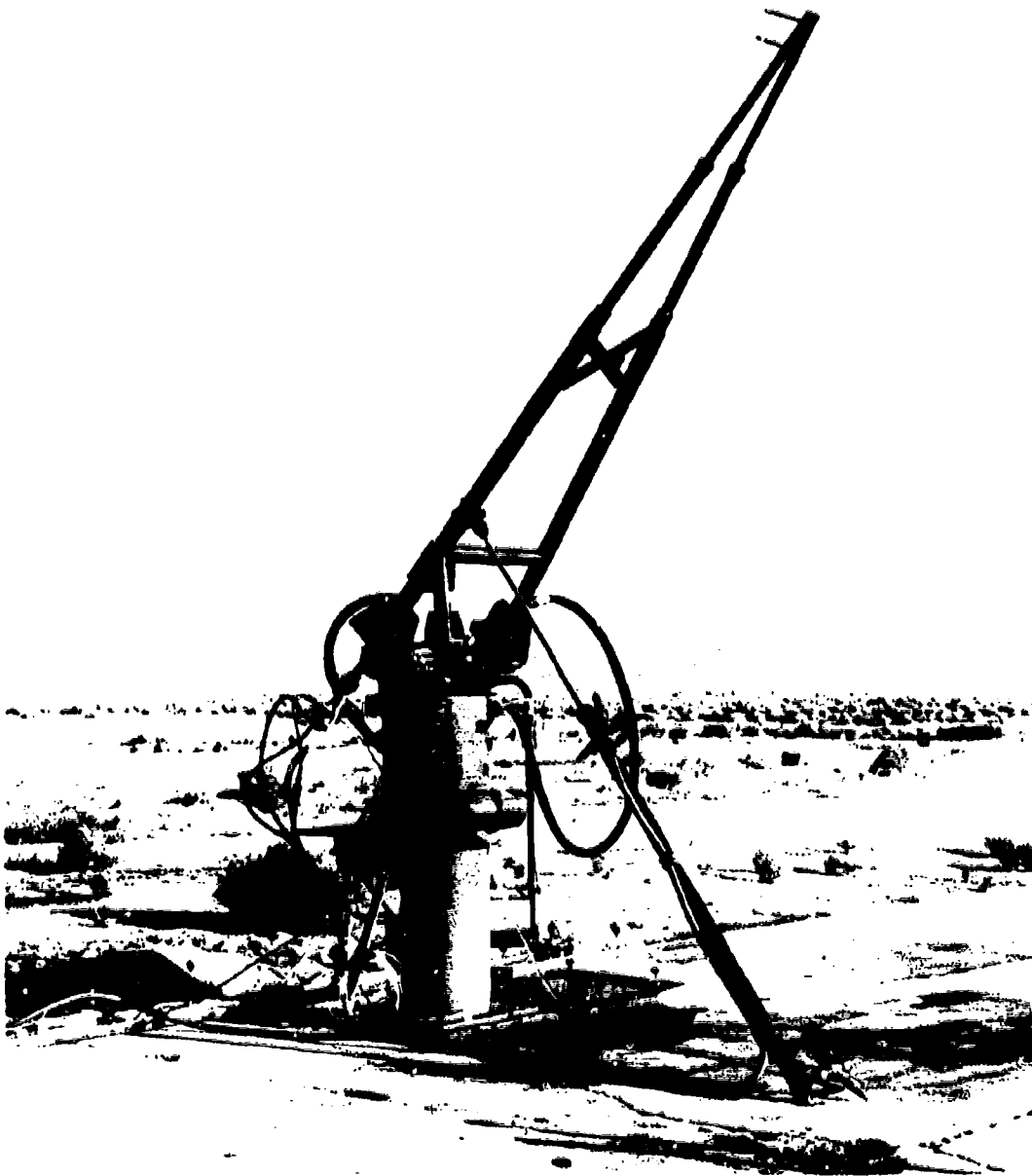


Figure 10. Low Temperature Probe System with Pneumatic Damper Added for Improved Stability.

The gaseous emissions analysis system consisted of four separate analyzers, all manufactured by Beckman Instruments, Inc.; the system was assembled by General Electric. The CO (Model 855) and CO₂ (Model 864) analyzers were both nondispersive infrared (NDIR) instruments. To minimize water interference, the sample was dried by an ice trap before entering the NDIR instruments. The NO_x analyzer was a Model 951 heated Chemiluminescence Analyzer, and the HC analyzer was a Model 402 flame ionization detector (FID) instrument. No traps were used in the NO_x and FID lines, and the sample temperature was maintained above the maximum dewpoint (130° F) of the sample gas.

SECTION 4.0

ANALYTICAL PLUME MODEL DEVELOPMENT

A key part of the afterburner emissions measurement program was the development of a computerized analytical model of the simultaneous mixing and chemical reaction processes that can occur in the plumes of afterburning engines. This model was developed so that local concentrations of the various exhaust gases, at any axial station and radial position downstream of the engine exhaust nozzle, may be calculated from the initial exhaust plane values. This model not only permits calculation of final emissions levels from exhaust plane data, but also permits investigation of the effects of such factors as engine size, ambient conditions, altitude, flight Mach number, etc. Initial development of the model was accomplished in Phase I of the program, and refinement and validation occurred in Phase II.

This section contains a discussion of the analytical methods used in the development of the model. Comparison of the predictions of the model with actual plume measurements made at various axial locations behind afterburning engines is presented in Section 6.0 of this report.

4.1 METHODS OF ANALYSIS

The analytical model of the physical and chemical processes occurring in the exhaust plume of afterburning gas turbine engines was formulated from a series of computer programs. This formulation utilized existing programs where appropriate, and new programs were written as required. The major pre-existing elements, which formed a sound base on which to structure the model, were: (a) the steady-state turbulent gas jet mixing analysis used in the General Electric computer program JETMIX (Reference 2); (b) a formal solution of gas-phase chemical reaction kinetics equations developed by NASA-Lewis Research Center (Reference 3); and (c) an approximate combustion gas kinetics analysis formulated at General Electric as an extension of techniques developed for hydrogen-fueled hypersonic ramjets (Reference 4).

Physical parameters input to the model include: ambient air properties (temperature, pressure, humidity, flight speed); fuel properties (temperature, hydrogen content, heating value); engine cycle parameters (ram air temperature, bypass ratio, main combustor fuel-air ratio and CO and NO_x emissions indices, fan discharge temperature, exhaust jet diameter); and exhaust jet survey probe data at several points (radial location, impact pressure, gas sample analysis). The gas analysis requires volumetric determination of CO and CO₂ with the sample dried to saturation at 32° F, and total HC (as single-carbon-atom molecules) and total NO_x with sample water content as-sampled.

The composition and properties of the gas flow at each probe measurement point are derived from the measurements. In this derivation, the gas composition at a point in the flow is assumed to be heterogeneous or time-varying. This assumption was chosen in preference to a homogeneous gas with nonequilibrium chemical composition, because examination of chemical reaction kinetics indicated that, under high temperature afterburner conditions, the reactions would proceed to equilibrium in a few inches. The existence of nonequilibrium concentrations of CO and hydrocarbons in the gas samples is better explained by postulating that, over a part of the sampling time, the probe was immersed in a gas mixture much richer or much leaner than the mean fuel concentration of the sample.

The flow is assumed to be axisymmetric so that the gas properties at each sample point are applied to the flow in an annular streamtube. The time-average properties of the flow in each tube are also computed.

The intermixing of the annular streamtubes and the diffusion of the jet into the static or moving ambient air are computed by the JETMIX analysis (Reference 2), which performs a numerical solution of the differential equations of continuity of mass, momentum, energy, gas species, and turbulence kinetic energy. The flow initially in each of the streamtubes assigned to each sample point is treated as a separate gas, as is the ambient air. These gases are treated as homogeneous, inert, ideal gases with constant specific heats. Any increase in total temperature due to chemical reactions is calculated later, but it is assumed that the density change is not sufficient to influence the

mixing. In an afterburner, the combustion reactions should be essentially complete upstream of the exhaust nozzle, so that the reactions continuing into the exhaust plume are only consuming trace contaminants.

A differential equation governing the formation, convection, and decay of a characteristic of the gas heterogeneity is solved numerically throughout the flow field, using the previously calculated properties of the flow. This concept was taken from the works of Spalding (References 5, 6, and 7).

The nonreacting flow field solution provided by the JETMIX analysis and the Spalding heterogeneity solution are not used directly by the plume model, but rather are used to guide the mixing between and homogenization within a fixed number of computation tubes extended from the original streamtubes assigned to each sample point. This approach is taken to minimize the number of chemical kinetics calculations. The computation proceeds in axial steps through the plume. The gas composition in each tube is modified by inter-tube mixing and intra-tube homogenization at each step. After several steps, the gas composition is further modified by chemical reactions over a time increment corresponding to the step length and local velocity.

A choice of two chemical reaction kinetics analyses is provided. One of these, GCKP, consists of a numerical solution of simultaneous differential equations formed from the forward and reverse reaction rates of a system of 23 two- and three-molecule collision reactions. Although having a high degree of rigor, GCKP is computationally cumbersome. The alternate kinetics analysis, SCKP, utilizes approximations applicable to high-temperature combustion reactions to achieve computational efficiency. These approximations are associated with a radical pool in pseudo-equilibrium, the decay of which is paced by selected three-body reactions.

Neither chemical kinetics analysis treats consumption of unburned hydrocarbons. This is done with a phenomenological technique using an empirical relation of ignition delay for kerosene as a function of temperature.

At preselected axial locations, the model performs a summation of fuel and contaminant flow in each computation tube, providing predicted values of local and overall emissions indices. When all local gas temperatures have been reduced to the point where chemical reactions cease, the emissions indices will not change with length. These are then the true residual emissions.

4.2 TWO-PART MODEL OF HETEROGENEOUS GAS FLOW

A detailed description of the heterogeneous gas flow at each probe location in the engine exhaust plane is constructed from the probe impact pressure, the measured or assumed static pressure, and the gas sample analysis. For computational expediency, only two gas mixtures are assumed to exist at each point in space: the cold part contains all of the measured hydrocarbons, plus turbine discharge gas bearing a proportional amount of any CO and NO_x emitted from the main combustor and, optionally, some bypass fan air or nozzle secondary air; the hot part contains the balance of the fuel and air and is in chemical equilibrium at the nozzle exit plane.

4.2.1 Sample Fuel-Air Ratio and Emissions Indices

The fuel-air mass ratio of each gas sample, \bar{f}_s , and the emission indices (pounds contaminant per pound fuel) for CO, NO_x (as NO₂), and unburned hydrocarbons, are derived from the gas sample analysis. The procedure is to solve three linear equations for the unknown quantities \bar{f}_s , M_T (total moles of sample per pound of air), and M_D (moles of dry sample, water removed, per pound of air):

$$\begin{aligned} \frac{2.5n\bar{f}_s}{m_f} &= \left[1 - \left(\frac{1-2.5n}{10} \right) R_{HC} \right] M_T - .503101 (R_{CO} + R_{H_2}) M_D - \frac{1}{m_a} - \frac{\alpha}{m_{H_2O}} \\ &= \left(\frac{1+2.5n}{10} \right) R_{HC} M_T + [.503101 (R_{CO} + 3R_{H_2}) - 1] M_D + \frac{1}{m_a} \\ &= \frac{n}{4} R_{HC} M_T + .2515505 n(R_{CO} + R_{CO_2}) M_D - \frac{.000075 n}{m_a} \end{aligned} \quad (1)$$

These equations are derived in Appendix A, Part 1. The symbol n represents the hydrogen-to-carbon atom ratio of the fuel, m_f is the fuel molecular weight (the fuel molecule formula is assumed to be C₁₀H_{10n}), m_a is the molecular weight of dry air, α is the air humidity (lb water/lb dry air), m_{H_2O} is the molecular weight of water, R_{CO} and R_{CO_2} are the gas analyzer readings for CO and CO₂ (moles constituent per mole sample dried to 492° R saturation), R_{HC} and R_{NO_x} are gas analyzer readings for total hydrocarbons (as CH₄) and nitrogen oxides (moles constituent per mole undried sample), and R_{H_2} is moles H₂ per mole dried sample, derived from R_{CO} by an empirical relation:

$$\begin{aligned} \frac{R_{H_2}}{R_{CO}} &= 0.2 (100 R_{CO})^{0.16} & R_{CO} \leq 0.091022292 \\ & & \\ \frac{R_{H_2}}{R_{CO}} &= 0.0147 (100 R_{CO})^{1.342} & R_{CO} > 0.091022292 \end{aligned} \quad (2)$$

This empirical relation had been developed at General Electric from a study of a large number of gas analyses from a variety of burners.

The emissions indices are then calculated as

$$EI_{HC} = R_{HC} \left(\frac{mf}{IO} \right) \left(\frac{MT}{\bar{f}_s} \right) \quad (3)$$

$$EI_{CO} = R_{CO} M_{CO} \left(\frac{1.006202 MD}{\bar{f}_s} \right) \quad (4)$$

$$EI_{NO_x} = R_{NO_x} M_{NO_x} \left(\frac{MT}{\bar{f}_s} \right) \quad (5)$$

Emissions indices are handled internally in the model as pounds per pound of fuel, rather than the conventional pounds per thousand pounds of fuel.

4.2.2 Local Vitiated Air Properties

The cold part of the two-part heterogeneous gas stream is assumed to consist of vitiated air (air burned with main combustor fuel), plus the measured unburned hydrocarbons. The properties of the air that arrives at each probe sampling location in the exhaust gas stream are a function of certain engine operating parameters. The nomenclature used to describe these parameters uses engine cycle stations illustrated in Figure 12.

Work is extracted from the core air stream to compress the fan air. Neglecting work extracted from the main combustor fuel flow,

$$h_2 - ha_5 = \beta (h_{25} - h_2) \quad (6)$$

where h_2 and h_{25} are the wet air specific enthalpies corresponding to engine inlet and fan discharge total temperatures T_2 and T_{25} , ha_5 is the enthalpy of air that would react with fuel-air ratio f_5 to produce turbine discharge total temperature T_5 , and β is the engine bypass ratio

$$\beta = W_{25}/W_{2C} \quad (7)$$

Mixing of the fan and turbine discharge stream may be incomplete at the probe survey plane, so that the local effective bypass ratio may not be equal to the engine cycle bypass ratio. To provide for this contingency, a local bypass ratio β_L is defined so that the local ratio of main combustor fuel to dry air is

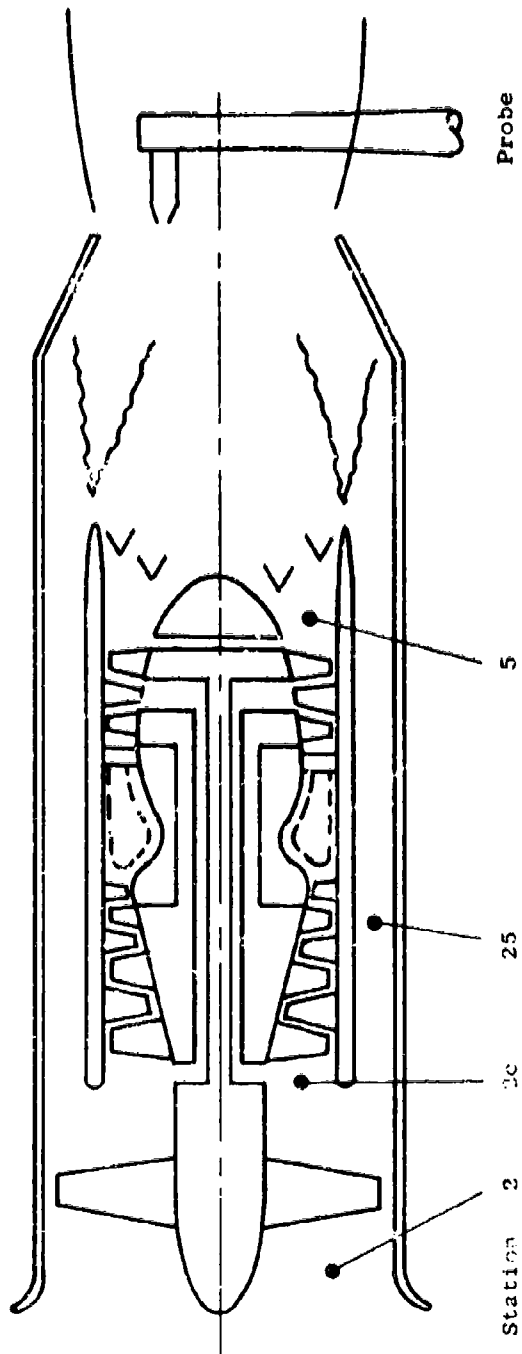


Figure 12. Augmented Turbofan Engine Schematic.

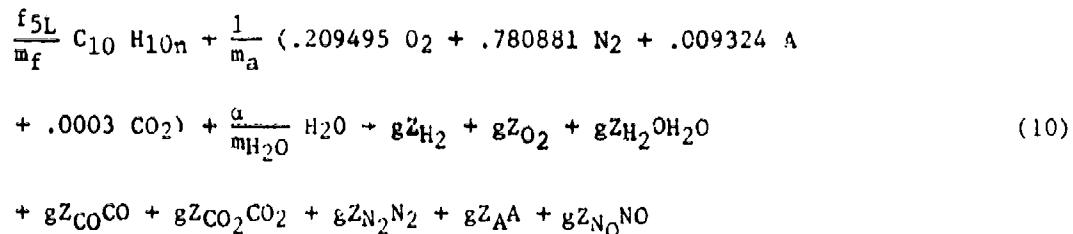
$$f_{5L} = \frac{f_5}{1 + \beta_L} \quad (8)$$

The value of β_L at each radial location may be estimated by measuring local fuel-air ratio with the engine at military power setting, where all fuel sampled is main combustor fuel, and assuming that the afterburner combustion does not alter the radial variation of β_L . For turbojet engines, $\beta = \beta_L = 0$, unless nozzle secondary air is sampled near the fringe of the jet, when a positive β_L may be required to account for $\bar{f}_s < f_5$.

The local effective air enthalpy is

$$h_{aL} = \frac{h_{a5} + \beta_L h_{25}}{1 + \beta_L} \quad (9)$$

The composition of the vitiated air which, with the measured unburned hydrocarbons, will form the cold part of the two-part heterogeneous gas mixture is computed by writing the formula for partial combustion of the main combustor fuel:



where $g = 1 + f_{5L} + \alpha$, and the Z_i 's are moles of species i per pound of mixture. The CO and NO_x emissions from the main combustor are assumed to remain in the vitiated air.

$$gZ_{CO} = f_{5L} (EI_{CO})_C / m_{CO} \quad (11)$$

$$gZ_{NO} = f_{5L} (EI_{NO_x})_C / m_{NO_2} \quad (12)$$

The hydrogen is assumed to be related to the CO by the same ratio as was used in Section 4.2.1 above:

$$Z_{H_2} = \left(\frac{RH_2}{R_{CO}} \right) Z_{CO} \quad (13)$$

Consistent mass balances then provide:

$$gZ_{H_2O} = \frac{5n f_{5L}}{m_f} + \frac{\alpha}{m_{H_2O}} - gZ_{H_2} \quad (14)$$

$$gZ_{CO_2} = \frac{10f_{5L}}{m_f} + \frac{.0003}{m_a} - gZ_{CO} \quad (15)$$

$$gZ_{N_2} = \frac{.780881}{m_a} = .5gZ_{O_2} \quad (16)$$

$$gZ_{O_2} = \left(\frac{.209495 + .0003}{m_a} \right) + .5 \left(\frac{\alpha}{m_{H_2O}} \right) - .5gZ_{CO} - .5gZ_{NO} - .5gZ_{H_2O} - gZ_{CO_2} \quad (17)$$

$$gZ_A = \frac{.005324}{m_a} \quad (18)$$

4.2.3 Proportion and Composition of Each Part of Heterogeneous Gas

The procedure for determining the properties of the two-part heterogeneous gas at each sample point is an iterative one, in which the mass fraction of hot gas in the sample is estimated, the composition and properties of both hot and cold parts are computed, then the calculated CO emissions index is compared with the measured value and a new estimate of the proportion of hot gas is made if necessary.

The hot and cold parts are assumed to be moving at the same stream velocity, and are assumed to remain separate in the sampling process until sufficient cooling to quench CO reaction has occurred. Because of gas density differences, the sampling rates for hot and cold gases are different, resulting in proportions of hot and cold parts in the sample somewhat different from those in the free stream; this effect is treated.

The cold part is assumed to contain vitiated air (as defined in Section 4.2.2 above) and the measured unburned hydrocarbons. The mass fraction of the cold gas consisting of unburned fuel is thus

$$F_u = \frac{\bar{F}_s (EIHC)}{1 - y_s} \quad (19)$$

where y_s is the estimated mass fraction of hot gas in the gas sample and

$$\bar{F}_s = \frac{\bar{i}_s}{1 + \bar{f}_s + \alpha} \quad (20)$$

is the mass fraction of total fuel in the mixed sample. The total fuel in the cold part is the sum of the unburned fuel and the main combustor fuel contained in the vitiated air:

$$F_c = F_u + F_{5L} (1 - F_u) \quad (21a)$$

where

$$F_{5L} = \frac{f_{5L}}{1 + f_{5L} + \alpha} \quad (21b)$$

The hot part contains the balance of the total fuel:

$$\bar{F}_s = y_s f_H + (1 - y_s) F_c \quad (22)$$

The total enthalpies of the hot and cold parts are computed from the local effective air enthalpy (Section 4.2.2) and the absolute enthalpy of the fuel (Appendix A, Part 3) assuming no heat conduction within the gas:

$$h_{TH} = (1 - F_H) h_{aL} + F_H h_f \quad (23)$$

$$h_{TC} = (1 - F_C) h_{aL} + F_C h_f \quad (24)$$

In expanding reversibly through the exhaust nozzle pressure ratio P_{T8}/P , the hot part would normally attain velocity

$$\frac{U_H^2}{2gJ C_{PH} T_{TH}} = 1 - \left(\frac{P_{T8}}{P} \right)^{\frac{\gamma-1}{\gamma}} \quad (25)$$

Similarly, for the cold part,

$$\frac{U_C^2}{2gJ C_{PC} T_{TC}} = 1 - \left(\frac{P_{T8}}{P} \right)^{\frac{\gamma-1}{\gamma}} \quad (26)$$

If the specific heats are not greatly different, then approximately,

$$U^2_H = \left(\frac{T_{TH}}{T_{TC}}\right) U_C^2 \quad (27)$$

However, in this model, the hot and cold streams are constrained to the same velocity U . Only part of the expansion work of the hot part produces kinetic energy; the rest is imparted to the cold part to increase its kinetic energy:

$$U^2 = yU^2_H + (1 - y)U_C^2 \quad (28)$$

The mass fraction of hot gas in the free stream (y) is not known at this point in the calculation; however, it has been observed that its value differs little from y_s , so that the approximate correction for kinetic energy transfer is derived from

$$U^2 = y_s \left(\frac{T_{TH}}{T_{TC}}\right) U_C^2 + (1 - y_s)U_C^2 \quad (29)$$

The static enthalpies of the hot and cold parts are thus

$$h_g = h_{TH} - \frac{\left(\frac{T_{TH}}{T_{TC}}\right) \left(\frac{U^2}{2gJ}\right)}{1 + \left(\frac{T_{TH}}{T_{TC}} - 1\right) y_s} \quad (30)$$

$$h_c = h_{TC} - \frac{\left(\frac{U^2}{2gJ}\right)}{1 + \left(\frac{T_{TH}}{T_{TC}} - 1\right) y_s} \quad (31)$$

The gas stream velocity U is not known a priori, but is estimated, and the estimate is subsequently revised until the calculated time-average probe impact pressure agrees with the measured value. This calculation will be described later in this section.

The composition of the cold gas consists of unburned fuel:

$$(Z_{HC})_C = \frac{F_u}{m_f} \quad (32)$$

and vitiated air:

$$(Z_i)_C = (1 - F_u) (Z_i)_{\text{vit.air}} \quad i = \text{H}_2, \text{O}_2, \text{etc.} \quad (33)$$

The static temperature of the cold gas is that at which the enthalpy of the gas mixture (Appendix A, Part 3) equals the cold stream static enthalpy:

$$h_C = R_o T_C \sum_i Z_i \left(\frac{H_i}{RT} \right)_{T_C} \quad (34)$$

The hot stream carries the balance of the measured nitrogen oxides:

$$y_S (Z_{\text{NO}})_H = \frac{\bar{F}_S (E_{\text{INOX}})}{m_{\text{NO}_2}} - (1 - y_S) (Z_{\text{NO}})_C \quad (35)$$

$$(Z_{\text{N}_2})_H = \left(\frac{1 - F_H}{1 + \alpha} \right) \left(\frac{.780881}{m_a} \right) - .5 (Z_{\text{NO}})_H \quad (36)$$

The remainder of the hot gas composition is computed as the chemical equilibrium composition (with NO regarded as inert; see Appendix A, Part 2) at the hot gas static temperature, which, in turn, is that at which the enthalpy of the gas mixture (Appendix A, Part 3) equals the hot stream static enthalpy:

$$h_H = R_o T_H \sum_i Z_i \left(\frac{H_i}{RT} \right)_{T_H} \quad (37)$$

For both the hot and cold gas mixtures, the thermodynamic properties are calculated as in Appendix A, Part 3, including specific heat (C_p), molecular weight (\bar{m}), specific volume (v), and sonic velocity (a). In addition, the ratio of specific heats is computed:

$$\gamma = \frac{C_p}{C_v} = \frac{C_p}{C_p - R_o/\bar{m}} \quad (38)$$

and the instantaneous Mach number:

$$M = U/a \quad (39)$$

and the total temperature:

$$T_T = T + \frac{U^2}{2gJc_p} \quad (40)$$

and the ratio of total (impact) to static pressure:

$$\frac{P_T}{P} = \left(1 + \frac{\gamma-1}{2} M^2\right)^{\frac{\gamma}{\gamma-1}} \quad \text{when } M \leq 1 \quad (41a)$$

$$\frac{P_T}{P} = \frac{\left(\frac{\gamma+1}{2} M^2\right)^{\frac{\gamma}{\gamma-1}}}{\left(\frac{2\gamma}{\gamma+1} M^2 - \frac{\gamma-1}{\gamma+1}\right)^{\frac{1}{\gamma-1}}} \quad \text{when } M > 1 \quad (41b)$$

These are well-known formulae (Reference 8, for example).

The mass fraction of hot gas in the free stream (which differs somewhat from that in the gas sample) is computed from the formula

$$y = \frac{1}{1 + \left(\frac{V_H}{V_C}\right) \left(\frac{W_H^*}{W_C^*}\right) \left[\frac{(P_T/P)_H}{(P_T/P)_C}\right] \sqrt{\left(\frac{m_H}{m_C}\right) \left(\frac{T_{TC}}{T_{TH}}\right) \left(\frac{1}{y_s} - 1\right)}} \quad (42a)$$

where

$$W^* = \frac{W}{P_{TA}^*} \sqrt{\frac{R_0 T_T}{g_m}} = \sqrt{\left(\frac{2}{\gamma+1}\right)^{\frac{\gamma+1}{2}}} \quad (42b)$$

The volume fraction of hot gas in the free stream is

$$\tau = \frac{\left(\frac{V_H}{V_C}\right) y}{1 + \left(\frac{V_H}{V_C} - 1\right) y} \quad (43)$$

The time-average probe impact pressure, to be compared with the measured value, is

$$\frac{\bar{P}_T}{P} = \frac{\left(\frac{P_T}{P}\right)_H \tau^2 + \left(\frac{P_T}{P}\right)_C (1-\tau)^2}{\tau^2 + (1-\tau)^2} \quad (44)$$

The preceding formulae for y , τ , and \bar{P}_T/P are derived in Appendix A, Part 4.

When the stream velocity has been adjusted to provide agreement between calculated and measured probe impact pressure, the CO emission index is calculated for comparison with that derived from the gas sample analysis:

$$EI_{CO} = \frac{m_{CO}}{F_S} \left[y_S (Z_{CO})_H + (1-y_S) (Z_{CO})_C \right] \quad (45)$$

If agreement is not attained, a new estimate of y_S (the mass fraction of hot gas in the sample) is made and the calculations are repeated.

In forming new estimates of y_S , three reference values are used. The maximum possible value is that at which the cold gas contains only the measured unburned hydrocarbons:

$$y_{\max} = 1 - \bar{F}_S (EI_{HC}) \quad (46)$$

As y_S is reduced, the fuel concentration in the hot gas increases. If the overall stoichiometry is fuel-lean, a point will be reached where the hot gas fuel concentration is exactly stoichiometric. As y_S is reduced from y_{\max} to y_{stoic} , the CO increases slowly due to equilibrium dissociation in the hot gas. As y_S is reduced below y_{stoic} , the CO will increase much faster due to oxygen starvation in the hot gas. The stoichiometric fuel-air ratio is

$$f_{\text{stoic}} = \frac{.209495 \text{ mf}}{10m_a (1 + .25n)} \quad (47)$$

The corresponding fuel mass fraction is

$$F_{\text{stoic}} = \frac{f_{\text{stoic}}}{1 + f_{\text{stoic}} + \alpha} \quad (48)$$

and the mass fraction of hot gas in the gas sample is

$$y_{\text{stoic}} = \frac{(\bar{F}_s - F_{5L}) - (1 - F_{5L}) \bar{F}_s (EI_{\text{HC}})}{F_{\text{stoic}} - F_{5L}} \quad (49)$$

The minimum value of y_s is that at which F_H is at the maximum value that can be accommodated by the procedure for calculation of equilibrium combustion gas composition (Appendix A, Part 2), which requires that sufficient air be present to oxidize all fuel to CO and H₂.

$$f_{\text{max}} = \frac{2(.209495)}{10} \left(\frac{m_f}{m_a} \right) \quad (50)$$

$$F_{\text{max}} = \frac{f_{\text{max}}}{1 + f_{\text{max}} + \alpha} \quad (51)$$

$$y_{\text{min}} = \frac{(\bar{F}_s - F_{5L}) - (1 - F_{5L}) \bar{F}_s (EI_{\text{HC}})}{F_{\text{max}} - F_{5L}} \quad (52)$$

The first few estimates of y_s are made using these reference values. Once the root has been spanned (that is, values of y_s have been identified that produce calculated values of EI_{CO} both higher and lower than the measured value), a quadratic interpolation procedure is used to guide convergence.

Once a set of properties is found for the two-part heterogeneous gas flow that is consistent with the probe measurements at that point, average gas properties are derived for use by the JETMIX analysis. The detailed two-part gas description is retained, of course, for use in the subsequent mixing, homogenization, and reaction calculations.

The mean fuel concentration of the gas in the free stream is

$$\bar{F} = yF_{H_i} + (1 - y) F_C \quad (53)$$

Similarly, the mean specific heat, molecular weight, and specific volume are

$$C_p = y(C_p)_H + (1 - y) (C_p)_C \quad (54)$$

$$\frac{1}{\bar{m}} = y \left(\frac{1}{m} \right)_H + (1 - y) \left(\frac{1}{m} \right)_C \quad (55)$$

$$\bar{v} = yv_H + (1 - y)v_C \quad (56)$$

For consistency, the mean static temperature is defined by the ideal gas law:

$$\bar{T} = \frac{144 P \bar{v} \bar{m}}{R_0 J} \quad (57)$$

The property characteristic of gas heterogeneity is, by definition,

$$G = y(F_H - \bar{F})^2 + (1 - y) (F_C - \bar{F})^2 \quad (58)$$

The variation of this heterogeneity property throughout the flow field will be used to guide the subsequent homogenization of the two-part mixtures. A maximum value of G may be defined, corresponding to a minimum value of y:

$$G_{\max} = \left(\frac{1 - y_{\min}}{y_{\min}} \right) (\bar{F} - F_C)^2 \quad (59)$$

A value of $y_{\min} = 0.3$ has been found useful.

4.3 STEADY-STATE TURBULENT GAS JET MIXING

Exhaust nozzles of most contemporary gas turbine engines generally operate near their ideal expansion ratios. In view of this, General Electric's initial efforts at the prediction of the flow field of a free jet relied on an aerodynamic analysis which includes only the effects of turbulent mixing. Specifically, this aerodynamic model is of the viscous, boundary-layer type. The computerized version of this analysis is referred to as the JETMIX computer program. This computer program solves the time-averaged turbulent boundary layer equations using boundary conditions which are appropriate for free jets. The turbulent Reynolds' stresses are included by means of a turbulence model which is based on a turbulent kinetic energy concept.

The flow field under consideration consists of a plane or axisymmetric turbulent jet exhausting into a region of constant (ambient) static pressure. For complete generality, the model would have included the effects of variations in static pressure throughout the plume. However, sufficiently detailed measurements at the engine exit to define the flow angles and initial static pressure field in order to permit subsequent calculation of downstream variable pressure fields would be very difficult to obtain. Furthermore, variation in static pressures, including the effects of expansion and compression waves and Mach discs, would involve considerable increased complexity in the model. Some exploration of jet mixing with supersonic unmatched static pressures showed only small effects on the turbulence generation. In addition, the moderate variation of the pressure fields expected in the cases to be analyzed would have only minor effects on the reaction kinetics calculations. Therefore, the analyses made and presented here all involve a uniform static pressure field assumption. The flow field is illustrated schematically in Figures 13 and 14 for subsonic and supersonic jets, respectively. The flow of diameter, or slot height, (d_p) discharges at an initial velocity (u_p) into a free stream of velocity (u_{ex}). The flow field is characterized by three distinct regions. Region 1 consists of a turbulent mixing layer which penetrates into the uniform parallel flow originating at the jet discharge. Upon disappearance of the potential core, the mixing characteristics undergo transition (Region 2) until at some distance downstream of the discharge plane the velocity profiles transverse to the jet axis become similar (Region 3).

The dependent variables of interest in the mixing problem are the streamwise velocity (u), the transverse velocity (v), the static temperature (T), the turbulence energy (e), and the constituent mole fractions (a_i). If transverse gradients are large, with respect to streamwise gradients, the equations of motion describing the flow field may be reduced to boundary layer form. For plane or axisymmetric flow, the governing boundary layer equations applicable to the free mixing problem are shown in Sections 4.3.1 through 4.3.4 below.

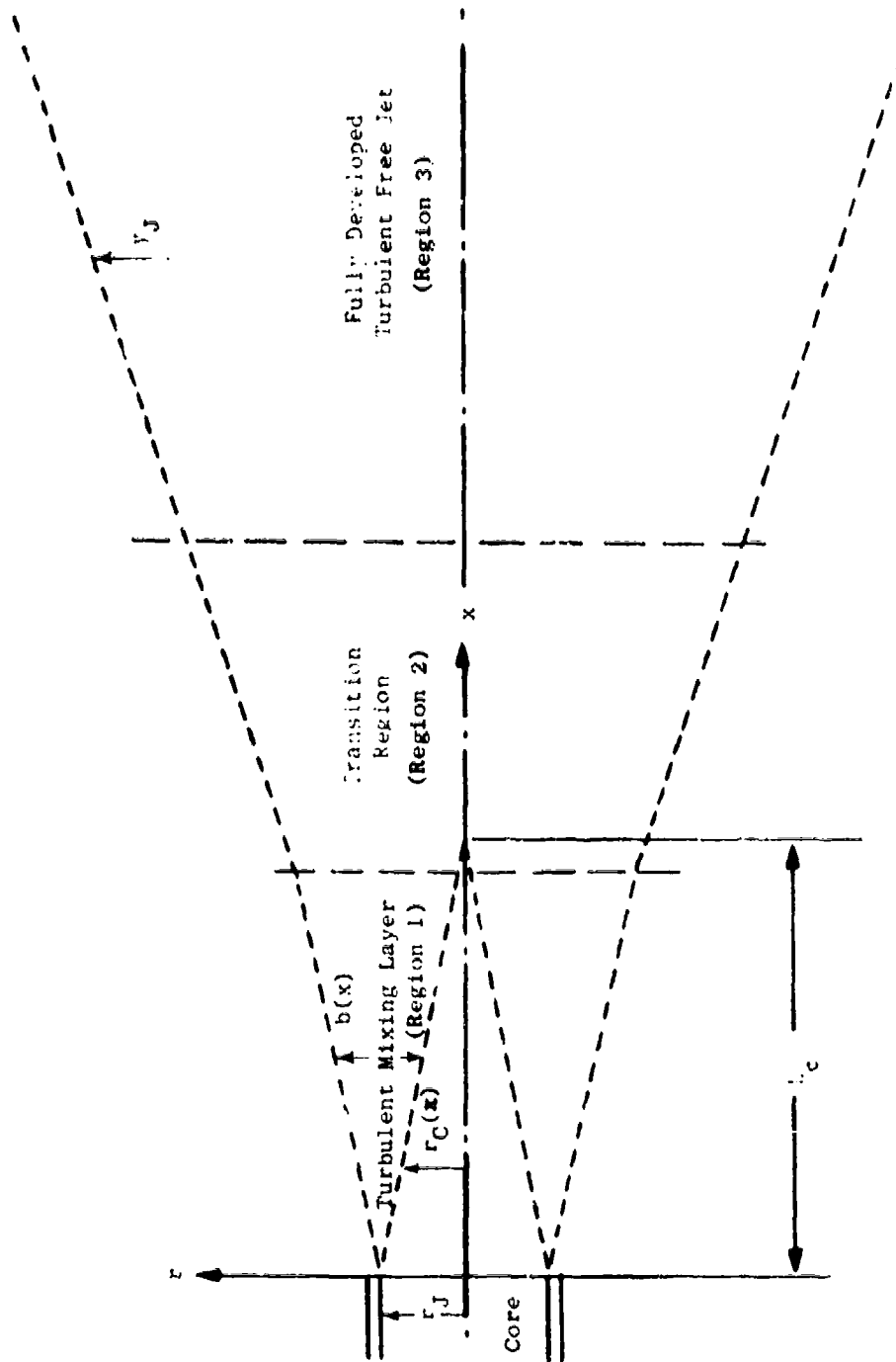


Figure 13. Subsonic Turbulent Jet.

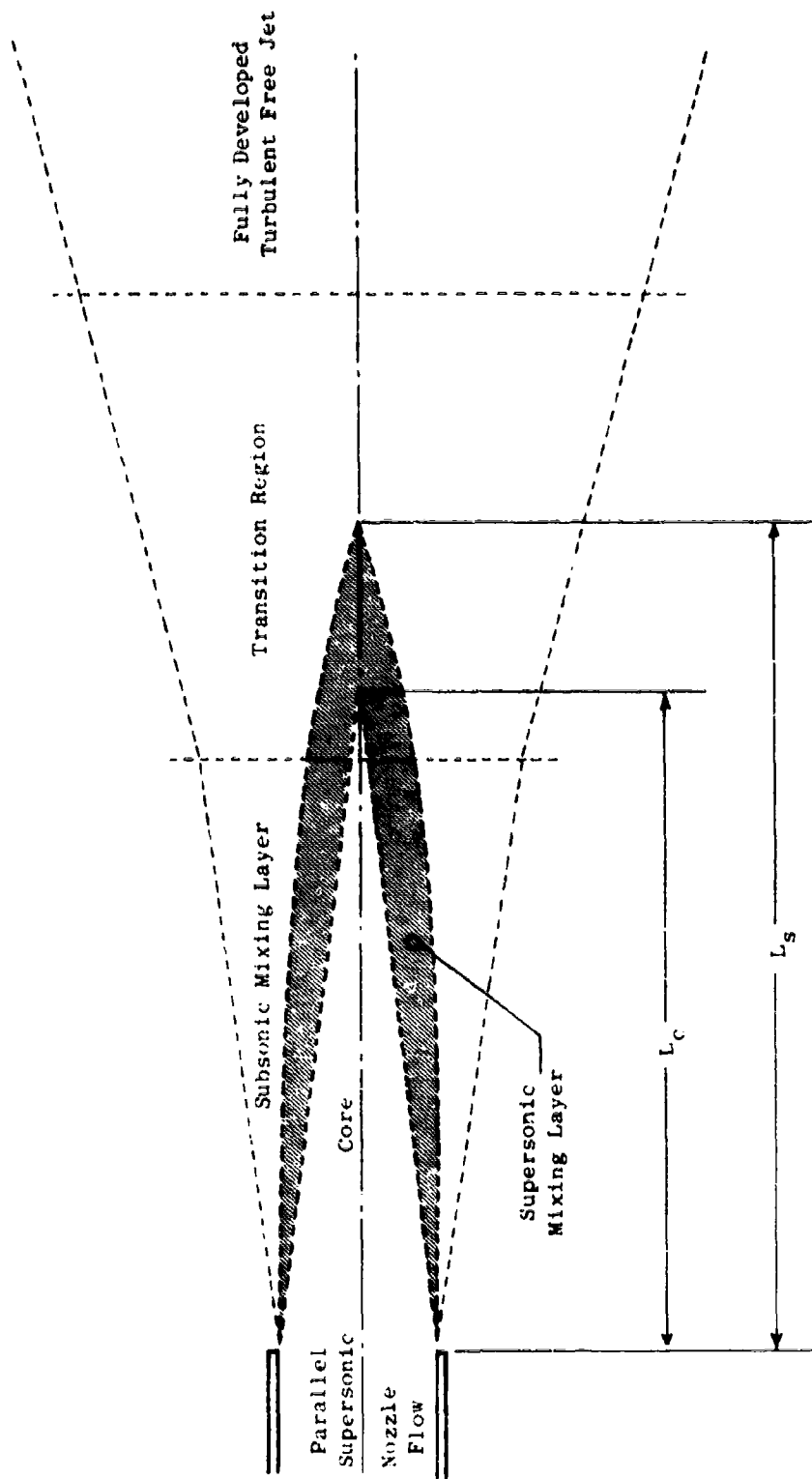


Figure 14. Supersonic Turbulent Jet.

4.3.1 Continuity Equation

$$\frac{\partial(\rho u y^\epsilon)}{\partial x} + \frac{\partial[(\rho v + \langle \rho' v' \rangle) y^\epsilon]}{\partial y} = 0 \quad (60)$$

where: $\epsilon = 0$, Plane Flow

$\epsilon = 1$, Axisymmetric Flow

where u and v are the streamwise and transverse mean flow velocities, respectively. The term $\langle \rho' v' \rangle$ represents the induced transverse mass flux of the fluctuating portion of the flow. Using order-of-magnitude arguments, Bradshaw (Reference 9) and Mellor (Reference 10) have shown that this term should be properly retained in the boundary layer form of the compressible equations of motion.

4.3.2 Species Continuity Equation

$$\rho u \frac{\partial \alpha_i}{\partial x} + (\rho v + \langle \rho' v' \rangle) \frac{\partial \alpha_i}{\partial y} = \frac{1}{y^\epsilon} \frac{\partial}{\partial y} \left(\frac{\mu_e y^\epsilon}{S_{ie}} \frac{\partial \alpha_i}{\partial y} \right) \quad (61)$$

where: S_{ie} = effective Schmidt number

μ_e = effective viscosity

4.3.3 X-Momentum Equation

The static pressure may be assumed constant for the free mixing analysis. In this case, the streamwise momentum equation becomes:

$$\rho u \frac{\partial u}{\partial x} + (\rho v + \langle \rho' v' \rangle) \frac{\partial u}{\partial y} = \frac{1}{y^\epsilon} \frac{\partial}{\partial y} \left(\mu_e y^\epsilon \frac{\partial u}{\partial y} \right) \quad (62)$$

4.3.4 Energy Equation

The Energy equation in terms of enthalpy is:

$$\begin{aligned} \rho u \frac{\partial h}{\partial x} + (\rho v + \langle \rho' v' \rangle) \frac{\partial h}{\partial y} &= \frac{1}{y^\epsilon} \frac{\partial}{\partial y} \left(k_e y^\epsilon \frac{\partial T}{\partial y} + \Gamma_e y^\epsilon \frac{\partial e}{\partial y} \right) \\ &+ \frac{\mu_e y^\epsilon}{M} \sum_i \left(\frac{h_i}{S_{ie}} \frac{\partial \alpha_i}{\partial y} \right) + \frac{\mu_e}{g_c J} \left(\frac{\partial u}{\partial y} \right)^2 + \frac{u}{J} \frac{dp_{ex}}{dx} - \rho u \frac{\partial e}{\partial x} - (\rho v + \langle \rho' v' \rangle) \frac{\partial e}{\partial y} \end{aligned} \quad (63)$$

where: h_i = constituent molar enthalpy
 \bar{M} = mixture molecular weight
 Γ_e = exchange coefficient

The static enthalpy of the mixture may be eliminated as an independent variable by using the following definitions:

$$h = \frac{1}{\bar{M}} \sum_i \alpha_i h_i \quad (64)$$

$$C_p = \frac{1}{\bar{M}} \sum_i \alpha_i C_{pi} \quad (65)$$

Differentiating,

$$\frac{\partial h}{\partial x} = \frac{1}{\bar{M}} \sum_i \alpha_i \frac{\partial h_i}{\partial x} + \frac{1}{\bar{M}} \sum_i h_i \frac{\partial \alpha_i}{\partial x} \quad (66)$$

$$\frac{\partial h}{\partial y} = \frac{1}{\bar{M}} \sum_i \alpha_i \frac{\partial h_i}{\partial y} + \frac{1}{\bar{M}} \sum_i h_i \frac{\partial \alpha_i}{\partial y} \quad (67)$$

Using Equation 64 and the species continuity Equation 61 yields the energy equation in terms of the mixture C_p and the static temperature (T).

$$\begin{aligned} \rho u C_p \frac{\partial T}{\partial x} + (\rho v + \langle \rho' v' \rangle) C_p \frac{\partial T}{\partial y} &= \frac{1}{y} \frac{\partial}{\partial y} \left(k_e y^\epsilon \frac{\partial T}{\partial y} \right) \\ + \frac{1}{y^\epsilon} \frac{\partial}{\partial y} \left(\Gamma_e y^\epsilon \frac{\partial e}{\partial y} \right) + \frac{\mu_e}{\bar{M}} \sum_i \frac{C_{pi}}{\epsilon_{ie}} \frac{\partial \alpha_i}{\partial y} \left(\frac{\partial T}{\partial y} \right) &+ \frac{\mu_e}{g_c J} \left(\frac{\partial u}{\partial y} \right)^2 \\ + \frac{u}{J} \frac{dP}{dx} - \rho u \frac{\partial e}{\partial x} - (\rho v + \langle \rho' v' \rangle) \frac{\partial e}{\partial y} \end{aligned} \quad (68)$$

The pressure, density, and temperature which appear in the above equations are related to each other by means of the perfect gas law:

$$P = \rho RT \quad (69)$$

where: R = mean gas constant for mixture.

The mean mixture heat capacity is considered to be a function of the static temperature T . For constant R then, C_p may be related to the isentropic exponent γ as:

$$C_p = \frac{\gamma R}{\gamma - 1} \quad (70)$$

Specification of γ as a function of temperature then enables calculation of C_p .

The Prandtl/Glushko/Spalding model which is discussed in the following section has been incorporated in Equations 61, 62, and 68.

4.3.5 Viscosity Model

Introduction of an eddy viscosity (μ_e) permits expression of the local shear stress in terms of an effective viscosity and the mean flow velocity gradient.

$$T = T_L + T_t = \mu (\partial u / \partial y) - \langle (\rho v)' u' \rangle \quad (71)$$

$$T = (\mu + \mu_t) \partial u / \partial y = \mu_e \partial u / \partial y \quad (72)$$

Phenomenological models, such as the Prandtl mixing length (Reference 11), have been used to relate the "eddy" or "turbulent" viscosity (μ_t) to the local mean velocity field. These models imply that the turbulence adjusts immediately to changes in mean flow conditions and that a universal relationship exists between the turbulent stresses and the mean strain rates. Experimental data have indicated that there is a delayed response of the turbulence structure to sudden changes in mean conditions. The turbulent kinetic energy equation proposed by Prandtl (Reference 12), and utilized by Glushko (Reference 13), and Spalding (Reference 14) provides a more fundamental modeling of the "eddy" viscosity. In the present work, the Prandtl-Kolmogorov relations, as given by Glushko and Spalding, are used to relate the "eddy" viscosity to the mean flow quantities. After Kolmogorov (Reference 15), the turbulent shear is taken as a universal function of the Reynolds number of turbulence:

$$T_t = \alpha R_t (\partial u / \partial y) = \mu_t (\partial u / \partial y) \quad (73)$$

where:

- α = Constant = 0.2
- R_t = Reynolds number of turbulence = $\frac{\rho \sqrt{e} L_t}{\mu}$
- e = Turbulence kinetic energy
- L_t = Length scale characterizing turbulence

The "effective" viscosity is defined as the sum of the laminar and turbulent parts.

$$\mu_e = \mu + \mu_t = \mu(1 + \alpha R_t) \quad (74)$$

Defining a turbulent Prandtl number as $Pr_t = \frac{C_p \mu_t}{k_t}$, the "effective" thermal conductivity is given as:

$$k_e = C_p \mu \left[\frac{1}{Pr} + \left(\frac{\mu_t}{\mu} \right) \frac{1}{Pr_t} \right] \quad (75)$$

The above relations introduce the turbulent kinetic energy as an additional dependent variable. The boundary layer equations cited previously may be augmented by an additional partial differential equation describing the conservation of turbulent kinetic energy. Specification or calculation of the characteristic length scale (L_t) then provides closure of the system of equations.

4.3.6 Turbulent Kinetic Energy

The turbulent kinetic energy equation, discussed in Hinze (Reference 16), represents the balance between the advection, diffusion, production, and dissipation of turbulent kinetic energy. In the Prandtl/Glushko (Reference 12 and 13) model, the pressure-velocity correlation term and triple velocity correlation term arising in the development of the turbulence energy equation are combined as a "gradient diffusion" term. The resulting turbulent kinetic energy equation is:

$$\rho u \frac{\partial e}{\partial x} + (\rho v + \langle \rho'v' \rangle) \frac{\partial e}{\partial y} = \frac{1}{y} \frac{\partial}{\partial y} \left(\Gamma_e y^e \frac{\partial e}{\partial y} \right) + \mu_t \left(\frac{\partial u}{\partial y} \right)^2 - D_e \quad (76)$$

In modeling the dissipation term (D_e), it is assumed that the small scale eddies responsible for the dissipation of mechanical energy are capable of handling all the energy transferred to them by the larger scale motion. The process is then assumed to be diffusion controlled, and both the exchange coefficient (Γ_e), and the dissipation term (D_e) are expressed in terms of an "intravortex" turbulent viscosity (D):

$$\Gamma_e = \mu D \quad (77)$$

$$D_e = \frac{(C_p D) e}{L_t^2} \quad (78)$$

The coefficient, D , is given by Glushko and Spalding as:

$$D = 1 + \alpha \eta R_t \quad (79)$$

where: $\eta = 0.586$ (empirical constant after Spalding)

The constant (C) in the dissipation term of the turbulence energy equation is assigned the value 2.59 (Spalding) for application to the turbulent mixing problem.

The principal uncertainty in the turbulence model resides in the characteristic length scale assigned to the turbulence (L_t). A partial differential equation for L_t , similar to the turbulence energy Equation 76, has been derived by Rotta (Reference 17). In the present analysis, however, the characteristic scale of the jet turbulence is assumed independent of the transverse coordinate (y), and is expressed in terms of the geometric parameters of the jet. Experimental data are used to define the constants in the model.

Referring to Figure 13, the mixing region of the single jet may be divided into three distinct zones. In Zone 1, the flow consists of a mixing layer which penetrates into a core region where only small or zero mixing occurs. The turbulence scale in the mixing layer is assumed proportional to the width of the mixing layer (b) (References 18 and 19):

$$L_{t(1)m} = C_{t1} b(1+C_{t2}M_j)^{-1} \quad (80a)$$

In the core region, however, the reference length for the scale calculation is more appropriately taken as the nozzle radius (r_j):

$$L_{t(1)c} = C_{t1} r_j(1+C_{t2}M_j)^{-1} \quad (80b)$$

To provide a smooth transition between these two regions, the following relations are used:

$$L_{t(1)} = L_{t(1)c} \quad r < .9r_c \quad (80c)$$

$$L_{t(1)} = L_{t(1)c} - \left[\frac{r - .9r_c}{.1(r_c + b)} \right] (L_{t(1)c} - L_{t(1)m}) \quad .9r_c < r < (r_c + .1b) \quad (80d)$$

In Zone 3, the velocity profiles are known to be similar. The turbulent scale for this fully developed region is defined, after Spalding (Reference 14), to be proportional to local radius or half-height of the jet.

$$L_{t(3)} = C_{t8} Y_j \quad (81)$$

The turbulence length scale in the transition zone (Region 2) is less well defined than those in Regions 1 and 3, in that experimental data are sparse or nonexistent. Two models are available for this region. In the first, an exponential increase in length scale is assumed to occur upon disappearance of the potential core.

$$L_t(2) = C_{t3} \left(1 + C_{t5} M_J\right)^{-1} \left(\frac{X}{L_c}\right) \exp \left[C_{t4} \left(C_{t6} + C_{t7} M_J \right) \right] \quad (82a)$$

The end of the transition zone is calculated as the axial station at which $L_t(2)$ first becomes equal to or greater than $L_t(3)$. The constants in this model must be determined from experimental data.

The second model assumes that the length of the transition zone is equal to the length of the potential core (L_c), and that the length scale varies linearly from the end of the core to the beginning of the fully developed region.

$$L_t(2) = C_{t1} Y_J \left(1 + C_{t2} M_J\right)^{-1} \left(2 - \frac{X}{L_c}\right) + C_{t8} Y_J \left(\frac{X}{L_c} - 1\right) \quad (82b)$$

Calculations based on this model have generally been found to show closer agreement with experimental data than those based on the model of Equation 82a.

The numerical values assigned to the constants C_{t1} through C_{t8} are:

$C_{t1} = 0.23$	$C_{t5} = 0.38$
$C_{t2} = 0.38$	$C_{t6} = 1.4$
$C_{t3} = 0.23$	$C_{t7} = 0.43$
$C_{t4} = 0.05$	$C_{t8} = 0.1875$

Using Equations 77 and 78, the turbulent energy Equation 76 may be written as:

$$\rho u \frac{\partial e}{\partial x} + (\rho v + \langle v'v' \rangle) \frac{\partial e}{\partial y} = \frac{1}{y} \frac{\partial}{\partial y} \left(\mu D y^{\epsilon} \frac{\partial e}{\partial y} \right) + \nu_t \left(\frac{\partial u}{\partial y} \right)^2 - \frac{C \mu D e}{L_t^2} \quad (83)$$

4.3.7 Determination of the Jet Edge and the Core Length

The determination of length scale and the location of the "effective" length of the core requires the location of the outer and inner edges of the mixing zone. Conventionally, the outer edge of the mixing region of a free jet is taken as the radius where the jet velocity approaches the ambient stagnation condition within a given tolerance. The inner edge is normally taken as the radius where the flow is no longer uniform and parallel. When velocity gradients exist in the core region, as in the case of the plume model, the conventional definition of the inner mixing zone radius is no longer valid. In this situation, the concentration of the ambient air is used to locate the inner edge of the mixing region. The inner radius is taken as the coordinate where the mole fraction of ambient air has reached

a value of 0.0001 due to turbulent diffusion. The core length, in this instance, then becomes the point where the mole fraction of ambient air becomes $> .0001$ on the jet axis. The outer edge of the jet is arbitrarily defined as the point where the velocity relative to the free-stream velocity is 0.02 of the centerline velocity.

4.3.8 Boundary Conditions

Considering the jet to be symmetric about the line $y = 0$, the applicable boundary conditions are:

$$\text{@ } y = 0 \quad \frac{\partial u}{\partial y} = \frac{\partial e}{\partial y} = \frac{\partial T}{\partial y} = \frac{\partial \alpha_i}{\partial y} = 0 \quad (\text{symmetry}) \quad (84)$$

$$\begin{aligned} \text{@ } y = y_{ex} \quad u &= u_{ex} \\ T &= T_{ex} \\ e &= e_{ex} \\ \alpha_i &= \alpha_{iex} \end{aligned}$$

4.3.9 Transformation of Differential Equations

The preceding equations may be cast in a more convenient form by nondimensionalizing with respect to the primary jet diameter and the discharge flow field variables u_p , e_p , T_p . The requisite relations are:

$$X = \frac{x}{d_p}, \quad Y = \frac{2y}{d_p} \quad (85)$$

$$U = \frac{u}{u_p}, \quad V = \frac{v}{u_p}, \quad E = \frac{e}{e_p}, \quad T = \frac{T}{T_p}$$

$$V' = \frac{v'}{u_p}$$

Substitution in Equations 60 through 63 and Equation 83 yields:

Continuity

$$\frac{\partial(\rho U Y^E)}{\partial X} + 2 \frac{\partial}{\partial Y} [(\rho V + \rho' V') Y^E] = 0 \quad (86)$$

X-Momentum

$$\rho U \frac{\partial U}{\partial X} + 2(\rho V + \rho' V') \frac{\partial U}{\partial Y} = \left(\frac{4}{u_p d_p Y^E} \right) \frac{\partial}{\partial Y} \left(\mu_e Y^E \frac{\partial U}{\partial Y} \right) - \frac{\rho C}{u_p} \frac{dP_{ex}}{dX} \quad (87)$$

Turbulent Kinetic Energy

$$\rho U \frac{\partial E}{\partial X} + 2(\rho V + \langle \rho' v' \rangle) \frac{\partial E}{\partial Y} = \left(\frac{4}{u_p d_p} \right) \frac{\partial}{\partial Y} \left(\mu D Y^\epsilon \frac{\partial E}{\partial Y} \right) + \left(\frac{4 u_p}{g_c J d_p} \right) \mu_t \left(\frac{\partial U}{\partial Y} \right)^2 - \frac{\mu C D d_p E}{u_p L_t^2} \quad (88)$$

Species Continuity

$$\rho U \frac{\partial \alpha_i}{\partial X} + 2(\rho V + \langle \rho' v' \rangle) \frac{\partial \alpha_i}{\partial Y} = \left(\frac{4}{u_p d_p} \right) \frac{\partial}{\partial Y} \left(\frac{\mu_e Y^\epsilon}{S_{ie}} \frac{\partial \alpha_i}{\partial Y} \right) \quad (89)$$

Energy

$$\rho U \frac{\partial \theta}{\partial X} + 2(\rho V + \langle \rho' v' \rangle) \frac{\partial \theta}{\partial Y} = \left(\frac{4}{C_p u_p d_p} \right) \frac{\partial}{\partial Y} \left(k_e Y^\epsilon \frac{\partial \theta}{\partial Y} \right) + \left(\frac{U}{U_p J C_p T_p} \right) \frac{dP_{ex}}{dX} + \left(\frac{4e_p}{C_p u_p T_p d_p} \right) \frac{\partial}{\partial Y} \left(\mu D Y^\epsilon \frac{\partial E}{\partial Y} \right) + \left(\frac{4u_p \mu_e}{C_p g_c J T_p d_p} \right) \left(\frac{\partial U}{\partial Y} \right)^2 + \frac{4u_e}{u_p d_p} \sum_i \frac{C_{pi}}{S_{ie}} \frac{\partial \alpha_i}{\partial Y} \left(\frac{\partial \theta}{\partial Y} \right) - \frac{e_p}{C_p T_p} \left(\rho U \frac{\partial E}{\partial X} + (\rho V + \langle \rho' v' \rangle) \frac{\partial E}{\partial Y} \right) \quad (90)$$

The boundary conditions become:

$$\begin{aligned} @ Y = 0 & \quad \frac{\partial U}{\partial Y} = \frac{\partial E}{\partial Y} = \frac{\partial \theta}{\partial Y} = \frac{\partial \alpha_i}{\partial Y} = 0 \\ @ Y \rightarrow Y_{ex} & \quad U = U_{ex} \\ & \quad E = E_{ex} \\ & \quad \theta = \theta_{ex} \\ & \quad \alpha_i = \alpha_{iex} \end{aligned} \quad (91)$$

The continuity Equation 86 may be identically satisfied by introduction of the stream function coordinate (ψ) as one of the independent variables (Von Mises transformation). Define a modified stream function, satisfying continuity, as follows:

$$\frac{\partial \psi}{\partial Y} = \frac{1}{2} \rho U Y^c, \quad \frac{\partial \psi}{\partial X} = -(\rho V + \langle \rho' V' \rangle) Y^c \quad (92)$$

Introduce the following new variables:

$$\begin{aligned} \xi &= \xi(X), \quad \eta = X \\ \psi &= \psi(X, Y) \end{aligned}$$

Then, using the chain rule, the following operators may be defined:

$$\begin{aligned} \frac{d}{dX} &= \frac{\partial}{\partial \xi} - (\rho V + \langle \rho' V' \rangle) \frac{\partial}{\partial \psi} \\ \frac{\partial}{\partial Y} &= \frac{1}{2} \rho U Y^c \frac{\partial}{\partial \psi} \end{aligned}$$

Using these relations in Equations 87 through 89 removes the transverse velocity components (v, V'), resulting in the following final set of differential equations:

X-Momentum

$$\frac{\partial U}{\partial X} = \left(\frac{1}{u_p d_p} \right) \frac{\partial}{\partial \xi} \left(\mu_e \rho U Y^{2c} \frac{\partial U}{\partial \psi} \right) - \left(\frac{g_c}{\rho U u_p^2} \right) \frac{dP_{ex}}{dX} \quad (93)$$

Turbulent Kinetic Energy

$$\begin{aligned} \frac{\partial E}{\partial X} &= \left(\frac{1}{u_p d_p} \right) \frac{\partial}{\partial \xi} \left(\mu_e \rho U Y^{2c} \frac{\partial E}{\partial \psi} \right) \\ &+ \left(\frac{u_p \mu_t}{g_c J d_p e_p} \rho U Y^{2c} \right) \left(\frac{\partial U}{\partial \psi} \right)^2 - \frac{u_c D d_p}{\rho U u_p l_t^2} E \end{aligned} \quad (94)$$

Species Continuity

$$\frac{\partial \alpha_i}{\partial X} = \left(\frac{1}{u_p d_p} \right) \frac{\partial}{\partial \xi} \left(\frac{\mu_c}{S_{ie}} \rho U Y^{2c} \frac{\partial \alpha_i}{\partial \psi} \right) \quad (95)$$

Energy

$$\begin{aligned}
 \frac{\partial \theta}{\partial X} = & \left(\frac{1}{u_p d_c} \right) \frac{\partial}{\partial \Psi} \left(k_c \rho U Y^{2\epsilon} \frac{\partial \theta}{\partial \Psi} \right) \\
 & + \left(\frac{e_p}{C_p u_p d_T} \right) \frac{\partial}{\partial \Psi} \left(\mu D \rho U Y^{2\epsilon} \frac{\partial E}{\partial \Psi} \right) + \left(\frac{1}{\rho C_p J T_p} \right) \frac{dP_{ex}}{dX} \\
 & + \left(\frac{u_p \mu_c}{g_c J C_p d T_p} \rho U Y^{2\epsilon} \right) \left(\frac{\partial U}{\partial \Psi} \right)^2 \\
 & + \left(\frac{\mu_c}{d U M c_p} \rho U Y^{2\epsilon} \right) \sum_i \frac{C_{pi}}{S_{ie}} \frac{\partial \alpha_i}{\partial \Psi} \left(\frac{\partial \theta}{\partial \Psi} \right) - \left(\frac{e_p}{C_p T_p} \right) \frac{\partial E}{\partial X} \quad (96)
 \end{aligned}$$

Taking the lower boundary at the zero streamline ($\Psi = 0$), the boundary conditions become:

$$@ \Psi = 0 \quad \frac{\partial U}{\partial \Psi} = \frac{\partial E}{\partial \Psi} = \frac{\partial \theta}{\partial \Psi} = \frac{\partial \alpha_i}{\partial \Psi} = 0 \quad (97)$$

$$\begin{aligned}
 @ \Psi \rightarrow \Psi_{ex} \quad U &= U_{ex} \\
 E &= E_{ex} \\
 \theta &= \theta_{ex} \\
 \alpha_i &= \alpha_{iex}
 \end{aligned}$$

The physical coordinate Y can be recovered by integration of Equation 92 from $\Psi = 0$ to a given streamline:

$$Y^{\epsilon+1} = 2(1+\epsilon) \int_0^{\Psi} \frac{\partial \Psi}{\partial U} \quad (98)$$

4.3.10 Numerical Solution of Differential Equations

The system of nonlinear parabolic differential Equations 93 through 96, along with boundary conditions and suitably prescribed initial conditions, represents a properly posed initial value problem. The solution may be stepwise advanced in the positive X direction using a finite difference approach. The implicit numerical technique utilized in the present investigation closely parallels that of Patankar and Spalding (Reference 11). The general programs of these latter investigators were not available at the inception of this project. The differences between the two approaches arise primarily in the type of finite difference mesh and the methods of controlling the streamwise stepsize.

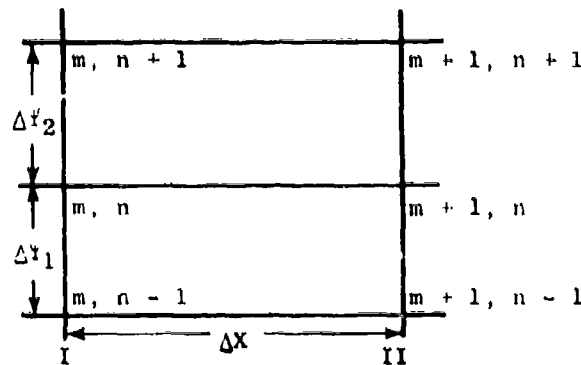
The Patanker method uses a fixed dimensionless streamline grid. The streamwise stepsize is controlled by explicitly monitoring the flow entrainment over a given step. In the present work, streamlines are added in a systematic fashion to cover the entire flow field. The streamwise stepsize is related to the local geometric parameters of the jet such as the width of the mixing zone or the distance to the effective edge of the jet.

The partial differential equations are all of the general "diffusion equation" form:

$$\epsilon \frac{\partial F}{\partial X} = \alpha \frac{\partial}{\partial \Psi} \left(\beta \frac{\partial F}{\partial \Psi} \right) + \gamma + \delta F + \eta \frac{\partial F}{\partial \Psi} \quad (99)$$

where F may represent any of the independent variables (U, E, θ). The equations are coupled principally through the normal derivative terms. Hence, a sequential solution technique may be utilized as opposed to direct simultaneous integration. The specific procedure consists of initially formulating the differential equations in terms of linear difference equations. The linearization is affected by evaluating the coefficients of the differential equations at the known upstream mesh points. The X -momentum equation is first solved for values of U and $\partial U / \partial \Psi$ at the downstream station. Using these quantities, the turbulent kinetic energy equation may be integrated to determine E and $\partial E / \partial \Psi$. Finally, the energy equation may be solved using the results of the preceding two solutions.

An implicit finite difference procedure is utilized to effect the solution of the above Equation 99. Consider a grid network as shown in the following sketch:



Conditions are known at station I and are to be determined at station II by solution of the following equation:

$$\epsilon \frac{\partial F}{\partial X} = \alpha \frac{\partial}{\partial \Psi} \left(\beta \frac{\partial F}{\partial \Psi} \right) + \gamma + \delta F + \eta \frac{\partial F}{\partial \Psi} \quad (100)$$

For the mesh indicated in the above sketch, the x derivative may be approximated by a backward difference and the ψ derivatives as noncentered 3-point differences in the following fashion:

$$\frac{\partial F}{\partial X} = \frac{(F_{m+1,n} - F_{m,n})}{\Delta X} \quad (101)$$

$$\frac{\partial F}{\partial \psi} = \frac{\Delta \psi_1^2 (F_{m+1,n+1} - F_{m+1,n}) + \Delta \psi_2^2 (F_{m+1,n} - F_{m+1,n-1})}{(\Delta \psi_1^2 \Delta \psi_2 + \Delta \psi_2^2 \Delta \psi_1)} \quad (102)$$

$$\frac{\partial^2 F}{\partial \psi^2} = \frac{2[\Delta \psi_1 F_{m+1,n+1} - (\Delta \psi_1 + \Delta \psi_2) F_{m+1,n} + \Delta \psi_2 F_{m+1,n-1}]}{(\Delta \psi_1^2 \Delta \psi_2 + \Delta \psi_2^2 \Delta \psi_1)} \quad (103)$$

Substituting these derivatives in Equation 100 yields:

$$\begin{aligned} & [(m+k) \Delta \psi_2^2 - \ell \Delta \psi_2] F_{m+1,n-1} + [\epsilon + \ell (\Delta \psi_1 + \Delta \psi_2) + (m+k) (\Delta \psi_1^2 - \Delta \psi_2^2) - \delta \Delta X] F_{m+1,n} \\ & - [(m+k) \Delta \psi_1^2 - \ell \Delta \psi_1] F_{m+1,n+1} = \epsilon F_{m,n} + \gamma \Delta X \end{aligned} \quad (104)$$

$$\text{where: } \ell = \ell_{m,n} = \frac{2\alpha\beta\Delta X}{(\Delta \psi_1^2 \Delta \psi_2 + \Delta \psi_2^2 \Delta \psi_1)}$$

$$m = m_{m,n} = \frac{\alpha \left(\frac{\partial \beta}{\partial \psi} \right) \Delta X}{(\Delta \psi_1^2 \Delta \psi_2 + \Delta \psi_2^2 \Delta \psi_1)}$$

$$k = k_{m,n} = \frac{n \Delta X}{(\Delta \psi_1^2 \Delta \psi_2 + \Delta \psi_2^2 \Delta \psi_1)}$$

Evaluation of the quantities $\epsilon, \alpha, \beta, \gamma, \delta, n, F$ at the known station 1 results in a set of linear simultaneous equations of the form:

$$a_n F_{m+1,n-1} + b_n F_{m+1,n} + g_n F_{m+1,n+1} = h_n \quad n = 2, 3, \dots, N-1 \quad (105)$$

$$\text{where: } a(i) = (m+k) \Delta \psi_2^2 - \ell \Delta \psi_2$$

$$b(i) = \epsilon + \ell (\Delta \psi_1 + \Delta \psi_2) + (m+k) (\Delta \psi_1^2 - \Delta \psi_2^2) - \delta \Delta X$$

$$g(i) = -(m+k) \Delta \psi_1^2 - \ell \Delta \psi_1$$

$$h(i) = \epsilon F_{m,n} + \gamma \Delta X$$

Inclusion of the boundary conditions in finite difference form closes the system of linear algebraic equations. For most cases, the use of forward or backward differences at the boundaries is adequate. The boundary conditions may then be written in a general form as the linear combination of the dependent variable F and its Ψ derivative.

$$\begin{aligned} \xi_1 F_1 + \eta_1 \left(\frac{dF}{d\Psi}\right)_1 &= \lambda_1 & n=1 \\ \xi_N F_N + \eta_N \left(\frac{dF}{d\Psi}\right)_N &= \lambda_N & n=N \end{aligned} \quad (106)$$

The coefficients corresponding to a, b, g, h in the preceding expressions are:

$$\begin{aligned} a_1 &= 0 & a_N &= -\eta_N/\Delta\Psi_N \\ b_1 &= \xi_1 - \eta_1/\Delta\Psi & b_N &= \xi_N + \eta_N/\Delta\Psi_N \\ g_1 &= \eta_1/\Delta\Psi_1 & g_N &= 0 \\ h_1 &= \lambda_1 & h_N &= \lambda_N \end{aligned}$$

The resulting set of N simultaneous equations may be written in the concise matrix form as:

$$U \bar{F} = J \quad (107)$$

where: \bar{F} = Solution vector
J = Vector of righthand sides

Since the U matrix is tri-diagonal, the solution may be readily obtained yielding the new values of F at station II.

4.3.11 Representation of Jet Properties and Initial Profiles

Nozzle exit plane measurements of aerodynamic and thermodynamic properties are used as initial conditions for the jet flow field calculations. The preparation of initial profiles in the form required by the analysis is performed in subroutine JETPRF. The jet is divided into as many as eleven annular rings at the nozzle exit with one corresponding to each radial gas sampling station. The gas originating in each region is identified as a distinct specie having properties determined from the appropriate gas sample.

The dividing radius between adjacent rings is set as the root mean square of the two sampling radii, and initial profiles of velocity, temperature, and heterogeneity parameter (G) are set using six points in each ring along with two points in the free stream (external flow). The profiles are "smoothed" somewhat by interpolation at the interface between adjacent rings to avoid abrupt discontinuities in the flow properties. The initial turbulence intensity is specified by the user.

4.4 CONSERVATION OF THE HETEROGENEITY PARAMETER

The concentration fluctuations that occur at a point in the turbulent nonreacting flow of a gas of nonuniform composition can be characterized statistically by a mean square intensity. If the local concentration (mass fraction) of a particular component is represented as the sum of mean and fluctuating quantities:

$$F = \langle F \rangle + F' \quad (108)$$

then the mean square intensity is defined by:

$$G = \langle F'^2 \rangle \quad (109)$$

A transport equation for G can be derived by multiplying the complete species continuity equation (for F) by F', time-averaging, and applying the boundary layer approximations. The resulting equation contains terms which represent the convection, diffusion, production, and dissipation of G. Unfortunately, these terms introduce additional unknown turbulence parameters (statistical correlations involving velocity and concentration fluctuations) which must be approximated in terms of quantities which are known or can be determined. It should be noted that the same situation is encountered in the formulation of the turbulent kinetic energy equation for the JETMIX flow field analysis (Section 4.3). The modeling procedures established by Spalding (Ref. 5, 6, and 7) have been utilized to obtain the following "simulated" form of the conservation equation for G:

$$\underbrace{\rho u \frac{\partial G}{\partial X} + (\rho v + \langle \rho' v' \rangle) \frac{\partial G}{\partial Y}}_{\text{convection}} = \underbrace{\frac{1}{Y} \frac{\partial}{\partial Y} \left(\frac{\mu_t}{\sigma_G} Y^e \frac{\partial G}{\partial Y} \right)}_{\text{diffusion}} + \underbrace{C_{G1} \mu_t \left(\frac{\partial F}{\partial Y} \right)^2}_{\text{production}} - \underbrace{C_{G2} \left(\frac{\mu_t}{\alpha_t L_t} \right)^2 G}_{\text{dissipation}} \quad (110)$$

where the brackets $\langle \rangle$ have been dropped from mean quantities for clarity and the exponent e is given by:

$$e = \begin{cases} 0 & \text{Plane (2-0) flow} \\ 1 & \text{Axisymmetric flow} \end{cases}$$

The eddy (or turbulent) viscosity (μ_t) is determined from:

$$\mu_t = \alpha_t \rho e^{1/2} L_t \quad (111)$$

where e is the turbulent kinetic energy and L_t is the turbulence length scale. The quantities C_{G1} , C_{G2} , α_t , and σ_G are constants.

The boundary conditions to be applied to the solution of Equation 110 are:

$$\begin{aligned} Y = 0: & \quad \frac{\partial G}{\partial Y} = 0 \quad (\text{symmetry}) \\ Y = Y_{\text{ex}}: & \quad G = G_{\text{ex}} \quad (\text{external flow}) \end{aligned} \quad (112)$$

In a multicomponent gas flow, Equation 110 can be used to calculate the distribution of concentration fluctuation intensity for any species for which the distribution of mean concentration is calculated. In a gas turbine engine exhaust plume, the gas composition can be characterized by the local fuel concentration (F) and mean-square fuel concentration fluctuation intensity (G).

Equation 110 can be solved simultaneously with the continuity, species continuity, axial momentum, energy, and turbulent kinetic energy (TKE) equations to obtain a description of the jet flow field. However, since the solution of the mean flow and TKE equations does not require knowledge of G , equation 110 can be uncoupled from the others and solved independently, using the previously determined solutions of the remaining coupled equations. This is the approach that was chosen in the present situation, primarily because of the availability of the JETMIX computer program for solution of the mean flow and TKE equations. A separate computer program (SPALDG) was developed to numerically solve the partial differential equation for G , using the JETMIX flow field definition as input.

The partial differential equation and boundary conditions for determination of G can be cast in more convenient form by nondimensionalizing with respect to initial jet diameter (d_j) and initial jet axial velocity (u_j). Define the following variables.

$$\begin{aligned} X &= \frac{x}{d_j}, & Y &= \frac{y}{d_j} \\ U &= \frac{u}{u_j}, & V &= \frac{v}{u_j}, & V^I &= \frac{v^I}{u_j} \end{aligned} \quad (113)$$

Substitution in Equation 110 yields:

$$\begin{aligned} \rho u \frac{\partial G}{\partial X} + 2 (\rho V + \langle \rho' V' \rangle) \frac{\partial G}{\partial Y} \\ = \left(\frac{4}{u_p d_p Y \epsilon} \right) \frac{\partial}{\partial Y} \left(\frac{\mu_t}{\sigma G} Y^2 \frac{\partial G}{\partial Y} \right) \\ + \left(\frac{4 C_{G1} \mu_t}{u_p d_p} \right) \left(\frac{\partial F}{\partial Y} \right)^2 - \left(\frac{C_{G2} \mu_t d_p}{\alpha_t^2 L_t^2 u_p} \right) G \end{aligned} \quad (114)$$

The boundary conditions become:

$$\begin{aligned} Y = 0: \quad \frac{\partial G}{\partial Y} = 0 \\ Y = Y_{ex}: \quad G = G_{ex} \end{aligned} \quad (115)$$

Recall from Section 4.3 that the continuity equation is identically satisfied by the introduction of the stream function coordinate (ψ) as one of the independent variables (Von Mises transformation). The stream function is defined by:

$$\frac{\psi}{Y} = \frac{1}{2} \left(U Y^2 \right) \quad (116)$$

$$\frac{\psi}{X} = - \left(V + \langle \rho' V' \rangle \right) Y^2$$

Applying the transformation to X- coordinates removes the transverse velocity components (V, V') from Equation 114, resulting in the following final form of the partial differential equation:

$$\begin{aligned} \frac{\partial G}{\partial X} = & \left(\frac{1}{u_p d_p} \right) \frac{\partial}{\partial \Psi} \left(\frac{\mu_t}{\sigma_G} \rho U Y^{2\epsilon} \frac{\partial G}{\partial \Psi} \right) \\ & + \left(\frac{C_{G1} \mu_t}{u_p d_p} \right) \rho U Y^{2\epsilon} \left(\frac{\partial F}{\partial \Psi} \right)^2 \\ & - \left(\frac{C_{G2} \mu_t d_p}{\rho U u_p \alpha_t^2 L_t} \right) G \end{aligned} \quad (117)$$

Taking the jet centerline as the zero streamline ($\Psi = 0$), the boundary conditions become:

$$\Psi = 0: \quad \frac{\partial G}{\partial \Psi} = 0 \quad (118a)$$

$$\Psi = \Psi_{ex}: \quad G = G_{ex} \quad (118b)$$

Equation 117 is of the general "diffusion" equation form:

$$\frac{\partial G}{\partial X} = \alpha \frac{\partial}{\partial \Psi} \left(\beta \frac{\partial G}{\partial \Psi} \right) + \gamma + \delta G \quad (119)$$

where:

$$\alpha = \frac{1}{u_p d_p}$$

$$\beta = \frac{\mu_t}{\sigma_G} \rho U Y^{2\epsilon}$$

$$\gamma = \left(\frac{C_{G1} \mu_t}{u_p d_p} \right) \rho U Y^{2\epsilon} \left(\frac{\partial F}{\partial \Psi} \right)^2$$

$$\delta = - \frac{C_{G2} \mu_t d_p}{\rho U u_p \alpha_t^2 L_t}$$

The equation is parabolic in character, and can therefore be solved by a step-by-step finite difference technique in which the solution propagates downstream through a series of axial stations (computation planes) from a given initial condition at $X = 0$.

The generalized Crank-Nicolson (implicit) finite difference procedure employing Gaussian elimination (Ref. 20) is used to obtain a solution to the partial differential equation for G . Consider the grid network shown in

Figure 15. A backward difference is used to approximate X-derivatives and central differences on both j^{th} and $(j+1)^{\text{st}}$ rows are used to represent ψ derivatives, in the following fashion:

$$\begin{aligned}
 \frac{\partial G}{\partial X} &= \frac{G_{i+1,j} - G_{i,j}}{\Delta X} \\
 \alpha \frac{\partial}{\partial \psi} \left(\beta \frac{\partial G}{\partial \psi} \right) &= \frac{\partial \theta}{\Delta \psi^2} \left[\beta_{i+1, j+\frac{1}{2}} (G_{i+1, j+1} - G_{i+1, j}) \right. \\
 &\quad \left. - \beta_{i+1, j-\frac{1}{2}} (G_{i+1, j} - G_{i+1, j-1}) \right] \\
 &+ \frac{\alpha(1-\theta)}{\Delta \psi^2} \left[\beta_{i, j+\frac{1}{2}} (G_{i, j+1} - G_{i, j}) \right. \\
 &\quad \left. - \beta_{i, j-\frac{1}{2}} (G_{i, j} - G_{i, j-1}) \right] \\
 \gamma + \delta G &= \theta (\gamma_{i+1, j} + \delta_{i+1, j} G_{i+1, j}) \\
 &+ (1-\theta) (\gamma_{i, j} + \delta_{i, j} G_{i, j})
 \end{aligned} \tag{120}$$

Note that the formulation assumes equal mesh spacing in the cross-stream coordinate (ψ). The value chosen for the weighting factor ($0.0 \leq \theta \leq 1.0$) in the finite difference representation determine the character of the formulation. In particular:

$$\theta \begin{cases} 0, \text{ explicit} \\ 1/2, \text{ Crank-Nicolson (implicit)} \\ 1, \text{ fully implicit} \end{cases}$$

Collecting terms, Equation 119 is expressed in finite difference form as:

$$C_{Rj} G_{i+1, j+1} + C_{Cj} G_{i+1, j} + C_{Lj} G_{i+1, j-1} = R_j \tag{121}$$

$$2 \leq j \leq (n-1)$$

where n is the total number of streamlines at axial station $(i+1)$. The coefficients are given by:

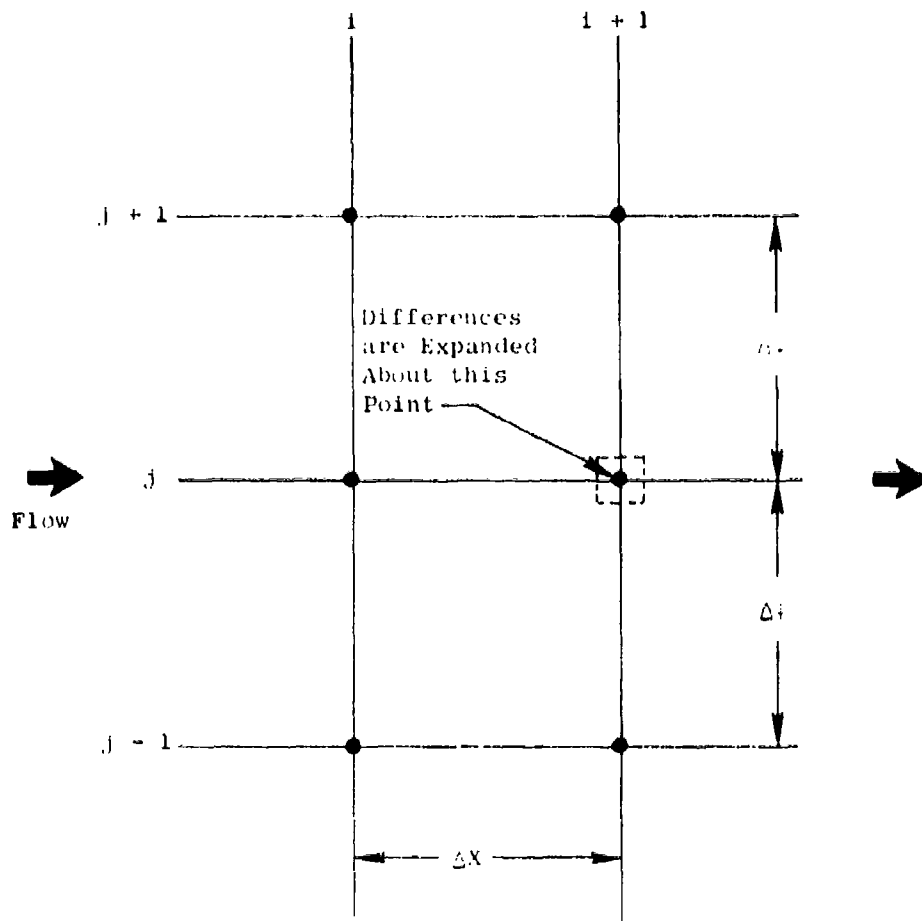


Figure 15. Finite Difference Grid Network.

$$\begin{aligned}
C_{Rj} &= - \frac{\alpha \theta (\Delta X)}{(\Delta \Psi)^2} \beta_{i+1, j+\frac{1}{2}} \\
C_{Uj} &= 1 + \frac{\alpha \theta (\Delta X)}{(\Delta \Psi)^2} (\beta_{i+1, j+\frac{1}{2}} + \beta_{i+1, j-\frac{1}{2}}) - \theta (\Delta X) \delta_{i+1, j} \\
C_{Lj} &= - \frac{\alpha \theta (\Delta X)}{(\Delta \Psi)^2} \beta_{i+1, j-\frac{1}{2}} \\
R_j &= \left[\frac{\alpha (1-\theta) (\Delta X)}{(\Delta \Psi)^2} \beta_{i, j+\frac{1}{2}} \right] G_{i, j+1} + \left[1 - \frac{\alpha (1-\theta) (\Delta X)}{(\Delta \Psi)^2} (\beta_{i, j+\frac{1}{2}} + \beta_{i, j-\frac{1}{2}}) \right. \\
&\quad \left. + (1-\theta) (\Delta X) \delta_{i, j} \right] G_{i, j} + \left[\frac{\alpha (1-\theta) (\Delta X)}{(\Delta \Psi)^2} \beta_{i, j-\frac{1}{2}} \right] G_{i, j-1} \\
&\quad + \theta (\Delta X) \gamma_{i+1, j} + (1-\theta) (\Delta X) \gamma_{i, j} \tag{122}
\end{aligned}$$

Application of Equation 121 to mesh points $j = 2$ through $(n - 1)$ results in a set of $(n - 2)$ simultaneous linear algebraic equations with n dependent variables. The system is closed by expression of the boundary conditions in finite difference form. The value of G on the jet centerline ($\Psi = 0$) is determined by passing a second-degree polynomial $G(\Psi)$ through the first mesh points, and requiring that Equation 118a be satisfied at the first point ($j=1$). This leads to the expression:

$$G_{i+1, 1} = \frac{4}{3} G_{i+1, 2} - G_{i+1, 3} \tag{123}$$

The second boundary condition, Equation 118b, is satisfied by specifying:

$$G_{i+1, n} = G_{ex} \tag{124}$$

Equations 123 and 124 can be used to eliminate the variables $G_{i+1, 1}$ and $G_{i+1, n}$ from Equation 121, yielding a set of $(n-2)$ simultaneous equations with a tridiagonal coefficient matrix. Gaussian elimination is then used to obtain a solution.

In addition to specified initial (and external) boundary conditions, a finite difference solution of Equation 119 requires that the coefficients $(1, \alpha, \theta, \dots)$ be evaluated at each mesh point. From equations 111 and 119, it is seen that the following information is therefore needed:

1. Physical characteristics of the nozzle exit (d_p, u_p).
2. Aerodynamic properties (ρ, U, F, e, L_t) at each mesh point.
3. Values of constants ($C_{G1}, C_{G2}, \alpha_t, \sigma_G$) in the turbulence model.

The information in the first and second items is obtained from output of the JETMIX computer program. The nozzle exit plane parameters, which are originally input to JETMIX as part of the problem description, are taken directly from the output. The aerodynamic properties are obtained by streamwise interpolation between calculated profiles at the JETMIX output stations. The values of the constants in item 3 can be specified through input to SPALDG. The constant α_t must be set as:

$$\alpha_t = 0.2 \quad (125)$$

to maintain consistency with the JETMIX analysis. The recommended values of the remaining quantities are:

$$\begin{aligned} C_{G1} &= 2.7 \\ C_{G2} &= 0.134 \\ \sigma_G &= 0.7 \end{aligned} \quad (126)$$

These values were taken from Reference 5, where they were chosen to yield good agreement of analytical predictions with the data of Reference 21.

4.5 MIXING AND HOMOGENIZATION OF THE HETEROGENEOUS GAS

The changes in the detailed composition of the two-part heterogeneous gas due to mixing, homogenization, and chemical reaction throughout the plume flow field are computed after completion of the steady-state turbulent inert gas jet mixing calculation. The procedure is to extend a computation tube from each area of the nozzle exit plane represented by a probe measurement, defining the tube boundaries so as to maintain constant fuel flow in each tube. Since the air entrained into the plume carries no fuel, no new computation tubes are created as mixing proceeds. The calculation proceeds out from the nozzle exit plane in axial steps.

In each computation step the interchange of gases between adjacent tubes is computed, using the flow profiles generated by the preceding steady-state gas jet mixing calculation as a guide. In this interchange, the two parts of the heterogeneous flow are kept segregated; i.e., hot gas from one tube is transported only into the hot gas parts of the adjacent tubes. Ambient air is considered cold gas and is transported into the cold gas part of the outer tube.

After the mixing interchange is accomplished, homogenization of the gas in each tube is performed by blending some of the cold gas into the hot gas until the heterogeneity characteristic parameter of the two-part gas agrees with the value computed previously for the steady-state turbulent mixing flow field.

The chemical composition of the hot gas mixture is altered by interchange with the hot gases of adjacent tubes, and by introduction of cold gas during homogenization. The composition of the cold gas mixture is altered only by interchange with the cold gases of adjacent tubes.

4.5.1 Definition of New Computation Tubes

The solution for the steady-state turbulent inert gas jet mixing flow field is expressed in the form of tables of normalized radius and stream function, velocity, mole fractions of the dummy gases representing the initial flow in each computation tube, and other properties. The solution for the characteristic heterogeneity parameter is also tabulated, with a different set of stream functions. A set of tables exists for each of several axial positions throughout the flow field.

A definite location for the outer edge of the flow field is required. In the original solution, the properties at the outer radii are feathered smoothly into the ambient flow, making the outer boundary indeterminate. The outer edge is arbitrarily defined as the point where the mole fraction of the dummy gas representing ambient air is 0.98. The value of the stream function corresponding to this point is determined by interpolation.

After locating the outer edge of the jet, the points at which flow properties are tabulated are redistributed by interpolation so that an approximately equal number of points is located within each computation tube.

The normalized stream function ψ' is converted to units of pounds per second by the formula:

$$\psi = \frac{U_j D_j^2}{144} \psi' \quad (127)$$

where U_j and D_j are the reference velocity (ft/sec.) and diameter (inches) of the initial exhaust jet. The normalized radius Y is converted to units of inches by:

$$R^2 = \left(\frac{1}{2} D_j\right)^2 Y^2 \quad (128)$$

the square of the radius is used for interpolation, because it is a more linear function with respect to stream function than is the radius.

In general, the axial location at which flow property profiles are required does not correspond to one of the axial locations at which property tables exist. It is necessary to construct tables at the present axial position by interpolation between available tables. The interpolation is performed between corresponding entries of the tables, without regard to the values of the properties.

At each point j in the profile, the mixture molecular weight is computed:

$$\bar{m}_j = \sum_i X_{kj} m_k \quad (129)$$

where m_k is the molecular weight of dummy gas k , and x_{kj} is the mole fraction of gas k at point j . The mole fractions are then converted to mass fractions:

$$Y_{kj} = X_{kj} \left(\frac{m_k}{\bar{m}_j} \right) \quad (130)$$

and the mass fraction of fuel at point j is computed:

$$F_j = \sum_k Y_{kj} F_k \quad (131)$$

Here, F_k is the fuel concentration in dummy gas k .

By the definition of the stream function, the mass flow between point j and its inner neighbor ($j-1$) is

$$\dot{W}_j = \dot{f}_j - \dot{f}_{j-1} \quad (132)$$

The cumulative flow (the total flow inside of point j) of dummy gas k is

$$\bar{W}_{kj} = \sum_{i=2}^j \frac{1}{2} (Y_{k(i-1)} + Y_{ki}) \dot{W}_i \quad (133)$$

and the cumulative fuel flow is

$$\bar{W}_{Fj} = \sum_{i=2}^j \frac{1}{2} (F_{i-1} + F_i) \dot{W}_i \quad (134)$$

To remove the effects of small continuity errors that may have occurred in the numerical calculations, each W_{Fj} is multiplied by the ratio of total fuel flow in the engine exit plane to the cumulative fuel flow in the present profile at the outer edge of the flow field.

The computation tubes are defined as tubes of constant fuel flow. To define the tube boundaries, the squares of the radii in the profile at the present station are tabulated against the cumulative fuel flow, and the values of radius are selected by interpolation at values of fuel flow that correspond to the tube boundaries. Similarly, the flow of each dummy gas in each tube is determined by tabulating cumulative gas flows against cumulative fuel flow and interpolating. If tube n has inner boundary n and outer boundary $(n + 1)$, the flow of dummy gas k in tube n at present axial station is

$$\hat{W}_{kn} = \bar{W}_k(n+1) - \bar{W}_{kn} \quad (135)$$

A correction factor is applied to each \hat{W}_{kn} to maintain continuity of flow of each dummy gas k ; that is,

$$\sum_n \hat{W}_{kn} = (W_{kk})_{x=0} \quad (136)$$

The total flow in each tube is also computed:

$$\hat{W}_{Tn} = \sum_k \hat{W}_{kn} \quad (137)$$

The mean velocity and heterogeneity parameter in tube n are determined by numerical integration with respect to cumulative fuel flow:

$$\bar{U}_n = \frac{\int_n^{n+1} U_d \bar{W}_F}{\bar{W}_F(n+1) - \bar{W}_{Fn}} \quad (138)$$

$$\bar{G}_n = \frac{\int_n^{n+1} U_d \bar{W}_F}{\bar{W}_F(n+1) - \bar{W}_{Fn}} \quad (139)$$

The entrainment of ambient air from the previous to the present axial station is computed by the difference in total airflow in all tubes. The air to be entrained is placed in an extra computation tube at the previous station.

$$W_{aa} = \sum_n (\hat{W}_{an} - W_{an}) \quad (140)$$

The residence time for chemical reactions in each tube is computed for the axial step:

$$(\Delta t)_n = \frac{\Delta X}{U_n} \quad (141)$$

4.5.2 Mixing and Homogenization

The interchange of gas due to mixing between adjacent computation tubes in an axial step is derived from the dummy gas flows in the tubes at the present and previous stations. The parameter α_{mn} is defined as the fraction of flow in tube m at the previous station that is transferred to tube n at the present station. In any one step, the interchange of gas is limited to adjacent tubes.

In the following development, W_{km} is the flow of dummy gas k in tube m at the previous station, and \hat{W}_{kn} is the flow of gas k in tube n at the present axial station.

The relations used to evaluate the α 's depend upon whether the tube is located within or outside the "potential core" of the mixing jet. A tube is defined to be outside the potential core if the flow of the dummy gas representing ambient air exceeds one percent of the total flow in the tube.

If the tube n is within the potential core, the flow of dummy gas n in its parent tube is used to evaluate the α 's.

$$\sum_m W_{nm} \alpha_{mn} = \hat{W}_{nm} \quad (142)$$

If tube n is outside the potential core, the total flow in the tube is used:

$$\sum_m W_{Tm} \alpha_{mn} = \hat{W}_{Tn} \quad (143)$$

Other relations used are fuel conservation.

$$\sum_m W_{fm} \alpha_{mn} = W_{fn} \quad (144)$$

where W_{fn} is the fuel flow in tube n (constant by definition of the computation tube), and the requirement that all the flow in a tube must go somewhere:

$$\sum_n \alpha_{mn} = 1 \quad (145)$$

The calculation of the α 's proceeds from tube to tube, starting at the centerline. If tube 1 is within the potential core, the above relations reduce to:

$$W_{11} \alpha_{11} + W_{12} \alpha_{21} = \hat{W}_{11} \quad (146)$$

$$W_{f1} \alpha_{11} + W_{f2} \alpha_{21} = W_{f1} \quad (147)$$

These equations are solved for α_{21} :

$$\alpha_{21} = \frac{W_{11} - \hat{W}_{11}}{W_{11} \left(\frac{W_{f2}}{W_{f1}} \right) - W_{12}} \quad (148)$$

If tube 1 is outside the potential core, this becomes

$$\alpha_{21} = \frac{W_{T1} - \hat{W}_{T1}}{W_{T1} \left(\frac{W_{f2}}{W_{f1}} \right) - W_{T2}} \quad (149)$$

The fraction of gas in tube 2 transferred to tube 1 must be within the limits $0 \leq \alpha_{21} \leq 1$, and must not move more fuel from tube 2 to tube 1 than can be moved from tube 1 to tube 2:

$$\alpha_{21} \leq \left(\frac{W_{f1}}{W_{f2}} \right) \quad (150)$$

with α_{21} determined, α_{12} is determined by fuel continuity

$$\alpha_{12} = \left(\frac{W_{f2}}{W_{f1}} \right) \alpha_{21} \quad (151)$$

and

$$a_{11} = 1 - a_{12} \quad (152)$$

The formulae for tube 2 must include the mass transfer between tubes 1 and 2 (already determined) as well as the transfer between tubes 2 and 3. If tube 2 is within the potential core,

$$a_{32} = \frac{W_{22} - \hat{W}_{22} + \left[W_{21} - \left(\frac{W_{F1}}{W_{F2}} \right) W_{12} \right] a_{12}}{\left(\frac{W_{F3}}{W_{F2}} \right) W_{22} - W_{23}} \quad (153)$$

or, if tube 2 is outside the potential core,

$$a_{32} = \frac{W_{T2} - \hat{W}_{T2} + \left[W_{T1} - \left(\frac{W_{F1}}{W_{F2}} \right) W_{T2} \right] a_{12}}{\left(\frac{W_{F3}}{W_{F2}} \right) W_{T2} - W_{T3}} \quad (154)$$

Again, a_{32} must be within the limits $0 \leq a_{32} \leq 1$, and

$$a_{32} = \left(\frac{W_{12}}{W_{F3}} \right) (1 - a_{21}) \quad (155)$$

After determination of a_{12} , a_{23} is determined by fuel continuity:

$$a_{23} = \left(\frac{W_{13}}{W_{F3}} \right) a_{12} \quad (156)$$

and

$$a_{22} = 1 - a_{21} - a_{23} \quad (157)$$

The procedure for tube 3 is repeated for each successive tube until the last fuel-inlet tube is reached, tube N . There is no fuel transferred outward from tube N , so

$$a_{N+1,N} = 0 \quad (158)$$

Tube N absorbs all of the flow in the extra tube containing the entrained air;

$$\alpha(N+1)N = 1 \quad (159)$$

Once the α 's have been derived, they are used to construct the detailed properties of the heterogeneous flow in each tube. The flows of hot and cold gases in tube n at the present station before homogenization are derived from the flows in all tubes at the previous station:

$$\hat{W}_H = \sum_m W_{Tm} \alpha_{mn} Y_m \quad (160)$$

$$\hat{W}_C = \sum_m W_{Tm} \alpha_{mn} (1 - Y_m) \quad (161)$$

Similarly, the flows of fuel in the hot and cold gases are:

$$\hat{W}_{FH} = \sum_m W_{Tm} \alpha_{mn} F_{Hm} Y_m \quad (162)$$

$$\hat{W}_{FC} = \sum_m W_{Tm} \alpha_{mn} F_{Cm} (1 - Y_m) \quad (163)$$

The mean fuel concentration in tube n at the present station is:

$$f_n = \frac{\hat{W}_{FH}}{\hat{W}_H + \hat{W}_{FC}} \quad (164)$$

The fuel concentration in the hot gas is:

$$f_{nH} = \frac{\hat{W}_{FH}}{\hat{W}_H} \quad (165)$$

The fuel concentration in the cold gas in the present station is:

$$\hat{y}' = \frac{\hat{w}_H}{\hat{w}_H + \hat{w}_C} \quad (166)$$

The mass fraction of hot gas after homogenization (\hat{y}) and the fuel concentration in the hot gas (\hat{F}_H) are derived from the value of the Spalding heterogeneity parameter at the present station. This is done by solving the equations

$$\bar{F} = \hat{y} \hat{F}_H + (1 - \hat{y}) \hat{F}_C \quad (167)$$

$$G = \hat{y} (\bar{F} - \hat{F}_H)^2 + (1 - \hat{y}) (\bar{F} - \hat{F}_C)^2 \quad (168)$$

The fraction of the cold gas that is transferred to the hot gas to accomplish the homogenization is

$$\tau = \frac{\hat{y} - \hat{y}'}{1 - \hat{y}'} \quad (169)$$

The composition and enthalpy of the cold and hot gases in tube n at the present station are computed by the formulae

$$\hat{H}_C = \frac{\sum_m \hat{E}_{cm} \alpha_{mn} (1 - y_m) W_{Tm}}{\hat{w}_C} \quad (170)$$

$$\hat{H}_H = \frac{\sum_m \hat{E}_{im} \alpha_{mn} y_m W_{Tm} + \tau \sum_m \hat{E}_{cm} \alpha_{mn} (1 - y_m) W_{Tm}}{\hat{y} (\hat{w}_H + \hat{w}_C)} \quad (171)$$

where \hat{E} represents, in turn, the concentrations of the chemical species Z_H, Z_O , etc. and the total enthalpy

$$h + \frac{U^2}{2g_c J}$$

4.6 CHEMICAL REACTION KINETICS

The plume model computer program provides the user a choice of two analytical procedures for modelling the gas-phase chemical reaction kinetics that govern the consumption of CO and the consumption or generation of NO_x in the plume. In practice, the two procedures have been found to produce almost identical results under conditions found in afterburner exhaust plumes.

The first procedure, GCKP, is a modified version of the NASA General Chemical Kinetics Program (Reference 3). It provides a formal numerical solution of simultaneous differential equations derived from a system of 23 molecular collision reactions. GCKP was included because of the high confidence in the accuracy of its predictions, and the added capability of examining such effects as departure of the radical pool from pseudo-equilibrium and conversion of NO to NO₂.

The alternative procedure, SCKP, makes use of some analytical approximations to gain computational efficiency. The two-body collision reactions which determine the concentrations of the free radicals relative to each other are assumed to be equilibrated. The decay of this radical pool is governed by selected rate-controlled three-body reactions. The consumption of CO and the generation of NO are computed independently by selected rate-controlled reactions.

The consumption of unburned hydrocarbons is not treated by either of the chemical kinetics procedures because of the formidability of the task of constructing a system of reactions and rates for the decomposition and oxidation of heavy hydrocarbon molecules. Although such a system can be found in the literature for methane oxidation (Reference 22), researchers confronted with more complex hydrocarbons have usually resorted to a "global reaction" approximation (Reference 23). Rather than pursue this approach, it was judged that equal accuracy could be attained by simply comparing residence time of the local gas mixture with empirically determined ignition delay times for kerosene at the local temperature.

4.6.1 General Chemical Kinetics (GCKP)

A general chemical kinetics computer program for complex gas mixtures, developed by David A. Bittker and Vincent J. Scullin of NASA Lewis Research Center, was adapted for use as a subprogram in the plume model computer program. Quoting from Reference 34, "this program can be used for any homogeneous reaction in either a flowing or a static system. It has the advantages of flexibility, accuracy, and ease of use. Moreover, any chemical system may be used for which species thermodynamic data and reaction rate constants are known. The program handles several types of reactions. These include bimolecular exchange reactions, unimolecular decompositions, bimolecular decompositions, and the reverse recombination process. The solution method is a rapid one based on the implicit finite-difference technique of Klee,el and Tyson. A unique step-size control system is used to estimate the optimum step-size for each step."

Reference 3 provides a "complete description of the chemical kinetics computer program and the implicit numerical integration method it uses. The theoretical kinetics differential equations solved by the program are also given in detail." There is no need to duplicate these descriptions here.

In modifying GCKP for use as a subprogram, considerable specialization was performed. The chemical reaction system, reaction rates, and species thermodynamic properties, normally presented to the program as input data, were all built into the subprogram version. The fluid dynamics options were set so that the problem is solved as a constant pressure adiabatic closed reactor, with residence time and initial gas temperature and composition specified.

The chemical reaction system included in GCKP is displayed in Table 3, along with Arrhenius equations for evaluating reaction rates. For some of the three-molecule reactions, some species are known to be more efficient collision partners than others. Those third-body efficiencies that could be evaluated are shown in Table 4; all others are 1.0.

CO is oxidized to CO₂ by two-body reactions 1 and 2. Of these, reaction 1 is dominant by factors of 10 or more, even in lean mixtures. The rate expression for reaction 1 was derived by fitting an Arrhenius-type equation to the more complex expression of Dryer, et al. (Reference 24). The coincidence is very close in the range 1500 < T < 4500 R.

NO is generated by reactions 12 through 14, recommended by Fenimore (Reference 25). Fenimore's rates were used for reaction 14, but for 12 and 13, faster rates were taken from the Leeds report (Reference 26). By this mechanism, NO is generated by the attack of oxygen atoms on nitrogen molecules.

The relative concentrations of hydrogen and oxygen atoms and hydroxyl radicals are regulated by two-body shuffle reactions 7 through 11. Rates for these reactions were obtained from Brokaw and Bittker (Reference 27), except for reaction 11, for which Hammond and Mellor (Reference 23) were consulted. These reactions are very fast compared to the three-body reactions, so are essentially equilibrated at high temperatures. At lower temperatures, departures from equilibrium are observed.

The decay of the radical pool toward overall equilibrium is governed by exothermic three-body recombination reactions 3 through 6 and 15. Rate expressions are those of Brokaw and Bittker, except Hammond and Mellor for reaction 5 with third-body efficiencies from the Leeds report. Of these, reaction 3 predominates in stoichiometric and fuel-rich mixtures. Reaction 15 becomes influential in lean mixtures where molecular oxygen concentrations are high.

To consume the hydroperoxyl radical (HO₂) produced by reaction 15, four two-body shuffle reactions among hydrogen-oxygen species are provided (reactions 16-19). On the recommendation of Brokaw and Bittker, an additional shuffle reaction between HO₂ and nitric oxide (NO) was included to provide for an observed sensitizing effect of NO on hydrogen-oxygen reactions at low

Table 3. Chemical Reaction System.

Reactions	Rate Constants (cgs Units)
1) $\text{CO} + \text{OH} \rightarrow \text{CO}_2 + \text{H}$	$k_1 = 1120.6042T^{2.486385}e^{-2574.743/RT}$ (d)
2) $\text{CO} + \text{O}_2 \rightarrow \text{CO}_2 + \text{O}$	$k_2 = 2.5(10^{12})e^{-48000/RT}$ (a)
3) $\text{H} + \text{OH} + \text{M} \rightarrow \text{H}_2\text{O} + \text{M}$	$k_3 = 1.0(10^{19})T^{-1}$ (a)
4) $\text{H}_2 + \text{M} \rightarrow 2\text{H} + \text{M}$	$k_4 = 1.12(10^{13})T^{0.5}e^{-92600/RT}$ (a)
5) $\text{H} + \text{O} + \text{M} \rightarrow \text{OH} + \text{M}$	$k_5 = 5.3(10^{15})e^{2780/RT}$ (b)
6) $\text{O} + \text{O} + \text{M} \rightarrow \text{O}_2 + \text{M}$	$k_6 = 8.15(10^{18})T^{-1.22}$ (a)
7) $\text{OH} + \text{H}_2 \rightarrow \text{H}_2\text{O} + \text{H}$	$k_7 = 2.3(10^{13})e^{-5200/RT}$ (a)
8) $\text{H} + \text{O}_2 \rightarrow \text{OH} + \text{O}$	$k_8 = 2.04(10^{14})e^{-16500/RT}$ (a)
9) $\text{O} + \text{H}_2 \rightarrow \text{OH} + \text{H}$	$k_9 = 4.0(10^{13})e^{-10200/RT}$ (a)
10) $\text{H}_2\text{O} + \text{O} \rightleftharpoons \text{OH} + \text{OH}$	$k_{10} = 8.4(10^{13})e^{-18000/RT}$ (a)
11) $\text{H}_2 + \text{O}_2 \rightleftharpoons \text{OH} + \text{OH}$	$k_{11} = 8.0(10^{14})e^{-45000/RT}$ (b)
12) $\text{N} + \text{NO} \rightarrow \text{N}_2 + \text{O}$	$k_{12} = 3.1(10^{13})e^{-334/RT}$ (e)
13) $\text{N} + \text{O}_2 \rightleftharpoons \text{NO} + \text{O}$	$k_{13} = 6.4(10^9)Te^{-6250/RT}$ (e)
14) $\text{N} + \text{OH} \rightarrow \text{NO} + \text{H}$	$k_{14} = 4.0(10^{13})$ (c)
15) $\text{H} + \text{O}_2 + \text{M} \rightarrow \text{HO}_2 + \text{M}$	$k_{15} = 1.0(10^{15})e^{1300/RT}$ (a)
16) $\text{H} + \text{HO}_2 \rightleftharpoons \text{OH} + \text{OH}$	$k_{16} = 7.0(10^{13})$ (a)
17) $\text{OH} + \text{HO}_2 \rightleftharpoons \text{H}_2\text{O} + \text{O}_2$	$k_{17} = 6.0(10^{12})$ (a)
18) $\text{O} + \text{HO}_2 \rightleftharpoons \text{OH} + \text{O}_2$	$k_{18} = 6.0(10^{12})$ (a)
19) $\text{H} + \text{HO}_2 \rightleftharpoons \text{H}_2 + \text{O}_2$	$k_{19} = 2.3(10^{13})$ (a)
20) $\text{NO} + \text{HO}_2 \rightarrow \text{NO}_2 + \text{OH}$	$k_{20} = 1.0(10^{13})$ (a)
21) $\text{NO}_2 + \text{H} \rightarrow \text{NO} + \text{OH}$	$k_{21} = 7.2(10^{14})e^{-1930/RT}$ (a)
22) $\text{NO}_2 + \text{O} \rightarrow \text{NO} + \text{O}_2$	$k_{22} = 1.9(10^{13})e^{-1060/RT}$ (a)
23) $\text{NO} + \text{O} + \text{M} \rightarrow \text{NO}_2 + \text{M}$	$k_{23} = 9.4(10^{14})e^{1930/RT}$ (a)

(a) Brokaw and Bittker, NASA TND-7024 (Ref. 27) (d) Driver, et. al. (Ref. 24)

(b) Hammond and Mellor, AIAA 71-711 (Ref. 22) (e) Leeds (Ref. 26)

(c) Fenimore, 13th Symposium (Ref. 25)

Table 4. Third Body Efficiencies.

<u>M</u>	<u>Reaction No.</u> <u>(3)</u>	<u>Reaction No.</u> <u>(15)</u>	<u>Reaction No.</u> <u>(23)</u>
CO	4.5	2.0	1.0
CO ₂	8.0	7.5	2.1
H ₂ O	18.0	32.5	6.1
O ₂	4.5	2.0	1.0
N ₂	3.6	2.0	1.4
OH	4.5	2.0	1.0
NO	4.5	2.0	1.4
H	1.07	1.0	0.75
O	1.07	1.0	1.0
H ₂	4.5	5.0	0.75

temperature. The last three reactions (21-23) serve to regenerate NO from the nitrogen dioxide (NO₂) produced by reaction 20.

4.6.2 Special Chemical Kinetics Procedure (SCKP)

The SCKP chemical kinetics program was developed by General Electric Company to provide a rapid calculation procedure for modeling the chemical kinetics of hydrocarbon combustion mixtures. To provide computational speed, the two-body collision reactions, which determine the concentration of free radicals, are assumed to be in pseudo-equilibrium. The decay of this radical pool toward overall equilibrium is monitored by a selected set of rate-controlled three-body recombination reactions. The consumption of CO and the generation of NO_x contaminants are evaluated independently by direct integration of the governing two-body CO and NO_x reactions.

Chemical Reaction System

The chemical reaction system utilized in the SCKP procedure consists of a subset of the GCKP reaction system. The pertinent chemical reactions, along with their rate constants, are shown in Table 5. As indicated by the table, they are identical to those used in GCKP, with exception of reaction 2, which is expressed in terms of a recombination rather than a dissociation reaction. The third body efficiencies for the three-body reactions are identical to those used in the GCKP program.

The three-body recombination reactions 1 to 5 each involve an equal reduction in the molarity of the system. The progress of the reaction may then be determined by monitoring the molecular weight \bar{m} , using the following expression:

$$\begin{aligned}
 -\frac{d\left(\frac{1}{\bar{m}}\right)}{dt} = & \frac{1}{T_0} \{k_1 (H) (OH) (M) - k_{-1} (H_2O) (M) + k_2 (H)^2 (M) - k_{-2} (H_2) (M) \\
 & + k_3 (H) (O) (M) - k_{-3} (OH) (M) + k_4 (O)^2 (M) - k_{-4} (O_2) (M) \\
 & + k_5 (H) (O_2) (M) - k_{-5} (HO_2) (M)\} \quad (172)
 \end{aligned}$$

Converting molar concentrations to mole fractions and combining the third-body efficiencies with the rate constants yields the following relation:

$$\begin{aligned}
 -\frac{d\left(\frac{1}{\bar{m}}\right)}{dt} = & \frac{\rho m^2}{T\bar{m}} \{k'_1 X_H X_{OH} - k'_{-1} X_{H_2O} + k'_2 X_H^2 - k'_{-2} X_{H_2} + k'_3 X_H X_O \\
 & - k'_{-3} X_{OH} + k'_4 X_O^2 - k'_{-4} X_{O_2} + k'_5 X_H X_{O_2} - k'_{-5} X_{HO_2}\} \quad (173)
 \end{aligned}$$

Table 5. SCKP Chemical Reaction System.

<u>Reactions</u>	<u>Rate Constants (cgs Units)</u>
1) $H + OH + M \rightleftharpoons H_2O + M$	$k_1 = 1.0(10^{19})T^{-1}$
2) $H + H + M \rightleftharpoons H_2 + M$	$k_2 = 3.3891(10^{13})T \cdot 109 e^{10594/RT}$
3) $H + O + M \rightleftharpoons OH + M$	$k_3 = 5.3 (10^{15})e^{2780/RT}$
4) $O + O + M \rightleftharpoons O_2 + M$	$k_4 = 8.15(10^{18})T^{-1022}$
5) $H + O_2 + M \rightleftharpoons HO_2 + M$	$k_5 = 1.0(10^{15})e^{1306/RT}$
6) $H + HO_2 \rightleftharpoons OH + OH$	$k_6 = 7.0(10^{13})$
7) $OH + HO_2 \rightleftharpoons H_2O + O_2$	$k_7 = 6.0(10^{12})$
8) $O + HO_2 \rightleftharpoons OH + O_2$	$k_8 = 6.0(10^{12})$
9) $H + HO_2 \rightleftharpoons H_2 + O_2$	$k_9 = 2.3(10^{13})$
10) $CO + OH \rightleftharpoons CO_2 + H$	$k_{10} = 1120.6042T^{2.4863852}e^{2574.743/RT}$
11) $N + NO \rightleftharpoons N_2 + O$	$k_{11} = 3.1(10^{13})e^{-334/RT}$
12) $N + O_2 \rightleftharpoons NO + O$	$k_{12} = 6.4(10^9)Te^{-6250/RT}$
13) $N + OH \rightleftharpoons NO + H$	$k_{13} = 4.0(10^{13})$

The hydroperoxyl radical (HO_2) is not considered a major species in the SCKP procedure and is eliminated using the "steady state" approximation $d[\text{HO}_2]/dt|_{ss} = 0$ in conjunction with the rate expressions for reactions 5 through 9. Using these reactions, the effective rate constant for the hydroperoxyl reactions may be established as:

$$\bar{k}'_5 = k'_5 \left\{ 1 - \left(\frac{k'_5}{k'_5} \right) \frac{[\text{HO}_2]}{[\text{H}][\text{O}_2]} \right\} \quad (174a)$$

where:

$$\left(\frac{k'_5}{k'_5} \right) \frac{[\text{HO}_2]}{[\text{H}][\text{O}_2]} = \frac{k'_{-5} \rho_m + \left(\frac{k'_{-5}}{k'_5} \right) \left\{ k'_{-6} \frac{X_{\text{OH}}^2}{X_{\text{H}} X_{\text{O}_2}} + k'_{-7} \frac{X_{\text{H}_2\text{O}}}{X_{\text{H}}} + k'_{-8} \frac{X_{\text{OH}}}{X_{\text{H}}} + k'_{-9} \frac{X_{\text{H}_2}}{X_{\text{H}}} \right\}}{(k'_{-5} \rho_m + (k_6 + k_9) X_{\text{H}} + k_7 X_{\text{OH}} + k_8 X_{\text{O}})} \quad (174b)$$

Equation 173 is then rewritten as:

$$-\frac{d\left(\frac{1}{\bar{m}}\right)}{dt} = \frac{\rho_m^2}{\bar{m}} \left\{ k'_1 X_{\text{H}} X_{\text{OH}} - k'_{-1} X_{\text{H}_2\text{O}} + k'_2 X_{\text{H}}^2 - k'_{-2} X_{\text{H}_2} + k'_3 X_{\text{H}} X_{\text{O}} - k'_{-3} X_{\text{OH}} + k'_4 X_{\text{O}}^2 - k'_{-4} X_{\text{O}_2} + \bar{k}'_5 X_{\text{H}} X_{\text{O}_2} \right\} \quad (175)$$

Integration of the Three-Body Rate Expression

The final relation for the three-body kinetics is a nonlinear first order differential equation and cannot be integrated in closed form. In Reference 4, it was observed that reaction 1, which has the largest rate constant, was the prime contributor to the heat release of the overall combustion reaction. It was further established that the combustion rate was proportional to the (H) (OH) product over a wide range of temperatures, equivalence ratios, and combustion efficiency levels. The combustion efficiency parameter (ρ) is defined in terms of the molecular weight \bar{m} as:

$$\rho = \frac{\left(\frac{1}{\bar{m}}\right) - \left(\frac{1}{\bar{m}_u}\right)}{\left(\frac{1}{\bar{m}_c}\right) - \left(\frac{1}{\bar{m}_u}\right)} \quad (176)$$

where: \bar{m}_u , \bar{m}_c are the unreacted and completely recombined molecular weights (Appendix A, Part 2).

The condition $\beta = 0$ corresponds to the unreacted mixture molecular weight resulting from the inefficient combustion of the hydrocarbon to CO and H₂ combustion products. The condition $\beta = 1$ corresponds to the completely recombined mixture molecular weight. Using the procedure followed in Reference 4, the rate expression equation may be approximately rewritten in terms of the combustion efficiency parameter β as:

$$\frac{d\beta}{dt} = - \frac{d(1-\beta)}{dt} = A' [(1-\beta)^2 - (1-\beta_{eq})^2] \quad (177)$$

where: β_{eq} = combustion efficiency level at full equilibrium.

The parameter A' is related to the forward rates of the recombination reactions and may be expressed as:

$$A' = \frac{\sum_{m=1}^2 \left\{ k'_1 X_H X_{OH} + k'_2 X_H^2 + k'_3 X_H X_O + k'_4 X_O^2 + k'_5 X_H X_{O2} \right\} \left(\frac{1}{m_c} - \frac{1}{m_u} \right)}{\left(\frac{1}{m} - \frac{1}{m_c} \right)^2} \quad (178)$$

If it is assumed that the integration time step (t_1 to t_2) is small and the parameter A' may be evaluated at the beginning of the step, Equation 177 may be integrated in closed form to yield

$$\beta_2 = 1 - (1-\beta_{eq}) \left[\frac{(2-\beta_{eq}-\beta_1)e^{2(1-\beta_{eq})A'\Delta t} + (\beta_{eq}-\beta_1)}{(2-\beta_{eq}-\beta_1)e^{2(1-\beta_{eq})A'\Delta t} - (\beta_{eq}-\beta_1)} \right] \quad (179)$$

where: $\Delta t = t_2 - t_1$

β_1, β_{eq}, A' are evaluated at t_1

CO Consumption

The consumption of CO in the plume is evaluated by direct integration of the rate expression for reaction 10.

$$\frac{dX_{CO}}{dt} = - c_m k_{10} \left\{ X_{CO} X_{OH} - \frac{1}{K_{10}} X_{CO_2} X_H \right\} \quad (180)$$

where $K_{10} = \frac{k_{10}}{k_{-10}}$

Using the carbon atom balance to eliminate the CO_2 ,

$$\frac{dX_{\text{CO}}}{dt} = aX_{\text{CO}} + b \quad (181)$$

where:

$$a = -v_m k_{10} \left(X_{\text{OH}} + \frac{X_{\text{H}}}{K_{10}} \right)$$

$$b = \frac{v_m k_{10} X_{\text{H}}}{n k_{10}} (X_{\text{H}} + 2X_{\text{H}_2} + X_{\text{OH}} + 2X_{\text{H}_2\text{O}})$$

$n = \text{fuel H/C atom ratio}$

Considering the coefficient a and b constant over the time step, Equation 181 may be integrated in closed form to give:

$$[X_{\text{CO}}]_2 = \left([X_{\text{CO}}]_1 + \frac{b}{a} \right) e^{a\Delta t} - \frac{b}{a} \quad (182)$$

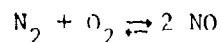
The CO_2 composition may be calculated from the C atom balance, and the H_2O and H_2 compositions adjusted to preserve the system molarity at the end of the time step.

NO_x Generation/Consumption

The generation/consumption of the NO_x contaminants is also determined independently using reactions 10 to 13. As in the case of the hydroperoxyl reactions, the N atom is not considered as a major species and may be removed from explicit consideration by use of the "steady state" approximation $dX_{\text{N}}/dt|_{\text{ss}} = 0$. The overall rate for the NO reactions may be written as:

$$\frac{dX_{\text{NO}}}{dt} = \frac{2v_m [k'_{-11} X_{\text{N}_2} X_{\text{O}} (k'_{12} X_{\text{O}_2} + k'_{13} X_{\text{OH}}) - k'_{11} X_{\text{NO}}^2 (k'_{-12} X_{\text{O}} + k'_{-13} X_{\text{OH}})]}{k'_{11} X_{\text{NO}} + (k'_{12} X_{\text{O}_2} + k'_{13} X_{\text{OH}})} \quad (183)$$

The differential rate expression is integrated numerically over the given time interval using a Runge Kutta technique. At the completion of an integration step, the molecular nitrogen and oxygen concentrations are adjusted to reflect the overall stoichiometry of the NO reactions using:



SCKP Calculation Procedure

Initially, the residence time for each streamtube, as determined by the mixing/homogenization relations, is divided into a series of small incremental time steps. The conditions at the beginning of the step are evaluated using the given mixture enthalpies and molecular weights. After determination of the full equilibrium composition, using the procedures defined in Appendix A, Part 2, the CO composition at the end of the intermediate time step is evaluated using Equation 182. The parameter β_2 is then determined by integration of the three-body recombination expression (Equation 179). Holding the CO and NO composition fixed, the composition of the free radical pool is evaluated using a "pseudo-equilibrium" procedure. Finally, the NO composition at the end of the step is determined by integration of Equation 183. The above steps are repeated for each streamtube until the total residence time is traversed.

4.6.3 Consumption of Unburned Hydrocarbons (HYCARB)

As indicated previously, the consumption of unburned hydrocarbons is not considered by either of the chemical kinetics procedures, due to the difficulty of constructing a general system of reactions and rates for the decomposition and oxidation of the heavy hydrocarbon chains. The hydrocarbon consumption is determined, rather, by accumulating the residence time of the local gas mixture and comparing this parameter with an empirically determined ignition delay time.

Define a "reactive incipency" R for the hydrocarbon fuel as follows:

$$R = \sum_{\text{steps}} \frac{\Delta t}{t_{id}} \quad (184)$$

where: Δt = residence time in a given step

t_{id} = ignition delay time at the local conditions in the step

The "reactive incipency" is accumulated at the initial temperature of the time step. When the cumulative reactive incipency in a given reaction tube becomes greater than or equal to 1, it is assumed that all of the fuel burns instantaneously and completely to CO and H₂. From Reference 28, the ignition delay relation (kerosene) was given as a function of temperature by:

$$t_{id} = e^{(-17.671439 + 40290.88/T)} \quad (185)$$

The accumulation of the "reactive incipency" of the fuel in both the rich and lean fractions of each reaction tube is carried out for every mixing/homogenization step. To properly account for the mixing transfer of raw fuel, the hydrocarbon is weighted as follows:

$$R'_j = \frac{\sum_i W_i R_i^4}{W_{tot j}} \quad (186)$$

where: W_i raw fuel of reactive incipency R_i transferred to tube j
 R_i - "reactive incipency" of raw fuel in tube i .

In equation 186, $W_{tot j}$ includes the fuel poured in from the adjacent rich or lean fraction of the pertinent stream tube being considered. The rationale behind the R^4 weighting function is that the hydrocarbon combustion is normally characterized by an induction period during which the free radicals build up by many orders of magnitude. Fuel with high "reactive incipency" carries radicals with it, thus catalyzing the ignition of other fuel present in the reaction tube.

4.7 SUMMATION OF CONTAMINANT FLOWS

At selected axial locations, an analysis of the profile is performed to evaluate the overall residual levels of gaseous contaminant emissions and to derive properties of the flow in individual tubes for comparison with measurements.

The radial locations of the computation tube boundaries at the selected station were determined during definition of new computation tubes, section 4.5.1 above. The total gas flow W , the mass fraction of hot gas y , the fuel concentrations F_H and F_C in the hot and cold gas parts, the static enthalpies h_H and h_C , and the concentrations (moles per pound) of chemical species Z_{iC} in the cold gas were determined for each tube by the mixing and homogenization calculations, Section 4.5. The chemical composition of the hot gas in each tube, also evaluated by the mixing and homogenization, was subsequently modified by chemical reactions, Section 4.6.

The profile analysis is done by analyzing each computation tube in turn, beginning at the centerline of the plume. The temperatures of the hot and cold gases are computed by trial and error. The temperature is estimated, then the enthalpy of the gas mixture at the estimated temperature is computed by the methods given in Appendix B, Part 3. This enthalpy is compared with the known enthalpy of the mixture, and the temperature estimate is revised to produce agreement. The molecular weight, m , the specific heat, C_p , the specific volume, v , and the specific heat ratio, γ , of each gas mixture are also computed by the methods of Appendix B, Part 3.

The average fuel concentration in the two-part gas stream is computed using (initially) the mass fraction of hot gas that exists in the free stream:

$$\bar{F} = y F_H + (1 - y) F_C \quad (187)$$

The fuel-air ratio is $f = (1 + x) \left(\frac{\bar{F}}{1 - \bar{F}} \right)$ (188)

Similarly, other average properties are computed:

$$\bar{v} = y v_H + (1 - y) v_C \quad (189)$$

$$\frac{1}{\bar{m}} = y \left(\frac{1}{m_H} \right) + (1 - y) \left(\frac{1}{m_C} \right) \quad (190)$$

$$\bar{Z}_i = y Z_{iH} + (1 - y) Z_{iC} \quad i = H, O, H_2, \text{ etc.} \quad (191)$$

The local emission indices (pounds contaminant per pound fuel) in the tube under analysis are:

$$EI_{CO} = \frac{m_{CO} \bar{z}_{CO}}{\bar{F}} \quad (192)$$

$$EI_{HC} = \frac{m_f \bar{z}_{HC}}{\bar{F}} \quad (193)$$

$$EI_{NO_x} = \frac{m_{NO_2} (\bar{z}_{NO} + \bar{z}_{NO_2})}{\bar{F}} \quad (194)$$

To compute the gas analyzer readings (parts per million by volume), the average gas composition is converted to mole fractions:

$$\bar{x}_i = \bar{m} \bar{z}_i \quad i = H, O, H_2, \text{ etc.} \quad (195)$$

Hydrocarbons and nitrogen oxides are analyzed without drying the sample:

$$R_{HC} = 10^7 \bar{x}_{HC} \quad (196)$$

$$R_{NO_x} = 10^6 (\bar{x}_{NO} + \bar{x}_{NO_2}) \quad (197)$$

CO is analyzed with the sample dried to 32° F saturation:

$$R_{CO} = \frac{10^6 \bar{x}_{CO}}{1.006202 (1 - \bar{x}_{H_2O})} \quad (198)$$

The tube area is computed from the radial position of the boundaries:

$$A = \pi (r_o^2 - r_i^2) \quad (199)$$

Velocity is computed from mass continuity:

$$U = \frac{W_f \bar{v}}{A} \quad (200)$$

Fuel flow in the tube is

$$W_f = \bar{F} W \quad (201)$$

The apparent impact pressure and total temperature that would be measured by impact pressure and aspirated thermocouple probes immersed in the two-part heterogeneous stream are calculated by the methods of Appendix A, Part 4. The mass fraction of hot gas in a gas sample drawn from the stream is also computed, after which the calculations of mean fuel-air ratio, emission indices, and analyzer readings are repeated using this value instead of y .

When all computation tubes have been analyzed, the total flows of fuel and contaminants in all tubes of the profile are computed, using local fuel flows and emission indices computed from the free-stream values of y :

$$(W_f)_T = \sum W_f \quad (202)$$

$$(W_{CO})_T = \sum W_f EI_{CO} \text{ etc.} \quad (203)$$

The overall emissions indices are thus

$$(EI_{CO})_T = \frac{(W_{CO})_T}{(W_f)_T} \text{ etc.} \quad (204)$$

4.8 OVERALL DESCRIPTION AND CAPABILITY OF INTEGRATED MODEL

The analytical procedures just described were combined to form a model of the exhaust plume of an afterburning turbojet or turbofan engine. The model represents those features of the gas flow which influence the consumption of gaseous contaminant emissions in the plume. These features include the time-average turbulent mixing of each element of the axisymmetric exhaust jet into the adjacent elements, and the mixing of the ambient air into the hot gas; the time-varying composition (heterogeneity) of the gas flow past each point in space; the generation and decay of gas heterogeneity in the plume; the alteration of instantaneous gas composition by mixing with gas from adjacent parts of the flow and by homogenization; and the consumption of gaseous contaminants by rate-limited chemical reactions.

Input to the model includes data from a probe survey of the engine exhaust stream, together with properties of the fuel and ambient air and parameters of the engine cycle. Based on this input, the model predicts profiles of velocity, fuel, and contaminant concentrations at various axial locations in the plume, plus overall residual emissions indices derived from integration of these profiles.

Input to the model includes data from a probe survey of the engine exhaust stream, together with properties of the fuel and ambient air and parameters of the engine cycle. Based on this input, the model predicts profiles of velocity, fuel, and contaminant concentrations at various axial locations in the plume, plus overall residual emissions indices derived from integration of these profiles.

The plume model has been encoded in FORTRAN IV language for machine computation on the Honeywell 6000-series computer. A complete description of this computer program is contained in the Computer Program User's Manual which is Supplement 2 to this report.

The primary use intended for the model is to estimate the true residual emissions released into the atmosphere, based upon emissions measurements made at the afterburner exhaust plane. This procedure is useful in applications where direct sampling of the mixed and cooled exhaust plume is not practical, such as engine tests in enclosed test cells. The model is also capable of accommodating a moving environment, which makes it useful in estimating contaminant consumption in the plume under high-altitude, high-speed flight conditions for exhaust jets with reasonably uniform static pressure distributions.

The accuracy of the model has been established by comparison with experimental data obtained under this program elsewhere. These comparisons are presented in Section 6.0.

The analytical model in its present form does a good, but not perfect, job of predicting the consumption of emissions in the plume. The model was compared with experimental data from only turbojet afterburners, not mixed-flow turbofan augmentors. When data for turbofan engines become available, the

model should be verified for this type of augmentor also. In contrast to some analytical modeling efforts which proceed from relatively simple models to more complex and sophisticated treatments, this model began with a very sophisticated initial structure and simplifications were searched for as work progressed. The importance of taking this approach was thoroughly justified by the successful results. It was recognized at the outset that this modeling problem involved very complex phenomena, including some for which no experimental definitions were available. The adoption of the already existing programs, JFTMIX and GCKP, was a very valuable starting point, and the inclusion of treatment of time inhomogeneities proved to be essential. Data were available on the character of time inhomogeneities in the developed plume and were adopted in the treatment, but information on the detailed time inhomogeneities at the end of the engine exit and through the potential core do not exist, except perhaps as can be inferred from this present work. It is believed that the most fruitful approach for improvement in the accuracy of emission consumption in the plume lies in revised representations of the time inhomogeneities in the early plume.

The present model, with some revision, could permit the examination of additional time inhomogeneity representations to approach a more perfect agreement with measured data.

SECTION 5.0

INITIAL AFTERBURNER EMISSIONS TESTS OF J85-5 AND J79-15 ENGINES

The primary purpose of the Phase II tests was the complete plume mapping of the emissions levels from two different afterburning engines, a J85-5 and a J79-15. Emissions were measured at radial locations to the edges of the plumes and axially aft of the engines to a point where temperatures were low enough that reactions were complete and the true emissions levels were obtained. The two engines are representative of two different sizes of afterburning engines currently in wide use on military aircraft.

The following is a brief description of each engine along with some details of the afterburner components and function.

5.1 ENGINE DESCRIPTION

5.1.1 J85 Engine

The original J85 engine was qualified in 1960 as the powerplant for the GAM 72 decoy drone. Within three years, the first version of the engine designed to power manned flight passed its Military Qualification Test. Presently, J85 engines power a number of manned and unmanned military aircraft, among them the Northrup F-5 lightweight fighter and the T-38 trainer. A turbofan version of the J85 is also used to power twin-engined business jets.

5.1.1.1 Engine Specifications

The following are the important specifications for the J85-5 engine:

Weight	584 lb
Length (cold)	104.6 in.
Maximum Diameter (cold)	21 in.
Pressure Ratio	6.6
Airflow	44.0 lb/sec
RPM	16,500
Maximum Thrust (SLS)	3850 lb
Military Thrust (SLS)	2680 lb

5.1.1.2 Engine Description

The J85-5 engine is a compact, high-thrust, lightweight, afterburning turbojet engine comprised of an eight-stage axial-flow compressor coupled

directly to a two-stage turbine. The engine incorporates a through-flow, annular-type combustion system, controlled compressor interstage bleed, and an afterburner with a variable-area exit nozzle.

5.1.1.3 Afterburner Description

Thrust augmentation is provided by injecting additional fuel into the diffuser behind the turbine. This fuel is ignited, burned, and ejected through the variable-area nozzle. The afterburner thus increases engine thrust by increasing the temperature and velocity of the exhaust gases.

The diffuser assembly for the J85-5 is shown in Figure 16. This assembly consists of a casing which houses a center cone, flameholder, and diffuser liner. Mounted on the diffuser liner are 16 shielded main spraybars with integral flow dividers, 2 main spraybar fuel manifolds, 4 pilot spraybars, and 3 pilot spraybar manifolds. The single flameholder, in addition to its function as a pilot burner, maintains the flame front in a position that assures complete combustion of the exhaust gas-fuel mixture in the afterburner.

The pilot burner spraybars are located at the 3, 6, 9, and 12 o'clock positions on the afterburner diffuser assembly and are designed to initiate afterburning and prevent afterburner blowout. They spray directly into the four flameholder air scoops.

The 16 main spraybars are the principle source of fuel for thrust augmentation. They consist of three tubes and three orifices and a pressure-operated valve (150 psig). They spray the fuel in a circumferential direction just downstream of the forward end of the flameholder air scoops. The afterburner fuel control schedules fuel to the main afterburner and pilot burner spraybars, as a function of power lever position and compressor discharge pressure. The control also regulates, as a function of power lever angle, the variable exhaust nozzle area until it is overridden by the turbine discharge control system.

Figure 17 shows the J85-5 afterburner casing, liner, and variable exhaust nozzle assembly. The afterburner casing and liner provide the volume necessary for the complete combustion of the exhaust gas-fuel mixture before it is ejected through the exhaust nozzle. The variable nozzle provides the exit passage for the exhaust gas stream. During afterburner operation, and when exhaust gas temperatures increase above the normal limit, the nozzle area is increased. When the afterburner is not in operation, the exhaust nozzle area is reduced for optimum engine performance.

5.1.2 J79 Engine

Design studies on the J79 were begun in 1952, and it became the world's first Mach 2-plus powerplant, with eventual selection as the engine for

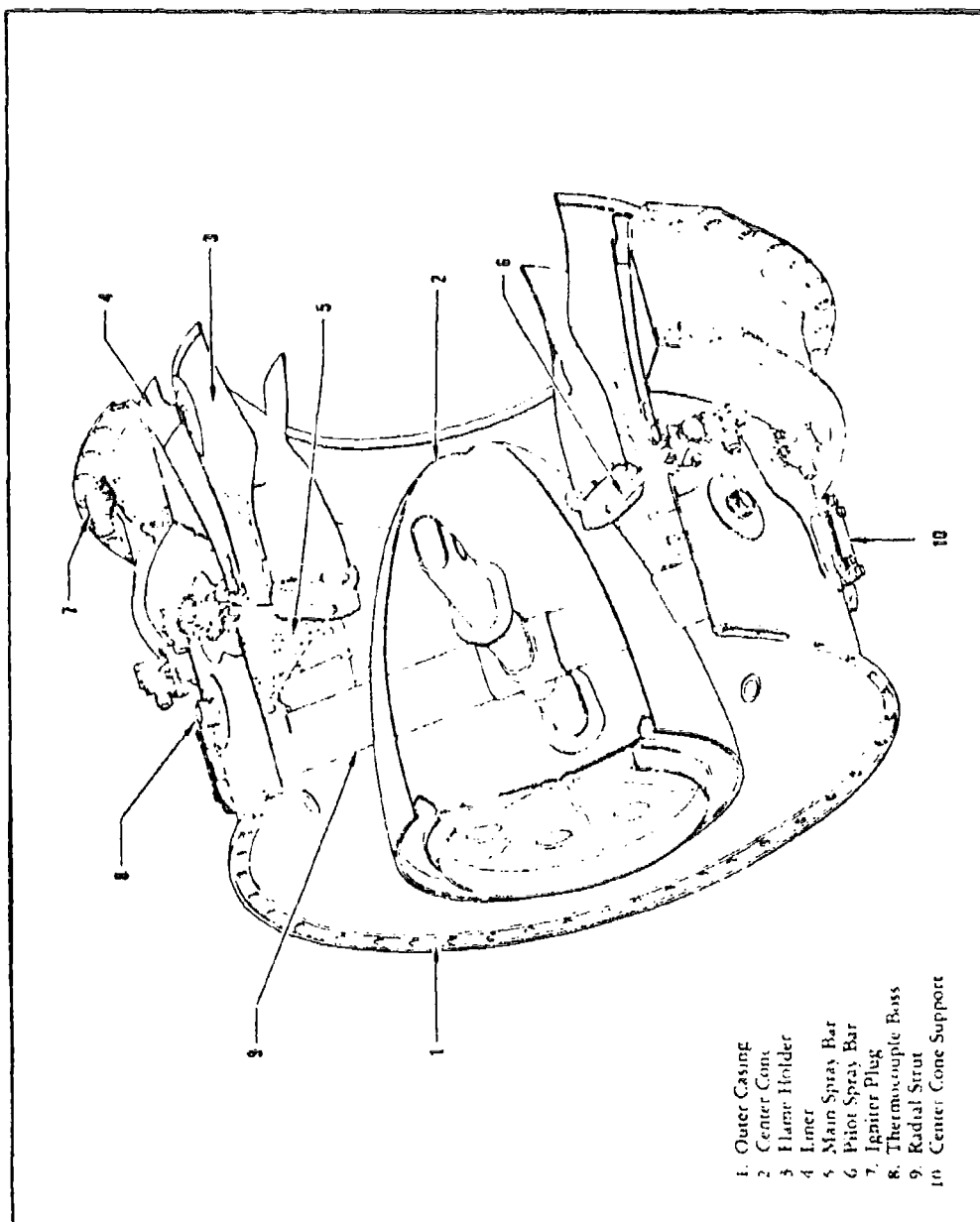


Figure 16. J85-5 Diffuser Assembly.

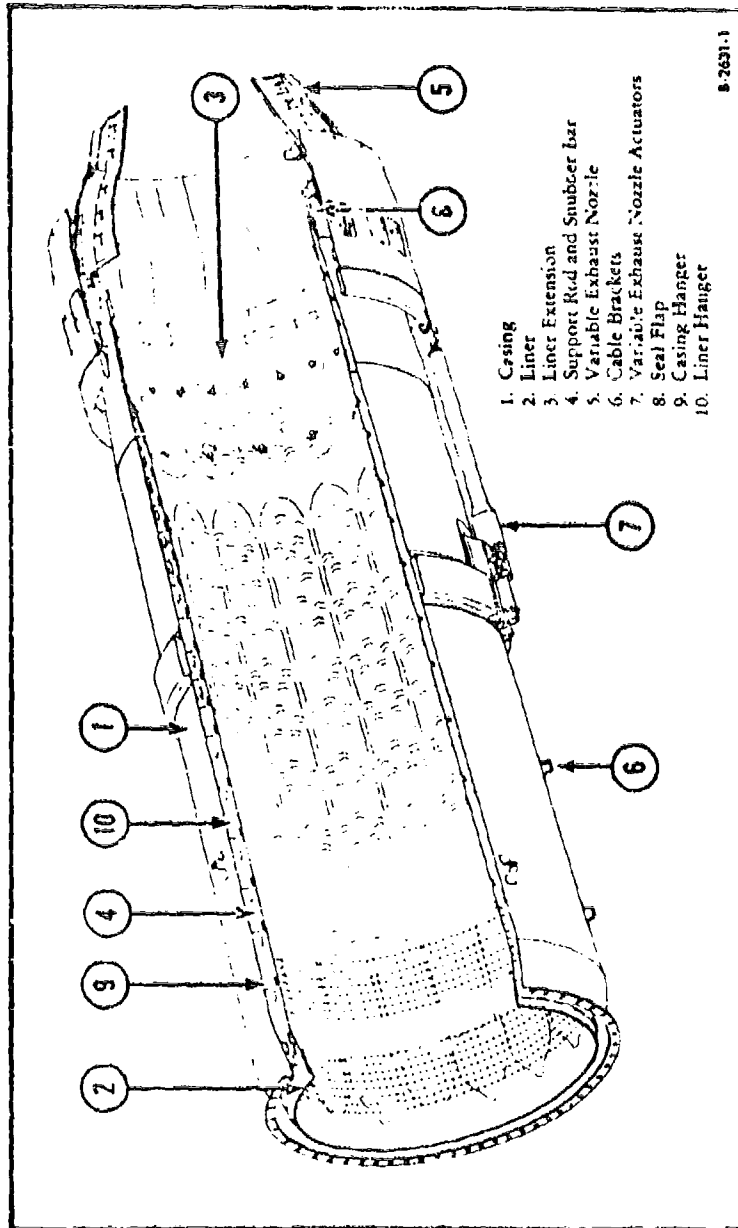


Figure 17. J85-5 Afterburner Casing and Variable Exhaust Nozzle Assembly.

several advanced aircraft, including the General Dynamics B-58 (the world's first supersonic bomber), the Lockheed F104, the McDonnell-Douglas F-4, and the Rockwell International RA-5C. A commercial version, the CJ805, powers the Convair 880 and 990 commercial transport aircraft.

5.1.2.1 Engine Specifications

The following are the important specifications for the J79-15 engine; the J79-8 is the U.S. Navy version and has similar specifications:

Weight	3685 lb
Length (cold)	2208.45 in.
Maximum Diameter (cold)	38.3 in.
Pressure Ratio (mil)	12.9
Airflow	169 lb/sec
RPM	7685
Maximum Thrust (SLS)	17,000 lb
Military Thrust (SLS)	10,900 lb

5.1.2.2 Engine Description

The J79-15 engine is an axial-flow turbojet engine with variable afterburner thrust. It incorporates a 17-stage compressor, of which the angles of the inlet guide vanes and the first 6 stages of vanes are variable; a combustion system which consists of 10 individual combustion liners situated between an inner and outer combustion casing; a 3-stage turbine rotor, which is coupled directly to the compressor rotor; and an afterburner system, which provides afterburner thrust variation through fuel flow scheduling and actuation of the variable-area, converging-diverging-type exhaust nozzle. The rotors are supported by three main bearings. Various engine systems control engine thrust by regulating engine speed, vane angle, fuel flow, exhaust nozzle area, and exhaust gas temperature. Interconnecting signals integrate the various controls so that the systems function as a single unit in response to the throttle.

5.1.2.3 Afterburner Description

To initiate afterburner operation, the throttle must be advanced beyond 76.5 degrees and the engine speed must exceed 90.3 percent. Figure 18 shows the afterburner and exhaust nozzle assembly. The afterburner fuel-air mixture is ignited by a torch igniter which extends into the exhaust duct. The flame of the torch igniter is provided by combining fuel from the main fuel manifold with air from the outer combustion casing. Flame stabilization is accomplished by three V-gutter-type flameholders.

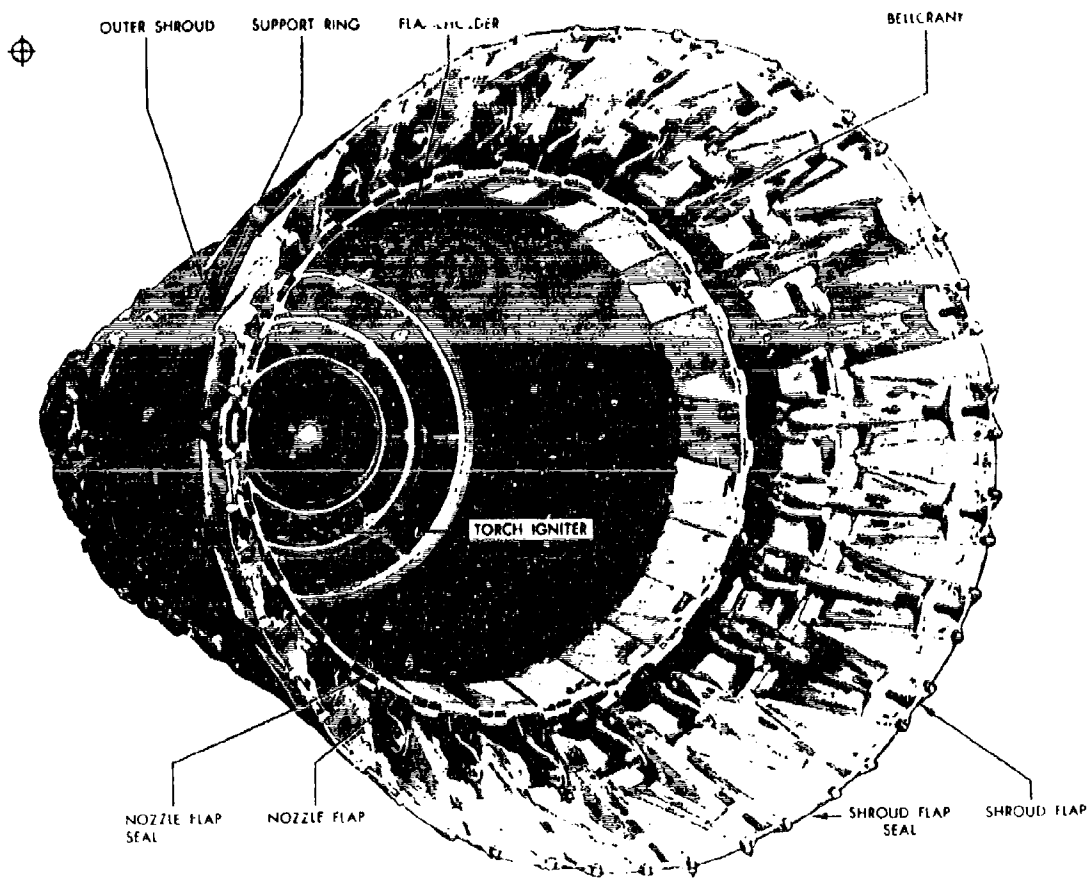


Figure 18. J79-15 Afterburner and Exhaust Nozzle Assembly.

Fuel is distributed by four fuel manifolds to 21 spraybars located in the exhaust diffuser section. Afterburner fuel flows to the fuel pressurizing valve consisting of four valves which divide the core fuel flow into primary core and secondary core, and the annulus fuel flow into primary annulus and secondary annulus. This division ensures that adequate pressures are maintained to prevent vaporization within the afterburner fuel tubes. Each pressurizing valve ports fuel to a fuel manifold, which delivers fuel to the spraybars. Each spraybar contains four separate tubes, one for each manifold. Holes in the sides of the tubes spray fuel into the exhaust gases. The primary and secondary core tubes inject fuel near the center of the exhaust gas stream; the primary and secondary annulus tubes spray fuel into the outer portion of the exhaust gas stream.

The exhaust nozzle causes the velocity of the air stream to increase by restricting its flow. The velocity of the exhaust gases past the throat (smallest) area is limited to the speed of sound within the gases. The exhaust nozzle assembly consists of 24 nozzle flaps and seals interconnected by flap actuators and bellcranks to the support ring. Attached to the support ring are 24 shroud flaps and seals. The support ring telescopes into the outer shroud. Through this arrangement, movement of the support ring toward the rear of the engine causes a simultaneous increase in the opening area of the primary and secondary exhaust nozzles.

5.2 ENGINE TEST FACILITY

All afterburner emissions measurements on this program were conducted at the North Site Test Facility at the General Electric Edwards Flight Test Center, Edwards Air Force Base, California. The North Test Site is in a relatively remote location, normally used for acoustic and infrared testing.

All engine controls, instrumentation readout, data acquisition equipment, and emissions analysis equipment were located in the control room. Figure 19 is a partial view of the interior of the control room. The two cabinets in the background contain the gas analysis instrumentation. On the right is the smoke measurement console, and the engine control console is in the foreground.

The engine support structure, stressed for the F101 engine thrust level, was mounted on the thrust table. The support structure was designed so as to support any of the engines with their centerline 12 feet above ground level. At that height, interference of the ground with the plume was prevented out to the farthest measurement station.

Figure 20 shows the J79-15 engine mounted on the test stand at the North Site Test Facility. The high temperature probe stands and actuators (with probes removed) are mounted on a moveable table so that the stands can be moved axially from the nozzle exit plane to a position 15 feet aft of the nozzle exit plane. Use of this arrangement facilitated changing of the axial location of the high temperature probes. In Figures 20, the low temperature probes are attached to the concrete pad at the 60-foot axial station.

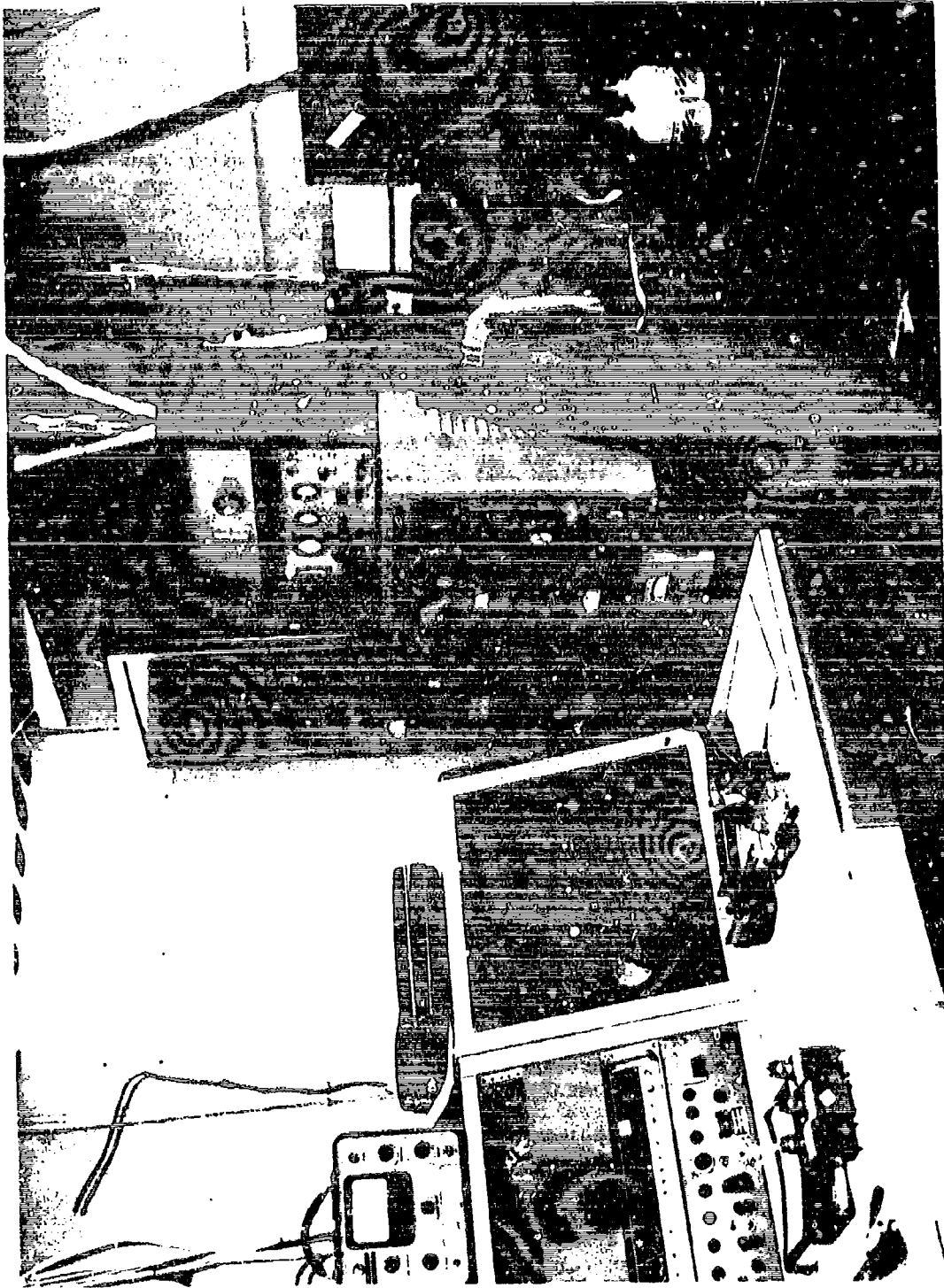


Figure 19. GE-Edwards Flight Test Center North Site Control Room Showing Gas Analysis System (Background), Smoke Console (Right), and Engine Run Console (Foreground).

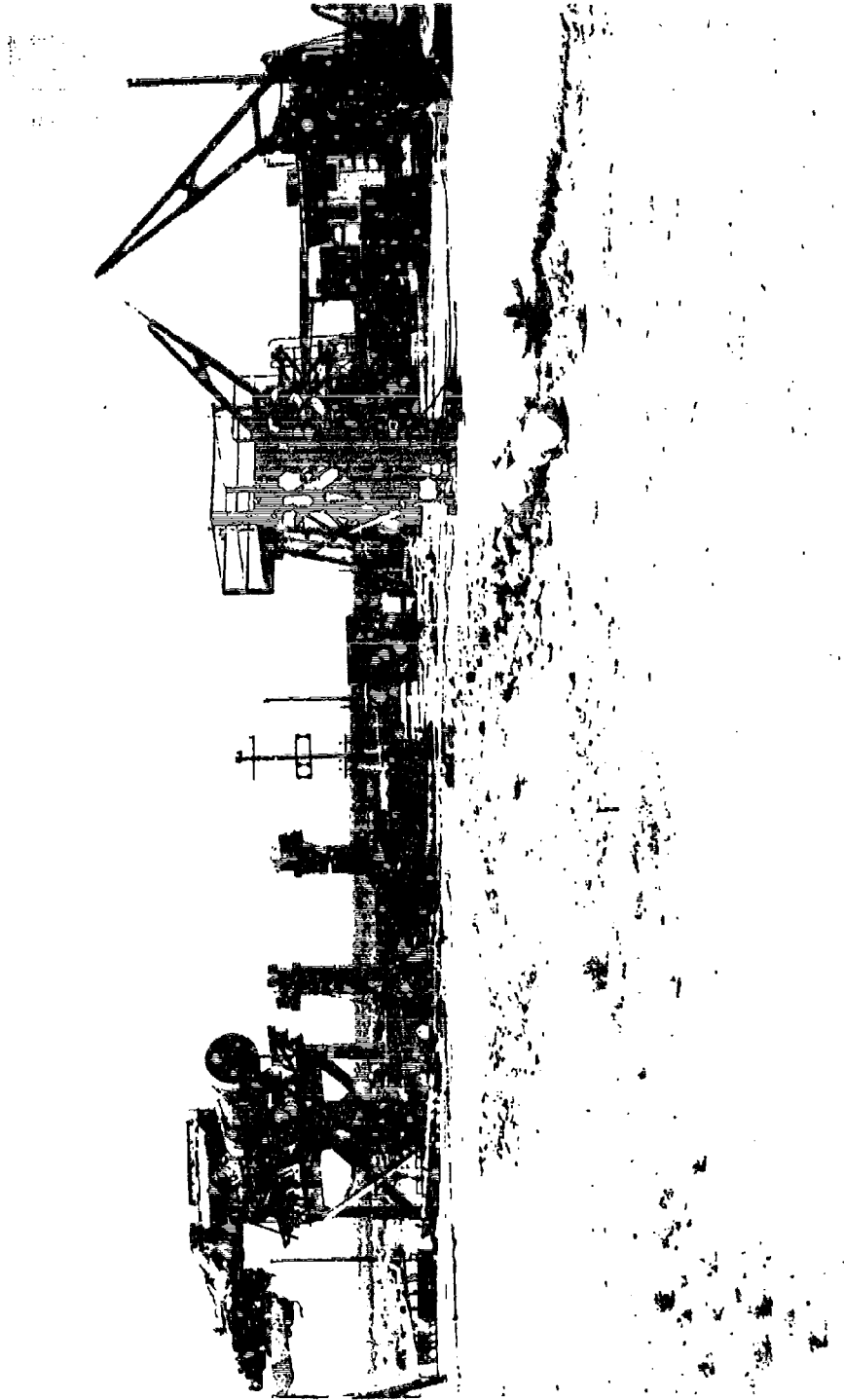


Figure 20. J79-15 Engine on Test Stand at GE-Edwards North Site Test Facility.

The control room at this test facility is partially underground and is located about 60 feet from the engine. Total sample line length was as long as 140 feet at the sampling station farthest from the engine. The engine inlet faced generally into the prevailing wind, and the engine exhausted over the dry lake bed.

Engineering drawings were made and issued at Edwards for the engine support structure and the low temperature probes. Drawings were made and issued at Evendale for the high temperature probes. A complete list of the drawings prepared for this program is given in Table 6.

5.3 DATA REDUCTION PROCEDURES

In the Phase II afterburner engine emissions tests, automated data acquisition equipment and computerized data reduction procedures were utilized as far as practical. The entire data reduction procedure was somewhat complicated by the fact that, in order to calculate true emissions levels, it was necessary to properly account for variations in local flow rates across the plume. The local flow rates were calculated from the total and static pressures and the total temperatures. At axial stations where the temperature was too high for total temperature and static pressure measurements, the total temperatures were calculated from the gas composition using an enthalpy balance procedure, and the static pressure was estimated to be the same as the ambient pressure. From the local flow rate and gas composition, the local emission flow rate and local fuel flow rate were calculated. Integration of these local values across the sampling plane gave the total emission flow rate and fuel flow rate at that axial station. Total emission index was calculated from the total emission flow and total fuel flow at a particular station. The total integrated fuel flow at each station was compared to the measured engine total fuel flow as a check on the consistency of the data.

The basic emission parameters (concentrations, total and static pressures) measured at the exhaust plane were also input to the plume model. The model was then used to calculate emission levels at the locations downstream of the nozzle for comparison with the measured values.

A brief description of the data acquisition and processing steps is given below.

5.3.1 PCM System

The PCM (pulse code modulation) system is a digital data acquisition system which was used to record all test data on magnetic tape. The test data included engine operating data along with the plume data. After appropriate preprocessing to convert to engineering units, additional calculations were performed with the plume data using the computer program described below.

Table G. Afterburner Emissions Tests - List of Drawings

	<u>Drawing Title</u>	<u>Drawing No.</u>	<u>Location</u>
1)	Support Assembly (A/B Emission Test)	56J117327	Edwards
2)	Modification - J93 Thrust Stand (A/B Emissions Test)	56J117329	Edwards
3)	Engine Mounting Systems - J79, J85, F101 (A/B Emissions Test)	56J117330	Edwards
4)	Mounting System - F101 Engine (A/B Emissions Test)	56J117331 Sheets 1 & 2	Edwards
5)	Low Temperature Rake (A/B Emissions Test)	56J117332	Edwards
6)	Support Assembly - Bellmouth, F101 (A/B Emissions Test)	56E117333	Edwards
7)	Sampling Probe - High Temperature	4013100-805	Evendale
8)	Probe Support Body	4013100-807	Evendale
9)	Clamp - Probe	4013100-808	Evendale
10)	Arm - Support	4013100-809	Evendale
11)	Clamp - Tube	4013100-810	Evendale
12)	Clamp- Tube	4013100-811	Evendale
13)	Tube - Cooling Details	4013100-812 Sheets 1 & 2	Evendale

CAROL Program: The CAROL computer program was an adaptation of an existing time-sharing data reduction program which basically calculates local composition and emission indices from the output of each analyzer (from the PCM system) and the analyzer calibration data, which was manually obtained before each test. The program was modified to include calculation of the radial probe position.

The equations used in calculating local fuel-air ratio and emission indices were, in general, those specified in ARP 1256 (Reference 29). However, a change was made in calculating local fuel-air ratio, in that the ambient air CO₂ content was not assumed to be zero as in the ARP 1256, but was taken as 0.03%, the standard air value. This difference was quite appreciable when samples were taken in very dilute regions of the plume where CO₂ concentrations approached ambient levels.

In order to calculate probe radial position, the probe was first set so that its projection passed through the projected engine centerline. In this position, the probe orifice to engine centerline distance was a small value, l (see Figure 21). The probe potentiometer was then calibrated as angular position θ versus potentiometer voltage. The orifice radial distance, R , from the engine centerline could then be calculated from the law of cosines, as shown in Figure 21, knowing the probing length L .

Output of the CAROL program was filed in the time-sharing system.

AREA Program: The AREA computer program was also a time-sharing system (TSS) program that used the CAROL output file for input. The AREA program converts the radial position of each probe measurement to an element of flow area to be represented by the measurement, and rewrites selected data in a second file. This program thus performed area weighting of the emissions measurements.

The data files written by CAROL and modified by AREA were manually supplemented by additional information not derived from the probe measurements, and were then transmitted directly to one of two batch computer programs, depending on whether the low temperature or the high temperature probe system was used.

EGT7 Program: Since temperature was not measured by the high temperature probes, program EGT7 was used to calculate gas temperature from the gas composition data. Computer program EGT7 is an existing batch program which calculates temperature using an enthalpy balance procedure. Basically, the total mixture enthalpy is first calculated from the inlet temperature and fuel-air ratio. An iterative procedure is then used to arrive at a final gas temperature which causes the sum of the enthalpies of the individual gas components to equal the total mixture enthalpy. Total mass balance and pseudo-equilibrium criteria are used to obtain concentrations of H₂, Ar, O₂, N₂, and OH.

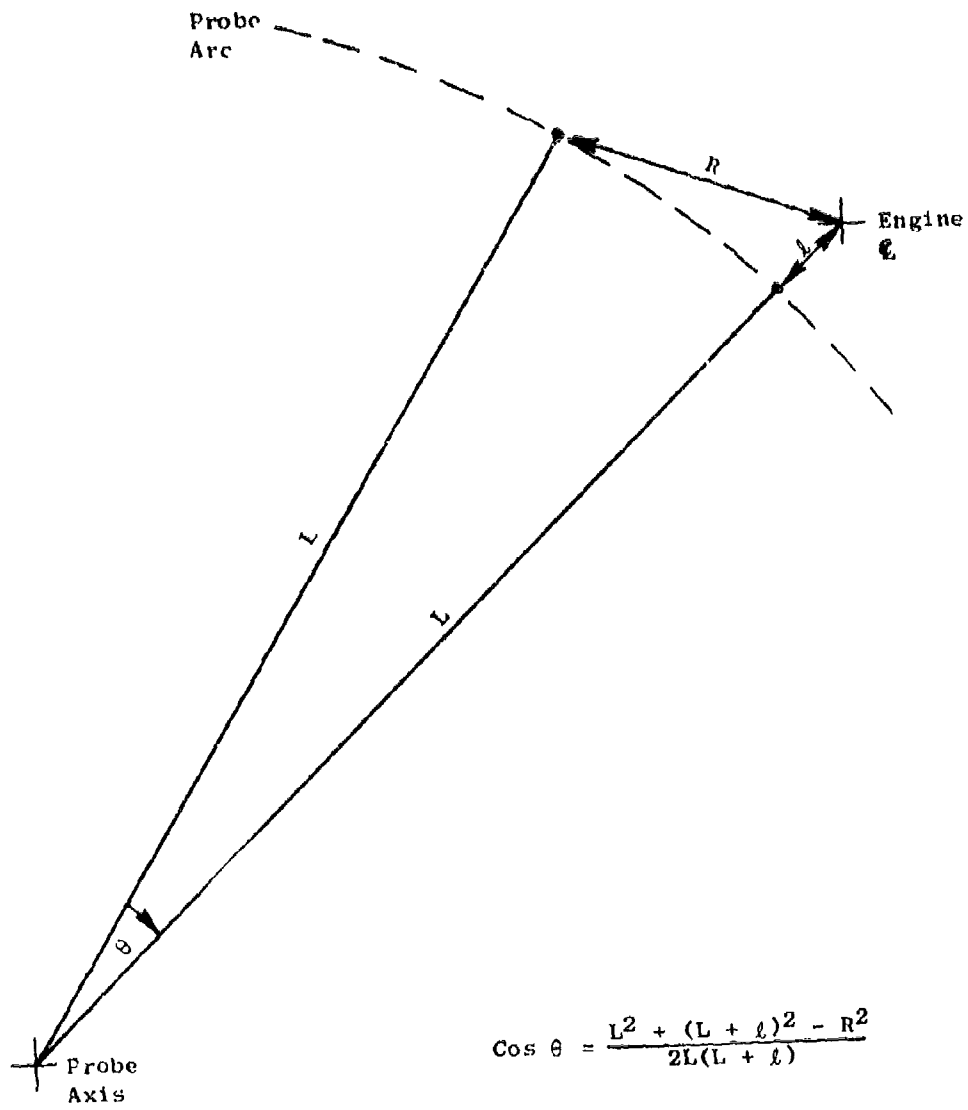


Figure 21. Relation of Probe Angle to Radial Position.

Using the calculated temperature, together with the measured total temperature and static (ambient) pressure, the local total mass flow (pounds per second per square inch) is calculated for each measured probe position. Local fuel flow rate (pounds per second per square inch) is calculated from the local total mass flow rate and local fuel-air ratio (from gas composition). Calculated values are entered, along with the flow area represented by the measurement, on a TSS file for subsequent input to program SCAPP (described below).

EGV1 Program: Computer program EGV1 is used with low temperature probe measurements. Local flow calculations procedures are similar to those used in EGT7 except that local total temperature is measured rather than calculated, and measured local static pressures, rather than ambient pressure, are used. As with EGT7, an output TSS file is created for subsequent input to SCAPP.

SCAPP Program: The SCAPP computer program (TSS) obtains emission indices directly from the CAROL output file and the local fuel flows and areas from EGV1 or EGT7, as appropriate. The local contaminant flow rate (pounds per second per square inch) and the contaminant flow, integrated across the plume, are calculated for each contaminant. The integrated fuel flow, along with the integrated contaminant flow, is used to calculate the overall (or integrated) emission index.

Figure 22 is a diagram showing the data processing steps. Raw data from the PCM system was obtained on magnetic tape and subsequently transferred to computer tape. Processing by a tape reader produced a printout of the raw data which was then examined for obvious errors. The corrected tape was then run through the engine preprocessor program and the plume preprocessor program. The plume preprocessor program output was put onto paper tape and subsequently transferred to a file in the time-sharing system (TSS). Up to this point, all data processing was done at Edwards Flight Test Center. The GE time-sharing system is accessible from both Edwards and Evendale, and subsequent processing was performed at Evendale. A permanent record of all plume preprocessor output was made on punch cards.

The data was then processed through the CAROL computer program, which gave a printed output and also a series of output cards (A, B, C, P, and T) for subsequent input to succeeding programs. Auxiliary programs NEWRAD and ABE, shown in Figure 22, are described later in this report.

5.4 J85-5 AFTERBURNER EMISSIONS TESTS

5.4.1 J85 Engine Setup and Instrumentation

The engine used was Model J85-5H, Serial Number 230-499, and was newly overhauled with total accumulated running time of 4827 hours. Table 7 is a listing of the engine and emissions instrumentation which were monitored by the PCM system. There were 90 channels of the PCM system available for test

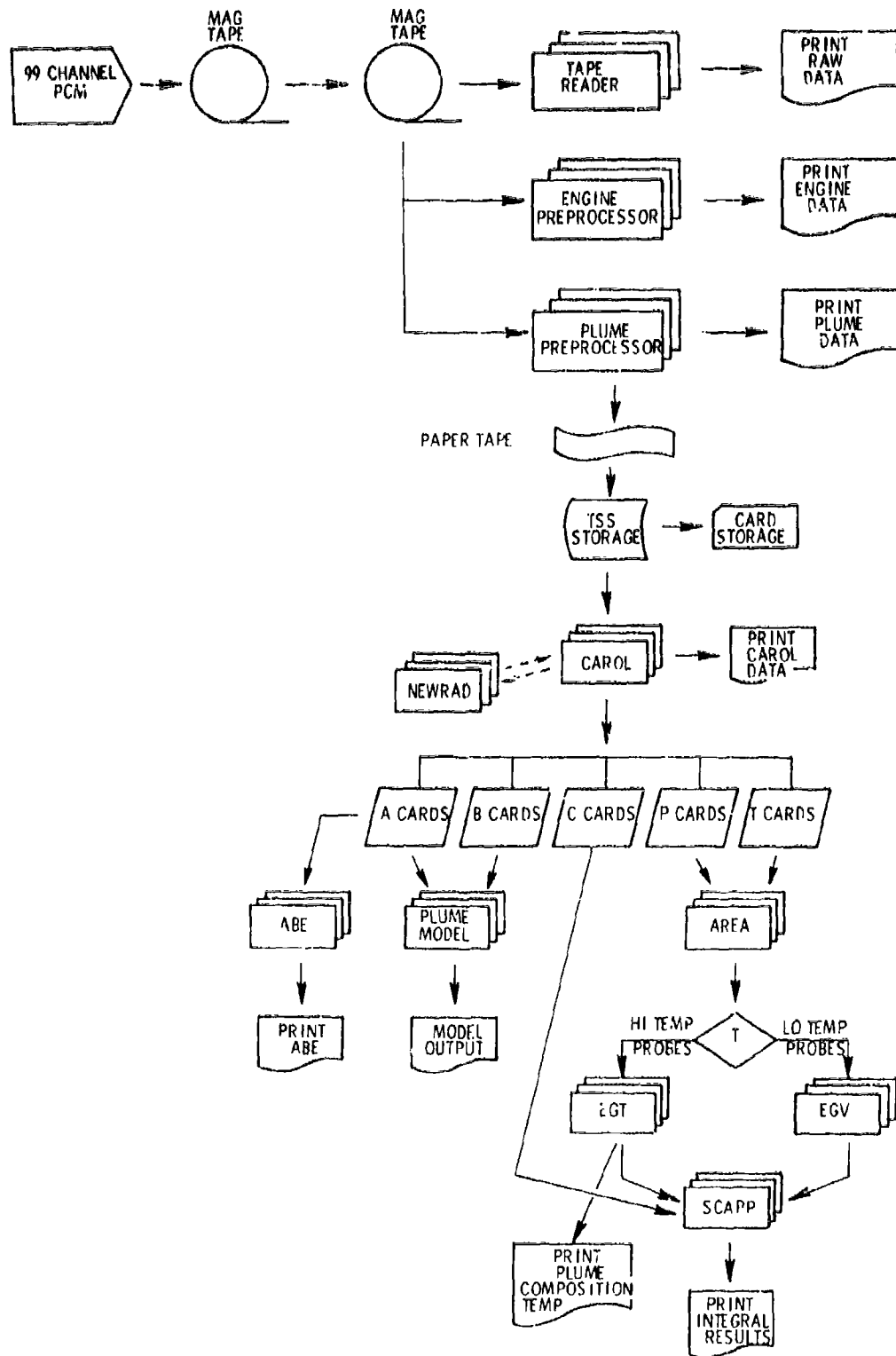


Figure 22. Engine Test Data Flow Chart.

Table 7. Instrumentation List for Afterburner Emissions Tests.

Item	No. Sensors	Extrg. Units	Description	Item	No. Sensors	Extrg. Units	Description
NG	1	rpm	Engine speed.	15CO	1	psig	Support #1 coolant outlet pressure.
T54	1	deg. C	Turbine Discharge temperature.	25CO	1	psig	Support #2 coolant outlet pressure.
PT2	4	psia	Engine inlet total pressure (bellmouth).	WPM	1	ppm	Main engine fuel flow.
PT3	4	psia	Engine inlet static pressure (bellmouth).	TFI	1	ppm	Total engine fuel flow.
TT1	2	deg. F	Engine inlet total temperature (bellmouth).	MFT	1	deg. F	Main fuel temperature.
TT2	1	deg. F	Compressor discharge total temperature.	TFI	1	deg. F	Total fuel temperature.
PT3	1	psia	Compressor discharge total pressure.	CO2A	1	--	Switch signal for CO analyzer range.
H1P	1	psia	High temperature probe #1 total pressure.	CO2RA	1	--	Switch signal for CO ₂ analyzer range.
H2P	1	psia	High temperature probe #2 total pressure.	CO2RA	1	--	Switch signal for CO ₂ analyzer range.
L1P	1	psia	Low temperature probe #1 total pressure.	HGRA	1	--	Switch signal for H ₂ analyzer range.
L2P	1	psia	Low temperature probe #2 total pressure.	HGRA	1	--	Switch signal for H ₂ analyzer range.
L3P	1	psia	Low temperature probe #1 static pressure.	PS30	1	--	Switch signal for probe number 1 of NO _x .
L4P	1	psia	Low temperature probe #2 static pressure.	NO-NOM	1	--	Switch signal for NO or NO ₂ reading.
L5P	1	psia	Low temperature probe #2 static pressure.	CO-CFLL	1	--	Switch signal for CO cell temp at start.
PT7	1	deg. R	Low temperature probe #1 total temperature.	PS1A	1	--	Switch signal for probe station.
PT8	2	deg. R	Low temperature probe #2 total temperature.	CO	1	ppm	CO analyzer output.
PT9	8	deg. F	Sample line temperature.	CO ₂	1	ppm	CO ₂ analyzer output.
PI1P	1	psia	Probe #1 sample pump inlet pressure.	HC	1	ppm	HC analyzer output.
PI2P	1	psia	Probe #2 sample pump inlet pressure.	NO	1	ppm	NO analyzer output.
PI3P	1	psia	Analyzer pump inlet pressure.	WQC	1	--	Counter for reading number.
ST	1	deg. F	Steam temperature.	PIA	1	deg.	Power lever angle.
IC1P	1	psig	Probe #1 coolant inlet pressure.	A6	1	in ²	Engine nozzle throat area.
IC2P	1	psig	Probe #2 coolant inlet pressure.	FC	1	lbs	thrust.
IC3P	1	psig	Probe #1 coolant outlet pressure.	PIP	1	mv	Probe #1 position potentiometer output.
IC4P	1	psig	Probe #2 coolant outlet pressure.	P2P	1	mv	Probe #2 position potentiometer output.
2G0F	1	psig	Probe #2 coolant outlet pressure.	PIV	1	volt	Probe #1 position potentiometer input.
				P2V	1	volt	Probe #2 position potentiometer input.

instrumentation, of which typically 70 to 80 were used. Selected channels (up to 10) could also be monitored continuously on digital meters. In addition to monitoring on the PCM system, the output of each analyzer along with probe position and total pressure were recorded on an eight-channel direct-writing recorder (Beckman Instruments, Type RC Dynograph).

The testing proceeded as planned, with a total of 20 separate test points, which consisted of engine operation at four power settings (military, minimum afterburner, mid-afterburner, and maximum afterburner). At each of the four power settings, complete plume profiles were obtained at five axial stations (nozzle exit, 3.75, 7.5, 15, and 30 feet aft). The 5 axial stations corresponded to approximately 0, 3, 6, 12, and 24 nozzle diameters downstream.

The J85 engine is normally limited to operation for five minutes at maximum afterburning power. Since each test point required 40 to 50 minutes of engine operation, excessive cycling of the engine would have been involved if the five-minute limit had been followed. After appropriate consultation, it was decided to adhere to a 30-minute limit at maximum A/B, since this would result in less total engine operating time. In addition, the consensus of opinion was that less engine distress would occur from the prolonged steady operation than from the repeated cycling.

5.4.2 J85 Emissions Test Data

The detailed emissions test data are tabulated in Supplement I of this report. Tables presented there give composition, fuel-air ratio, emission indices, total and static pressure, total temperature, and fuel and contaminant flow rates at each radial position for each test point. Selected parameters are plotted in this section of Volume I to illustrate the variation with radial and axial position and with engine power level.

Table 8 is a summary of the J85 engine test data. Each entry is the numerical average of all data taken for that particular test point. Most of the column headings are described in Table 7. Note that WFAB is the afterburner fuel flow. Ambient conditions of temperature (T_0), pressure (P_0), absolute humidity, and wind speed and direction were manually recorded at various times during each test. In the case of a double entry in the wind speed and direction columns, the numbers indicate maximum and minimum values. In setting test points, throttle setting alone was used for the military power condition. At the A/B power points, a total fuel flow was chosen and maintained in setting each power condition.

JP4 fuel was used for all tests. Fuel samples were taken periodically during the Phase II tests and submitted for analyses. Table 9 gives the fuel analyses for both the J85 and J79 tests. All values reported were within limits given in Specification MIL-T-5624J.

Figure 23 shows the effect of power level on the radial fuel-air ratio distribution at the nozzle exit for Probe No. 1. A general increase of fuel flow with power setting occurs, with the fuel being injected mainly into the annular flame stabilization region. Figure 24 shows similar profiles obtained at the 7.5-foot axial station. At this station, mixing has resulted in the development of typical plume profile shapes. Note that this station is near the end of the potential core, as previously planned, and, as indicated by the fact that the centerline fuel-air ratio and temperature, is about the same as at the nozzle exit location. Figure 25 shows fuel-air profiles obtained at the 30-foot axial station. At this distance, the plume is quite diluted by mixing with surrounding air, and concentrations near the edge of the plume are approaching ambient levels. It may be noted that the standard air concentration for CO₂ (0.03%) corresponds to a fuel-air ratio of about 0.00015. Data from Probe No. 2 shows similar radial profiles, but are not included on the plots in order to maintain clarity.

Figure 26 shows the NO_x radial profile at the nozzle exit plane for the various power levels. Note that little NO_x is formed in the afterburner at minimum A/B power. Some NO_x is formed at the higher A/B power settings, mainly in the high temperature burning region. Figure 27 shows similar NO_x profiles at the 7.5-foot station, where the typical plume distribution has developed. Note that the centerline concentration of NO_x actually increases between 0 and 7.5 feet even though the total NO_x remains constant, as will be shown later. The reason for the increase in centerline NO_x is that the centerline concentration is lower than in the surrounding annular region at the nozzle exit, and thus increases with distance as it mixes with the gas of higher concentration. Figure 28 shows NO_x radial profile 30 feet aft of the nozzle exit plane at various power levels. As with the fuel-air ratio data, extremely low NO_x levels were obtained near the edge of the plume. However, the NO_x levels at the 30-foot station seem to be high in proportion to the fuel-air ratio.

Figure 29 shows the CO concentration profile at various axial distances at minimum A/B power level. The centerline concentration remains essentially constant to the end of the potential core (7.5 feet), which indicates little consumption of CO. Beyond 7.5 feet, mixing occurs into the centerline, and the plume spreads more rapidly.

Figure 30 shows the CO concentration profile at various axial distances at maximum A/B power level. In contrast to the data at minimum A/B, the centerline concentration decreases at each successive axial station, indicating considerable consumption of CO in the plume.

Smoke measurements were made on the J85 engine at the nozzle exit plane. Very little, if any, smoke was obtained, as judged by the appearance of the smoke tapes. It was suspected that smoke was being lost, either in the sample line or the pump, and further smoke measurements on the J85 were not made. The sampling system is not well-suited to the measurement of low smoke numbers.

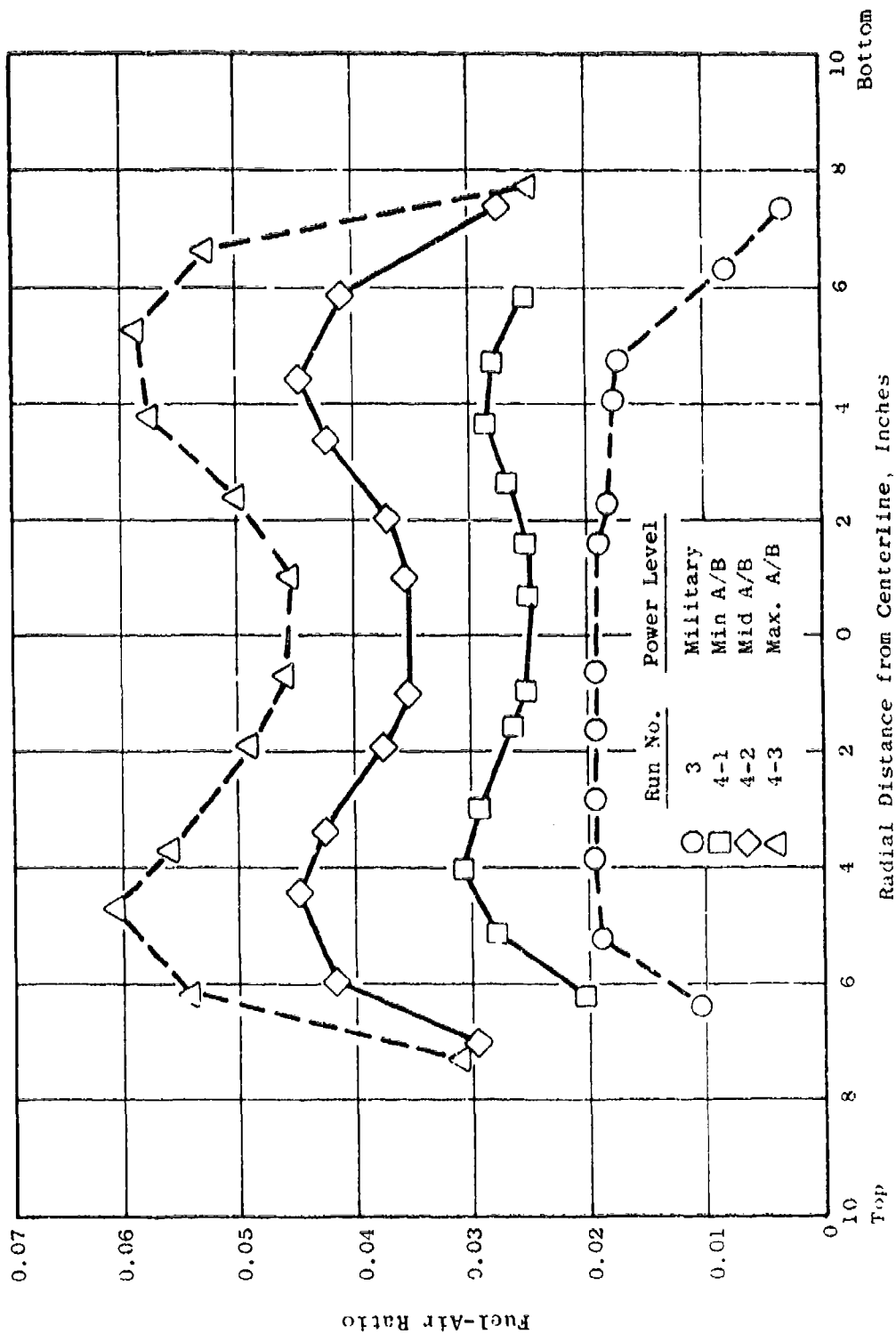


Figure 23. Effect of Power Level on Radial Distribution of Fuel-Air Ratio at Nozzle Exit, J85-5 Engine, Probe No. 1.

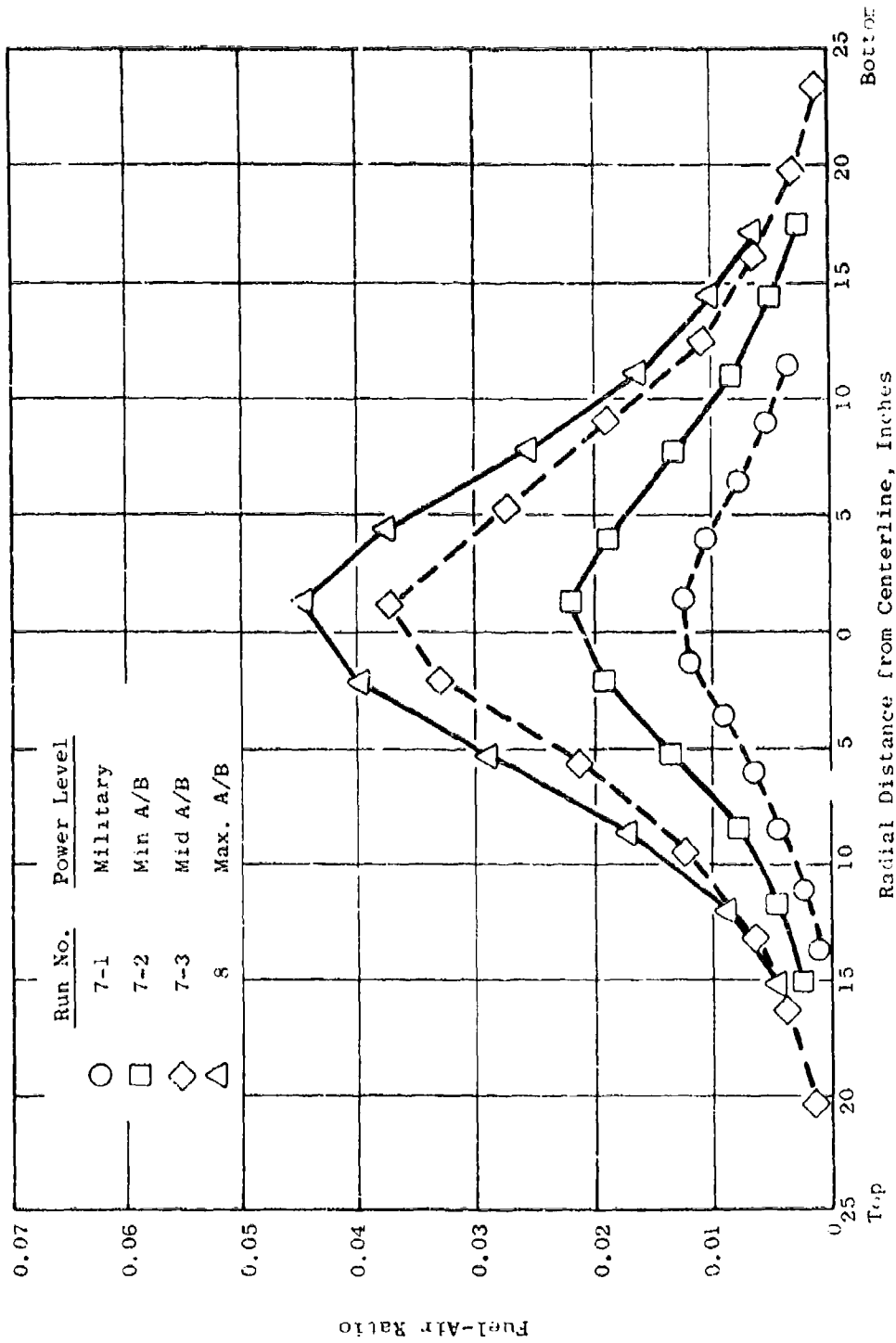


Figure 24. Effect of Power Level on Radial Distribution of Fuel-Air Ratio 7.5 feet Aft of Nozzle Exit, J85-5 Engine, Probe No. 1.

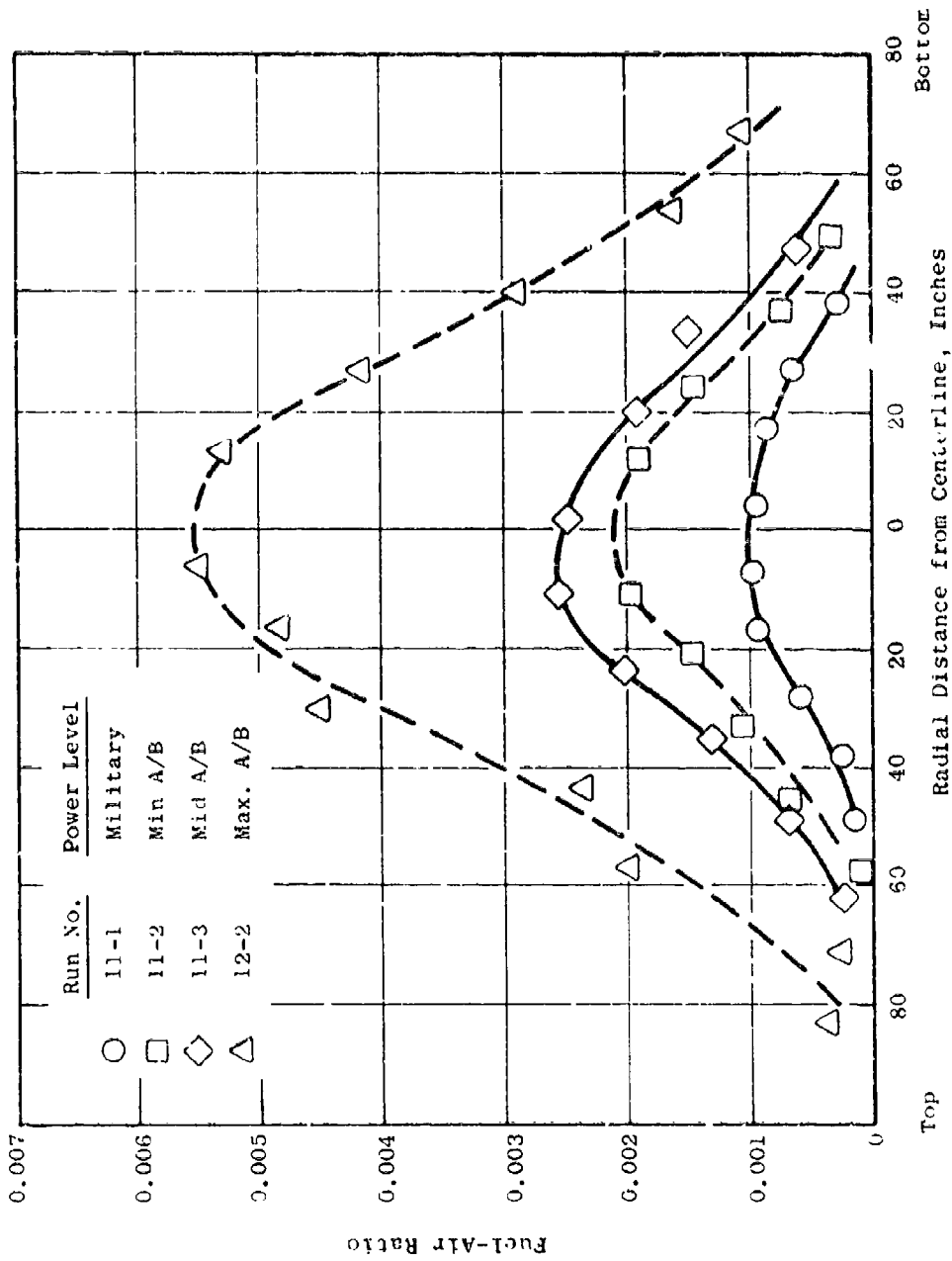


Figure 25. Effect of Power Level on Radial Distribution of Fuel-Air Ratio 30 feet Aft of Nozzle Exit, J85-5 Engine, Probe No. 1.

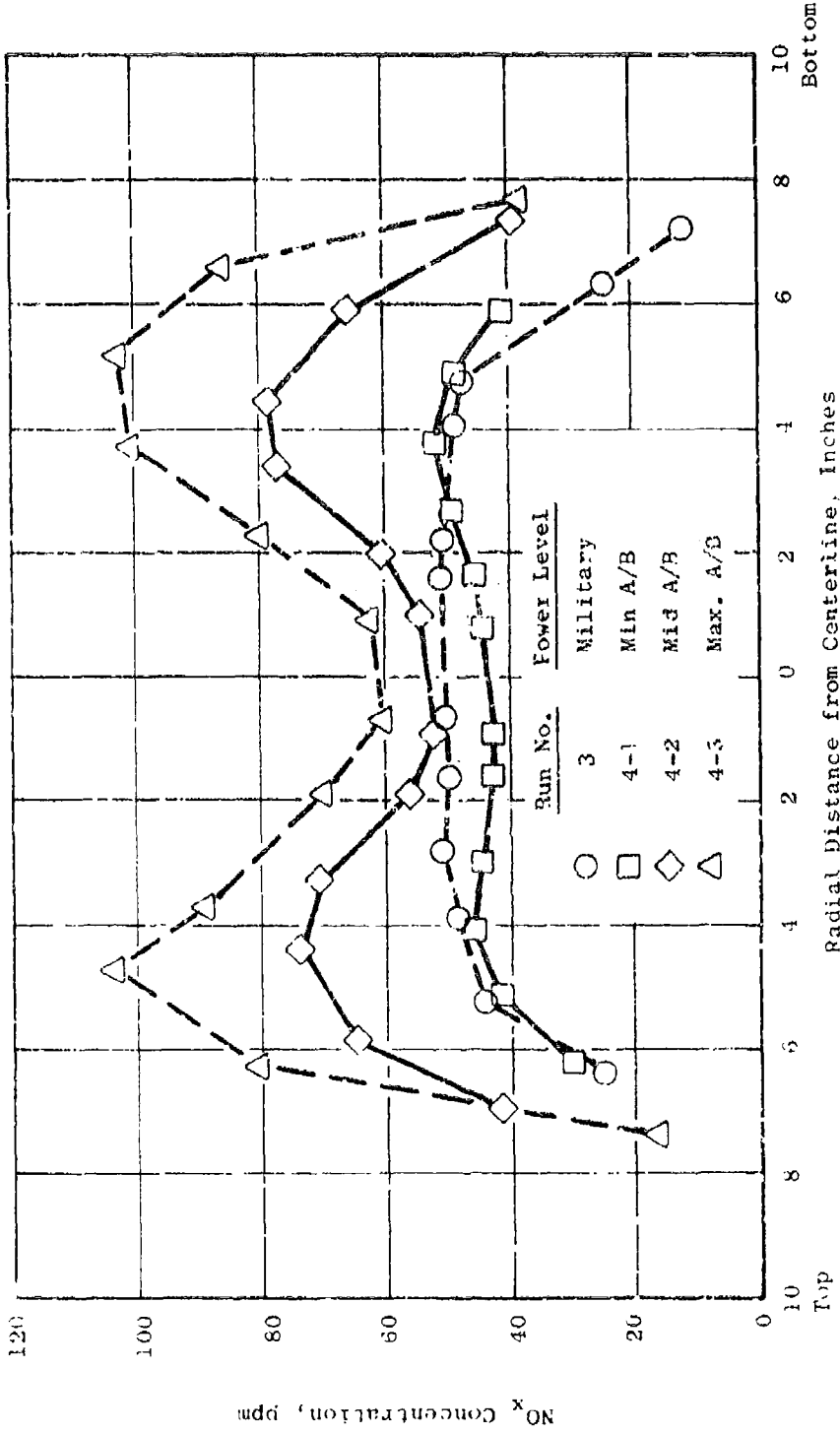


Figure 26. Effect of Power Level on Radial Distribution of NO_x at Nozzle Exit, J85-5 Engine. Probe No. 1.

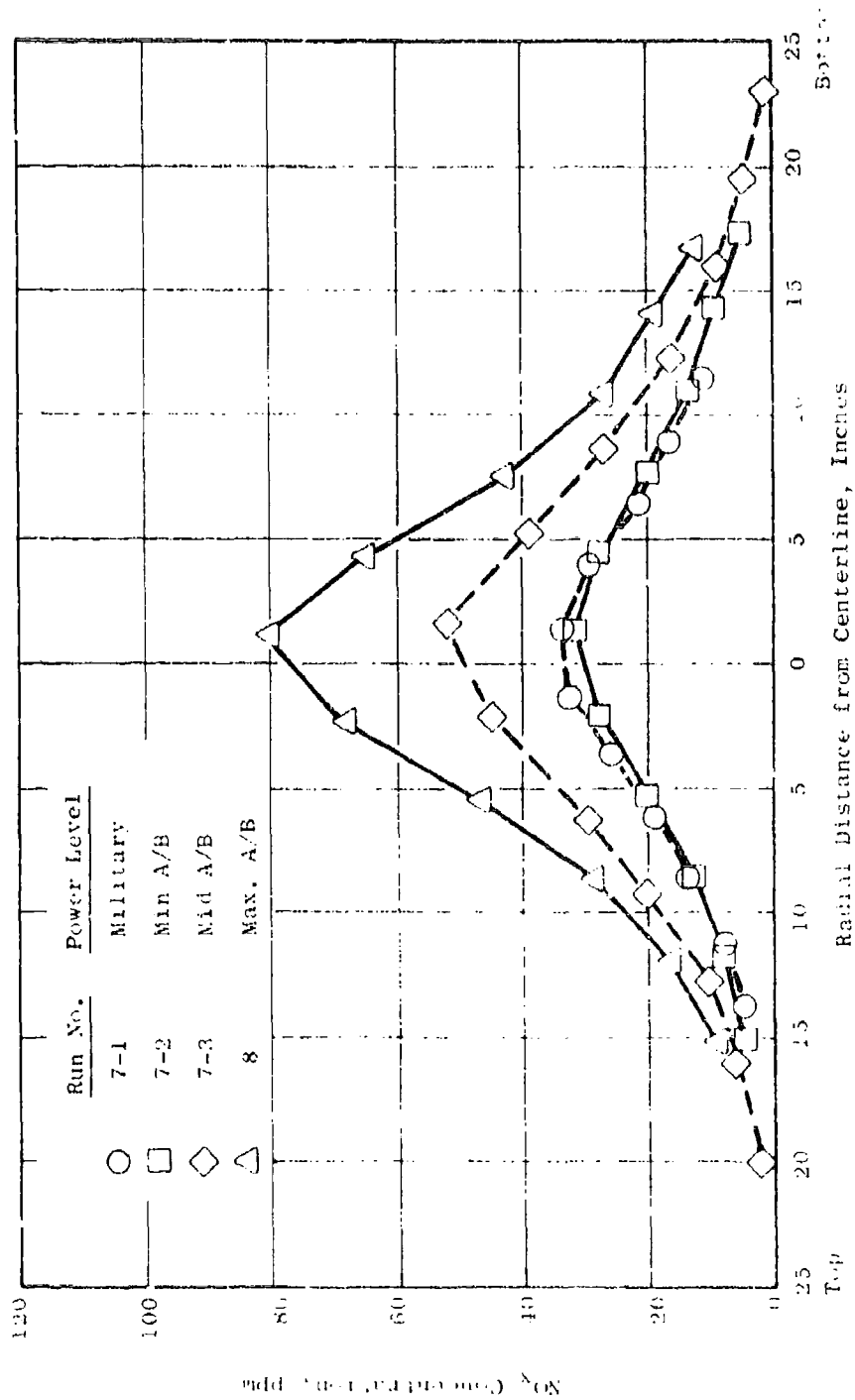


Figure 25 Effect of Power Level on Radial Distribution of NO_x 7.5 feet Aft of Nozzle Exit.
 185-5 Engine, Probe No. 1.

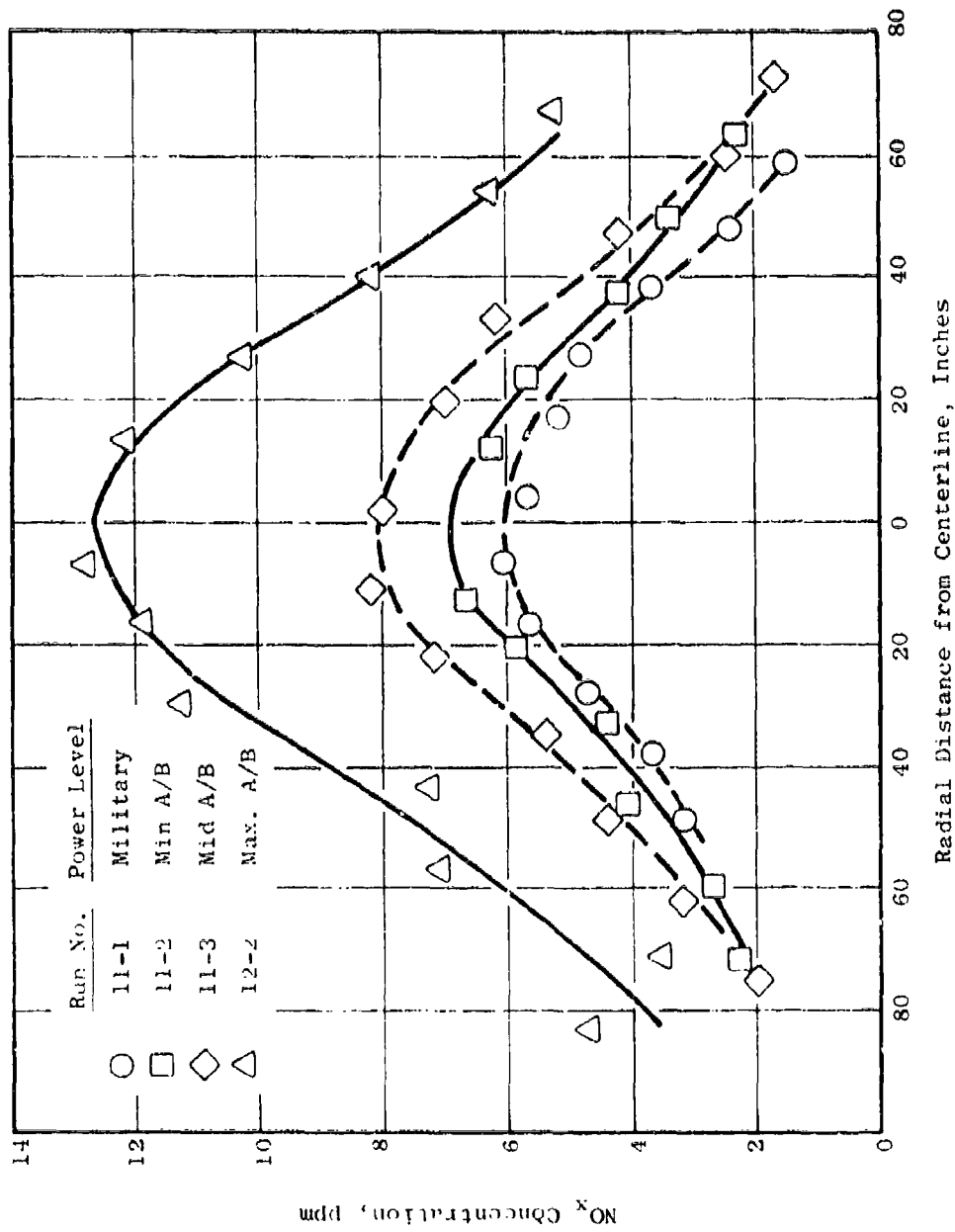


Figure 28. Effect of Power Level on Radial Distribution of NO_x 30 feet Aft of Nozzle Exit, J85-5 Engine, Probe No. 1.

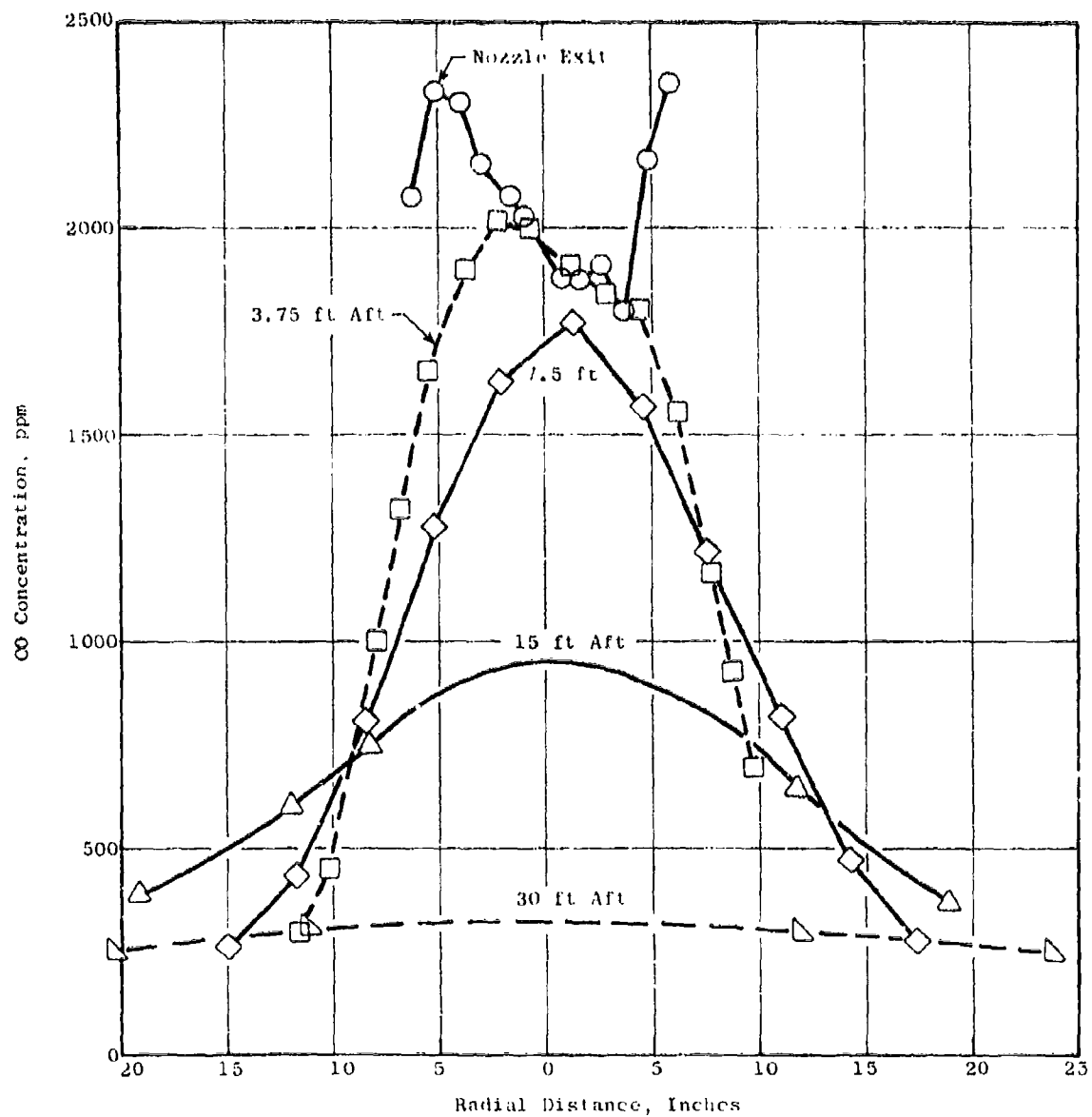


Figure 29. CO Concentration Profile at Various Axial Distances for J85-5 Engine at Min. A/B Power (Probe No. 1).

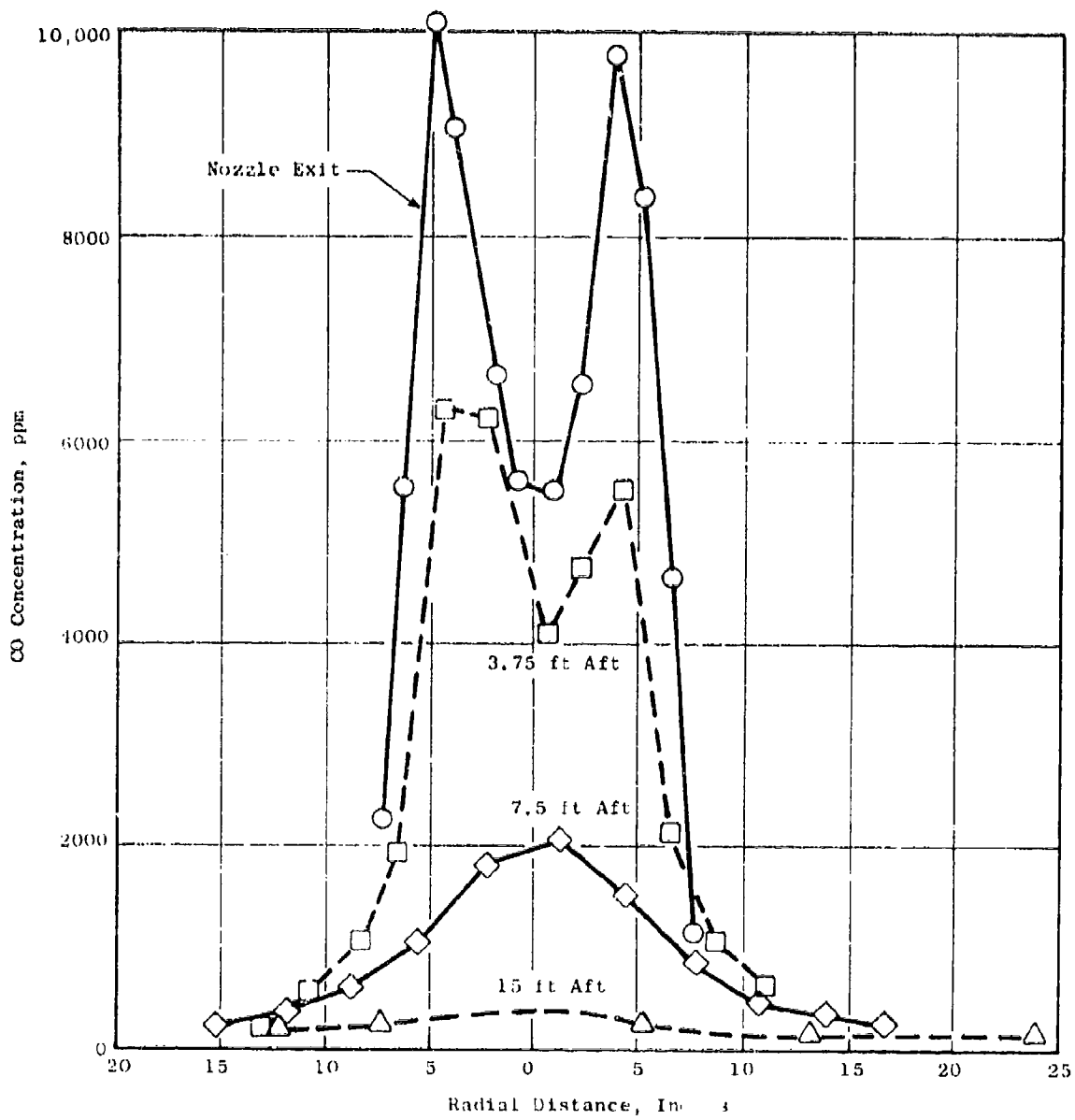


Figure 30. CO Concentration Profile at Various Axial Distances for J85-5 Engine at Max. A/B Power (Probe No. 1).

5.4.3 Adjustment for Plume Symmetry

It was noted that, at the farthest downstream locations (15 and 30 feet aft), the apparent plume centerline did not coincide with the projected engine centerline. An analytical method was devised for locating the center of symmetry of the plume in relation to the engine centerline. At the farthest downstream locations, the integration over the plume area was then performed with respect to this axis of symmetry, rather than around the projected engine centerline.

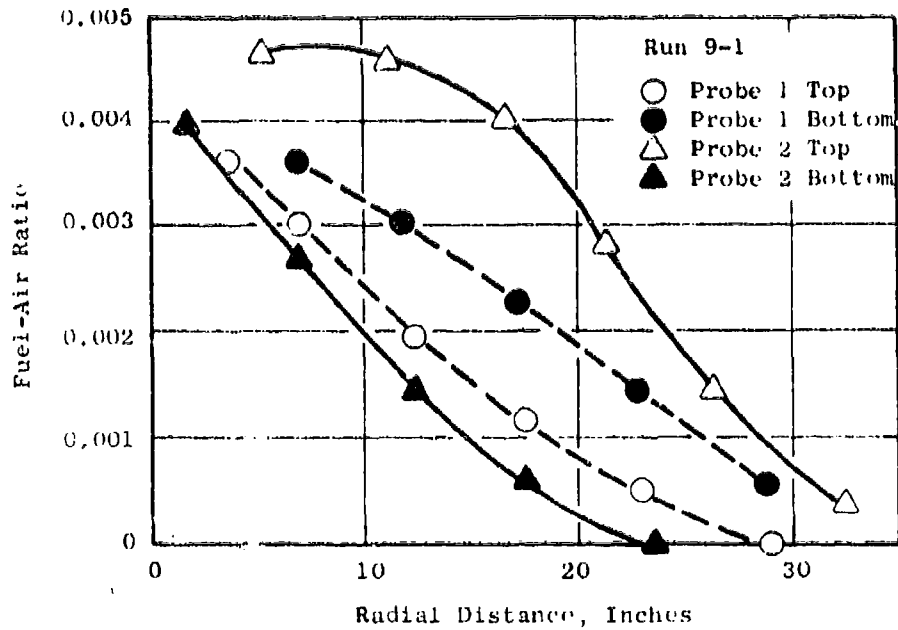
Figure 31 demonstrates this effect on the fuel-air ratio profile. Figure 31(a) shows the fuel-air ratio profile at military power, 15 feet aft of the nozzle exit with the origin at the projected engine centerline. Figure 31(b) shows the same data after adjusting for symmetry. The origin is shifted 3.7 inches downward along the path of Probe 1 and 6.8 inches upward along the path of Probe 2, for a total shift of 7.7 inches. This is an angular separation of 2.5 degrees.

It should be noted that this shifting of the origin involves no additional assumptions, since the assumption of circular symmetry of the plume is already contained in the area integration calculations. The adjustment for circular symmetry generally results in a decrease in calculated flow for all species, compared to that calculated with the origin not at the center of symmetry. An additional computer program (NEWRAD) was written to perform this calculation, and all data at the 15 and 30-foot axial stations were adjusted for symmetry. All radial distances quoted in this report have been adjusted for plume symmetry. The adjustments required to shift the origin to the center of symmetry for the J85 are tabulated in Table 10.

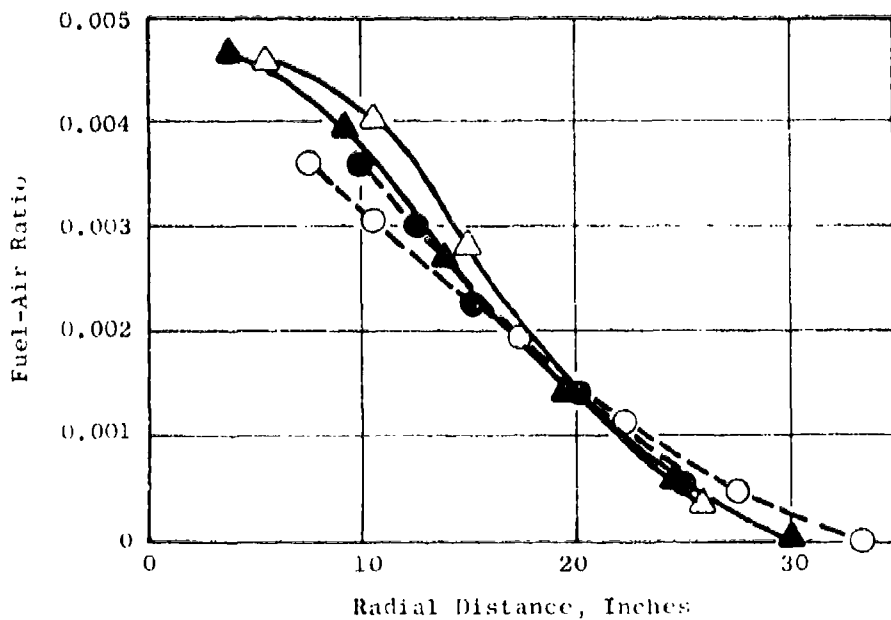
Although the detailed causes for the apparently unsymmetrical plume have not been determined, it is believed that a part of the discrepancy is due to inaccurate measurement of the projected engine centerline. Additional factors may be that the engine does not exhaust precisely along its centerline, or that the engine is slightly loose in its mounting so that its axis can vary slightly. Note that a small shift in the center of symmetry could cause appreciable error in the integrated values. It should also be noted that the true center of symmetry cannot be located with a single diametral probe sweep.

5.4.4 Calculation of Integrated Results for J85

All J85 plume data were processed through the integral computer programs (Figure 22) to yield the integral flow rates for fuel, CO, HC, and NO_x along with the corresponding emission indices. These values are given in Table 11 along with the metered fuel flow. A very valuable test of the validity of the data is the agreement between the calculated and metered fuel flow at each axial station. Examination of these data show that generally good agreement between the calculated and measured fuel flow is obtained for axial stations near the nozzle exit plane (0, 3.75, and 7.5 feet aft of nozzle), while con-



(a) Origin at Projected Engine Centerline



(b) Origin Shifted 7.7 Inches for Symmetry Adjustment

Figure 31. Radial Fuel-Air Ratio Profiles for J85-5 Engine at Military Power, 15 feet Aft of Nozzle Exit, With and Without Symmetry Adjustment.

Table 10. Adjustment of Plume Centerline Required to Shift Origin to Center of Symmetry for J85 Engine.

<u>Run No.</u>	<u>Axial Station (ft.)</u>	<u>Power Setting</u>	<u>Probe 1 Change (in.)</u>	<u>Probe 2 Change (in.)</u>	<u>Total Adjustment (in.)</u>	<u>Angular Separation (degrees)</u>
9-1	15	Mid	+3.7	+6.8	7.7	2.5
9-2	15	Min A/B	0	+7.3	7.3	2.3
9-3	15	Mid A/B	+5.1	0	5.1	1.6
10-2	15	Max A/B	+3.5	+1.4	3.8	1.2
11-1	30	Mid	+5.2	-3.7	6.4	1.0
11-2	30	Min A/B	-4.7	-7.5	8.9	1.4
11-3	30	Mid A/B	-5.5	0	5.5	0.9
12-2	30	Max A/B	-1.0	-4.1	5.6	0.9

Notes: a. Positive change is upward along the probe orifice path; negative change is downward.

b. Angular separation is the displacement as measured from the center of the exhaust nozzle.

Table 11. Integrated Results - J85-5 Afterburner Emissions Tests.

Run No.	Power Level	Axial Station, ft.	Metered Fuel Flow, pps	Calculated Flow Rate,			Emission Index, lb/1000 lb fuel			
				Fuel	CO	HC	CO	HC	NO _x	
3	Mid	0	0.683	0.687	0.0263	0.0009	0.0030	38.4	1.3	4.4
5	Mid	3.75	0.689	0.614	0.0232	0.0011	0.0029	37.8	1.8	4.7
7-1	Mid	7.5	0.708	0.654	0.0269	0.0012	0.0030	41.1	1.8	4.7
9-1	Mid	15.0	0.719	0.508	0.0329	0.0021	0.0040	55.0	3.5	6.7
11-1	Mid	30.0	0.714	0.280	0.0193	0.0000	0.0029	68.9	0.0	10.3
4-1	Min A/B	0	1.196	1.343	0.1077	0.1031	0.0033	80.1	76.8	2.4
6-1	Min A/B	3.75	1.169	0.943	0.0851	0.0482	0.0026	90.2	51.1	2.8
7-2	Min A/B	7.5	1.173	1.173	0.1042	0.0587	0.0029	88.8	50.1	2.5
9-2	Min A/B	15.0	1.176	0.984	0.1274	0.0644	0.0036	129.0	65.4	3.7
11-2	Min A/B	30.0	1.172	0.569	0.0739	0.0416	0.0020	130.0	73.1	3.4
4-2	Mid A/B	0	1.690	1.811	0.1076	0.0161	0.0047	59.4	8.9	2.6
6-2	Mid A/B	3.75	1.734	1.785	0.0665	0.0028	0.0042	37.3	1.6	2.4
7-3	Mid A/B	7.5	1.726	2.139	0.0589	0.0021	0.0049	27.5	1.0	2.3
9-3	Mid A/B	15.0	1.739	1.828	0.0642	0.0027	0.0059	35.1	1.5	3.2
12-1	Mid A/B	30.0	1.713	0.897	0.0460	0.0000	0.0048	51.2	0.0	5.4
4-3	Max A/B	0	2.184	2.017	0.2458	0.0020	0.0051	122.0	1.0	2.5
6-3	Max A/B	3.75	2.250	2.396	0.1600	0.0005	0.0056	66.8	0.2	2.3
8	Max A/B	7.5	2.323	2.232	0.0872	0.0008	0.0063	39.1	0.3	2.8
10-2	Max A/B	15.0	2.289	2.263	0.0475	0.0000	0.0069	21.0	0.0	3.0
12-2	Max A/B	30.0	2.234	1.790	0.0575	0.0035	0.0077	32.1	2.0	4.3

Note: Profiles at 15 and 30-foot stations adjusted for symmetry.

siderable discrepancy between metered and calculated fuel flow exists at the downstream locations (15 and 30 feet aft).

Considerable evidence links this discrepancy to an error in the CO₂ measurement causing the measured CO₂ value to be slightly less than the true values. This was later found to be caused by an electrical interaction between the PCM system and the CO₂ analyzer. Since the effect was small, no significant error was introduced for high CO₂ concentrations, such as were obtained near the nozzle exit. At the very low concentrations encountered for the downstream locations, considerable error was introduced.

The erroneously low CO₂ value at the downstream locations is consistent with the calculated local temperatures lower than measured values (see Supplement 1 data tabulation) and the emission indices, both local and integral values, higher than values which would be consistent with the nozzle exit location values. The contaminant flow rate is nearly independent of CO₂ value and forms a more consistent set of data.

Note that integrated contaminant flow rate and corresponding emission index should generally remain constant or decrease with axial distance. There seems to be one exception to this, as indicated by the increase in CO emission index between the nozzle exit plane and 3.75 feet aft at Min A/B power level. This is explained by the partial oxidation of HC to CO in the same axial range. The decrease in HC is more than sufficient to account for the increase in carbon as CO.

With the foregoing observations in mind, the following conclusions concerning the axial variation of contaminant flow may be made for the J85:

1. No significant change in NO_x concentration occurs in the plume at any power level.
2. At military power, no significant change in CO or HC occurs.
3. At minimum A/B power, a small increase in CO occurs along with a decrease in HC.
4. At mid A/B and maximum A/B power, significant decreases in both CO and HC occur, with HC values ultimately approaching zero.

5.5 J79-15 AFTERBURNER EMISSIONS TESTS

5.5.1 J79 Emissions Test Data

The engine tested was a J79-15, Serial Number 439-012, and was newly overhauled with a total accumulated running time of 2317 hours. Engine and emissions instrumentation was basically the same as that for the J85, listed in Table 7. As with the J85, 20 separate test points were run, consisting of the four power settings with plume profiles obtained at each of 5 axial stations ((nozzle exit, 7.5, 15, 30, and 60 feet aft). As with the J85, the 5 axial stations corresponded to approximately 0, 3, 6, 12, and 24 nozzle diameters downstream.

Engine operating data for the Phase II emissions tests are given in Table 12. Column headings are the same as for the J85 tabulation except W_2 (engine airflow). Detailed emissions data for the J79 tests are presented in Supplement 1 of this report. Selected parameters are plotted in this section of the report to illustrate the variation with radial and axial position and with engine power levels.

As previously mentioned, the afterburner on the J79-15 engine has a fuel system with four manifolds and fuel injection tubes: primary core, secondary core, primary annulus, and secondary annulus. As afterburner fuel flow increases, the fuel pressurizing valve operates to deliver fuel to the four manifolds in succession. The afterburner emissions test points are such that at minimum A/B power, there is partial core flow; at mid A/B power, there is full core flow and partial primary annulus; at maximum A/B, there is full flow to all four manifolds.

Figure 32 shows the fuel-air ratio profiles for the J79 at the nozzle exit, for the four power settings. With increasing afterburner fuel flow, the peak fuel-air ratio moves toward the outside as proportionally more fuel flows to the annulus manifolds. Little change in fuel-air ratio near the engine centerline occurs over the entire range of afterburner operation. The increase in exhaust diameter with afterburner power level is due to the opening of the exhaust nozzle. Figure 33 shows similar fuel-air ratio profiles 7.5 feet aft of the nozzle exit where considerable mixing has already occurred. Figure 34 shows fuel-air profiles at 15 feet aft of the nozzle exit, which is near the end of the potential core, as indicated by the fact that ambient air has not mixed to the centerline. At this location, typical plume profiles of fuel-air ratio have developed.

Rather severe gradients, especially in HC, may be encountered at the nozzle exit location for afterburner operation. The gradients are particularly steep for the J79 at mid A/B power level, as shown in Figure 35 where HC concentration (log scale) is plotted against radial position at the nozzle exit. The minimum in the HC curve corresponds to those regions in the afterburner where the combination of good flame stabilization and favorable fuel-air ratio leads to excellent combustion efficiency. The flame does not effectively spread outside these regions, and relatively poor burning occurs.

The change in shape of the HC concentration profile with axial distance is shown in Figure 36. Note that at the 7.5-foot station the extremely high HC concentration along the centerline has been completely consumed. Considerably higher concentrations exist near the top of the plume (left side in the figure) and this asymmetry persists out to 60 feet. The hydrocarbons that mix toward the center of the plume are consumed in the high temperature gases at least down to 15 feet, where a depression still persists in the center. At 30 feet aft, the centerline temperature is too low for rapid consumption of HC, and the concentration near the center is increasing. The centerline concentration is thus a maximum at the nozzle exit and rapidly decreases to zero with axial distance. After the centerline temperature reaches a low enough value, the centerline concentration rises to a second maximum and then gradually decreases as mixing with ambient air continues.

Table 12. J79-15 Engine Data for Phase II Afterburner Emissions Tests - JP-4 Fuel.

Notes	Time	Power (HP)	WFI (lb)	Fuel (lb/hr)	W (lb)	F _g (lb)	W _g (ppm)	P _{ad} (psia)	T ₃ (°F)	T ₅ (°F)	T ₅ (in ²)	Ans. Hous. (hr/lb)	T ₅ (in ²)	T ₅ (in ²)
1	1:00	4000	11.0	150.83	11.07	7671	163.46	376	27.1	11.512	30.1	11	62.1	425.6
1	1:01	4000	11.0	153.42	11.06	7673	160.09	384	26	11.2	30.1	11	62.1	425.6
1	1:02	4000	11.0	160.75	11.06	7653	162.51	394	26	11.2	30.1	11	62.1	425.6
1	1:03	4000	11.0	159.85	11.07	7675	164.21	361	24	11.2	30.1	11	62.1	425.6
1	1:04	4000	11.0	161.92	11.061	7675	165.3	351	24	11.2	30.1	11	62.1	425.6
1	1:05	4000	11.0	161.1	11.07	7675	161.09	377	27	11.2	30.1	11	62.1	425.6
1	1:06	4000	11.0	161.25	11.06	7675	159.75	366	24	11.2	30.1	11	62.1	425.6
1	1:07	4000	11.0	160.75	11.06	7675	162.46	366	27	11.2	30.1	11	62.1	425.6
1	1:08	4000	11.0	160.25	11.07	7675	161.43	366	27	11.2	30.1	11	62.1	425.6
1	1:09	4000	11.0	161.31	11.06	7675	164.76	364	26	11.2	30.1	11	62.1	425.6
1	1:10	4000	11.0	161.82	11.07	7675	165.34	374	26	11.2	30.1	11	62.1	425.6
1	1:11	4000	11.0	163.26	11.07	7679	163.45	373	23	11.2	30.1	11	62.1	425.6
1	1:12	4000	11.0	160.21	11.06	7675	161.55	373	22	11.2	30.1	11	62.1	425.6
1	1:13	4000	11.0	155.71	11.061	7675	162.09	375	24	11.2	30.1	11	62.1	425.6
1	1:14	4000	11.0	157.71	11.061	7675	161.60	369	24	11.2	30.1	11	62.1	425.6
1	1:15	4000	11.0	156.51	11.07	7671	162.35	373	26	11.2	30.1	11	62.1	425.6
4/2	1:16	4000	11.0	161.34	11.062	7675	164.37	354	21	11.2	30.1	11	62.1	425.6
4/1	1:17	4000	11.0	161.17	11.07	7675	165.36	363	22	11.2	30.1	11	62.1	425.6
1	1:18	4000	11.0	161.45	11.065	7675	164.08	357	23	11.2	30.1	11	62.1	425.6
1	1:19	4000	11.0	161.37	11.061	7675	161.05	382	25	11.2	30.1	11	62.1	425.6
1	1:20	4000	11.0	161.37	11.061	7675	161.05	382	25	11.2	30.1	11	62.1	425.6

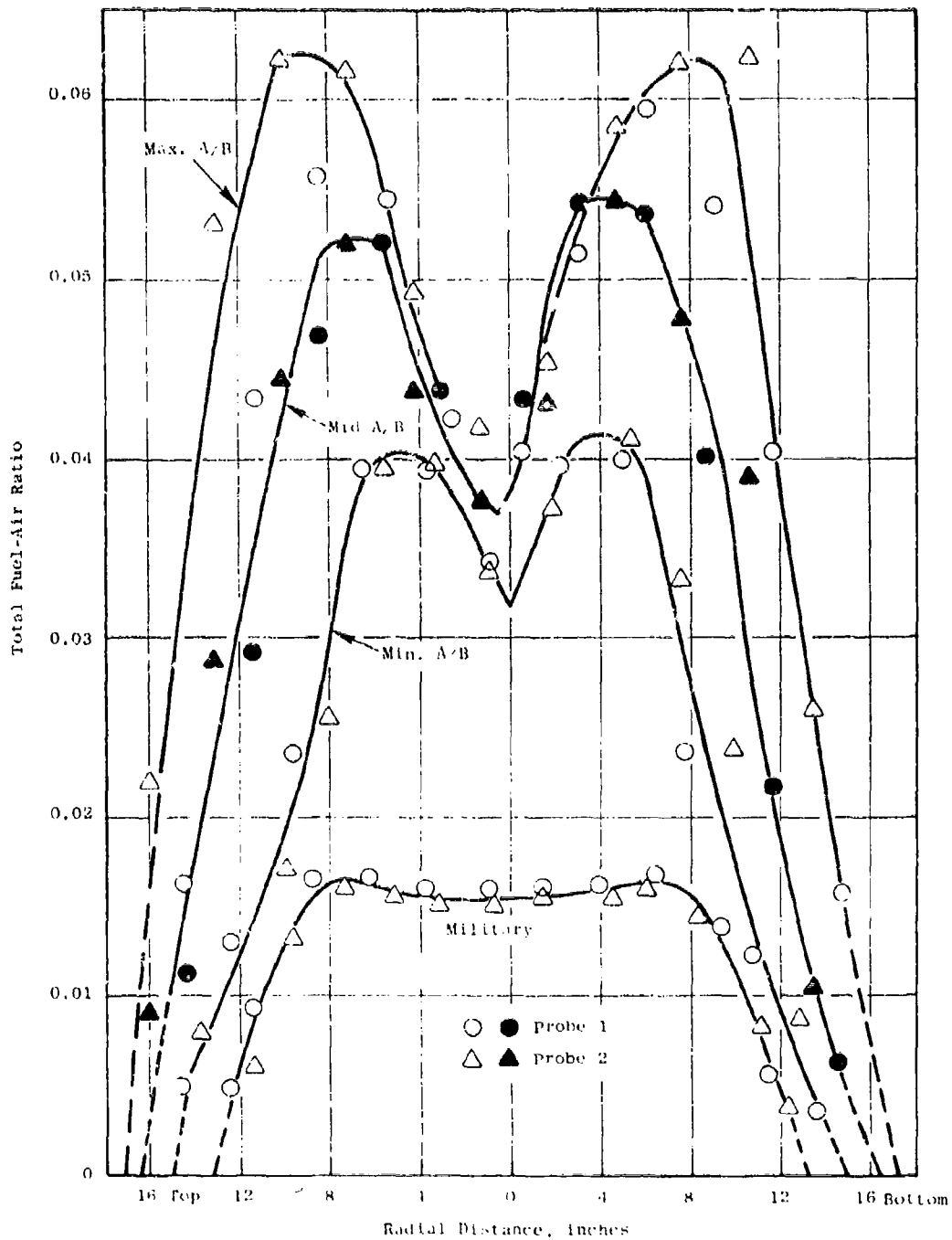


Figure 32. Radial Fuel-Air Ratio Profiles at Nozzle Exit for J79-15 Engine at Various Engine Power Levels.

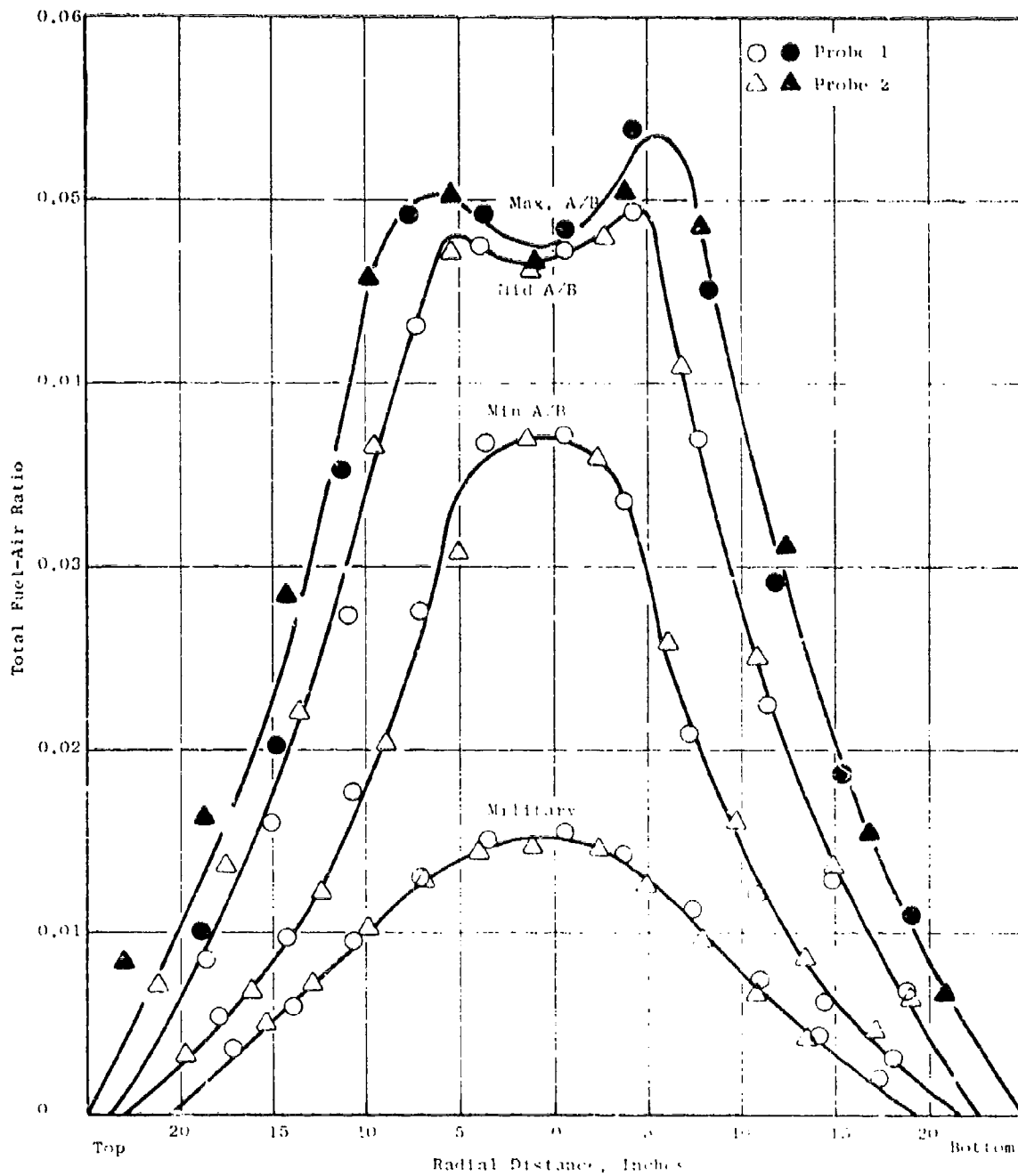


Figure 33. Radial Fuel-Air Ratio Profiles for J79-15 Engine at 7.5 feet Aft of Nozzle Exit for Various Power Levels.

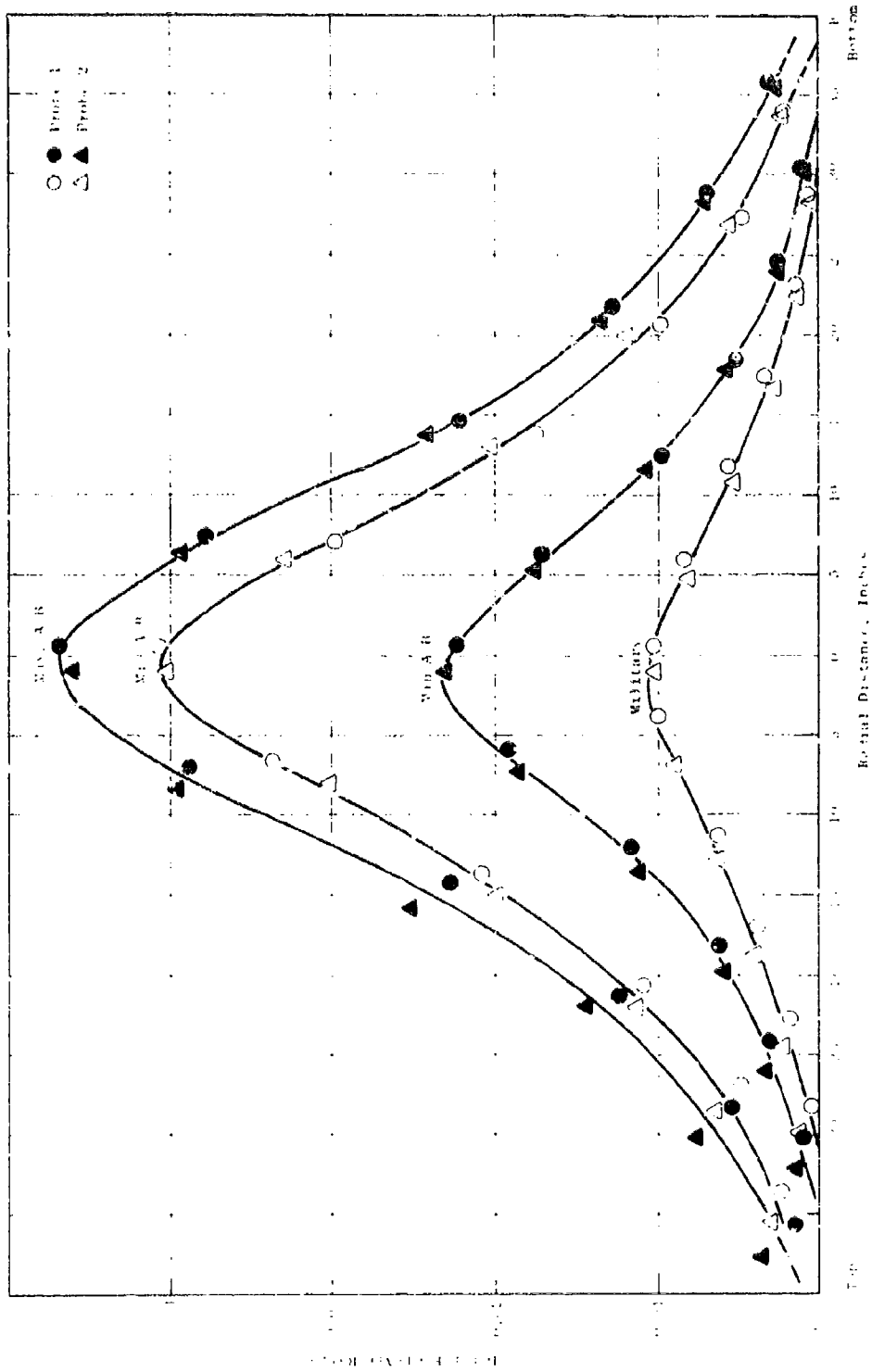


Figure 34. Radial Fuel-Air Ratio Profiles for J79-13 Engine at 15 feet Aft of Nozzle Exit for Various Power Levels.

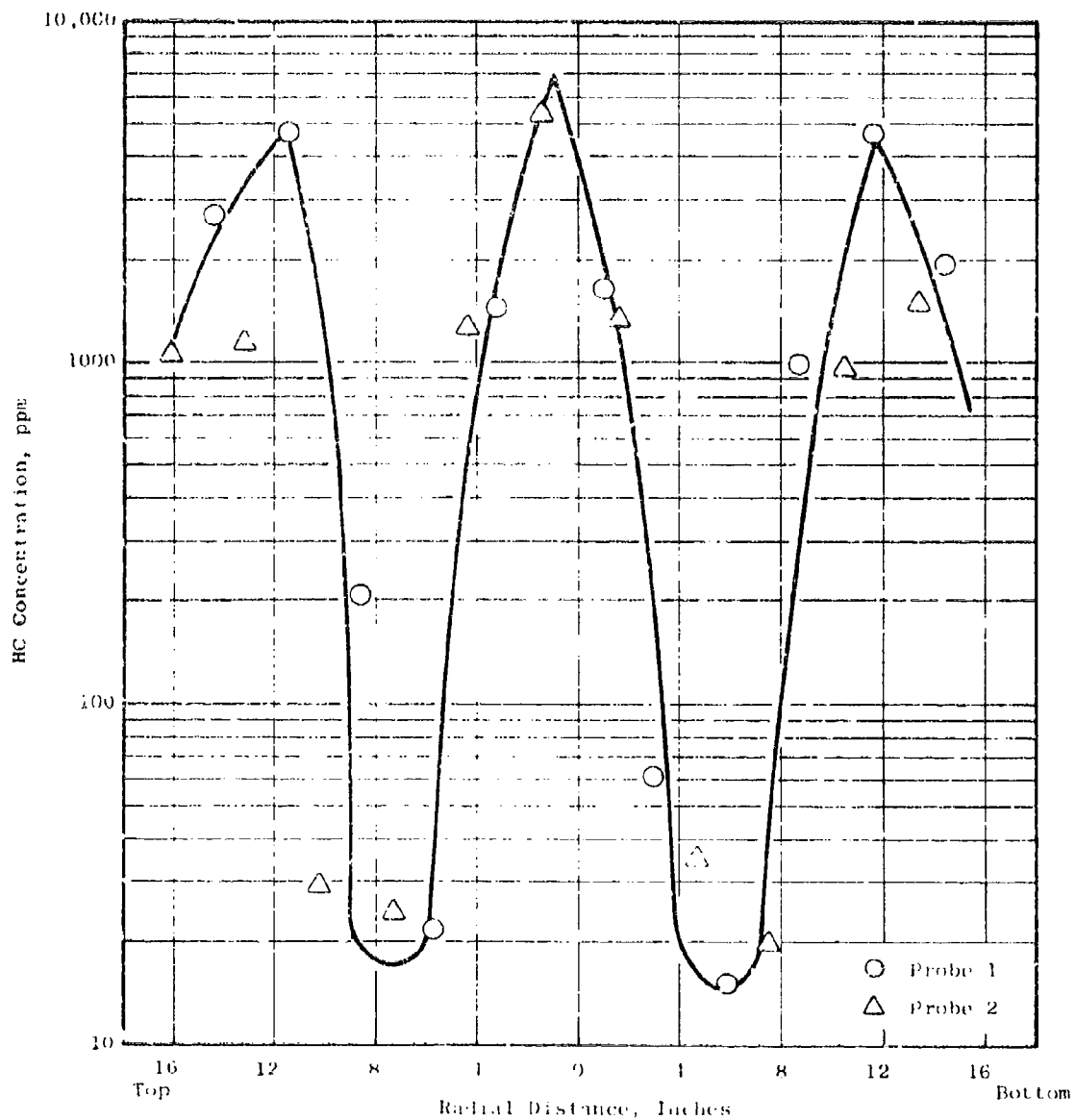


Figure 35. Radial HC Concentration Profile at Nozzle Exit for J79-15 Engine at Mid A-B Power Level.

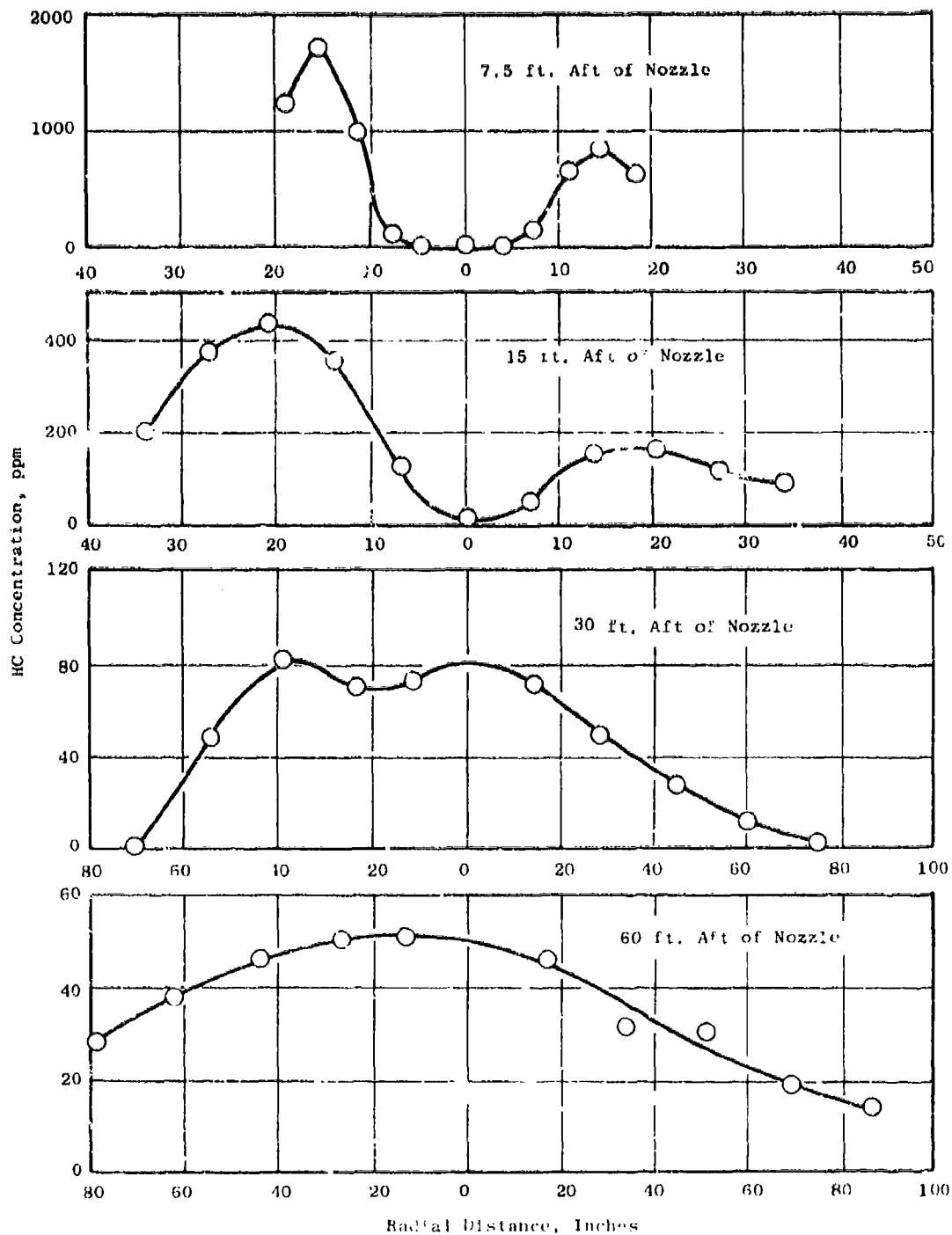


Figure 36. HC Concentration Radial Profile, J79-15 Engine at Mid. A/B Power Level.

5.5.2 Calculations of Integrated Results for J79

All J79-15 engine afterburner data from the Phase I engine tests were processed through the integral computer programs to give integral flow rates and the corresponding emissions indices. The profiles at the 30- and 60-foot stations were adjusted for symmetry using the NEWRAD computer program, as described in the previous section on the J85.

Adjustments required to move the origin to the apparent center of symmetry of the plume for the J79 are listed in Table 13 for each run at the 30- and 60-foot axial stations. A positive change is upward along the probe orifice path and a negative change is downward. The total adjustment is the diagonal shift, calculated from the two mutually perpendicular changes. The angular separation, as measured from the center of the engine exhaust nozzle, is quite small at the 60-foot axial station, being less than one degree in each case. At the 30-foot station, angular separations are greater, being between 1.0 and 1.5 degrees in each case.

Results of the calculations of integrated values for the J79 are given in Table 14. At the sampling stations closest to the engine (0, 7.5, and 15 feet), generally good agreement between the calculated and the metered fuel flows was obtained. At the 30- and 60-foot sampling stations, considerable discrepancy exists between the calculated and measured fuel flow for several of the runs. As with the J85 integrated data, the major portion of this discrepancy is attributed to an electrical interaction between the PCM system and the CO₂ analyzer which was found and corrected before the Phase III engine tests.

Qualitatively, the general trends shown by the J79 plume measurements are similar to the J85 measurements in that HC is most reactive in the plume, with CO somewhat less reactive, and NO_x the least reactive, with essentially no change occurring in the plume. For the J79, the highest residual HC level occurred for mid A/B power setting where, for the J85, the highest residual HC level occurred at minimum A/B.

The smoke numbers given in Table 14 are the averages of the smoke measurements, and no attempt has been made to properly mass weight the smoke data. As was expected, the smoke number decreases with increasing afterburner power setting and with increasing axial distance from the exhaust nozzle. The absolute value of the smoke number obtained is subject to some question due to the sampling procedures used.

5.6 INTERPRETATION OF DATA AT DOWNSTREAM LOCATIONS

It has already been pointed out that at the far downstream locations (15 and 30 feet for the J85, and 30 and 60 feet for the J79), generally poor agreement between calculated and metered fuel-air ratio has been observed. A major factor in this discrepancy is a small shift in zero of the CO₂ analyzer caused by interaction with the PCM system. An additional factor is that quite good instrument sensitivity and stability is required to obtain accurate measurements at very low concentrations. This is obvious if one

Table 13. Adjustment of Plume Centerline Required to Shift Origin to the Center of Symmetry for J79.

<u>Run No.</u>	<u>Axial Station (ft)</u>	<u>Power Setting</u>	<u>Probe 1 Change (in)</u>	<u>Probe 2 Change (in)</u>	<u>Adjustment (in)</u>	<u>Angular Separation (degrees)</u>
23-2	30	Mil	+0.71	+7.83	7.86	1.25
23-3	30	Min A/B	+5.67	+3.78	6.81	1.08
22	30	Mid A/B	-3.00	+8.50	9.01	1.43
23-1	30	Max A/B	-4.44	+7.77	8.95	1.42
28-1	60	Mil	-1.16	-2.31	2.59	0.20
28-1	60	Min A/B	0	-1.17	1.17	0.10
28-2	60	Mid A/B	-2.35	-10.57	10.82	0.87
28-4	60	Max A/B	+2.35	-7.04	7.42	0.58

Notes: Positive change is upward along probe orifice path, negative change is downward.

Angular separation is the displacement as measured from the center of the engine exhaust nozzle.

Changes calculated by computer program NEWRAD.

Table 14. Integrated Results - J79-15 Exhaust Emissions Tests.

Run No.	Power Level	Axial Station, ft	Metered Fuel Flow, pps	Calculated Flow Rate, PPS				Emission Index, lb/1000lb fuel			Avg. SAE Smoke Number
				Fuel	CO	HC	NO _x	CO	HC	NO _x	
24-1	Mid	0	2.344	2.228	0.0052	0	0.0267	2.3	0	12.0	38.8
25-3	Mid	7.5	2.273	2.167	0.0062	0	0.0275	2.8	0	12.7	33.6
27-1	Mid	15.0	2.306	2.065	0.0069	0	0.0303	3.4	0	14.7	25.1
23-2	Mid	35.0	2.372	1.574	0.0085	0	0.0364	5.4	0	19.3	--
28-1	Mid	60.0	2.390	1.949	0.0113	0	0.0263	5.8	0	13.5	--
26-2	Min A/B	0	3.915	4.069	0.1386	0.0424	0.0289	34.2	16.5	7.1	15.2
27-4	Min A/B	7.5	3.776	3.867	0.1176	0.0104	0.0392	30.4	2.7	7.8	17.8
27-2	Min A/B	15.0	3.921	3.809	0.1188	0.0086	0.0319	31.2	2.3	8.4	14.2
23-3	Min A/B	30.0	3.931	6.004	0.1241	0.0092	0.0410	20.7	1.5	6.8	--
27-2	Min A/B	60.0	3.933	4.113	0.1272	0.0004	0.0379	30.9	0.1	9.2	--
25-1	Mid A/B	0	6.097	6.330	0.4339	0.1400	0.0320	68.6	22.1	5.1	9.5
26-2	Mid A/B	7.5	6.026	6.684	0.3934	0.1110	0.0323	58.9	16.6	4.8	5.1
27-3	Mid A/B	15.0	6.073	7.291	0.3571	0.0557	0.0357	49.0	7.6	4.9	3.5
22	Mid A/B	30.0	6.052	8.516	0.3435	0.0297	0.0419	40.3	3.5	4.9	--
28-3	Mid A/B	60.0	5.996	9.013	0.4144	0.0345	0.0465	46.0	3.8	5.2	--
25-2	Max A/B	0	7.537	8.189	0.8018	0.0150	0.0391	97.9	1.8	4.8	3.8
26-2	Max A/B	7.5	7.613	7.631	0.2510	0	0.0352	32.9	0.004	4.6	0.5
27-4	Max A/B	15.0	7.524	9.126	0.1199	0	0.0424	13.0	0	4.6	2.3
23-1	Max A/B	30.0	7.726	9.459	0.0944	0	0.0544	10.0	0	5.9	--
28-4	Max A/B	60.0	7.493	11.915	0.1053	0	0.0710	8.8	0	5.9	--

Note: Profiles at 30 and 60-foot stations adjusted for symmetry.

considers that, for example, a change of 1 ppm NO_x causes a change of 0.11 in emission index if the CO_2 concentration is 3%, but the same change in NO_x concentration causes a change in emission index of 1.1 if the CO_2 concentration is only 0.3%. Finally, at concentrations comparable to the ambient levels, the measurement of concentrations becomes almost meaningless without some correction for ambient levels. Thus, the accurate measurement of emission index at high air dilution values by the integral method, which includes the mass and area weighting procedures and correction for ambient levels, would become quite complex. This fact was recognized early in the program and a search was made for an alternate technique.

One approach considered, and finally adopted with some modifications, is based on the fact that the emission index should become constant, both radially and axially, at sampling stations far enough downstream that mixing and reactions are complete. This arises from an important fact concerning emission index; namely, that if an arbitrary unreacting gas composition is mixed with pure air, the emission index will not change. From this it follows that if one plots, for example, CO versus CO_2 , and if mixing and reactions are complete, the result must be a straight line with origin determined by the ambient levels. Figure 37 is a plot for CO versus CO_2 for the J79 at minimum A/B power and 60 feet aft of the exhaust nozzle. Although the data are quite linear, the intercept of the straight line does not pass through zero but is about +10 ppm on the CO axis. It is apparent that the emission index, calculated in the usual way, would increase without limit if the straight-line relationship were followed to zero on the CO_2 axis. This is the trend that has been generally observed, mainly at very high air dilution values.

The emission index may be calculated from the slope of the line and is about 26 for Figure 37, as compared to 30.9 calculated from the integral programs (Table 14). The emission index from the slope will tend to be lower than the integrated value if the y-intercept is positive, and higher than the integral value if the y-intercept is negative.

A number of such plots have been made and they show some rather interesting effects. Figure 38 shows CO plotted against CO_2 for the J79 at military power and at each of the five axial stations. It should be noted that remarkably consistent emission indices are obtained from the slopes of the individual lines, even with emission indices of only 2.2 to 2.9 and with CO concentrations as low as 4 ppm. Furthermore, the values of emission indices agree quite well with those obtained from the integrated values at axial stations near the exhaust nozzle, as shown in Table 14. The CO intercept lies between 2.1 and 4.8 ppm for each plot in Figure 38.

Figure 39 shows CO concentration plotted against CO_2 for the J79 at mid A/B power level and at each of the five axial stations. These curves demonstrate the appearance of the plots in cases of strong contaminant consumption in the plume. At the nozzle exit location, the exhaust is extremely nonuniform, and no particular pattern is evident. Local emission indices range from 27 to 180. At the 7.5-foot axial station, a characteristic hook-shaped curve develops which seems to be indicative of intense mixing and CO consumption. This is to be expected since maximum temperatures are near 3400°R . Local emission indices range from 127 to 17. At 15 feet aft of the nozzle, the curve is straightening somewhat. Maximum temperatures of

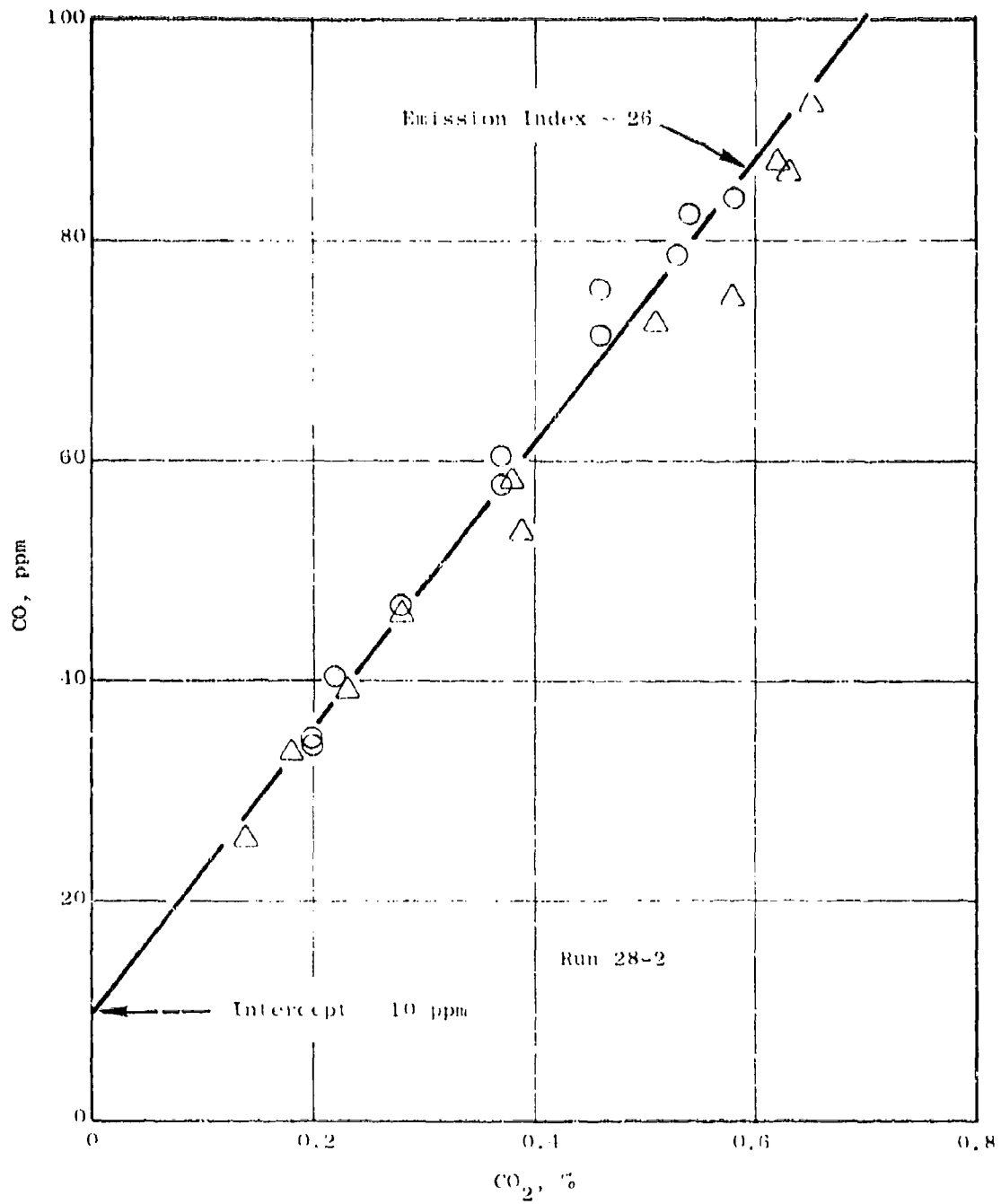


Figure 37. CO Vs. CO₂ Concentration for J79-15 Engine at Min A/B Power Level, 50 feet Aft of Exhaust Nozzle.

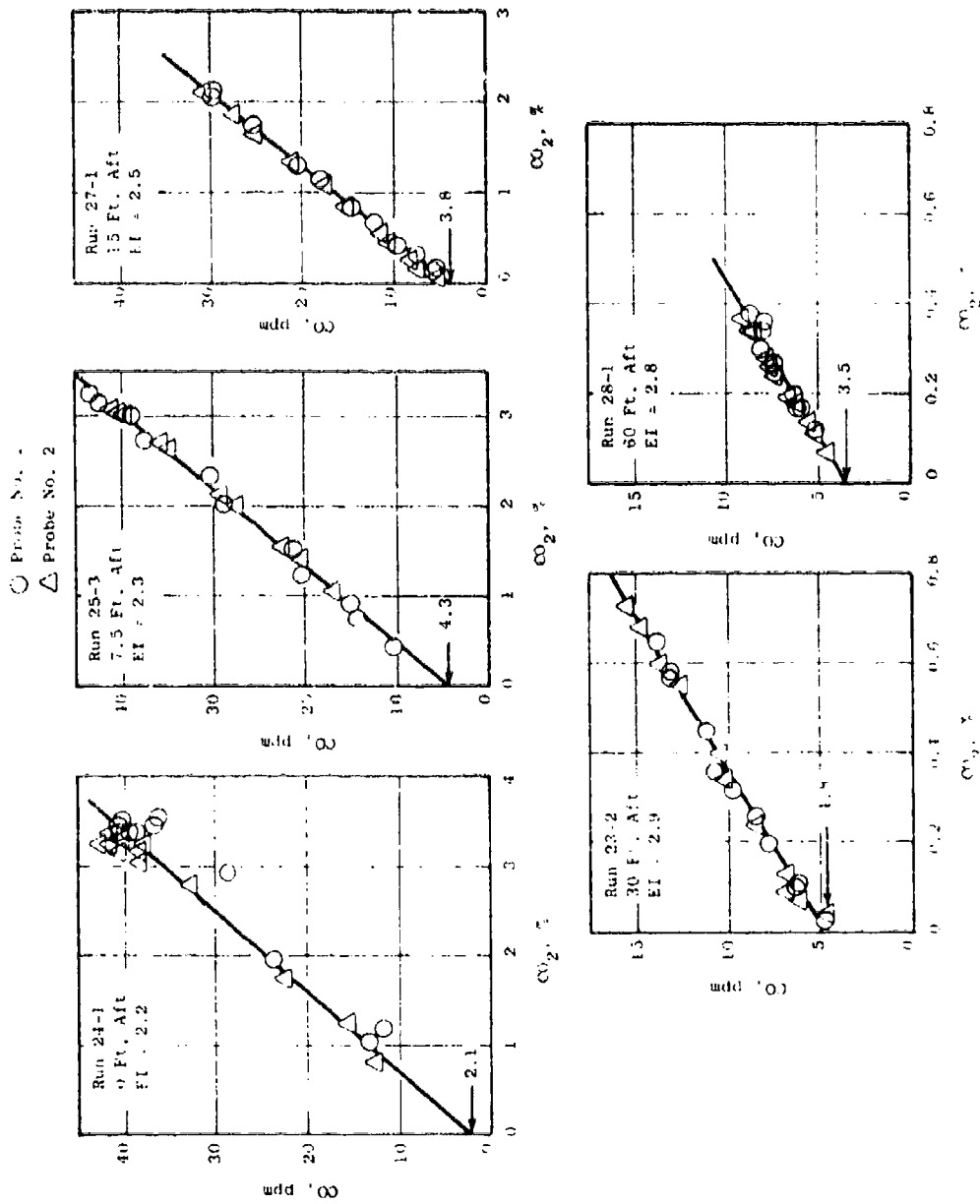


Figure 36. CO Plotted Against CO_2 Concentrations for J79-15 at Military Power and at Each of the Five Axial Stations. Emission Index (EI) Calculated from the Slope is Given on Each Plot.

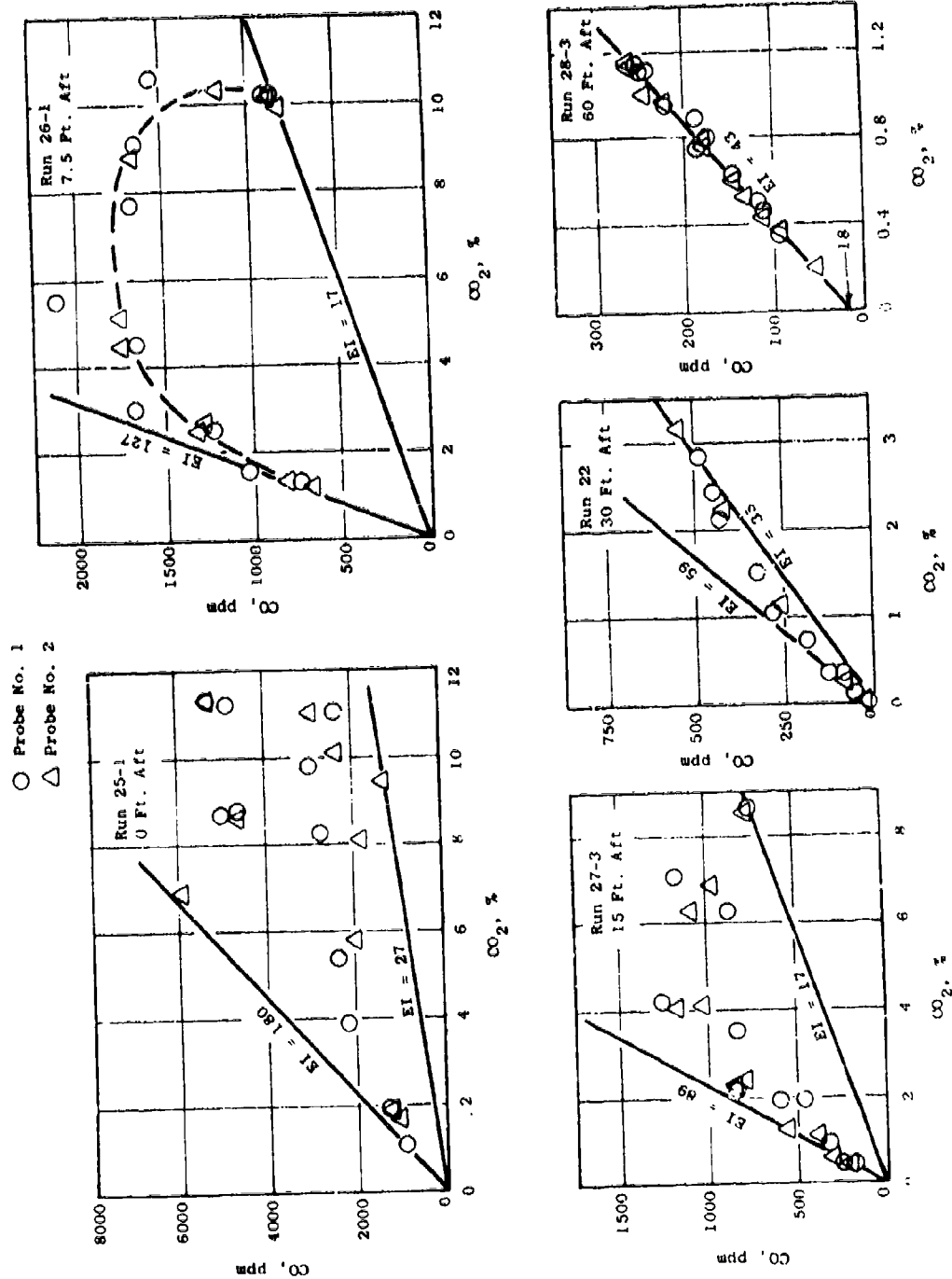


Figure 39. CO vs. CO₂ Concentration for J79-15 Engine at Mid. A/B Power, at Each of Five Axial Stations.

3040° R indicate that CO consumption is still quite rapid, as does the fact that the minimum local index is still 17 compared to the maximum of 89. At the 30-foot station the CO consumption rate is quite low since the maximum temperature is only 1680° R. Mixing is not yet complete, as indicated by the curvature of the plot. At the 60-foot station, mixing and reactions are complete, as indicated by the straight-line plot. An intercept of 18 ppm is indicated. The emission index is 43, as calculated from the slope, compared to 46 calculated from the integral programs.

Figure 40 demonstrates the application of the slope method to calculations of NO_x emission index for the J79 at maximum A/B power. At this power level, the NO_x is distributed with the CO₂, and a fairly straight line results, even at the nozzle exit location. Emission indices as calculated from the slopes are fairly constant at each of the five sampling stations. In each case, the NO_x intercept is quite small.

Figure 41 shows HC concentration plotted against CO₂ concentration for the J79 engine at minimum A/B power and at each of the five axial stations. At the nozzle exit location, the highest unburned HC concentration occurs near the engine centerline, while the highest CO₂ concentration (highest fuel-air ratio) occurs behind the flameholders. The HC near the centerline is rapidly consumed as the exhaust moves away from the nozzle and the centerline gases mix with the hot surrounding gases. This is apparent in the plots at the 7.5 and 15-foot locations. At the 30-foot location, the plot is nearly linear, indicating that HC consumption is completed and mixing is nearly complete. At the 60-foot location, the linear plot indicates that both mixing and reactions are complete. Note that for data at the 60-foot location, the negative HC values indicate an obvious negative shift in the HC analyzer zero setting. In spite of this, the slope method still yields a reliable value of the emission index. The weighted average emission index, calculated in the usual manner (from the integration program), is 0.1 lb per 1000 lb fuel, while the value obtained from the slope method is 1.7. The latter is obviously more nearly correct, as can be seen from examination of the plots of Figure 41.

Figure 42 shows similar data at mid A/B power level. In this case, the plot at the nozzle exit shows that high HC concentration initially occurs both inside and outside the flame stabilization region. As the exhaust moves away from the nozzle, the HC near the centerline is completely consumed while that near the outer plume edge is partially consumed, as shown by the plots at the 7.5- and 15-foot locations. At the 30-foot location, reactions are complete and mixing is nearly complete. Data at both the 15- and 30-foot locations indicate some circumferential nonuniformity, with both the upper right and upper left quadrants having high hydrocarbon concentration. At the 60-foot location, reactions and mixing are complete. Again, the plot for the 60-foot location yields a negative intercept on the HC axis, as did the minimum A/B data (Figure 41). This might be expected since the two test points were run in succession on the same day. It is interesting to compare the plots of Figure 42 with the radial profiles of the same data shown in Figures 36 and 37.

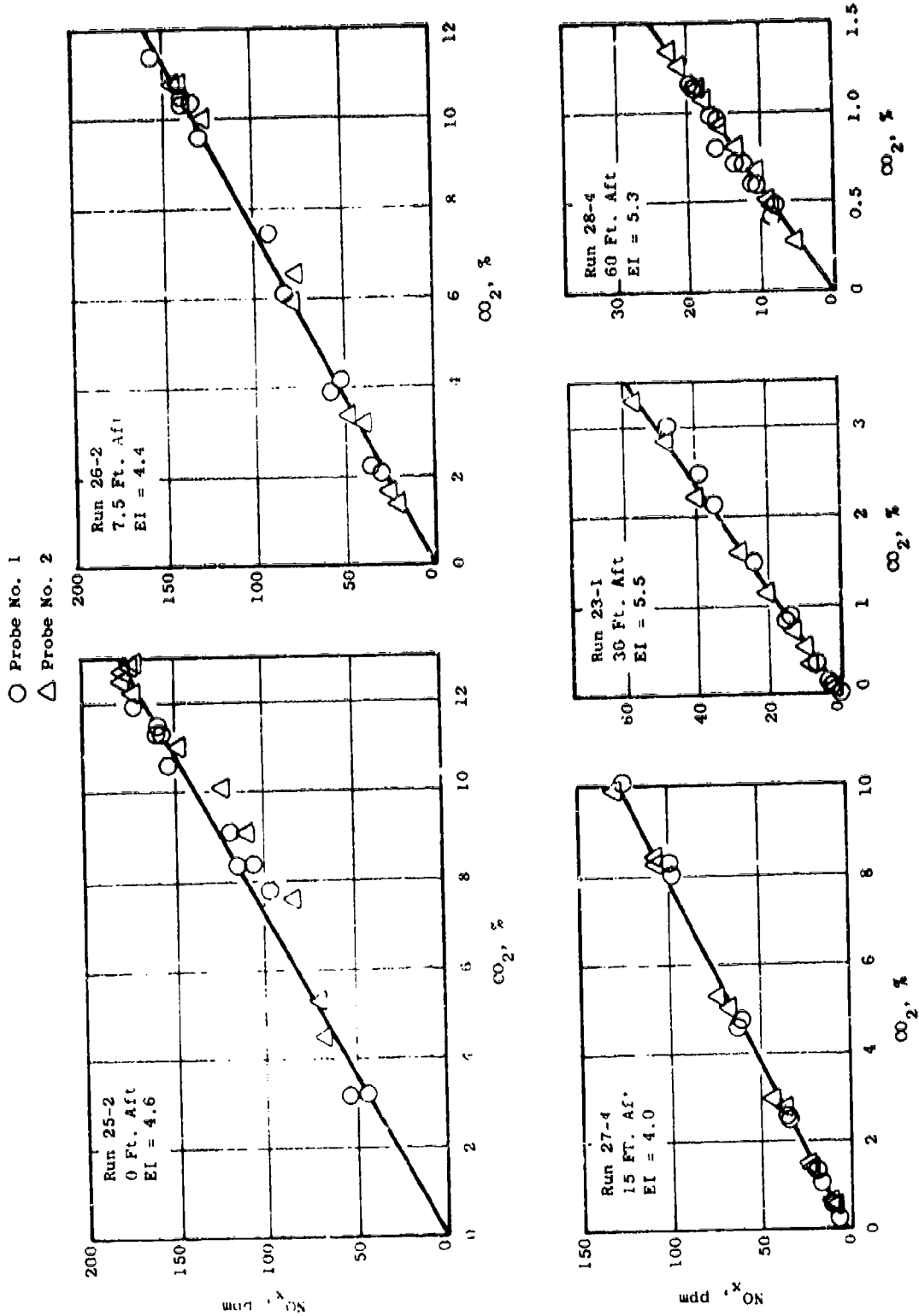


Figure 40. NO_x Vs. CO₂ Concentration for J79-15 Engine at Max. A/B Power, at Each of Five Axial Stations.

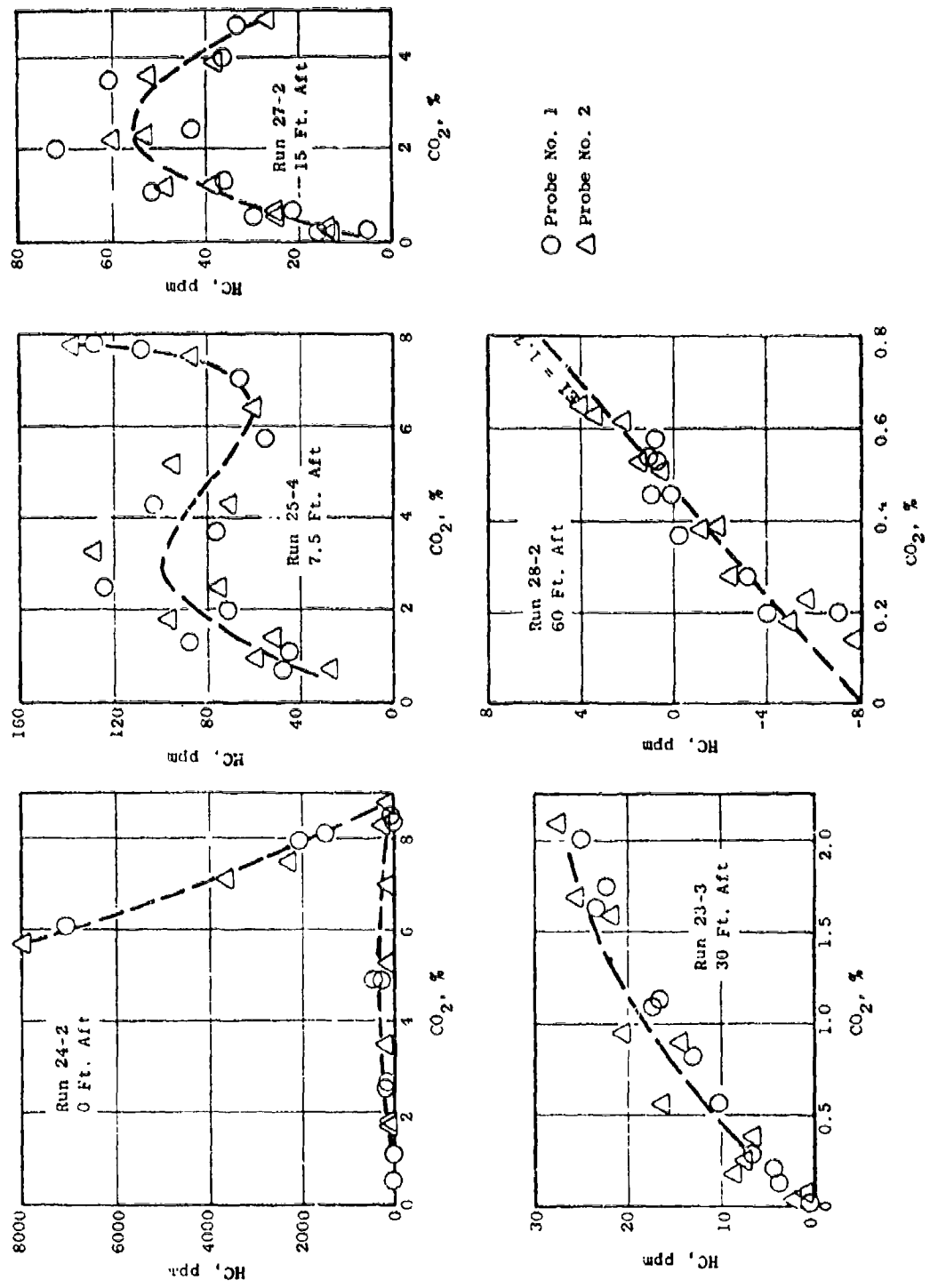


Figure 41. HC Vs. CO₂ Concentration for J79-15 Engine at Min. A B Power, at Each of Five Axial Stations.

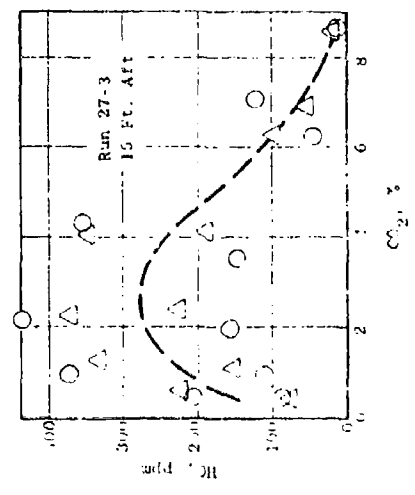
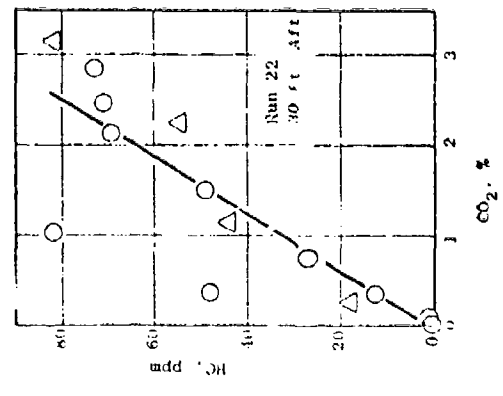
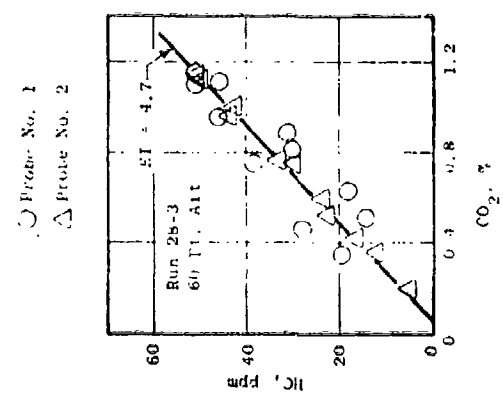
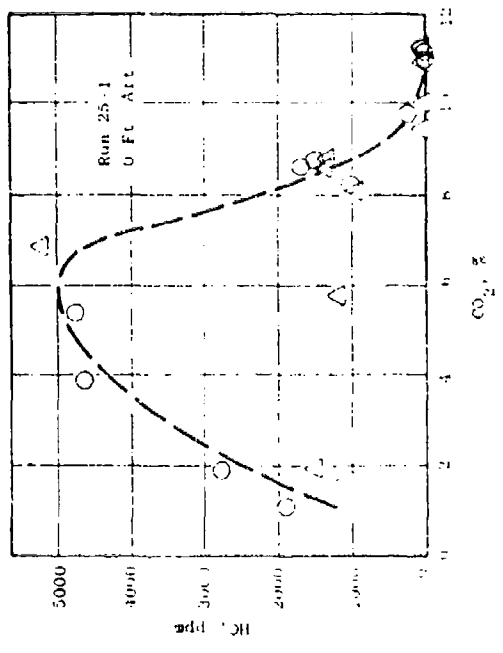
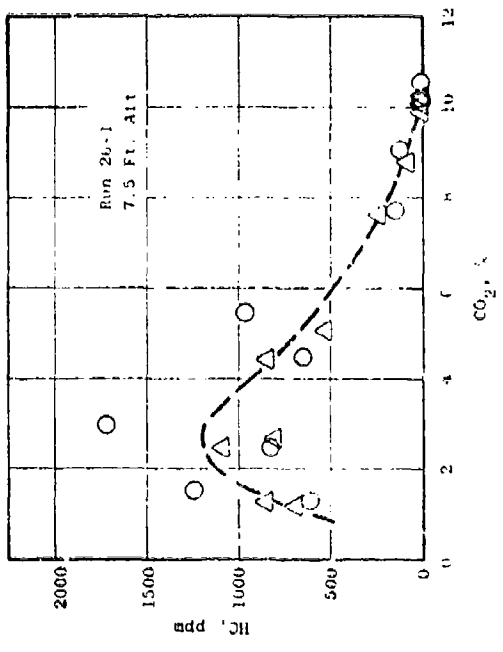


Figure 12. HC vs. CO₂ Concentration for J79-15 Engine at Mid. A/B Power, at Each of Five Axial Stations.

The emissions plots versus CO₂ are valuable as graphical displays which are interpretable in terms of the degree of mixing and reaction occurring in the plume. Under conditions where the local emission indices vary widely over the plume cross section, it is obvious that a weighting method, such as the integral technique used here, must be used for accurate evaluation of the overall emission index. In the case where the emission index has become constant across the plume, it appears that the slope of the emission concentration versus CO₂ gives a more reliable measure of the emission index, especially at very high air dilution values.

A computer program, called ABE, was written to calculate the linear fit of contaminant concentration against CO₂ concentration by the method of least squares. When mixing and reactions are complete, the linear relationship is closely followed, and the slope of the line is simply related to the emission index. This data treatment method is not only interpretable in terms of the degree of mixing and reaction in the plume, but is also amenable to statistical analysis.

Table 15 shows an example of the ABE program printout for a J79 engine test point. This particular test point, sampled 60 feet aft of the engine at military power, gives generally the lowest concentrations of the various measured species in the exhaust. The first column of the table gives the probe number and the second gives the probe angle. The probe is horizontal at 45 degrees, passes through the projected engine centerline at approximately 90 degrees, and is vertical at 135 degrees. The next five columns give measured exhaust concentrations of various species, corrected to a wet basis, that is, corrected for both combustion water and inlet air humidity. Each column of emission data is fit to the linear equation $Y = B_0 + B_1 \times CO_2$ by the method of least squares. In this equation Y is the emission concentration (CO, HC, NO_x, or CO), B₀ is the intercept on the Y axis, B₁ is the slope of the line, and CO₂ is the CO₂ concentration. The last four columns give the deviation (calculated minus actual values) of each data point from the calculated line.

In the lower part of the table are given the calculated B₀, B₁, correlation coefficient, emission index (EI), and standard deviations of the values. The correlation coefficient is an index of how closely the data follows a linear relationship. A perfect linear relationship with positive slope is indicated by the maximum correlation coefficient of 1.00. In this particular case, fairly good linear correlation is indicated by coefficients between 0.97 and 0.98.

The utility of this method of data reduction at very high air dilution values is illustrated by the fact that, even with these extremely low concentrations, calculated emission indices are in good agreement with values calculated from the integral programs at the nozzle exit locations. Further indication of data consistency is shown by the low relative standard deviation of the emission indices and fairly good linear correlation coefficients.

Table 15. Typical ABE Computer Program Printout.

Afterburner Emissions Curve Fit Calculations

Engine - J79
Run - 28-1

Power Setting - MIL
Humidity - 15.5

Station - 60
H/C Ratio - 2.00

Probe	Angle	Wet Concentrations				Calculated - Actual				
		CO ₂ PCT	CO ppm	HC ppm	NO _x ppm	NO ppm	CO ppm	HC ppm	NO _x ppm	NO ppm
1	46	0.168	6.0	0	6.6	5.8	0.1	0	0.6	1.3
1	55	0.205	6.4	0	7.8	7.6	0.2	0	0.6	0.7
1	64	0.268	7.4	0	10.0	10.1	0.0	0	0.9	0.2
1	73	0.343	7.9	0	12.4	11.8	0.5	0	1.3	1.0
1	82	0.379	8.7	0	14.2	13.5	0.2	0	0.6	0.5
1	91	0.383	8.7	0	14.6	13.8	0.3	0	0.5	0.3
1	100	0.363	7.9	0	13.9	13.0	0.7	0	0.5	0.5
1	109	0.298	8.1	0	12.9	10.7	-0.3	0	-0.9	9.6
1	118	0.253	7.4	0	10.1	9.9	-0.2	0	0.2	-0.1
1	127	0.172	6.1	0	8.2	7.1	0.0	0	-0.9	9.1
1	136	0.119	6.2	0	5.6	4.9	0.3	0	-0.2	0.6
2	46	0.137	5.7	0	5.2	6.7	0.0	0	0.9	-0.6
2	55	0.180	6.4	0	7.7	8.2	-0.1	0	-0.1	-0.7
2	64	0.237	7.5	0	10.3	10.2	-0.4	0	-0.4	-0.8
2	72	0.284	7.9	0	12.4	11.4	-0.3	0	-0.9	-0.5
2	81	0.343	8.8	0	14.4	13.5	-0.3	0	-0.7	-0.7
2	90	0.367	9.1	0	15.0	14.3	-0.3	0	-0.4	-0.7
2	99	0.339	8.6	0	14.2	13.4	-0.2	0	-0.6	-0.7
2	108	0.264	7.7	0	11.9	10.2	-0.3	0	-1.1	0.0
2	117	0.192	6.7	0	8.8	8.7	-0.3	0	-0.7	-0.9
2	125	0.109	5.3	0	5.0	5.6	0.1	0	0.1	-0.5
2	134	0.071	4.6	0	3.3	3.4	0.2	0	0.3	0.5

Least Squares Fit $Y = B_0 + B_1 \cdot CO_2$

	B ₀	B ₁	Corr Coeff	EI	Y	Standard Deviations		
						B ₀	B ₁	EI
CO	3.89	13.21	0.9729	2.64	0.303	0.702	0.187	0.037
HC	0	0	1.0000	0	0	0	0	0
NO _x	1.03	36.62	0.9799	12.06	0.723	1.676	0.446	0.146
NO	1.56	32.77	0.9793	10.74	0.654	1.514	0.403	0.132

Table 16 and 17 give a complete summary of results of the ABE computer program calculations for both the J79 and J85 afterburner emissions tests. As can be seen in these tables, for any given power level, the correlation coefficient generally increases and the standard deviation decreases, with increasing axial distance. This is a consequence of the fact that the emissions plotted against CO_2 becomes linear when chemical reactions and mixing are both complete. Good linearity is shown by correlation coefficients above about 0.96, with lower values indicating lack of complete mixing. With low values of correlation coefficient, the calculated emission index may be, of course, considerably in error. Many correlation coefficients for CO and NO_x are above 0.99, indicating excellent linearity.

Correlation coefficients for HC measurements are considerably lower than for CO and NO_x , and the intercept (BO) values are quite erratic. This behavior indicates a definite problem with the stability of the hydrocarbon analyzer. This problem was investigated prior to the Phase III engine tests and is discussed in a later section of this report.

This technique of determining emission indices from the slope of the emission concentration versus CO_2 linear plots appears, on the basis of results summarized here, to be the most reliable method of determining emission indices at very high air dilution values. This method was thus chosen to be the basis of the proposed afterburner emission measurement technique for sampling stations sufficiently far from the engine that mixing and reactions are complete.

Although the slope method of data evaluation is more accurate at high air dilution values, there is still some uncertainty in the data shown in Table 16 and 17 due to problems with the CO_2 analyzer, which was mentioned earlier in this report. The general tendency is for the emissions level of the Phase II data to be higher than the actual value due to these problems. (See Section 8 of this report for a comparison of all emissions data at each axial station for both the Phase II and Phase III engine test measurements.)

5.7 EFFECT OF AFTERBURNING ON NO_x EMISSIONS

Since there is no mechanism for consumption of total NO_x , either in the afterburner or in the plume, the NO_x produced in the mainburner passes through the afterburner and out into the surrounding atmosphere. In addition, NO_x may or may not be formed in the afterburner, depending mainly on the power level. Since fuel is added in the afterburner, it is not clear from the change in total emission index whether or not an actual increase in total NO_x flow has occurred.

The amount of total NO_x actually formed in the afterburner can best be evaluated by defining an afterburner emission index for NO_x , EI_{AB} , as the NO_x formed in the afterburner divided by the afterburner fuel flow. Such values, calculated for each of the two engines, are shown in Table 18. The total

Table 16. J79-15 Afterburner Emissions - ABE Program Summary.

Run No.	Axial Station (ft.)	Carbon Monoxide			Hydrocarbon			Nitrogen Oxides					
		Em. Index	Std. Dev.	Corr. Coeff.	BO (ppm)	Em. Index	Std. Dev.	Corr. Coeff.	BO (ppm)	Em. Index	Std. Dev.	Corr. Coeff.	BO (ppm)
Military Power													
24-1	0	2.3	0.4	.969	1.4	0	--	--	11.0	0.8	.993	6.9	
25-3	7.5	2.3	0.1	.996	4.3	0	--	--	11.2	0.5	.996	7.0	
27-1	15	2.5	0.04	.998	4.4	0	--	--	12.4	0.2	.988	6.2	
23-2	30	2.9	0.03	.995	4.9	0	--	--	16.3	0.2	.992	3.3	
24-1	60	2.6	0.04	.973	3.9	0	--	--	12.1	0.15	.980	1.0	
Min A/B Power													
24-2	0	54.4	108	.531	-100	20.1	106	.229	199	3.5	3.0	.820	41.4
25-4	7.5	40.6	12.1	.957	-131	0.6	1.1	.486	59	4.4	1.1	.969	26.7
27-2	15	28.3	1.0	.998	28.2	0.5	0.5	.441	26.9	6.2	0.4	.993	10.4
23-3	30	20.3	0.7	.990	7.2	1.2	0.1	.960	3.2	6.6	0.2	.994	1.3
28-2	60	24.9	0.3	.990	10.2	2.0	0.1	.957	-9.4	7.5	0.1	.990	1.8
Mid A/B Power													
25-1	0	57.0	130	.591	896	-28.7	73	-.547	3382	5.0	1.6	.983	4.4
26-1	7.5	0.8	35.2	.031	1224	-13.1	12.1	-.835	1226	4.8	0.5	.988	3.8
27-3	15	16.8	16.6	.677	410	-2.3	4.1	-.459	265	4.5	0.3	.999	3.8
27	30	33.5	2.1	.987	39.2	2.7	0.6	.868	7.4	4.6	0.1	.998	1.7
24-3	60	42.4	1.1	.990	13.3	4.6	0.3	.950	-3.6	4.7	0.1	.936	1.0
Max A/B Power													
25-2	0	127.4	226	.747	1009	-12.2	114	-.206	1796	5.1	2.3	.979	-10.4
26-2	7.5	37.1	43.1	.805	-140	0	0	--	0.2	4.7	0.8	.985	-1.3
27-4	15	9.6	2.2	.978	57.1	0	0	--	0	4.4	0.3	.998	2.3
23-1	30	7.3	0.7	.963	15.1	0	0	--	0	5.4	0.1	.997	1.1
28-4	60	6.9	0.1	.996	6.7	0	0	--	0	5.1	0.2	.989	1.6

Table 17. J83-5 Afterburner Emissions - ABE Program Summary.

Run No.	Axle I Station (ft.)	Carbon Monoxide			Hydrocarbon			Nitrogen Oxides					
		Em. Index	Std. Dev.	Corr. Coeff. (ppm)	Em. Index	Std. Dev.	Corr. Coeff. (ppm)	Em. Index	Std. Dev.	Corr. Coeff. (ppm)			
<u>Military Power</u>													
3	0	31.6	6.2	.961	107	0.3	0.5	.411	26.9	4.2	0.82	.961	3.2
5	3.75	34.3	2.6	.994	33.2	0.2	0.08	.826	32.9	4.3	0.14	.999	2.3
7-1	7.5	32.5	0.8	.997	53.3	0.5	0.06	.937	16.9	4.1	0.06	.999	2.3
9-1	15	44.1	0.2	.999	27.9	0.5	0.15	.337	13.9	4.9	0.04	.998	2.8
11-1	30	47.8	0.2	.990	17.0	0.6	0.01	.950	-4.7	5.7	0.05	.973	2.2
<u>Min A/B Power</u>													
4-1	0	--	--	--	--	--	--	--	--	--	--	--	--
6-1	3.75	65.7	12.0	.962	311	27.8	12.5	.821	639	2.7	0.12	.998	2.2
7-2	7.5	74.8	5.0	.992	140	32.3	4.4	.966	334	2.2	0.05	.999	2.1
9-2	15	113.9	1.5	.995	60.2	55.9	1.0	.992	74.3	3.0	0.05	.993	1.7
11-2	30	121.4	0.6	.994	55.5	65.9	0.5	.999	54.0	3.5	0.02	.988	2.3
<u>Mid A/B Power</u>													
4-2	0	--	--	--	--	--	--	--	--	--	--	--	--
6-2	3.75	16.8	17.6	.768	496	-0.6	-1.4	-.489	110	2.4	0.26	.997	-0.1
7-3	7.5	12.4	6.8	.825	178	-0.2	-0.3	-.497	35	2.3	0.10	.998	0.3
9-3	15	23.4	1.8	.982	30.3	0.3	0.07	.869	1.4	2.4	0.08	.997	1.4
10-1	30	29.3	2.6	.983	35.4	0.3	0.1	.789	0.8	2.5	0.14	.993	1.1
11-3	30	39.4	0.4	.994	22.8	0.7	0.01	.981	-3.3	3.6	0.03	.996	2.3
12-1	30	34.8	0.7	.996	34.8	0.4	0.02	.962	11.9	2.5	0.04	.998	3.0
<u>Max A/B Power</u>													
4-3	0	--	--	--	--	--	--	--	--	--	--	--	--
6-3	3.75	93.9	66.9	.919	-821	-0.03	-0.04	-.780	16.5	3.4	0.40	.996	-1.6
8	7.5	43.7	9.7	.980	-63.3	-0.02	-0.01	-.821	11.2	2.9	0.35	.994	-0.6
10-2	15	15.4	1.6	.967	31.0	-0.03	-0.01	-.826	-6.0	2.7	0.04	.999	1.5
12-2	30	23.3	0.5	.991	31.7	0.01	0.02	.048	14.1	2.9	0.06	.991	3.2

Table 1b. NO_x Formation in J85 and J79 Afterburners.

Power Level	J85-5			J79-15		
	Total NO _x Flow (pps)	NO _x Flow (NO _x Flow) MIL	EI _{AB}	Total NO _x Flow (pps)	NO _x Flow (NO _x Flow) MIL	EI _{AB}
Military	0.00297	1.00	--	0.0282	1.00	--
Mid A/B	0.00292	0.99	0	0.0303	1.07	1.4
Mid A/B	0.00460	1.55	1.6	0.0333	1.18	1.4
Max A/B	0.00567	1.91	1.8	0.0359	1.36	2.1

$$EI_{AB} = \frac{NO_x \text{ Flow} - (NO_x \text{ Flow})_{MIL}}{WFAE} \times 1000 \times 3600 \text{ (lb/1000 lb AB Fuel)}$$

NO_x flow is obtained from the integral computer program. The fractional NO_x increase (NO_x flow divided by NO_x flow at military power) is quite low for both engines at minimum A/B power level. At maximum A/B power, the total NO_x flow for the J85 increases by 91 percent over the value at military power, while the increase is but 38 percent for the J79, even though both engines have approximately the same afterburner emission index (1.8 and 2.1). The higher fractional increase in total NO_x for the J85 at maximum A/B is due to the fact that the J85 has a considerably lower NO_x emission index at military power (4.4 versus 12.0 for the J79). This, in turn, is a result of the lower engine pressure ratio and the lower combustor inlet temperature (T_3) of the J85.

Although only small increases in total NO_x occur in the afterburner at low A/B power levels as shown in Table 18, considerable conversion of NO to NO_2 can occur under these conditions, as shown in Figure 43. Figure 43 compares NO_x and NO profiles at the nozzle exit location for the J85 at military power. Under these conditions about 53 percent of the NO_x is NO. At minimum A/B power, however, considerable conversion of NO to NO_2 occurs, as shown in Figure 43. At minimum A/B power, only about 10 percent of the total NO_x is NO, even though the total NO_x formed is the same for the two power levels. Figure 44 shows similar data for the J79-15. For this engine, some increase in total NO_x occurs in the high temperature region, while considerable conversion to NO_2 occurs outside the high temperature region. The decrease in total NO_x along the engine centerline at minimum A/B power has not been explained.

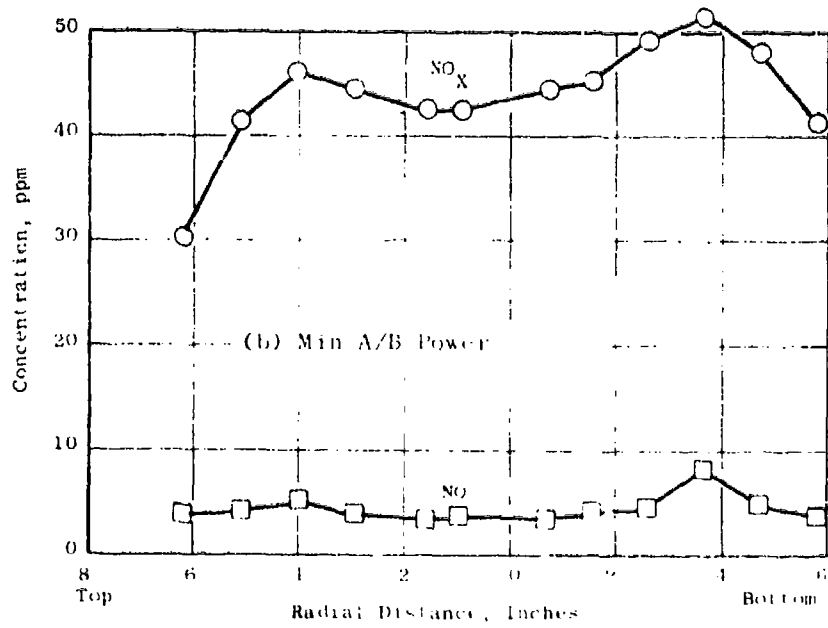
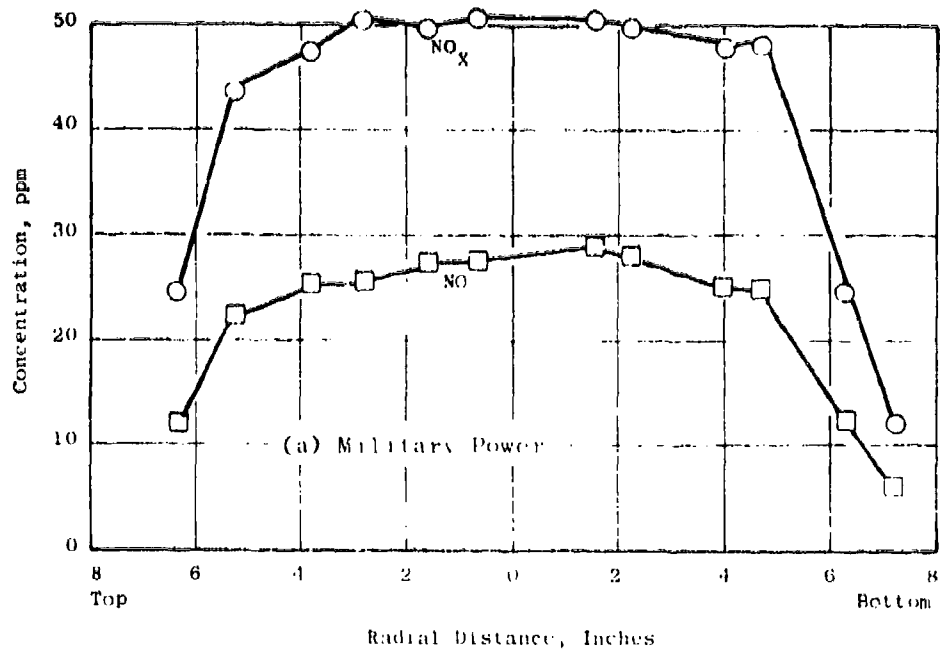


Figure 43. NO_x and NO Profiles for J85-5 Engine at Military and Min. A/B Power, Samples from Probe No. 1 at Nozzle Exit.

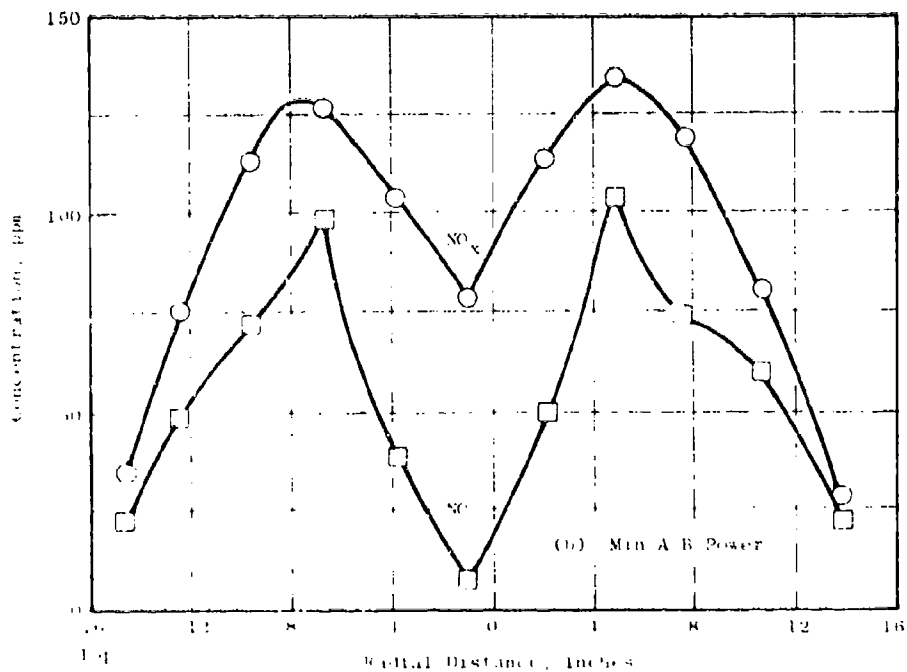
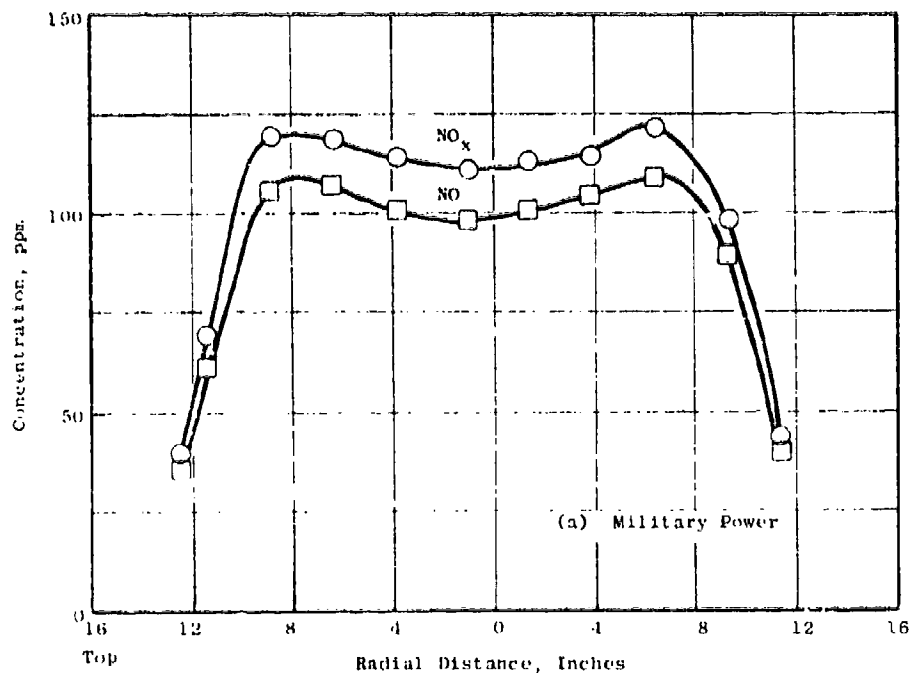


FIGURE 11. NO_x and NO Profiles for J79-15 Engine at Military and Min. A/B Power. Samples from Probe No. 1 at Nozzle Exit.

SECTION 6.0

PLUME MODEL VERIFICATION

Validation of the plume model began as part of the Phase II effort on this program and continued into Phase III. The integrated plume model was verified, after some modification and adjustment, by inputting nozzle exit gas sample data from the afterburner emissions tests of J85-5 and J79-15 engines described in Section 5.0 of this report; calculating the mixing, homogenization, and contaminant consumption reactions in the exhaust plumes; and comparing the predicted profiles with those measured in the tests at several distances from the engine. These comparisons are presented in this section of this report.

Some elements of the plume model were independently verified by comparison with experimental data drawn from the literature or generated previously. The comparison of JETMIX predictions with measured mixing profiles in turbulent inert gas jets was described by Heck (Reference 30). Empirical constants appearing in the Spalding heterogeneity formula were evaluated by comparison of calculations with measurements of Becker, Hottel, and Williams (Reference 31), although one of these constants was subsequently modified after integration into the plume model (see Section 4.4). The chemical reaction system used with GCKP was tested by comparison of calculated and measured decay of CO behind an ethylene-air flat flame (Reference 32), and SCKP was tested by comparison with GCKP.

6.1 COMPARISON WITH J85-5 TEST DATA

Test data acquired in the emissions tests of a J85-5 engine with afterburner, including engine operating parameters, fuel and ambient air properties, and total pressure and gas sample analyses from traversing probes located near the exhaust nozzle exit plane, were used as input to the plume model. Profiles of fuel-air ratio and contaminant concentration were calculated at various stations downstream from the engine and compared with measured profiles at those stations. Integrated emissions indices were calculated from the predicted profiles and compared to overall emissions indices derived from the measurements either by integration of the profiles, or by the slope method, as appropriate. These comparisons are presented in Figures 45 through 62.

Because the plume model can accommodate no more than eleven different radial gas compositions as input, whereas a typical survey consisted of 24 samples, it was necessary to select a representative set of samples from the full survey. The resulting initial profiles used by the plume model are compared with the full sets of measurements in Figures 45, 46, and 47. The overall emissions indices of the selected samples agreed with those of the full survey within 10 percent, as shown by the left-hand bars of Figures 50, 56, and 62.

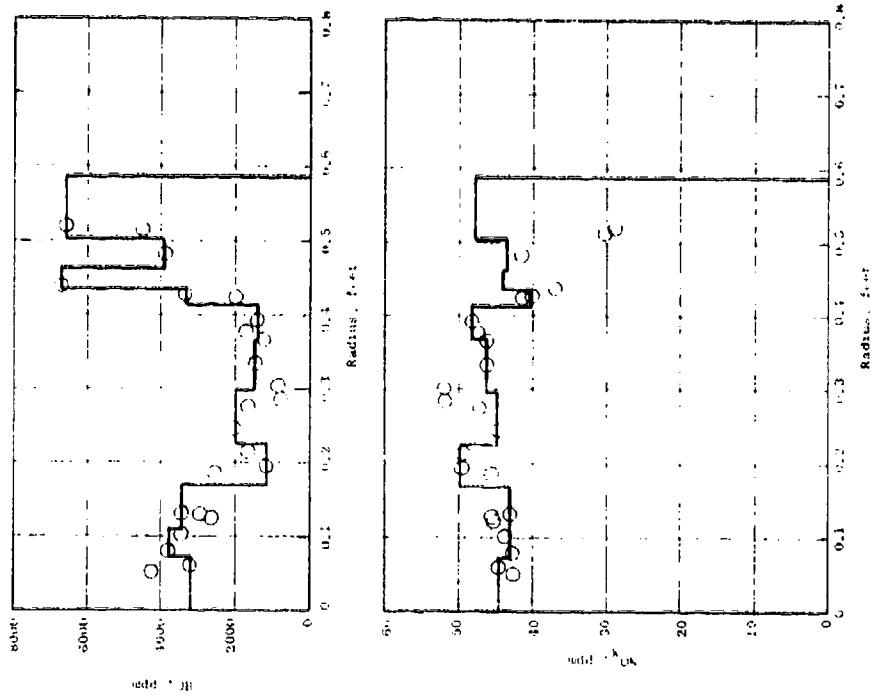


Figure 45. Plume Model Profile Predictions Compared with Phase II Test Data - J85-5 Engine,
 Min. A/B, X = 0 feet.

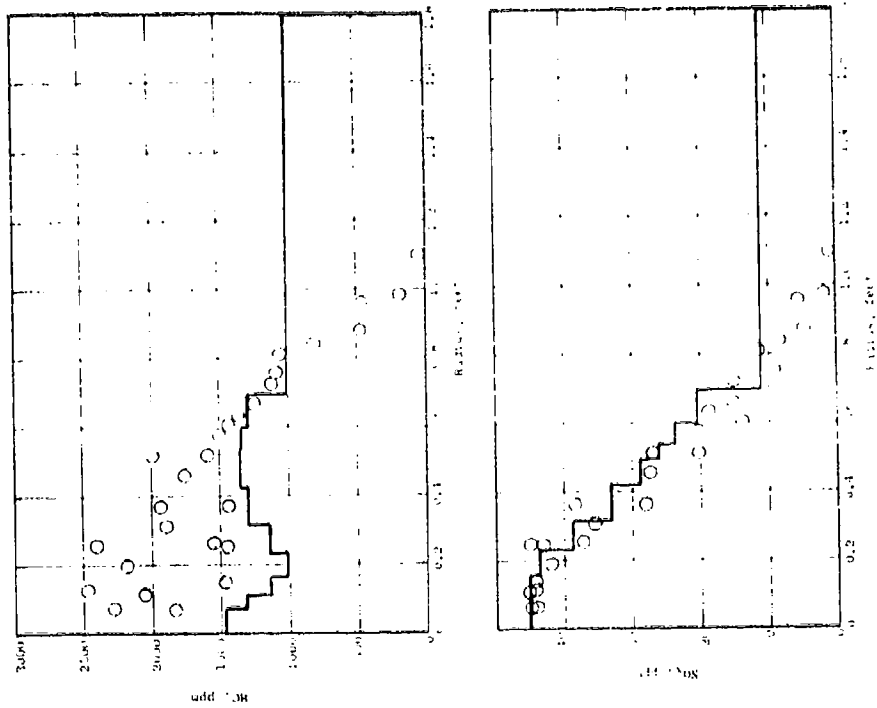


Figure 46. Plume Model Profile Predictions Compared with Phase II Test Data - J85-5 Engine, Min. A/B, X = 3.75 feet.

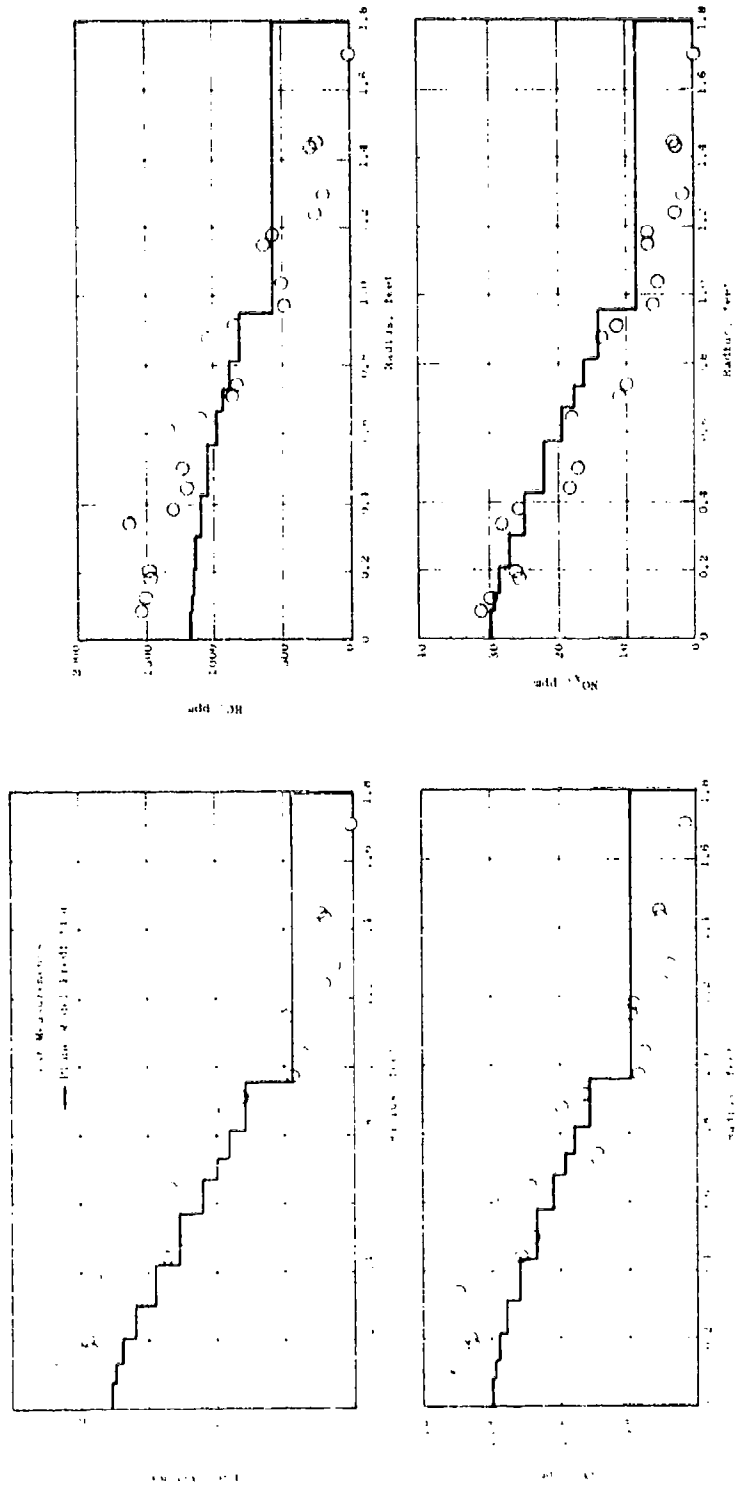


Figure 47. Plume Model Profile Predictions Compared with Phase II Test Data - J85-5 Engine, Min. A/B, X = 7.5 feet.

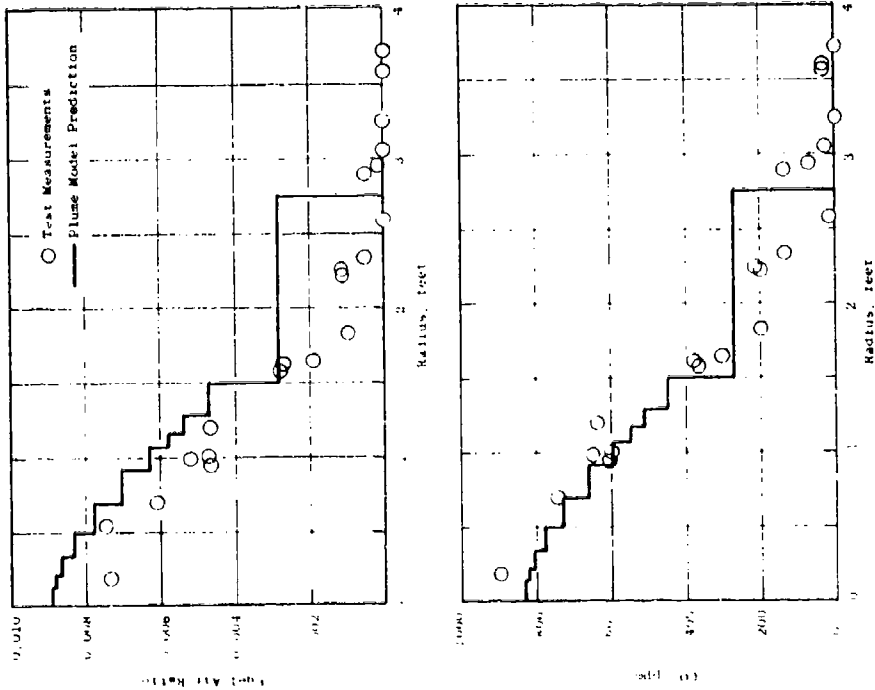
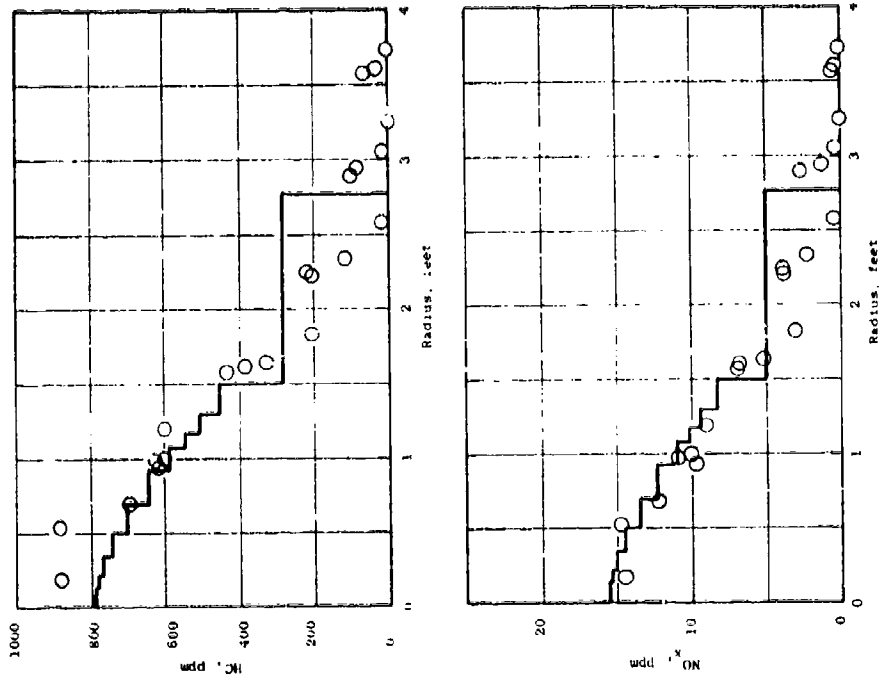


Figure 48. Plume Model Profile Predictions Compared with Phase II Test Data - J85-5 Engine, Min. A/B, X = 15 feet.

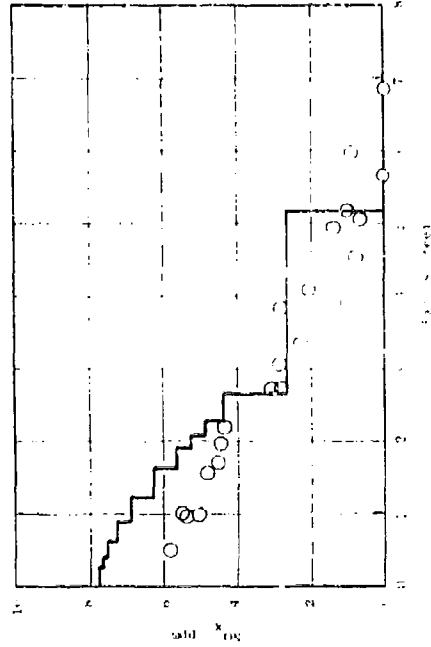
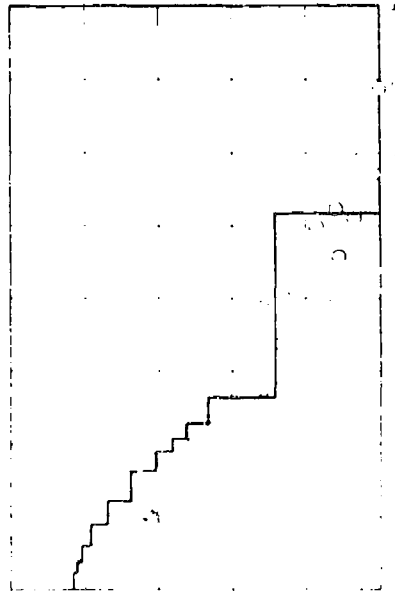
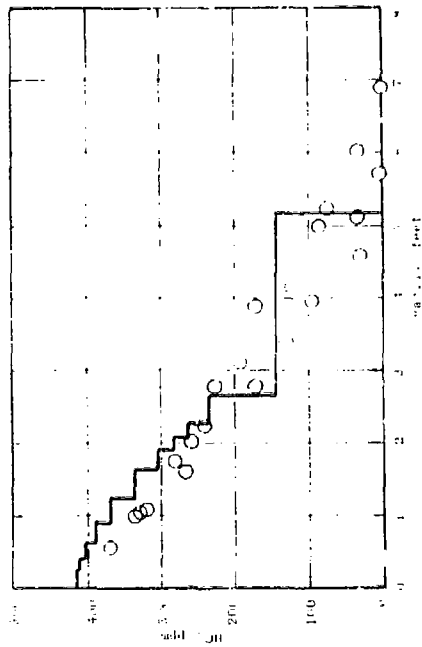
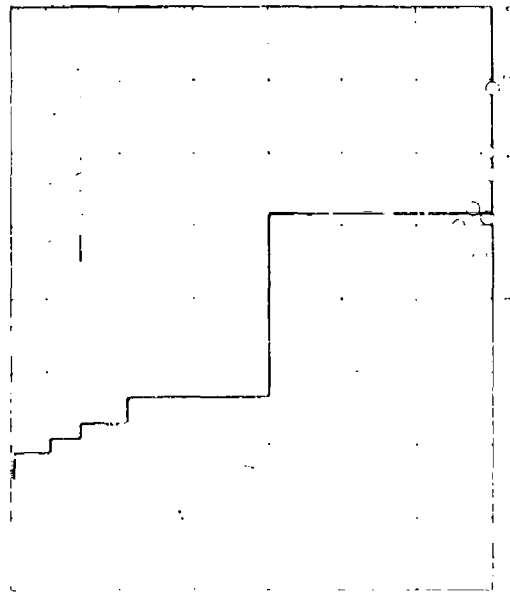


Figure 49. Plane Nozzle Profile Predictions Compared with Phase II Test Data - J85-5 Engine, Min. A/B, X = 30 feet.

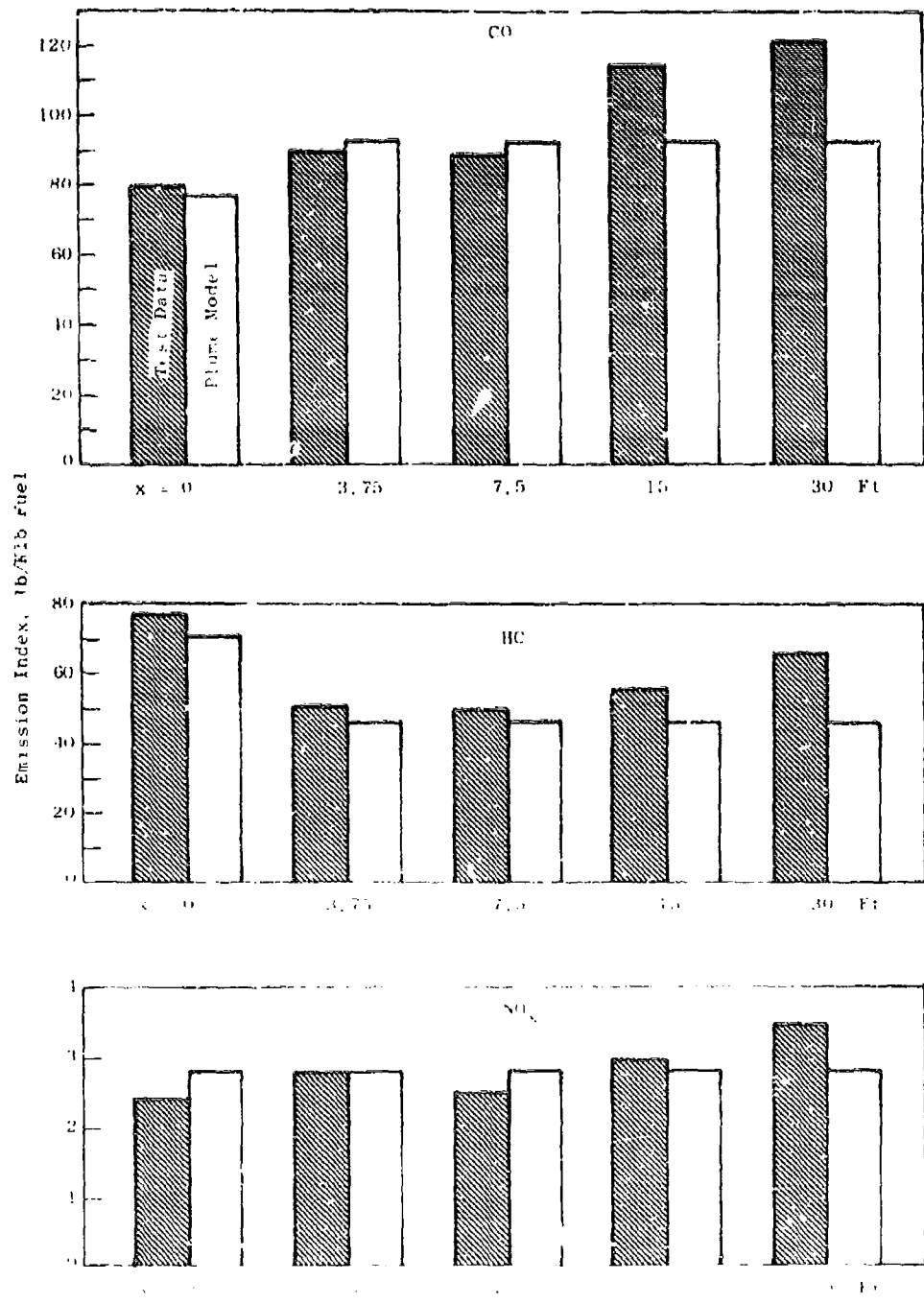


Figure 30. Plume Model Predictions of overall Emissions Indices Compared with Phase II Test Data - 180-5 Engine, MIP, A-B.

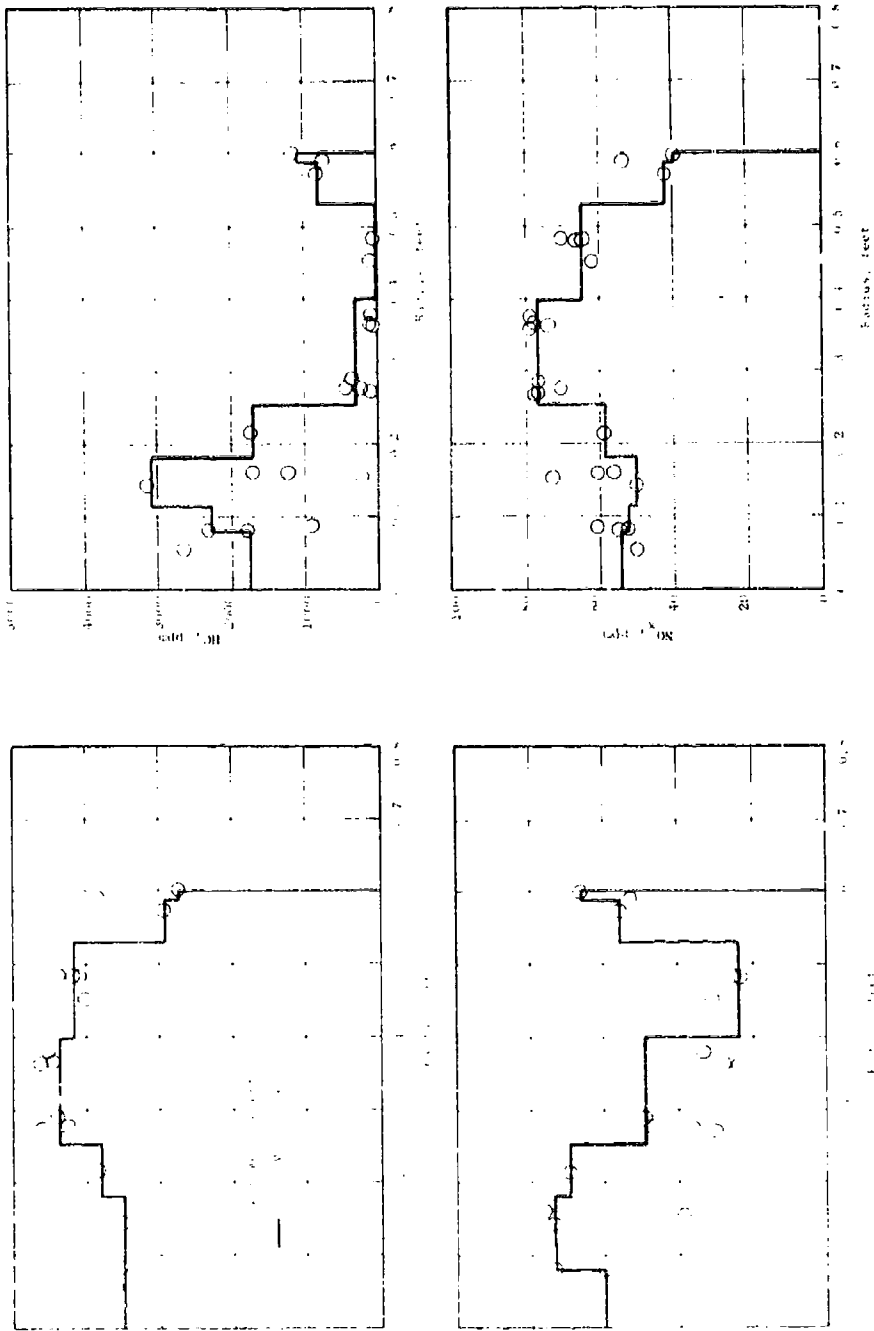


Figure 51. Plume Model Profile Predictions Compared with Phase II Test Data - J85-5 Engine, Mid. A/B, X = 0.

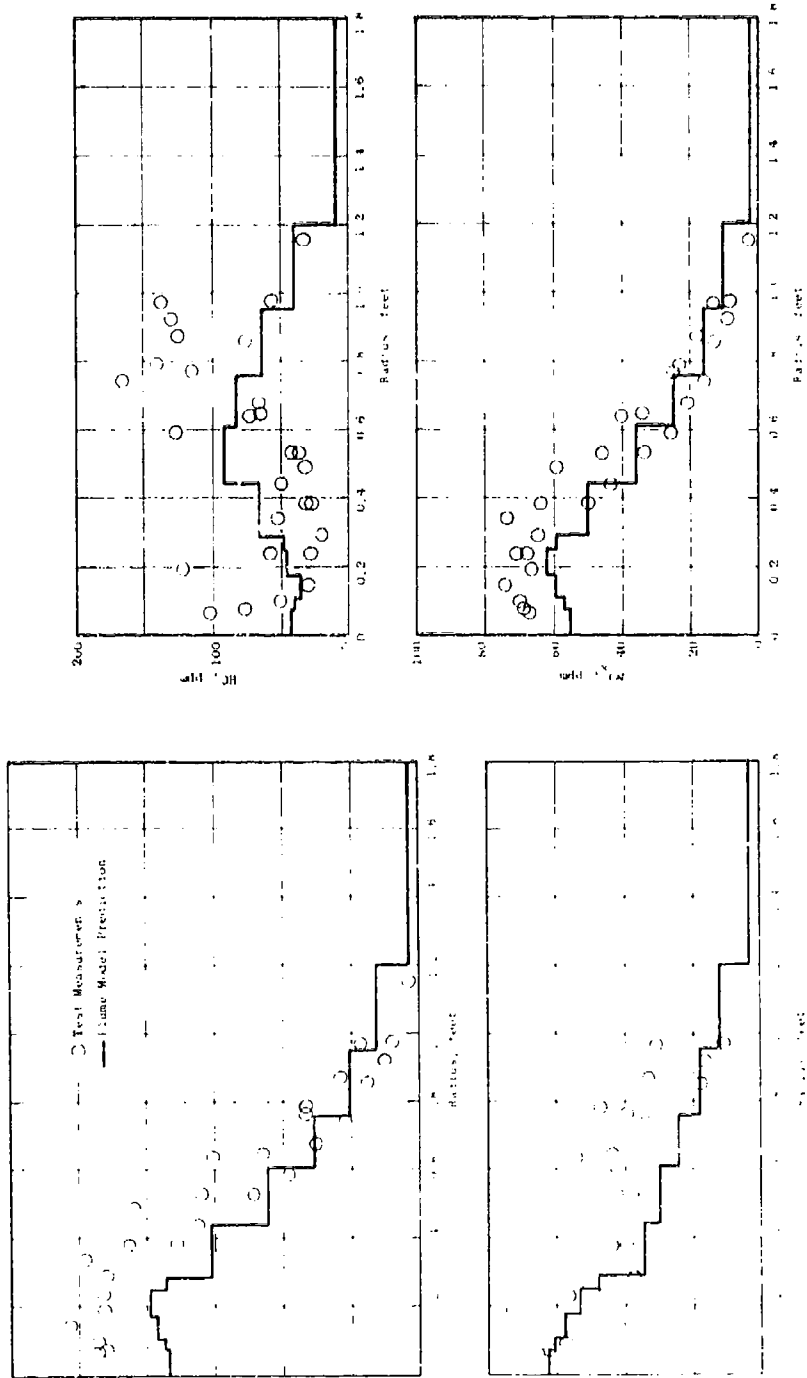


Figure 52. Plume Model Profile Predictions Compared with Phase II Test Data - J85-5 Engine, Mid. A/B, X = 3.75 feet

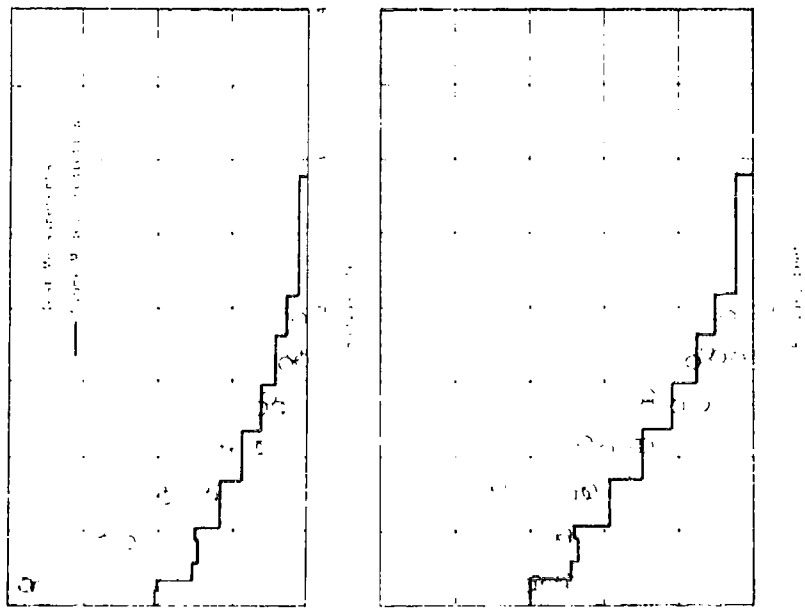
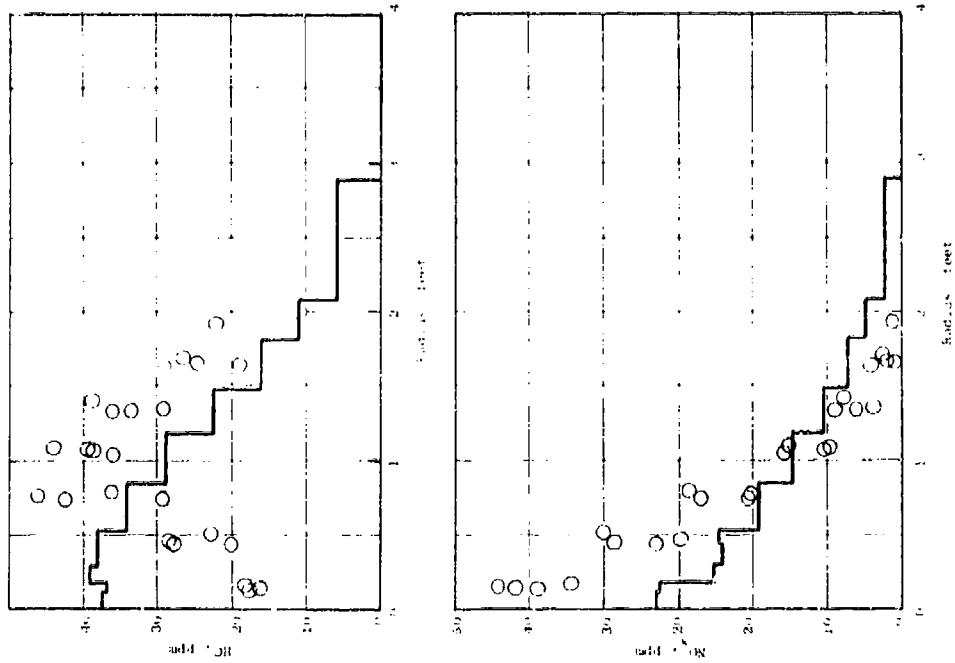


Figure 53. Flume Model Profile Predictions Compared with Phase II Test Data - J85-5 Engine, Mid. A/B, X = 7.5 feet.

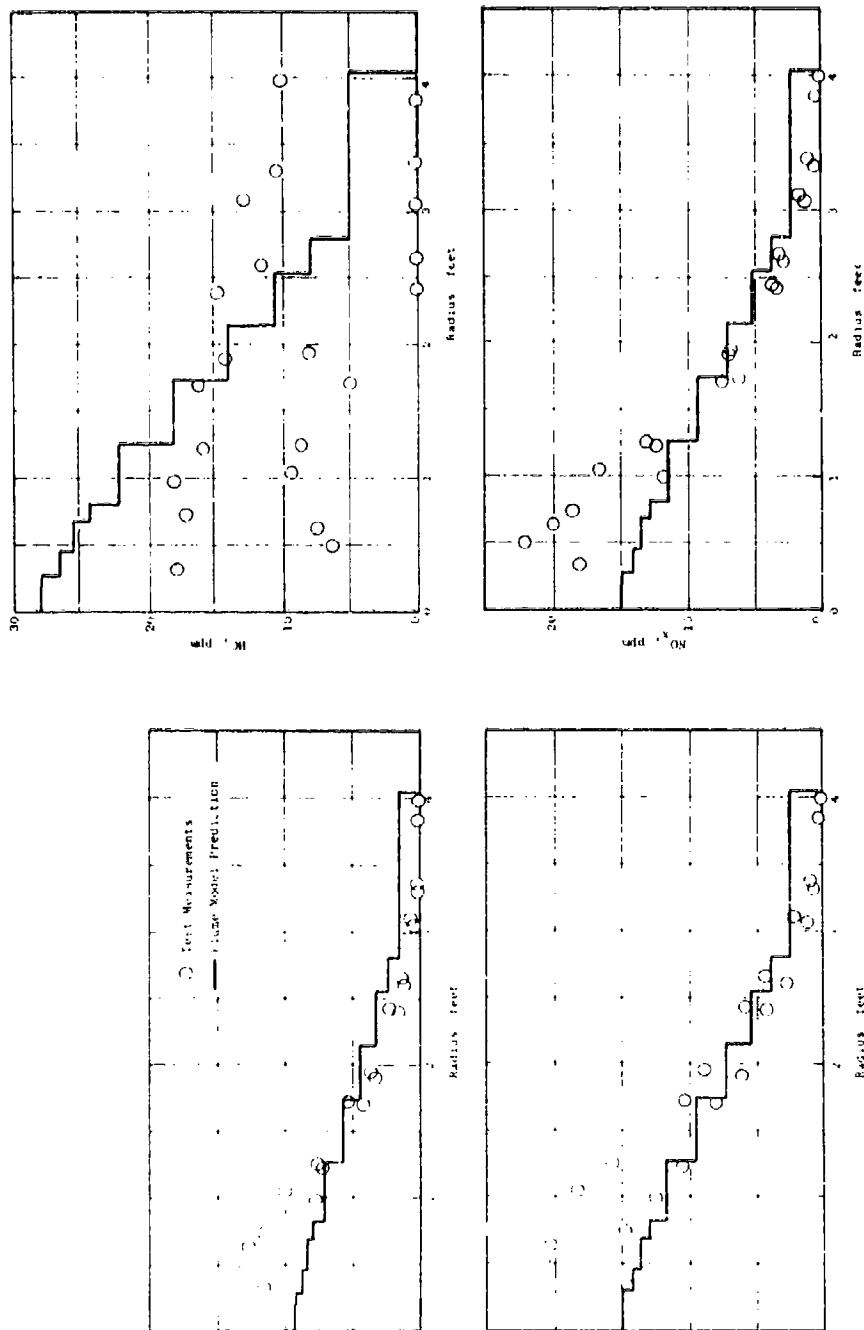


Figure 54. Plume Model Profile Predictions Compared with Phase II Test Data - J85-5 Engine, Mid. A/B, X = 15 feet.

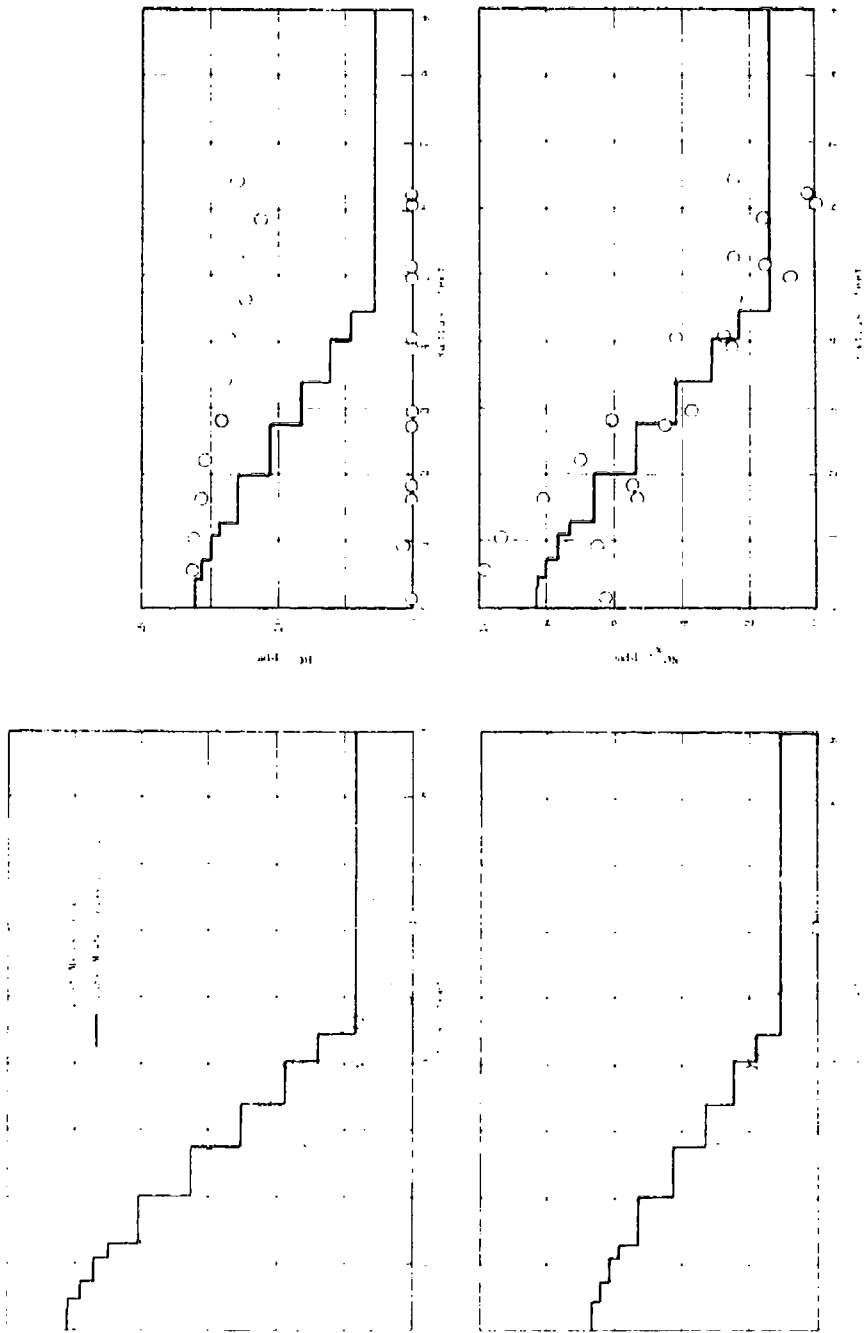


Figure 55. Plume Model Profile Predictions Compared with Phase II Test Data - J85-5 Engine, Mid. A.B., X = 30 feet.

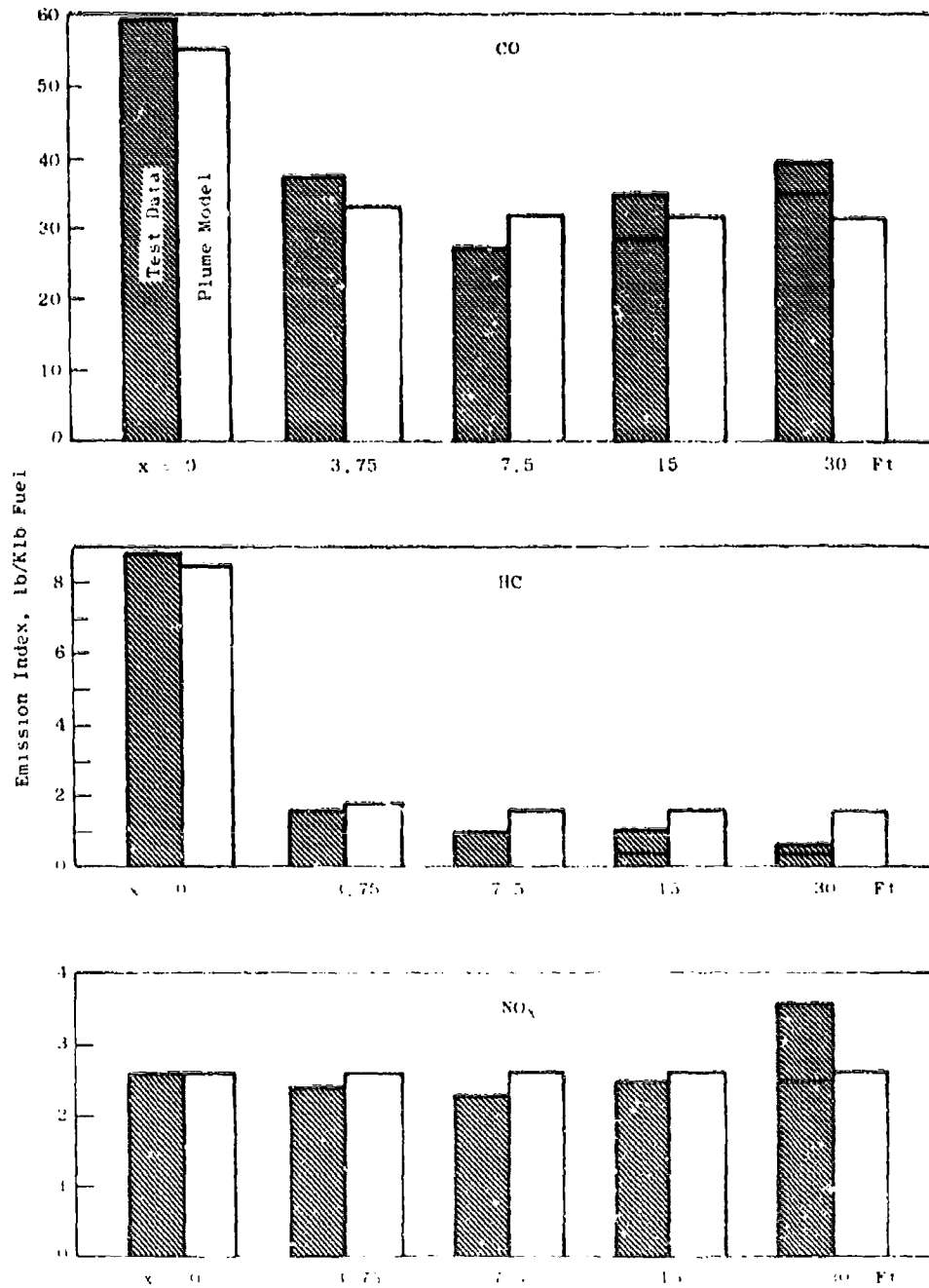


Figure 56. Plume Model Predictions of Overall Emissions Indices Compared with Phase II Test Data - J85-5 Engine, Mid. A-B.

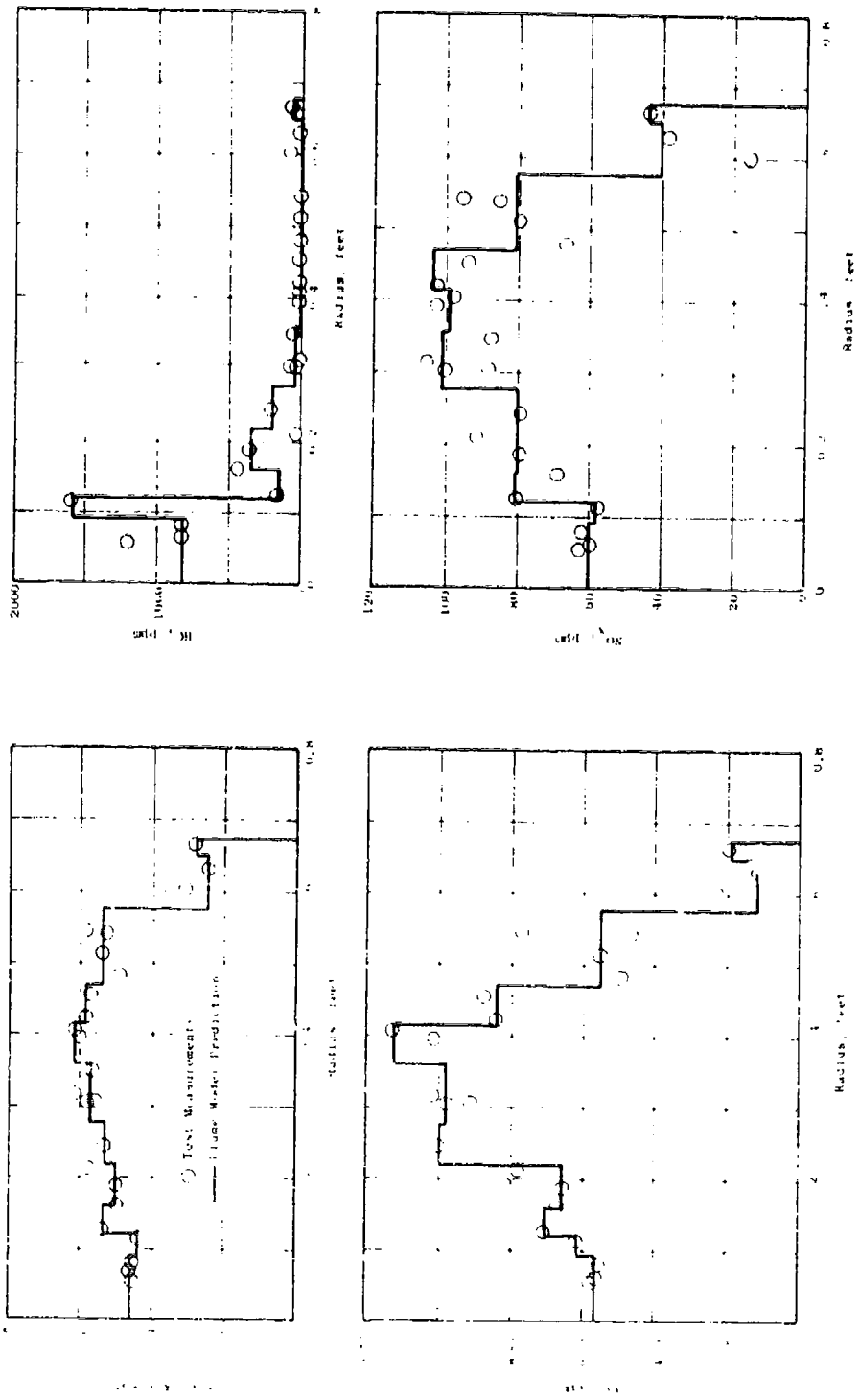


Figure J7. Plume Model Profile Predictions Compared with Phase II Test Data - J85-5 Engine, Max. A/B, X = 0.

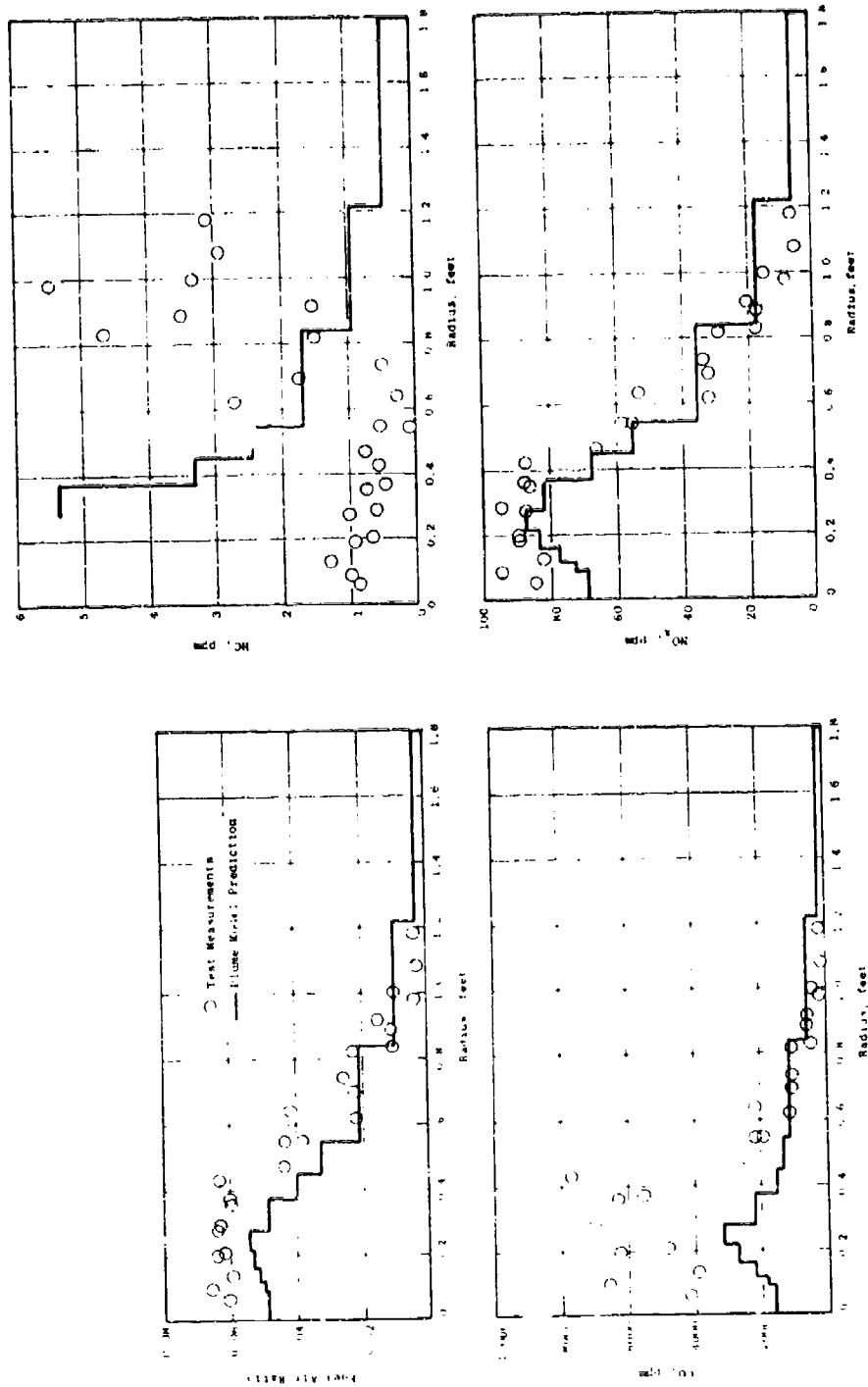


Figure 58. Plume Model Profile Predictions Compared with Phase II Test Data - J85-5 Engine,
Max. A/B, X - 3.75 feet.

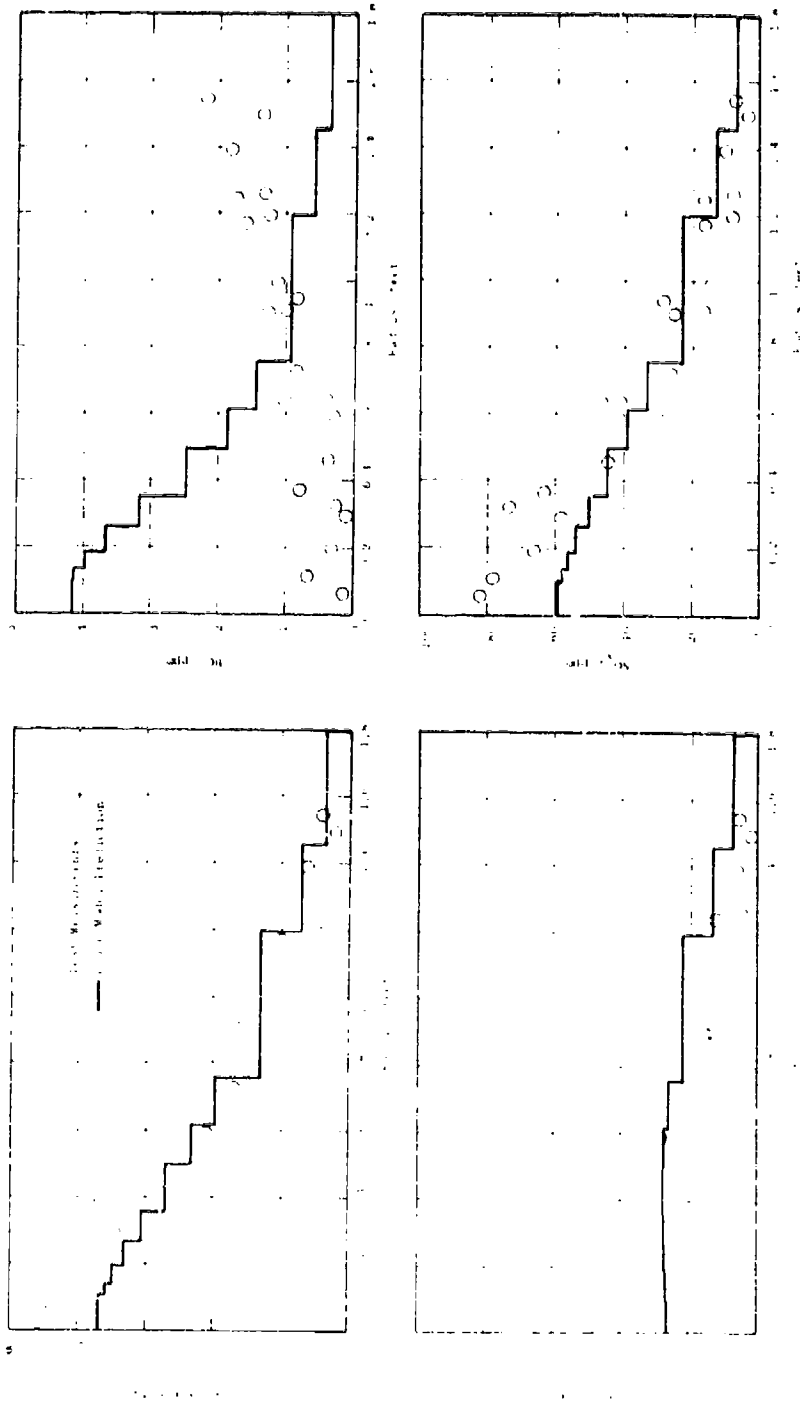


Figure 59. Plume Model Profile Predictions Compared with Phase II Test Data - J85-5 Engine,
 Max. A/B, X = 7.5 feet.

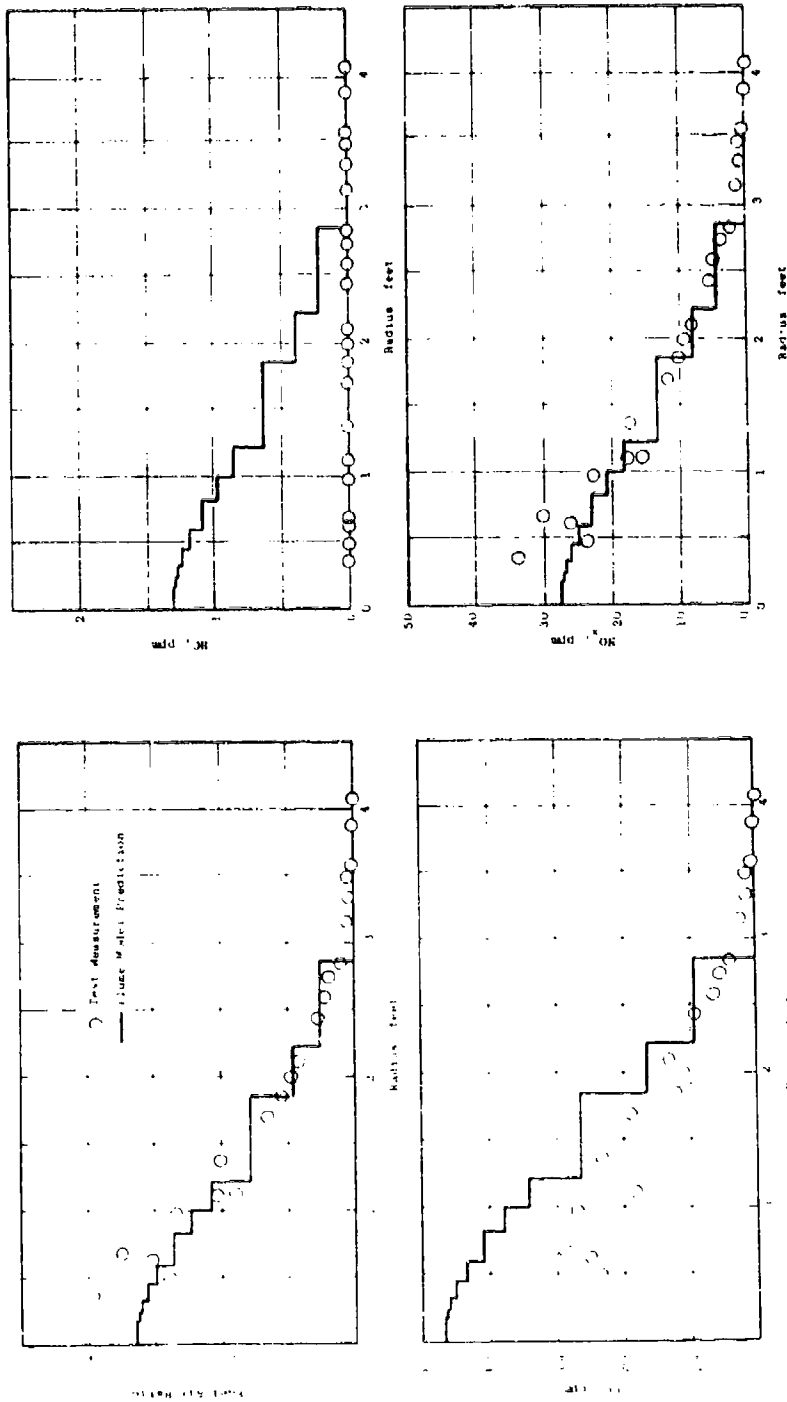


Figure 60. Plume Model Profile Predictions Compared with Phase II Test Data - J85-5 Engine, Max. A/B, X = 15 feet.

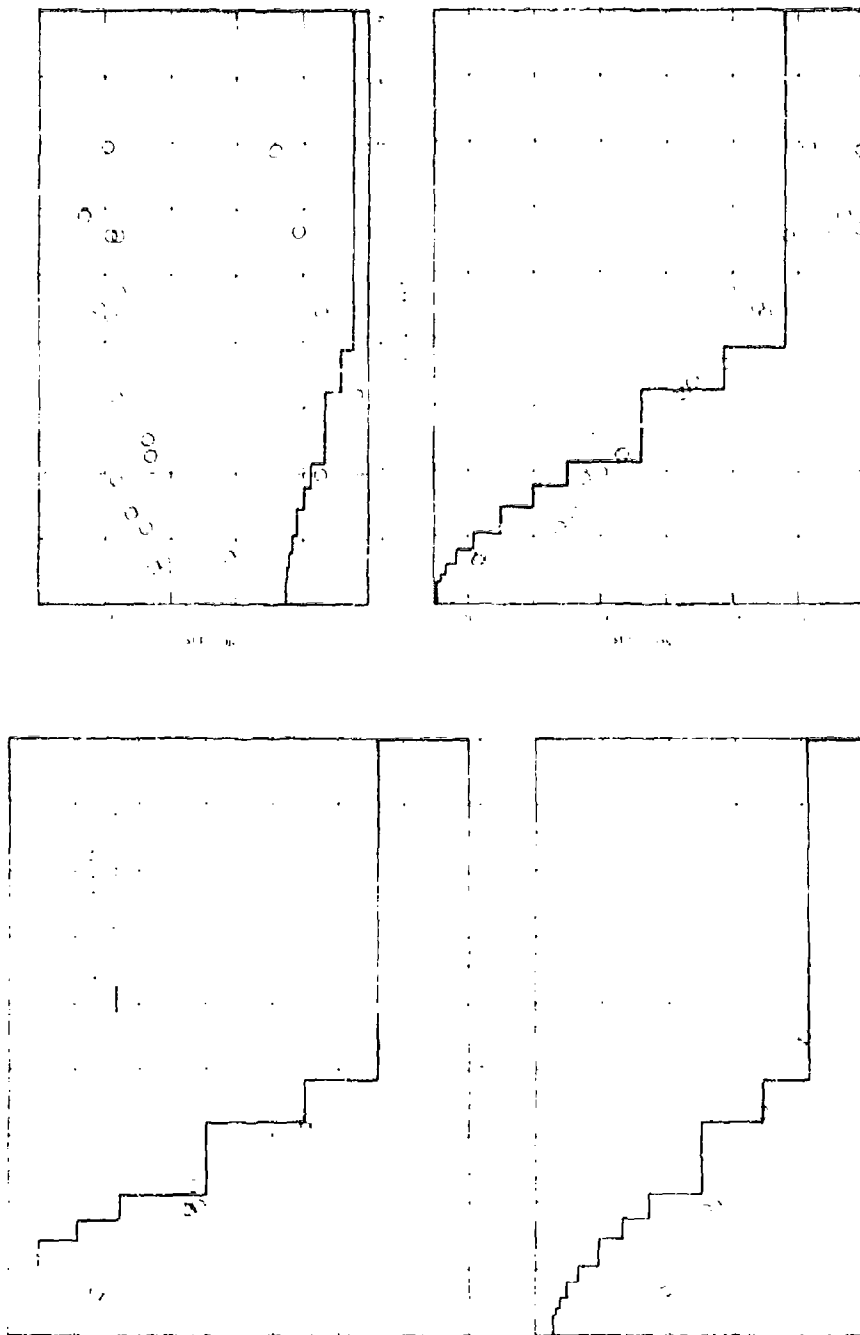


Figure 61. Plume Model Profile Predictions Compared with Phase II Test Data - J85-5 Engine,
Max. A/P, X = 30 feet.

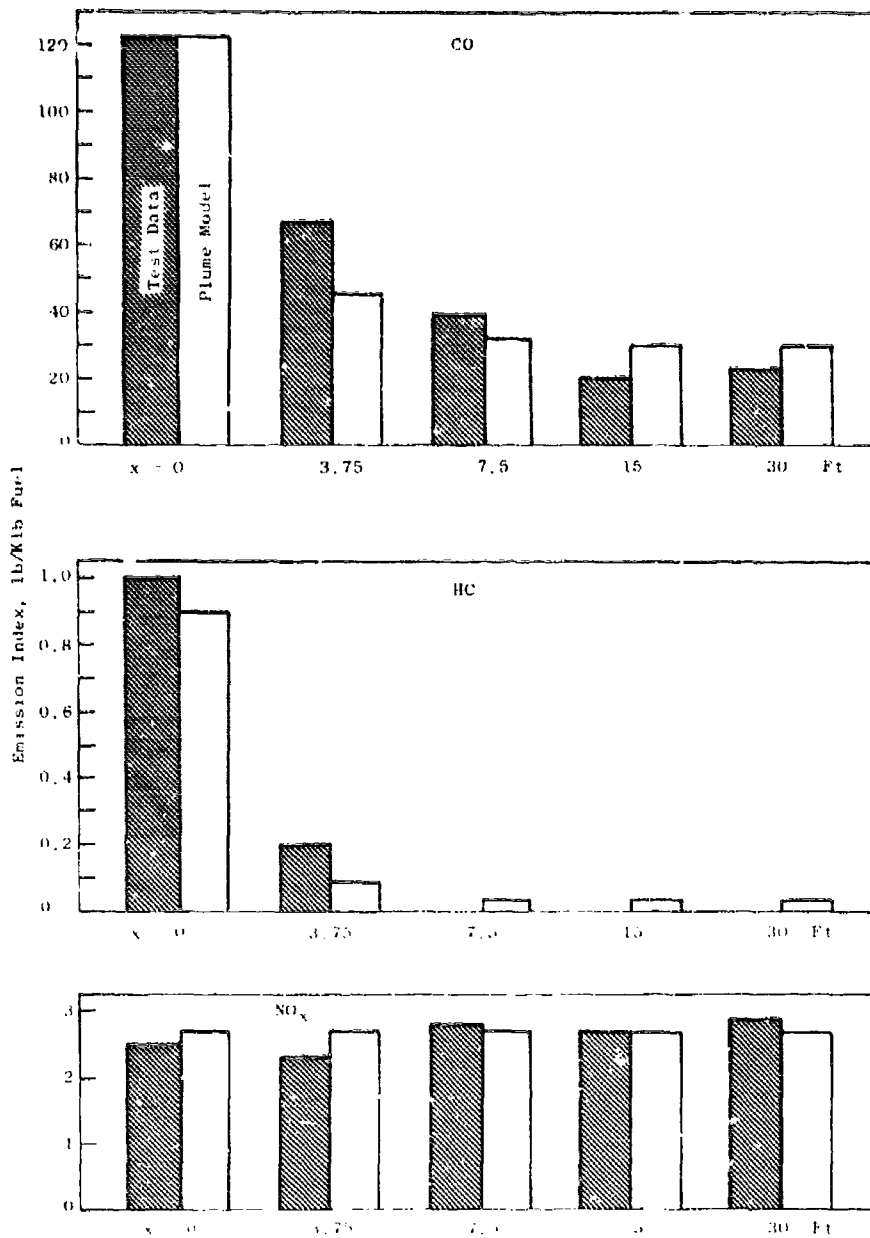


Figure 62. Plume Model Predictions of Overall Emissions Indices Compared with Phase II Test Data - J85-5 Engine, Max. A B.

Data and calculations for the lowest afterburning engine power setting (min A/B) are shown in Figures 45 through 50. The predicted profiles show acceptable agreement with the sample data points, except for the fuel-air ratio profile at $X = 30$ feet from the engine, where measured fuel concentrations are extremely low (Table 9 shows low fuel flow continuity for the measurements at this station). The predicted overall emissions indices at each station agree with those derived from the measurements, within reason. The predicted and measured net increase in CO from $X = 0$ to $X = 3.75$ feet is due to HC consumption, which generates CO faster than it can be consumed. The measured increase in CO from $X = 7.5$ to $X = 15$ is not confirmed by the model, and cannot be explained by HC consumption. The model predicts no change in NO_x , at any engine power setting; this prediction is verified by the measurements.

Data and calculations for the intermediate afterburning engine power setting (mid A/B) are shown in Figures 51 through 56. Acceptable agreement was obtained between predicted and measured profiles and overall emissions indices. The least satisfactory agreement was in the overall HC consumption, where the predicted consumption was somewhat less than measured.

Comparisons for the highest afterburning engine power setting (max A/B) are given in Figures 57 through 62. Again, agreement was generally satisfactory except for HC consumption in the streamtubes near the plume centerline, where predicted consumption lagged the measured values. Overall, however, the plume model predicted nearly complete consumption, as was measured.

6.2 COMPARISON WITH J79-15 TEST DATA

Test data from the emissions tests of an afterburning J79-15 engine were also used to validate the plume model, in the same manner as the J85 test data described in the preceding section. Since the J79 is roughly twice the diameter of the J85, the distances downstream at which calculated and measured profiles were compared were twice as great. The comparisons are presented in Figures 63 through 80. Figures 63, 69, and 75 illustrate the selection of eleven samples from the full survey to define initial ($X = 0$) profiles from which the plume model predicted the development of profiles further downstream.

Data and calculations for the minimum A/B engine power setting are shown in Figures 63 through 68. The agreement between predicted profiles and sample data points is excellent at all axial stations. As was observed for the J85, neither theory nor measurement indicates any NO_x consumption or generation in the plume at any power setting.

Data and calculations for the mid A/B engine power setting are compared in Figures 69 through 74. At the far downstream stations, the agreement is acceptable. The predicted overall residual level of HC is only about half of the measured residual, but in terms of percent of initial HC consumed in the plume, the agreement is much better. At intermediate stations, the calculations predicted more rapid consumption of both CO and HC than was measured.

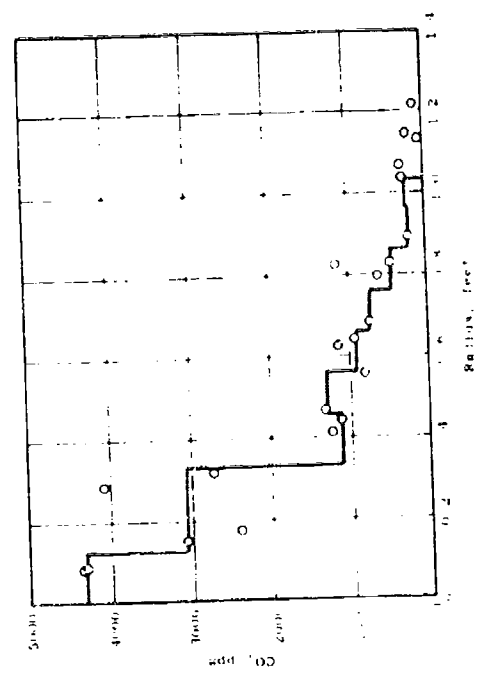
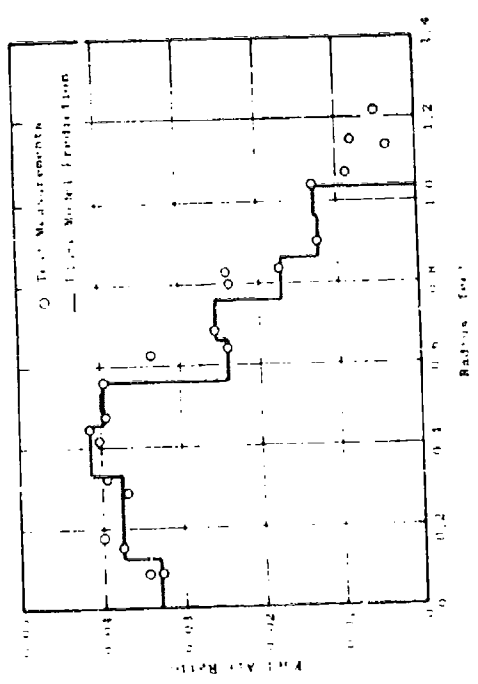
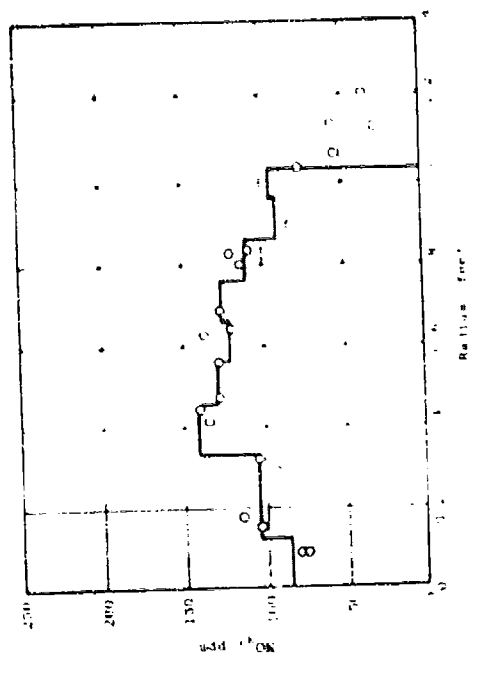
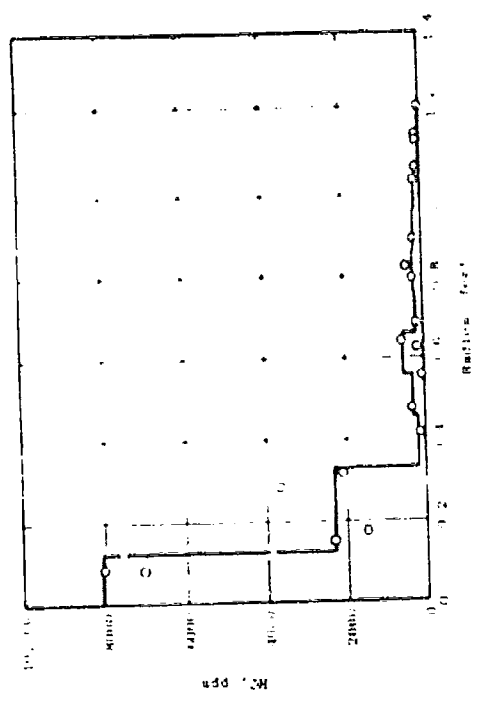


Figure 63. Plume Model Profile Predictions Compared with Phase II Test Data - J79-15 Engine.
 Min. A/B. X = 0.



Figure 64. Plume Model Profile Predictions Compared with Phase II Test Data - J79-15 Engine.
 Min. A/B, X = 7.5 feet.

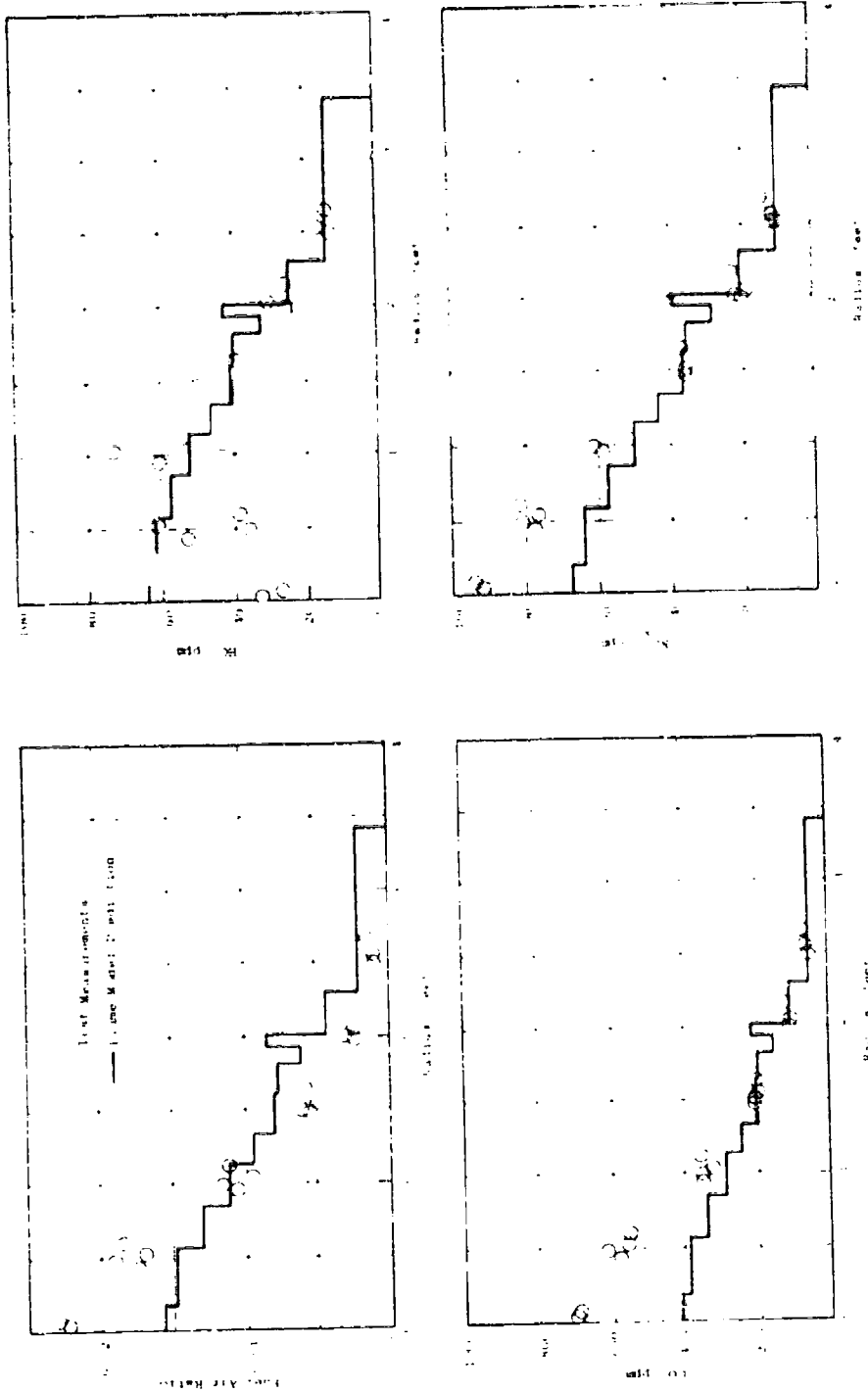


Figure 65. Plume Model Profile Predictions Compared with Phase II Test Data - J79-15 Engine.
 Min. A/B, X = 15 feet.

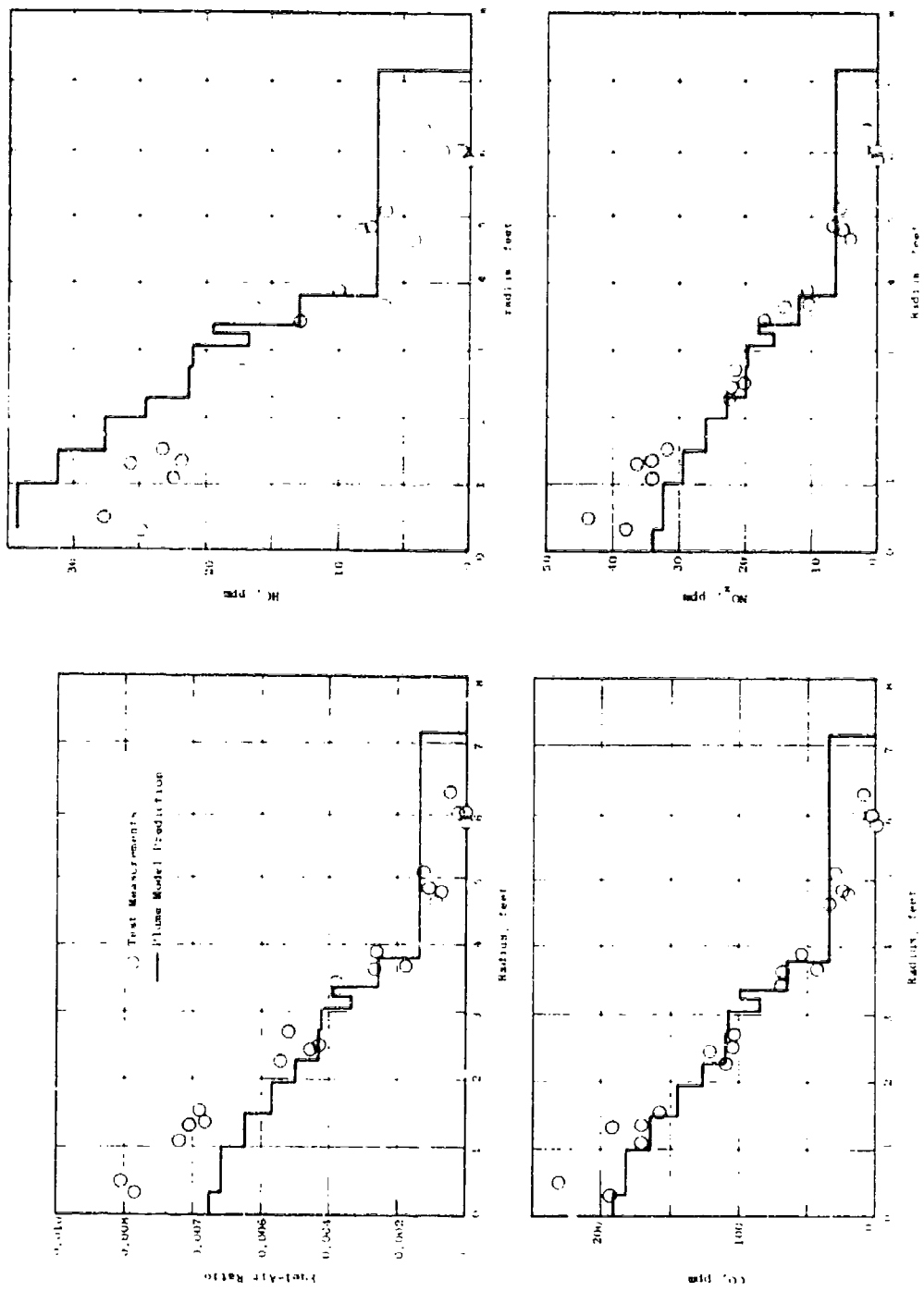


Figure 66. Plume Model Profile Predictions Compared with Phase II Test Data - J79-15 Engine, Min. A/B, X = 30 feet.



Figure 67. Plume Model Profile Predictions Compared with Phase II Test Data - J79-15 Engine. Min. A/B, X = 60 feet.

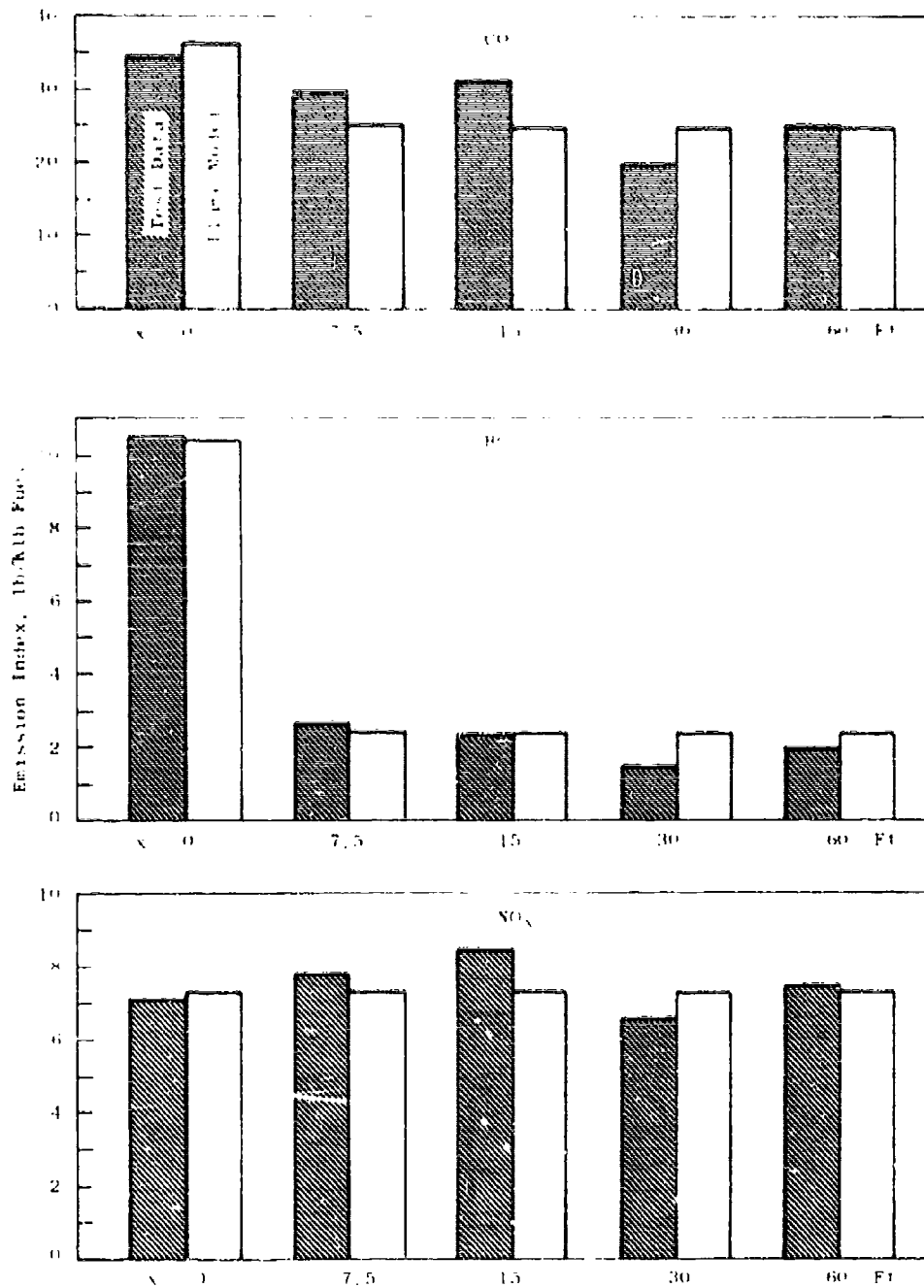


Figure 68. Plume Model Predictions of Overall Emissions Indices Compared with Phase II Test Data - J79-15 Engine, Min. A/B.

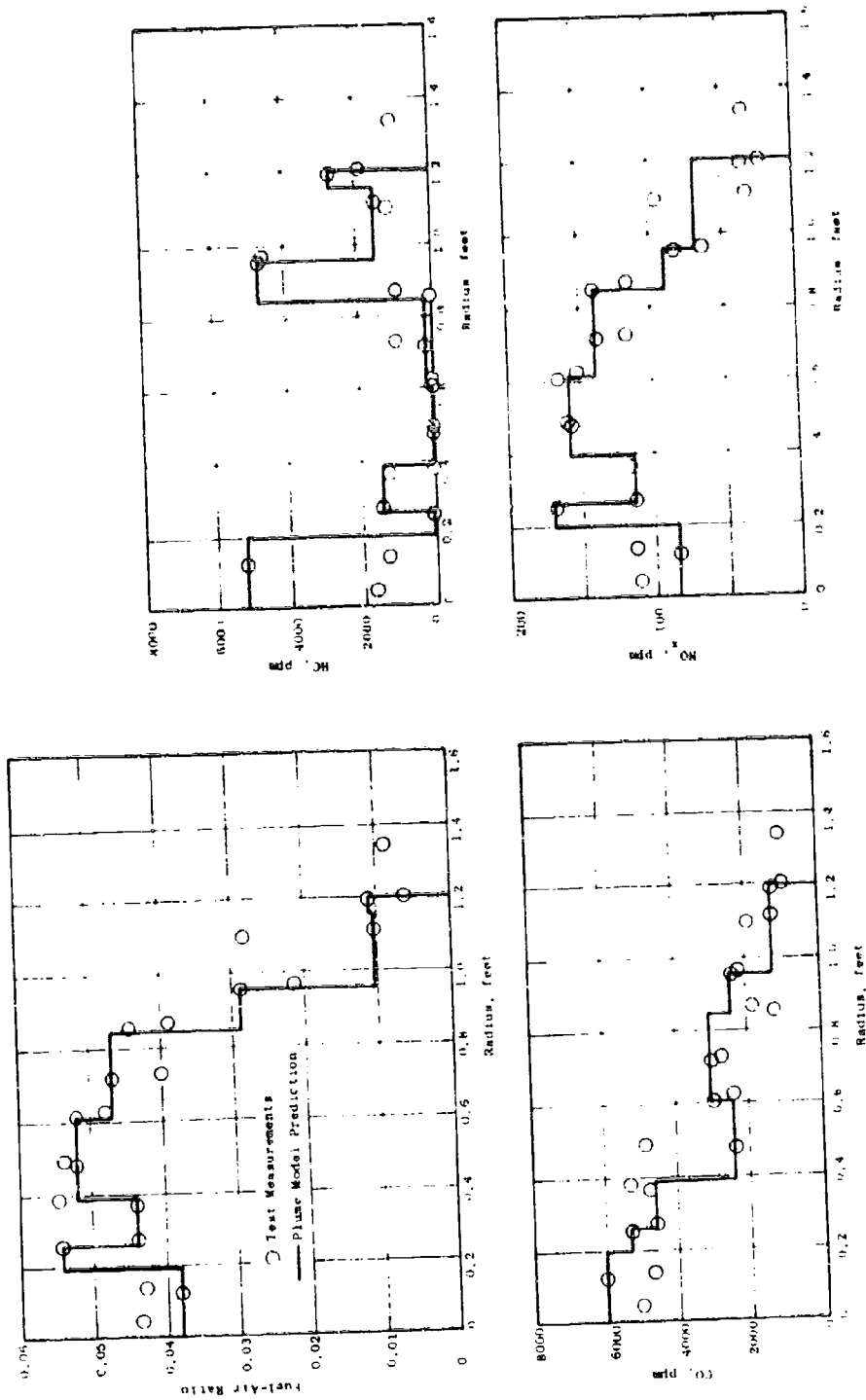


Figure 69. Plume Model Profile Predictions Compared with Phase II Test Data - J79-15 Engine, Mid. A/B, X = 0.

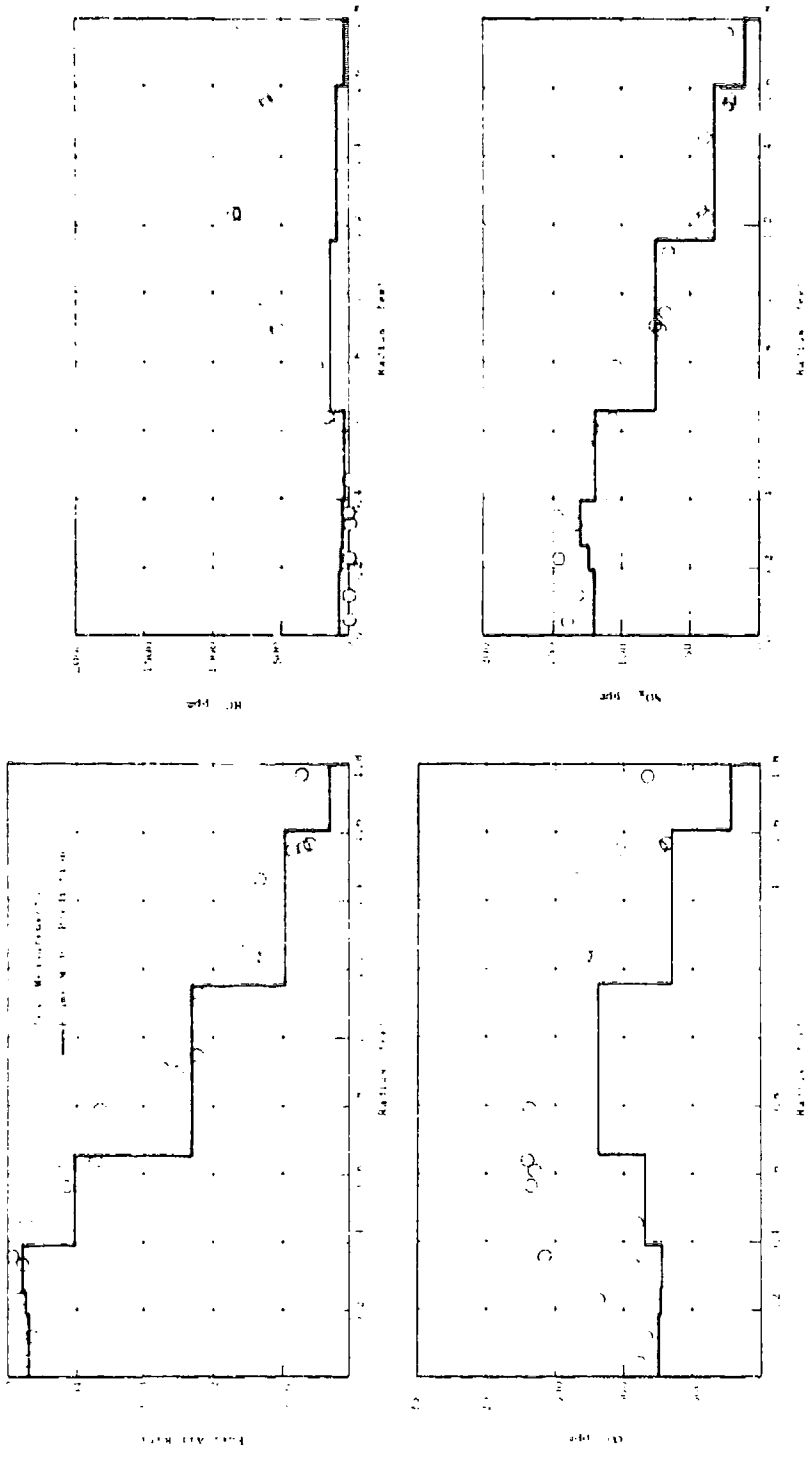


Figure 70. Plume Model Profile Predictions Compared with Phase II Test Data - J79-15 Engine.
Mid. A/B, X = 7.5 feet.



Figure 71. Plume Model Profile Predictions Compared with Phase II Test Data - J79-15 Engine, Mid. A/B, X = 15 feet.

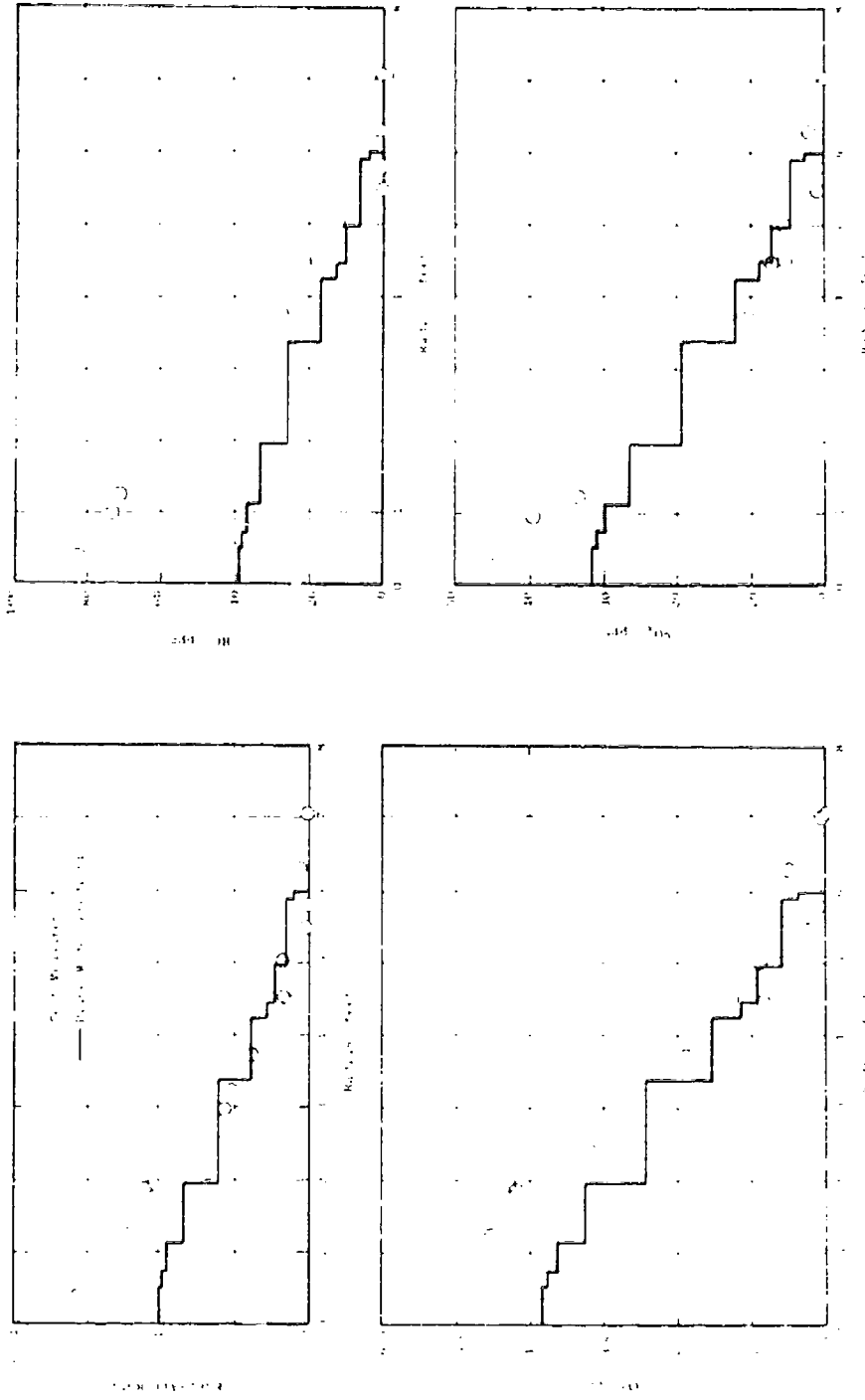


Figure 72. Plume Model Profile Predictions Compared with Phase II Test Data - J79-15 Engine. Mid. A/B, X = 30 feet.

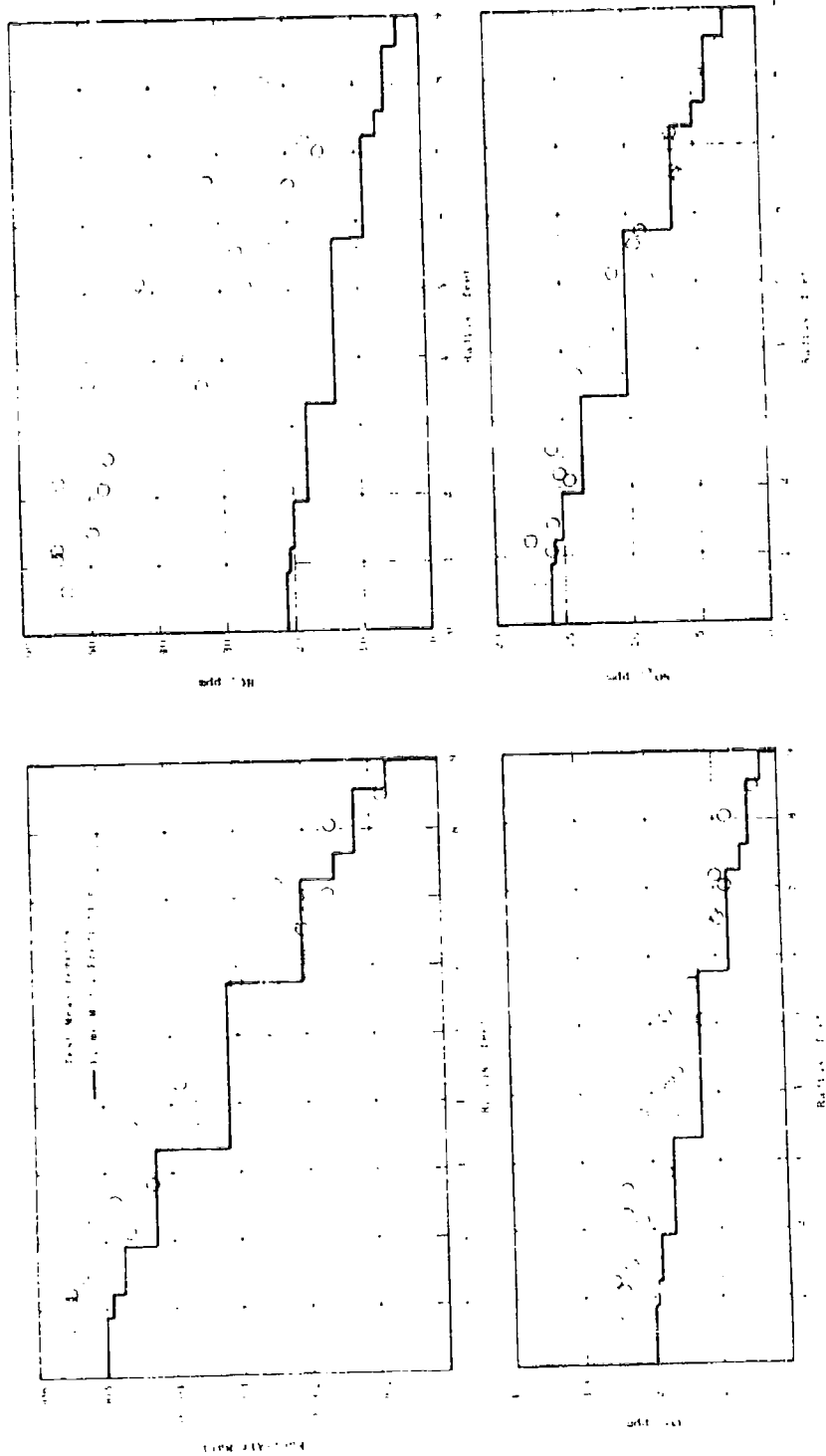


Figure 73. Plume Model Profile Predictions Compared with Phase II Test Data - J79-15 Engine, Mid. A/B, X = 60 feet.

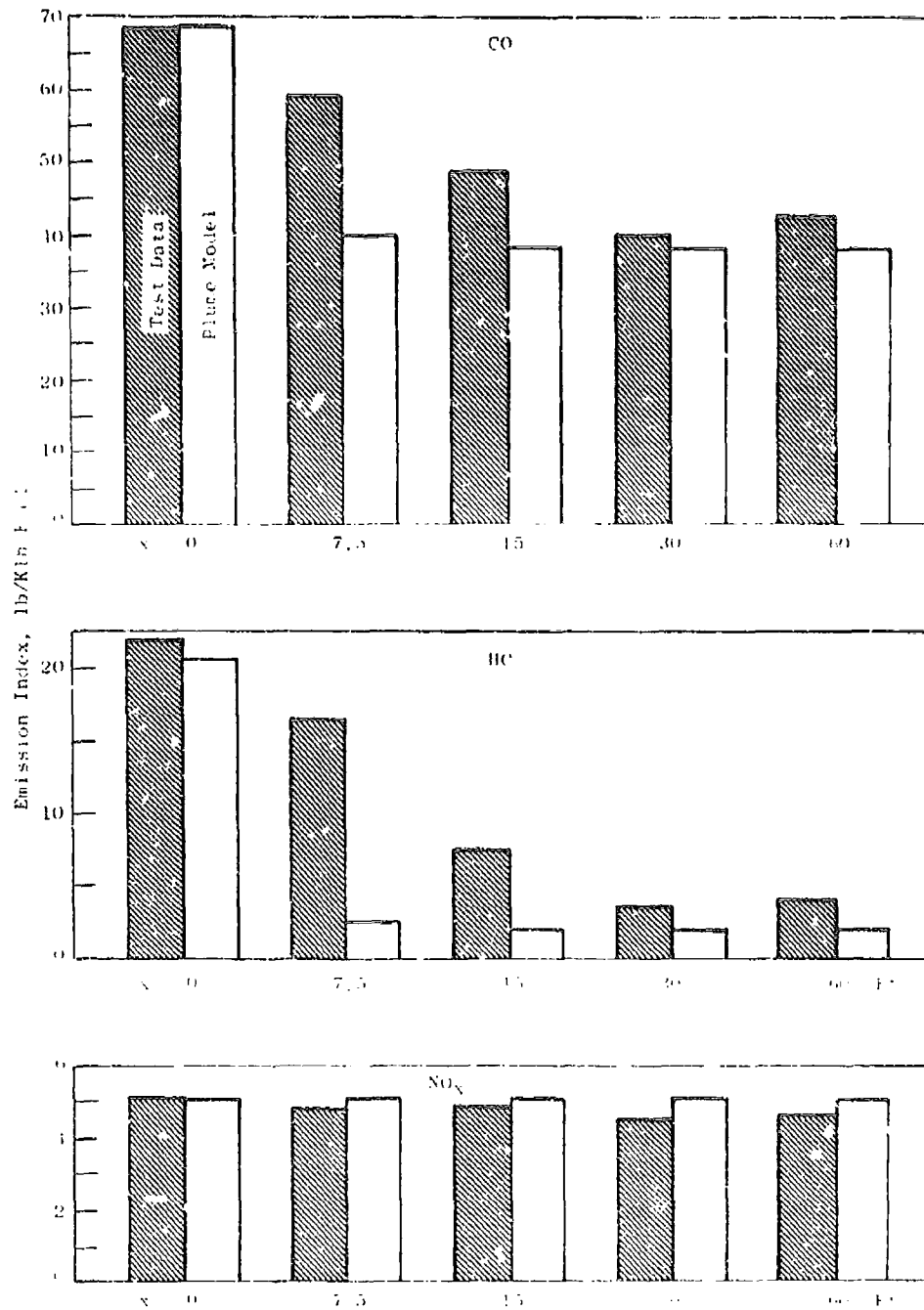


Figure 74. Plume Model Predictions of Overall Emissions Indices Compared with Phase II Test Data - J79-15 Engine, Mid. A/B.

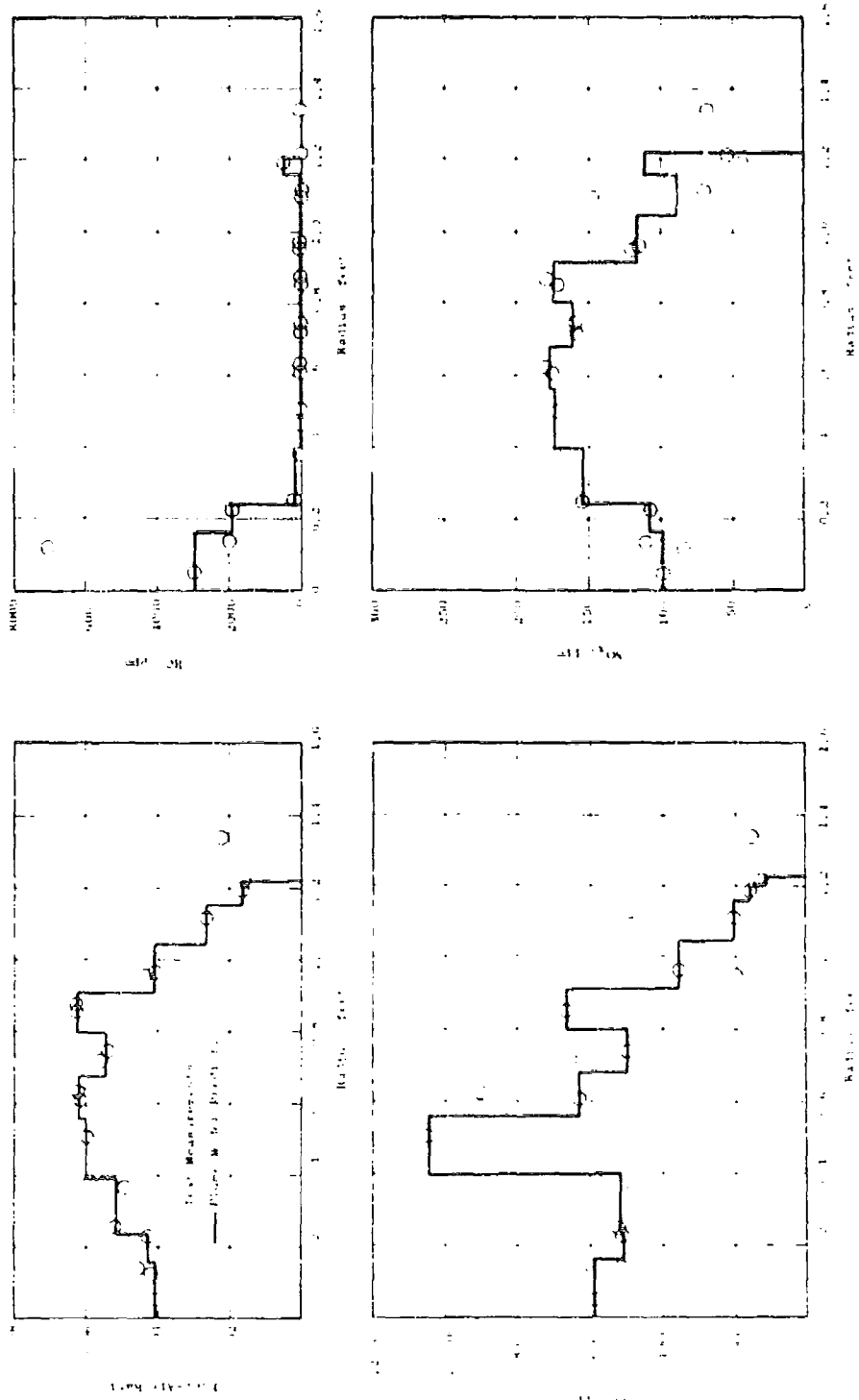


Figure 75. Plume Model Profile Predictions Compared with Phase II Test Data - J79-15 Engine, Max. A/B, X = 0.

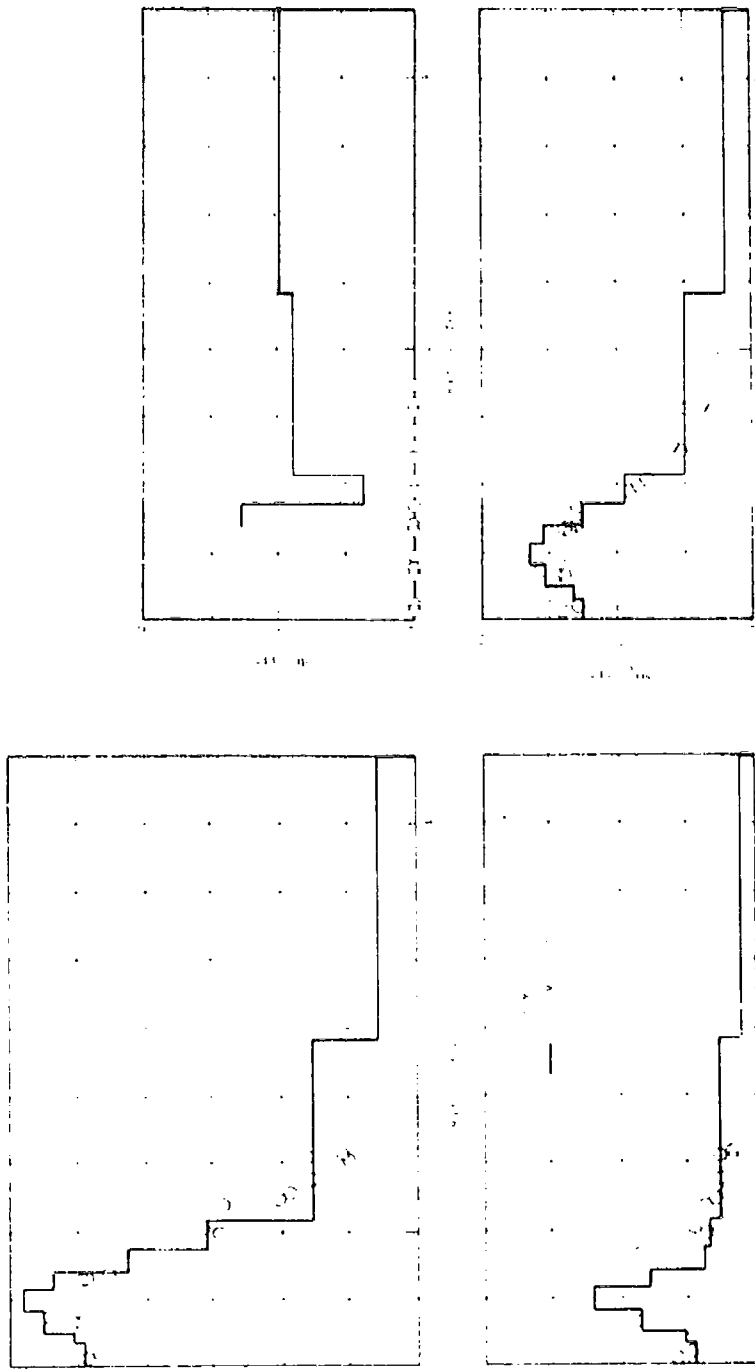


Figure 76. Plume Model Profile Predictions Compared with Phase II Test Data - J79-15 Engine,
 Max. A/B, X = 7.5 feet.

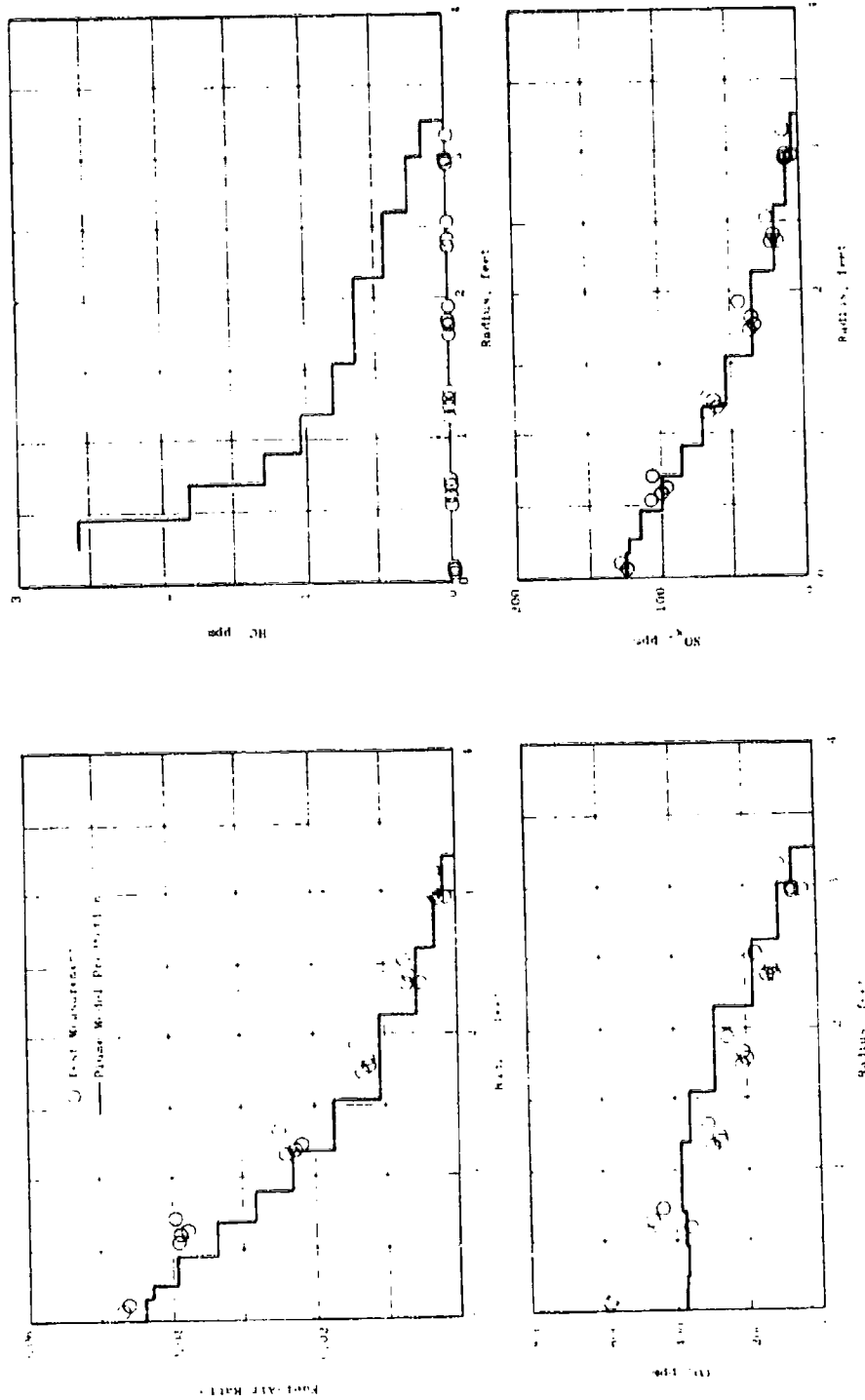


FIGURE 77. Plume Model Profile Predictions Compared with Phase II Test Data - J79-15 Engine, Max. A/B, X = 15 feet.

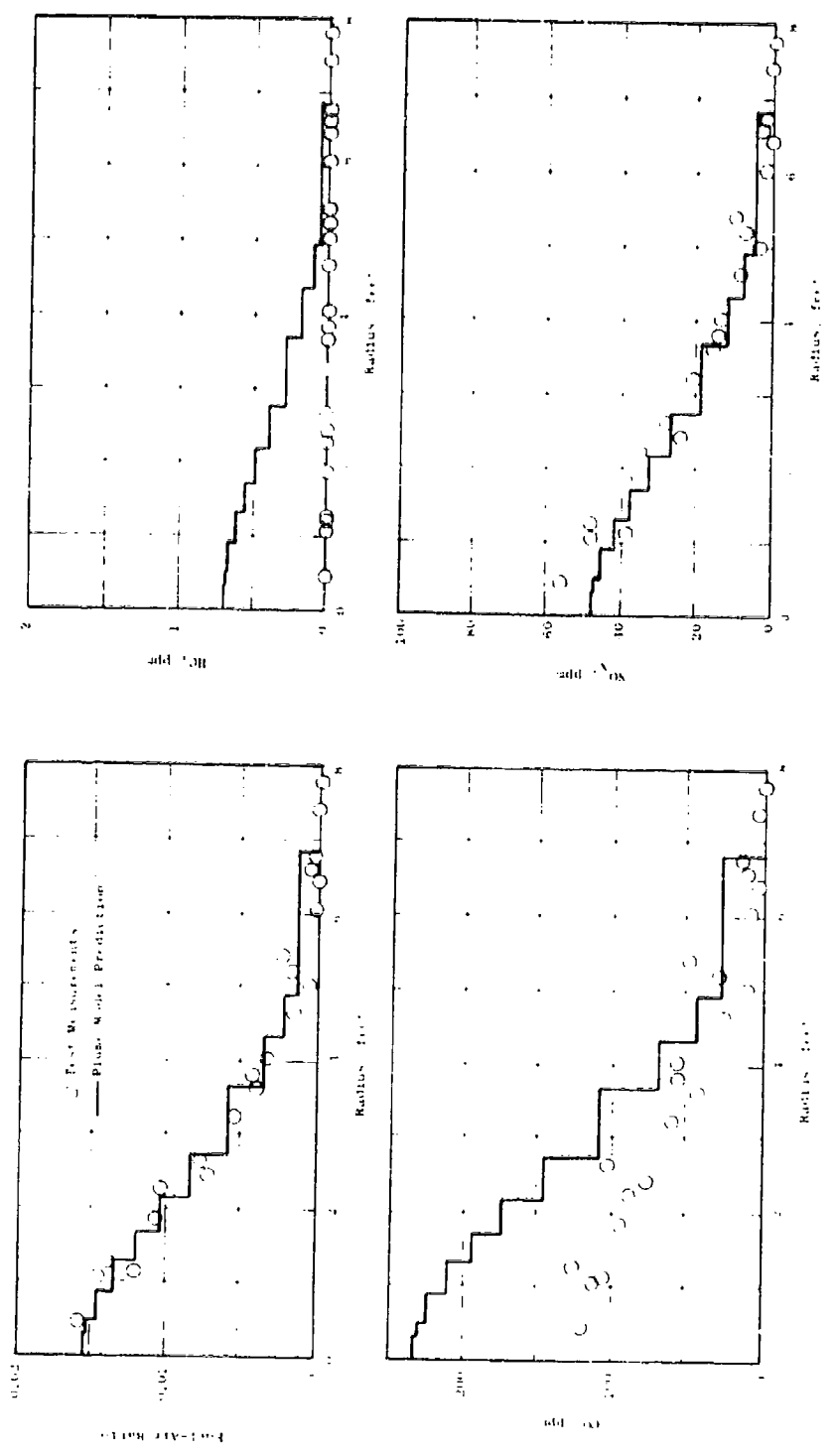


Figure 78. Plume Model Profile Predictions Compared with Phase II Test Data - J79-15 Engine, Max. A/B, X = 30 feet.

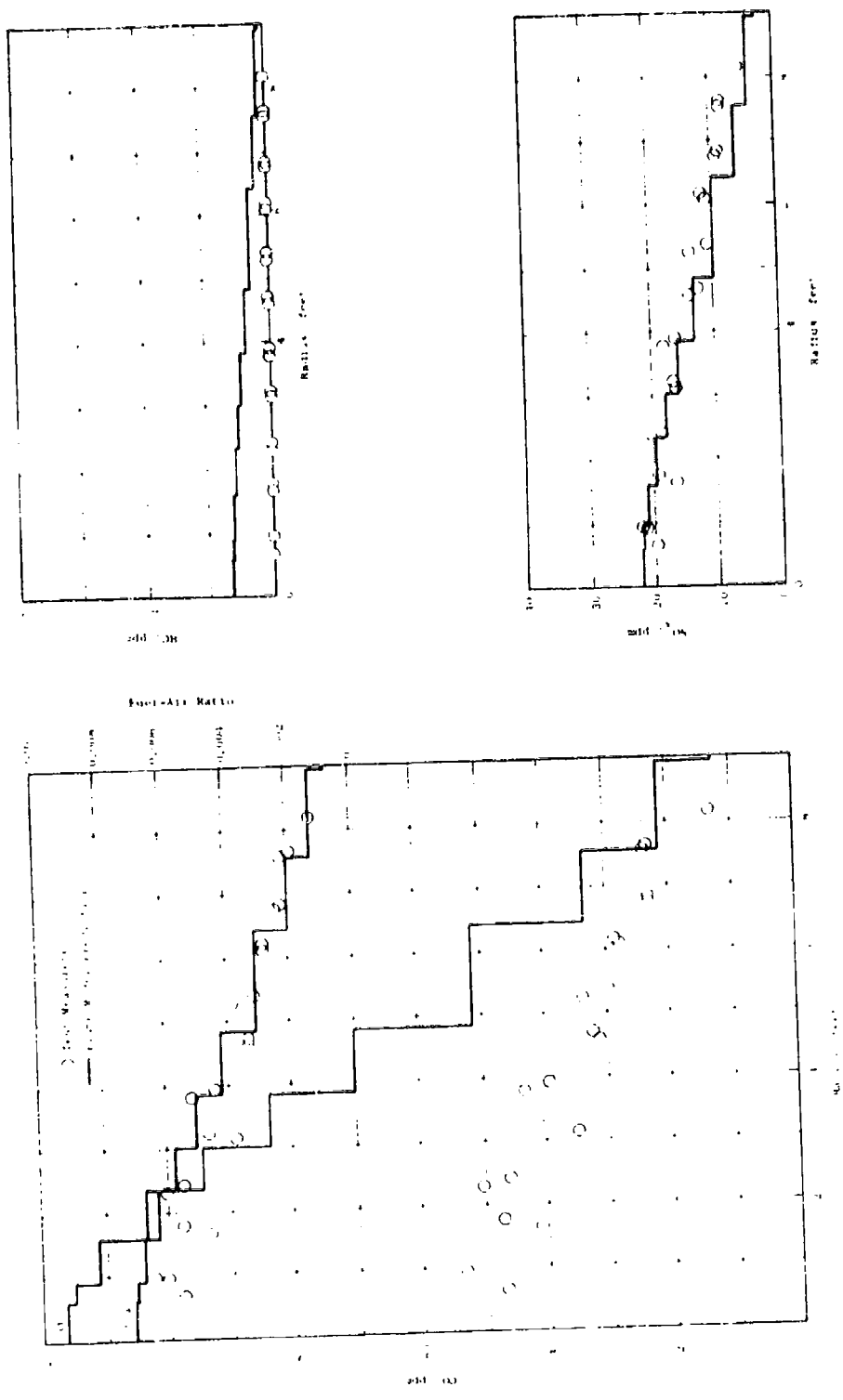


Figure 79. Plume Model Profile Predictions Compared with Phase II Test Data - J79-15 Engine, Max. A/B, X = 60 feet.

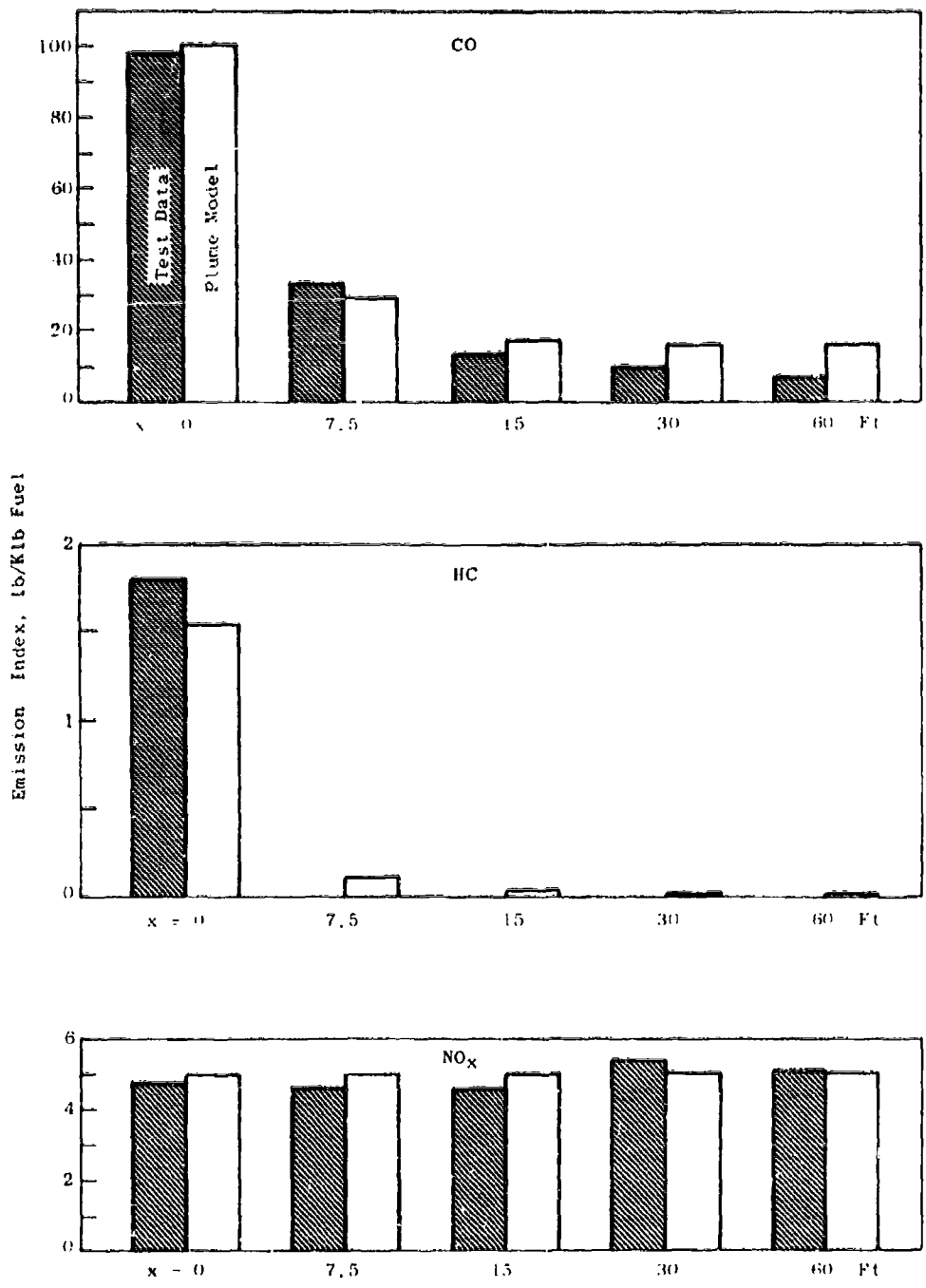


Figure 80. Plume Model Predictions of Overall Emissions Indices Compared with Phase II Test Data - J79-15 Engine, Max. A/B.

Comparisons for the maximum A/B engine power setting are given in Figures 75 through 80. Again, the agreement is acceptable when comparison is made on percent consumed. The analysis predicted quenching of the CO consumption reactions earlier than the data indicate, and the predicted HC consumption was to very low levels although not to the complete elimination indicated by the measurements.

All six cases in this and the preceding section were run using SCKP, the computationally efficient, approximate chemical kinetics routines. The J79 minimum A/B case was also run with GCKP, the NASA-developed formal kinetics routines. The results were essentially identical.

6.3 COMPARISON WITH ALTITUDE WIND TUNNEL DATA

In addition to predicting emissions consumption in exhaust plumes of afterburning engines undergoing sea-level static tests, the analytical plume model is capable of modeling engine exhaust plumes in a moving, high-altitude environment. This capability is potentially useful in predicting contaminants released into the upper atmosphere by aircraft with afterburning engines.

To validate the altitude capability of the plume model, gas sample data from a survey made near the exhaust nozzle of a J85 engine mounted in a supersonic wind tunnel were input to the model, and the model's predictions of plume development and contaminant consumption were compared with data obtained at axial stations farther downstream. The tests were performed for FAA at AEDC (Reference 33).

Predicted and measured fuel and contaminant profiles are compared in Figures 81 through 83. Agreement is generally satisfactory. The static pressure in the plume was 1.3 psia in these tests. At this pressure, the CO consumption reactions are essentially quenched. The model predicted 20 percent consumption of hydrocarbons, which seems to agree with the measurements. The emissions consumptions at altitude are much lower than at sea level static because of the low reaction pressure levels and the low static temperature resulting from the higher pressure ratio expansion. With these lower consumption levels, the model provides generally more accurate prediction than for sea level operation.

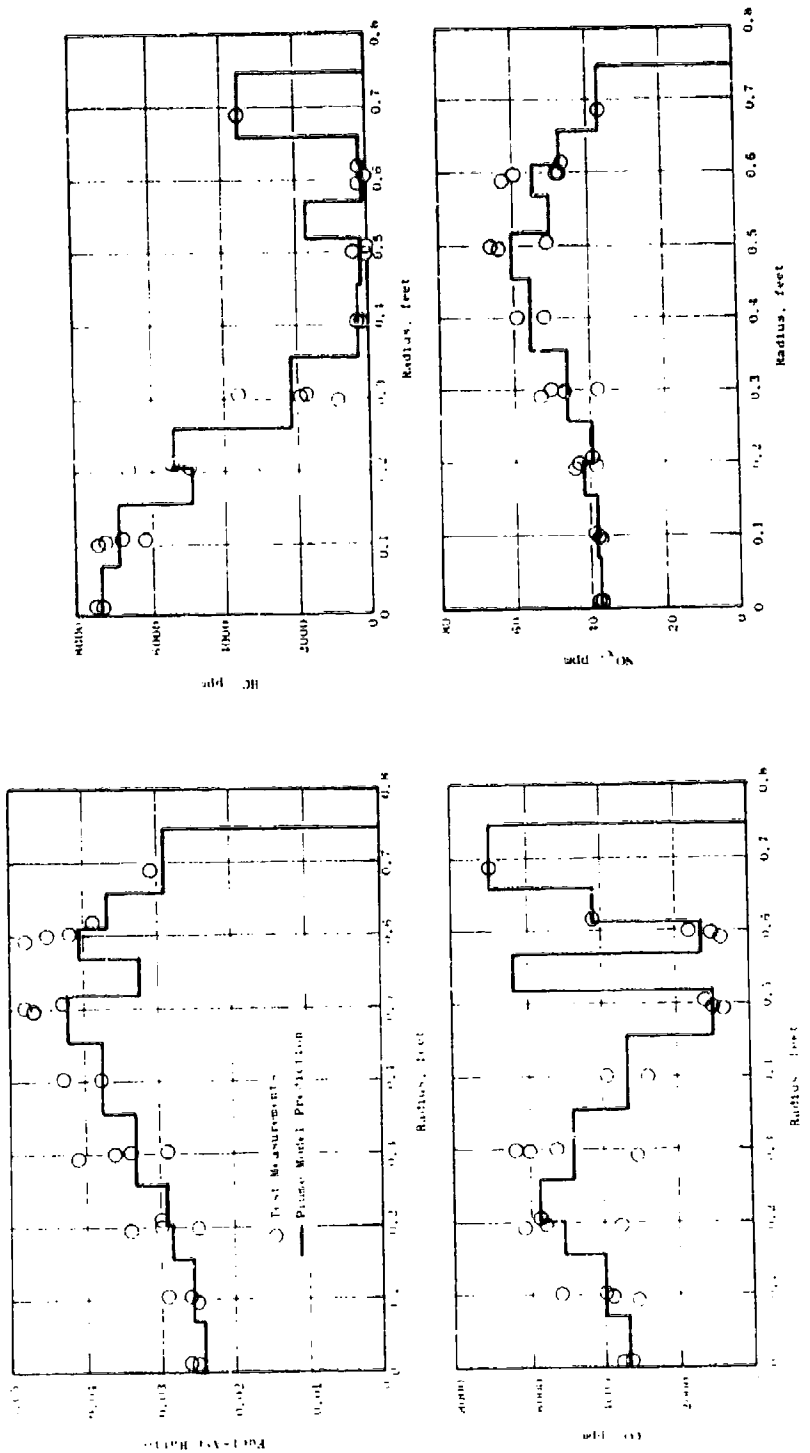


Figure 81. Plume Model Profile Predictions Compared with AEDC Test Data - J85-5 Engine, Mach 1.6/55,000 feet, $X = 0.4$ feet.

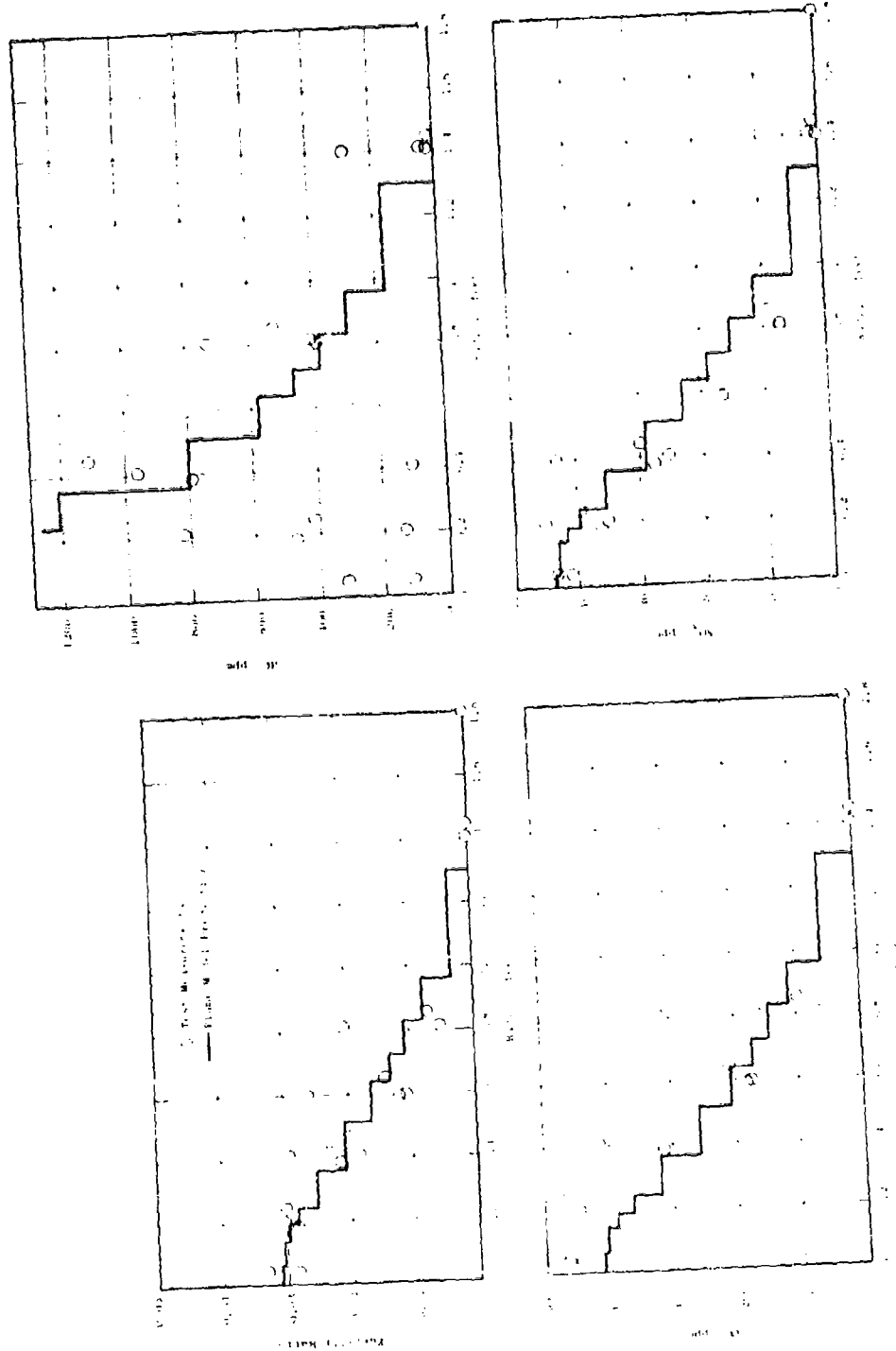


Figure 82. Plume Model Profile Predictions Compared with AEDC Test Data - J85-5 Engine, Mach 1.6/55,000 feet, $X = 13.9$ feet.

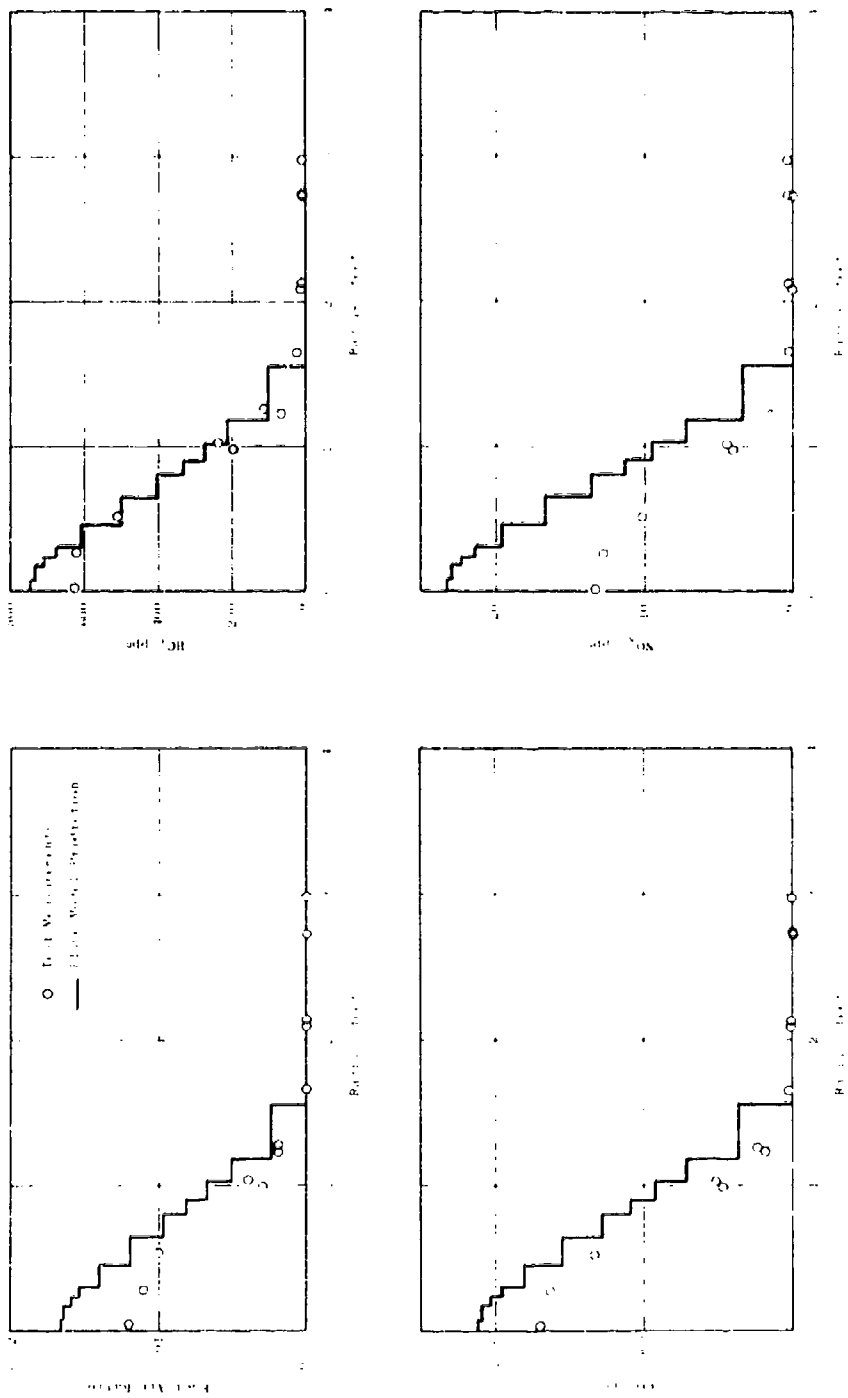


Figure 83. Plume Model Profile Predictions Compared with AEDC Test Data - J83-5 Engine, Mach 1.6755, 000 feet, X = 29.7 feet.

SECTION 7.0

DEVELOPMENT OF AFTERBURNER EMISSIONS MEASUREMENTS PROCEDURES

7.1 GENERAL CONSIDERATIONS

The Phase II afterburner emissions measurements on the J85 and J79 engines confirmed previously anticipated complexities encountered in assessing emissions levels at the nozzle exit plane. Sampling probes must be designed so as not only to withstand the severe environment but also to quench the reactions at the probe inlet. The exhaust is generally so nonuniform, both radially and circumferentially, that a relatively large number of samples are required, and local total pressure measurements are required to properly mass weight the individual measurements. Accurate probe position measurements are required to properly assess the area weighting factor for each local measurement. Finally, the local measurement must be processed through the extremely complex plume model computer program in order to evaluate emissions levels ultimately emitted into the atmosphere.

Measurement of emissions at an axial station far enough downstream of the engine that mixing and plume reactions are complete avoids many of the difficulties associated with the nozzle exit plane measurements. The low concentrations encountered at the downstream locations require measurement sensitivity somewhat better than that normally required for main engine emission measurements. A data reduction procedure was developed in Phase II which accounts for the ambient levels of emissions. Although the procedure does not evaluate carbon balance as a test for representative sampling, various statistical methods are available to check for overall data consistency.

The major potential drawback of the downstream measurement method is that it requires considerable open area behind the engine and would generally necessitate an outdoor test facility. Since this requirement might unduly restrict the applicability of the afterburner emissions measurement techniques, it was decided that the finalized procedure developed on this program would include both the downstream measurement method and the nozzle exit plane measurement method. The downstream method is the preferred method and is referred to as the "Far Plume" procedure. The nozzle exit plane method, referred to as the "Near Plume" procedure, is the alternative procedure which may be employed if no test facility is available which meets the requirements of the Far Plume procedure.

The finalized measurement procedure is presented in Appendix B of this report. The general format used is similar to that of SAE ARP 1256. In specifying the measurement equipment used, an effort was made to permit utilization of the same equipment as that used for main engine emissions measurements, as specified in ARP 1256.

The SAE ARP 1256 (Issued 10-1-71) has been followed in these procedures as far as practicable. However, the SAE document is becoming outdated, and efforts at revision are in progress at the time of this writing. Procedural differences between ARP 1256 and the afterburner emissions measurement procedures presented here arise either from anticipated revisions to ARP 1256 or from the basic requirements of the afterburner measurements. Major differences are listed below:

Equipment - ARP 1256 specifies NDIR and NDUV instruments for NO and NO₂ measurements, while the A/B procedures specify a chemiluminescence instrument with converter.

Sample Line Temperature - ARP 1256 specifies $302 \pm 9^\circ$ F, while the A/B procedures specify $300 \pm 27^\circ$ F, anticipating a similar revision in ARP 1256.

Sample Transit Time - The A/B procedures require 10-second sample transit time, while ARP 1256 requires 2 seconds.

Sampling - ARP 1256 permits mixed samples, while the A/B procedures require individual samples. Also, for the "Near Plume" procedure, 22 sample points are required rather than 12 in ARP 1256.

Probe Temperature - The probe temperature is not specified in ARP 1256, while the A/B procedures require the sample line within the probe to be maintained between 160 and 327° F.

Data Reduction - ARP 1256 requires averaged values to be reported. Considerably more extensive data reduction procedures are required for A/B emissions measurements.

Several other general comments regarding these procedures are appropriate at this point. Considerable conversion of NO to NO₂ at certain afterburning conditions was found in the Phase II afterburning emissions measurements. This conversion of NO to NO₂ in afterburners can be quite important since, in at least one reported case involving an afterburning engine (Reference 34), sufficient NO₂ existed in the exhaust that the plume was visible. In the proposed afterburner emissions measurement procedure, it is thus important that both total NO_x and NO measurements be made since, at least for some future engines, it may be necessary to set some limit on the NO₂ concentration in order to prevent plume visibility.

Due to the potentially high NO₂ concentration in the exhaust of afterburning engines, it is particularly important that the converter in the NO analyzer be highly efficient and that frequent checks be made to assure proper operation of the converter. This factor was considered in the proposed emissions measurement procedure.

It is recommended that smoke measurements not be required for engines at afterburning power levels. Smoke measurements made in Phase II on the J79-15 engine showed a decrease in smoke level with increasing reheat power level. This is to be expected since conditions in the mainburner are most conducive

to smoke formation, while the high temperature, low pressure conditions in the afterburner would tend to oxidize smoke particles and hence reduce the smoke level. The highest smoke levels, thus, are likely to occur under nonafter-burning conditions, and adequate procedures already exist for such measurements (e.g. SAE ARP 1179).

The finalized measurement procedure, described in a format similar to that used for SAE ARP 1256, is presented as Appendix B of this report. The finalized measurement procedure is divided into two parts: Part A - Far Plume Procedure, and Part B - Near Plume Procedure. Each part is divided into nine sections as follows:

1. Definitions
2. Analysis Equipment
3. Sampling Equipment
4. Equipment Layout
5. Instrument Routines
6. Reference Gases
7. Test Procedure
8. Minimum Information to be Recorded
9. Calculation of Results

Some discussion of specific details of the two measurement methods is contained in the following sections of this report.

1.2 FAR PLUME PROCEDURE (PART A)

Section A2 - Analysis Equipment - NDIR instruments are specified for CO and CO₂ measurements, flame ionization detector for HC, and chemiluminescence analyzer with converter for NO and NO_x. This follows the EPA equipment specifications (Federal Register, July 17, 1973) rather than the NDIR-NDUV combinations for NO-NO₂ measurements specified in ARP 1256. For the NDIR instruments, zero drift and span drift are specified as 0.5 percent per 1 hour, rather than 1 percent per 8 hours generally required. Repeatability and noise are specified at 2.5 percent, and sensitivity of 0.5 ppm for CO and 0.005 percent for CO₂ is required. These latter requirements are consistent with the lower concentration levels encountered with the Far Plume procedure. For the HC and NO analyzers, the noise, zero drift, and span drift are as specified in ARP 1256, since the more sensitive ranges available on these instruments result in total instrument sensitivity adequate for the Far Plume procedure.

Section A3 - Sampling Equipment - Conventional probe design is required with specified probe temperatures such as to permit either hot water or steam heating. In order to specify sampling locations, both axial and radial, the sampling system is scaled according to the engine nozzle diameter. A minimum of 11 sampling points is required, approximately equally spaced across a diameter. This number of samples permits meaningful statistical treatment of the data. Fewer samples can be taken with correspondingly reduced measurement accuracy. With only two samples, the statistical treatment is meaningless.

since a perfect straight line fit results. In principle, the method can be used with only one sample, if an independent measurement or estimate of the ambient levels is available.

Sample line temperature is specified at $300 \pm 27^\circ \text{F}$, which is consistent with the proposed revision to ARP 1256 now being considered by the SAE E-31 Committee. The tolerance is increased from 9°F over that required by the current ARP 1256 and the EPA requirement. There appears to still be some controversy concerning specification of sample line temperature.

Since very long sample lines would probably be involved with this procedure, no maximum sample line length is required. The requirement of 10-second gas transport time effectively limits the sample line length to a reasonable value.

Section A4 - Equipment Layout - The equipment layout is similar to that specified in ARP 1256.

Section A5 - Instrument Routines - Instrument routines are similar to those specified in ARP 1256. Additional checks of instrument zero and span drift, repeatability, and noise level are specified. Thermal converter efficiency check is as specified in the EPA procedure. This efficiency check is required at least monthly.

Section A6 - Reference Gases - Specified Reference Gases are similar to those required by ARP 1256.

Section A7 - Test Procedures - Strong crosswinds can deflect the plume, and a 5-mph crosswind limit is specified. Ambient air concentration limits are not specified in the procedure since the data reduction method takes ambient levels into account. The procedure does contain a caution against high ambient levels.

Section A9 - Calculation of Results - CO and CO₂ are first corrected to true sample moisture level, in case a dryer was used. A linear fit of each pollutant versus CO₂ is then made by the method of least squares. Correlation coefficients are calculated by standard statistical procedures. If the slope of the line is larger than 10, then the correlation coefficient is required to be greater than 0.95. This value was chosen after considerable deliberation concerning what was obtained during the Phase II and Phase III measurements and what might reasonably be obtained with some care.

Emissions indices are then calculated from the slopes of the linear fits. The emission flow rate (lb/hr) is then calculated from the overall engine fuel flow and the emission index. Emission standards or goals may be specified either in terms of emission indices or total flow rate of emissions. The problem of establishing Air Force standards or goals for afterburning engines is not addressed in this program.

7.3 NEAR PLUME PROCEDURE (PART B)

Section B2 - Analysis Equipment - With the exception of the chemiluminescence analyzer for NO and NO_x, the specified equipment is basically the same as that in ARP 1256.

Section B3 - Sampling Equipment - The sampling probe is required to be of the quenching type, and the pressure ratio across the orifice is required to be at least 5. Only general guidelines are given in regard to cooling of the probe structure, since the responsibility for the probe integrity must rest with the probe designer and operator. Total pressure measurement is permitted to be separated by no more than 0.2 inch from the sampling point, which permits use of a combination tip in which pressure and gas sample are obtained from separate orifices. The two measurements may then be obtained simultaneously.

The axial sampling plane is required to lie within eight inches of the exhaust plane. This would allow for normal growth of the engine and also for axial translation of the nozzle. A minimum of 22 sampling points are specified to lie across two diameters. The points are specified to be approximately equally spaced, although this results in somewhat inadequate coverage of the outer exhaust region. Equal area sampling, on the other hand, results in sparse coverage of the inner region where quite severe gradients have been encountered. To accurately locate the edge of the exhaust stream, as required for the plume model, the total pressure at the outermost sampling point is required to be between 1.05 and 1.10 times the ambient pressure. The actual edge of the stream is determined by extrapolation of the outermost point.

Section B9 - Calculation of Results - All required calculation of results is accomplished by the plume model. Assembly of the plume model input data, however, requires some effort. A difficulty that evolved over the course of this program is that, to conserve computer time, the plume model is set up to accommodate 11 samples or stream tubes. However, due to the circumferential gradients which can exist when afterburning, at least 22 samples are judged to be required to obtain representative sampling. A manual procedure is specified which effectively averages the data by plotting against radial position and drawing a smooth curve through the data points. Eleven values are then selected from the smooth curve for input to the plume model. These 11 values are selected to be in centers of 11 equal areas.

Several alternative approaches are possible which are not contained in the finalized procedure. The first is to revise the plume model to accommodate 22 or more individual samples. This would be a considerable task and would involve increased computation time in the data reduction. This should, however, result in more reliable overall data. The second approach is either to reduce the number of sampling points to 11, or to carefully select 11 sampling points from the 22, in order to reduce the plume model input to 11 sets of values. This latter approach would be the least reliable. The approach specified in the finalized procedure is recommended, since the moderate effort required should result in increased data reliability and, in addition, it is well to plot the curves in order to observe the radial and circumferential variations in concentrations and total pressure.

It is required that plume model output be computed at 0, 35, and 50 nozzle radii downstream of the exhaust nozzle in order to determine if reactions are completed, as determined by identical values at the 35 and 50 radii axial stations. If the two values are not the same within 5 percent, then the computer program shall be rerun for an axial distance of 70 nozzle radii downstream.

The computer program calculates total gas flow and fuel flow, along with emission indices and total contaminant flow. The standard or goal may thus be specified as either contaminant flow or emission index.

A check of data consistency or representative sampling is required which specifies that the calculated fuel flow shall agree with the metered fuel flow within ± 15 percent. However, a retest is not required if the agreement is not within ± 15 percent. It should be up to the standard-setting agency to specify the procedure if the data consistency check is not met.

The plume model is currently not programmed to calculate NO or NO₂ in the exhaust, even though the NO_x and the NO measurement are required. However, if NO₂ visibility criteria are developed in the future, the plume model should be modified to calculate total NO₂ flux at the various stations.

It might appear that substantial simplification of the total modeling approach could be developed. A possible method to accomplish this might be to use the complete model for a parametric study to generate a series of graphs from which consumption of species in the plume might be obtained. However, the engine afterburner emissions data obtained on this program have demonstrated that the distribution of CO and HC at the nozzle exit plane, along with its relation to the temperature profile, has an extremely important effect on subsequent consumption of these species in the plume. Quantities of these gases existing near the engine centerline are constrained to mix with the hot surrounding gases and thus tend to be largely consumed, while those existing near the exhaust boundary mix with cold surrounding gas and the reactions tend to be quenched. It is not clear how such distribution might be quantified for inclusion in the graphical approach referred to above. Basically, then, it is the dependence on distribution which prevents significant simplification of techniques employed for predictions of consumption in the plume.

SECTION 8.0

FINAL ENGINE EMISSIONS TESTS USING NEAR PLUME AND FAR PLUME PROCEDURES

After the final measurement procedures were defined early in Phase III of this program, another series of afterburner emissions measurements were made on the same J85 and J79 engines as had been used for the Phase II engine tests. Results of these Phase III engine tests are presented in this section of the report.

8.1 TEST SETUP AND INSTRUMENTATION

The proposed "Far Plume" procedure for afterburner emissions measurements necessitates accurate measurement of emissions levels considerably lower than those normally encountered in gas turbine emissions measurements. Special procedures were investigated to enable reliable measurements at the fractional part per million levels. The actual levels measured are close to normal ambient levels. It is obviously desirable to be able to use the same, or slightly modified, analysis equipment normally used at the nozzle exit locations for nonafterburning engines.

Accuracy of the concentration measurements at very low levels is determined primarily by the sensitivity and stability of the measurement instruments. An investigation of some factors affecting the sensitivity and accuracy of the analysis equipment was made. It was found that adequate sensitivity of all instruments can be obtained with a digital voltmeter readout having 1-millivolt sensitivity and a 5-volt range. This was the type of readout used in the Phase II engine tests. For CO, HC, and NO_x, the sensitivity was about 0.1 ppm with this readout, and better than 0.001% for CO₂. In some cases it was found that improved signal-to-noise ratio can be obtained with reduced instrument gain.

A check of instrument stability was made by observing the instrument output over a period of several hours with zero gas (N₂) flowing through the system. The total variation observed, expressed as equivalent concentration, was ± 0.35 ppm for CO; $\pm 0.001\%$ for CO₂; ± 1.3 ppm for HC; and ± 0.16 ppm for NO. Except for the HC analyzer, the stability measured was comparable to or better than that observed on other instruments used for GE engine testing and is within the manufacturer's specified stability limits. A representative of the manufacturer was consulted in an attempt to improve the stability of the HC analyzer. At his suggestion, a container of molecular sieve was put in the line to remove residual hydrocarbons from the zero gas. Considerable improvement in stability was obtained after this modification.

From these investigations of the behavior of the gas analyzers, it was reaffirmed that these instruments are suitable for reliable measurement of gas concentrations near ambient levels, provided that adequate precautions are taken to obtain sufficient sensitivity and stability.

Some revisions were made to the CAROL data reduction program in preparation for the Phase III engine tests. This time-sharing system computer program was used to perform initial calculations with the gas analysis data obtained during engine testing. The data from the test log was filed in the time-sharing system at Edwards. The program was then run either at Edwards or at Evendale. The digital data acquisition system (PCM) which had been used for the Phase II engine testing was not used for the Phase III engine tests, since the quantity of data required did not warrant its use. The test data was thus entered into the time-sharing system from the test log rather than via the digital data acquisition system. Data processing beyond the CAROL program, including input to the plume model, was handled as in the Phase II engine tests.

One other modification to the data reduction procedure involved incorporation of the ABE program directly into the CAROL program. The ABE program, which performs a linear fit of emission concentration versus CO₂ concentration by the method of least squares, was run as a separate program during Phase II engine testing. The ABE program is specifically intended to process data obtained at probe locations far removed from the nozzle exit plane (Far Plume procedure), where measured concentrations can approach ambient levels.

The sampling and analysis system used in the Phase III tests was basically the same as for the Phase II tests. One exception, however, was the addition of a sample pump immediately before the gas analysis system. This considerably speeded the sample transit time, since the pressure was reduced in the long length of sample line between the sample pump at the probe and the analysis system.

8.2 FINAL TEST RESULTS - J85-5 ENGINE

Afterburner emissions measurements on the J85-5 were made at four engine power settings (Military, Min A/B, Mid A/B, and Max A/B) using both the Near Plume (nozzle exit plane) and Far Plume (30 feet aft) measurement procedures.

Initially, attempts were made at measuring ambient levels near the inlet of the J85 engine. An open stainless steel tube was mounted near the side of the engine inlet screen which covered the bellmouth, and a sample from this tube was pumped to the analyzers. During engine operations, analysis of the samples showed high and erratic concentrations, especially for HC during A/B operation. It appeared that engine leakage or local recirculation patterns contributed to these erratic readings. Gross reingestion of exhaust was not the major problem since no large increases in engine inlet temperature occurred. It thus appeared that the ambient sample location adjacent to the engine inlet was a poor choice for these particular tests. Attempts to measure "ambient" levels in the vicinity of the engine were then abandoned. Note that direct measurement of the ambient levels is not required for the Far Plume procedure, since ambient levels are accounted for in the data reduction process.

Table 19 is a summary of the engine operating data for the J85-5 Phase III tests. Column headings are as in Table 8, which gave a summary of engine operating data for the Phase II tests.

Table 19. J85-5 Engine Data for Final Afterburner Emissions Tests (Phase III) - JP-4 Fuel.

Date	No.	Power (HP)	AP (in. Hg)	AT (in. Hg)	VAV (in. Hg)	T ₁ (°C)	V ₁ (ft/min)	T ₂ (°C)	T ₃ (°C)	T ₄ (°C)	P ₀ (in. Hg)	Speed (rpm)	VAV (in. Hg)	T ₅₀ (°C)	T ₇₂ (°C)	N ₂ (ppm)	N ₂ (ppm)	N ₂ (ppm)	N ₂ (ppm)
Initial Conditions for Test - Run #117																			
12-18	31	911	25.5	24.3	1	251.5	1000	366	36	27.207	7	90	21	681	61	0	10.5	94.2	
12-18	32	917	25.5	24.3	1	252.1	1000	373	36	27.229	7	91	21	680	61	20.3	12.22	117.5	
12-18	33	917	25.5	24.3	1	252.1	1000	375	36	27.217	7	91	21	680	61	41.4	13.31	137.4	
12-18	34	917	25.5	24.3	1	252.1	1000	379	36	27.698	7	91	21	680	61	39.3	14.44	138.8	
Average Initial Conditions - Run #117																			
12-18	31	912	25.5	24.3	1	251.5	1000	379	36	27.763	7	90	21	680	61		10.93	97.8	
12-18	32	917	25.5	24.3	1	252.1	1000	380	36	27.746	7	91	21	680	61	20	12.20	117.5	
12-18	33	917	25.5	24.3	1	252.1	1000	382	36	27.743	7	91	21	680	61	46	13.81	148.8	
12-18	34	917	25.5	24.3	1	252.1	1000	382	36	27.836	7	91	21	681	61	62	14.71	170.9	

Figure 84 shows fuel-air ratio profile for the J85 at the nozzle exit location at various power levels. Data are similar to those obtained during the Phase II engine tests. Figure 85 shows the fuel-air ratio profile for the J85 at 30 feet aft of the nozzle. The data indicate good symmetry around the engine centerline. Similarly symmetrical radial profiles for CO at 30 feet aft are shown in Figure 86.

Figures 87 through 90 show plots of the emissions concentrations versus CO₂ at the four engine power levels. The linearity of the relationships and the locations of the intercepts can be seen on these plots. It should be noted from these figures that apparently good sensitivity and accuracy at very low levels were obtained.

Table 20 is a summary of emissions data from both the Near Plume and Far Plume methods. Excellent agreement between measured fuel flow and calculated integral fuel flow was obtained with the Near Plume procedure. Fairly good agreement with Phase II test data was obtained, as will be shown in a later section of this report.

Table 21 is a summary of statistical parameters from the Far Plume procedure. Linear correlation coefficients are typically above 0.99, indicating excellent linearity of emission concentration versus CO₂. The exception is for very low slopes (B1 less than 10) where, as would be expected, much lower correlation coefficients are obtained). The values for B0, the y-axis intercept of the plot of emission concentration versus CO₂, correspond more closely to reasonable ambient levels than was the case with this procedure in the Phase II tests.

8.3 FINAL TEST RESULTS - J79-15 ENGINE

Afterburner emissions measurements were made on the J79-15 engine at four engine power settings (Military, Minimum A/B, Mid A/B, and Maximum A/B) using both the Near Plume and Far Plume measurement procedures. Measurements by the Far Plume method were made at the station 60 feet aft of the nozzle exit plane. Except for some delay due to exceedingly high winds in the test area, these tests proceeded essentially without incident.

Several modifications were made to the measurement system for the Far Plume measurements. A separate sample line was run to the sample plane, and the inlet was fixed at a position 11.9 feet from the projected engine centerline. For each test point, two samples were withdrawn from this point and included in the data reduction procedure. This line permitted taking samples closer to the edge of the plume, since the probe could only be moved to a position about 9.2 feet from the engine centerline.

A second modification to the system involved the use of a hydraulic damper to suppress vibration of the probe induced by the violent turbulence within the plume. The hydraulic damper, a cylinder fixed between the probe arm and the pad, seemed to be effective in reducing vibrations, although no

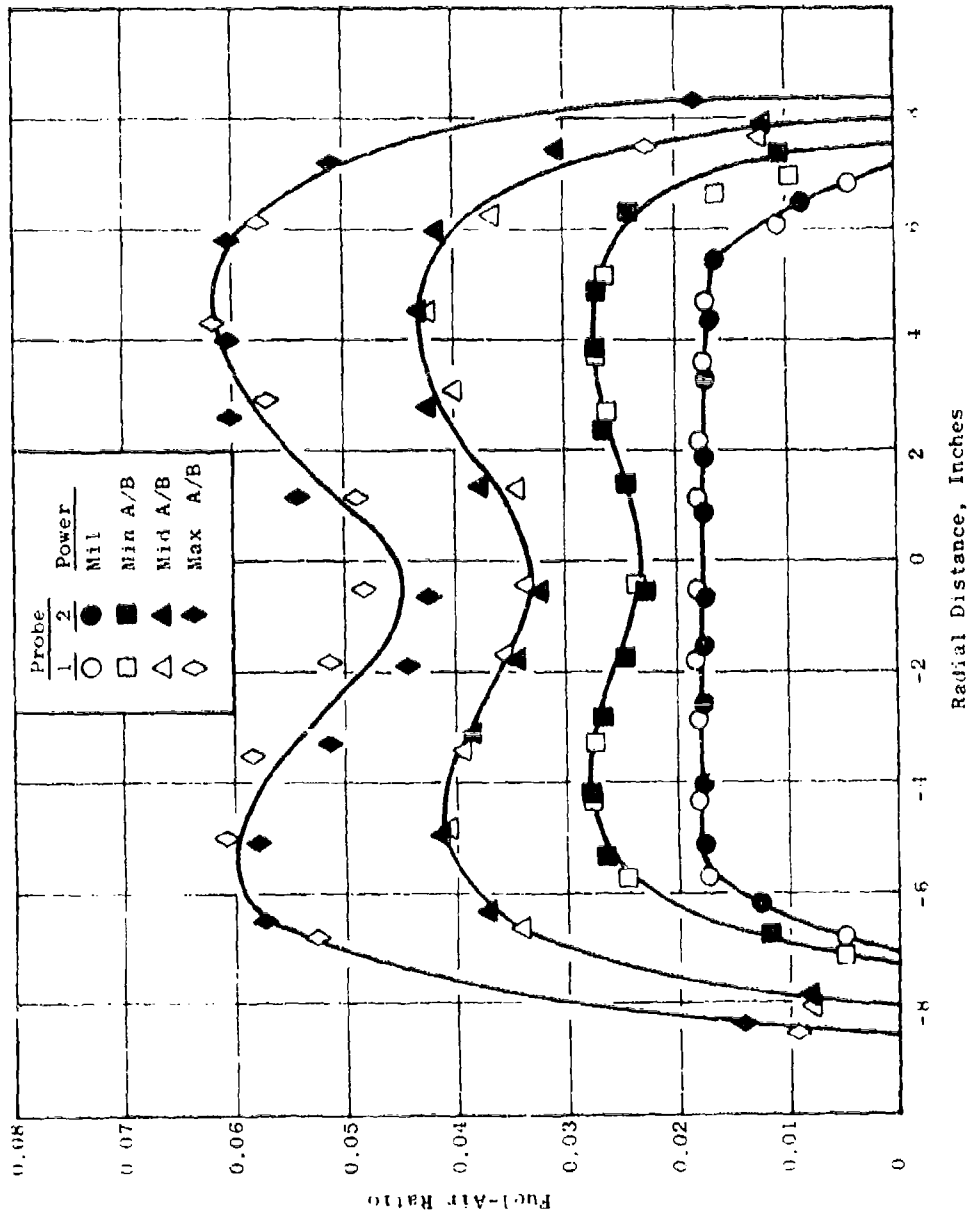


Figure 84. Fuel-Air Ratio Profile for J85-5 Engine at Nozzle Exit for Various Power Levels. Final Data by Near Plume Method.

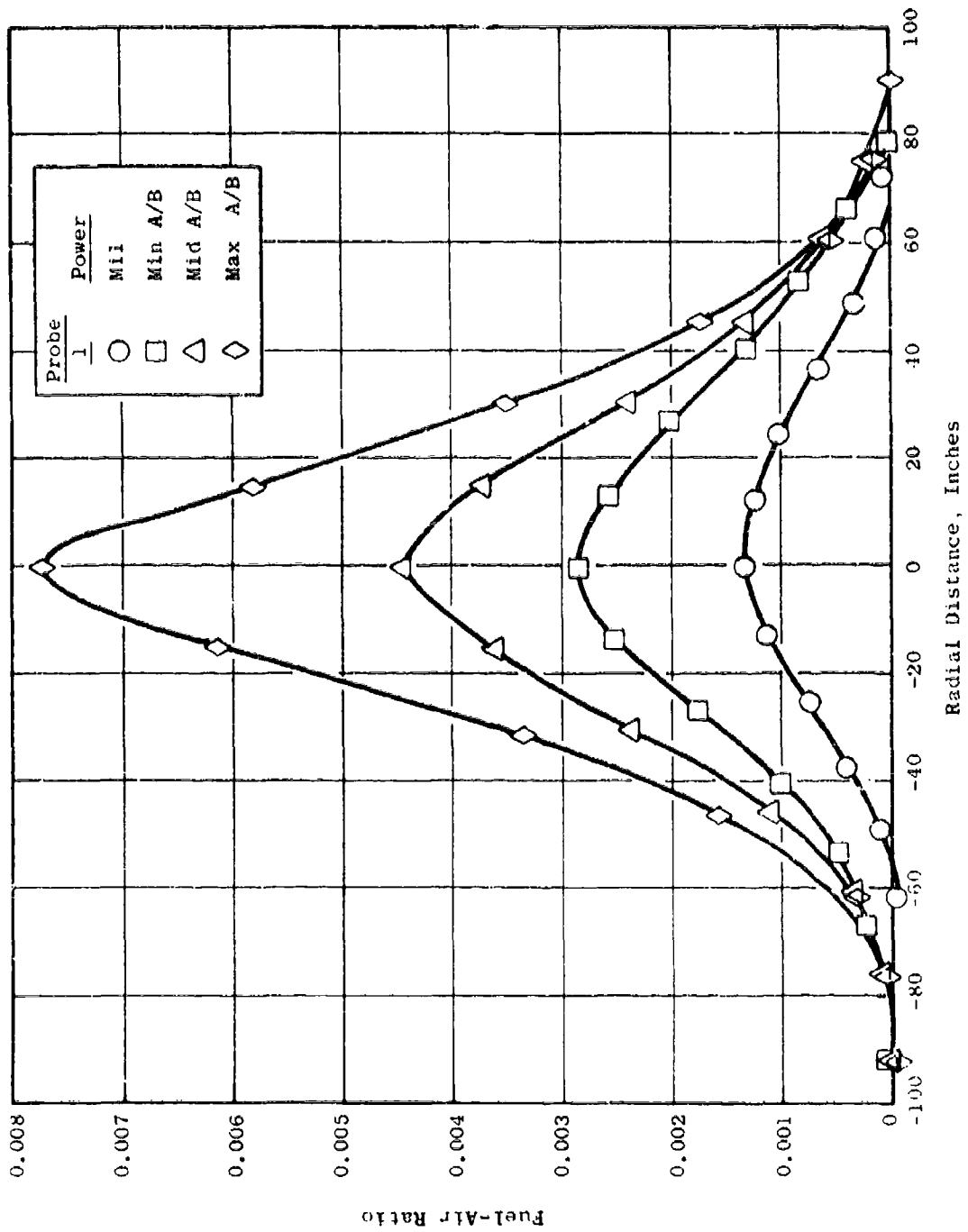


Figure 85. Fuel-Air Ratio Profile for J85-5 Engine 30 feet Aft of Nozzle for Various Power Levels. Final Data by Far Plume Method.

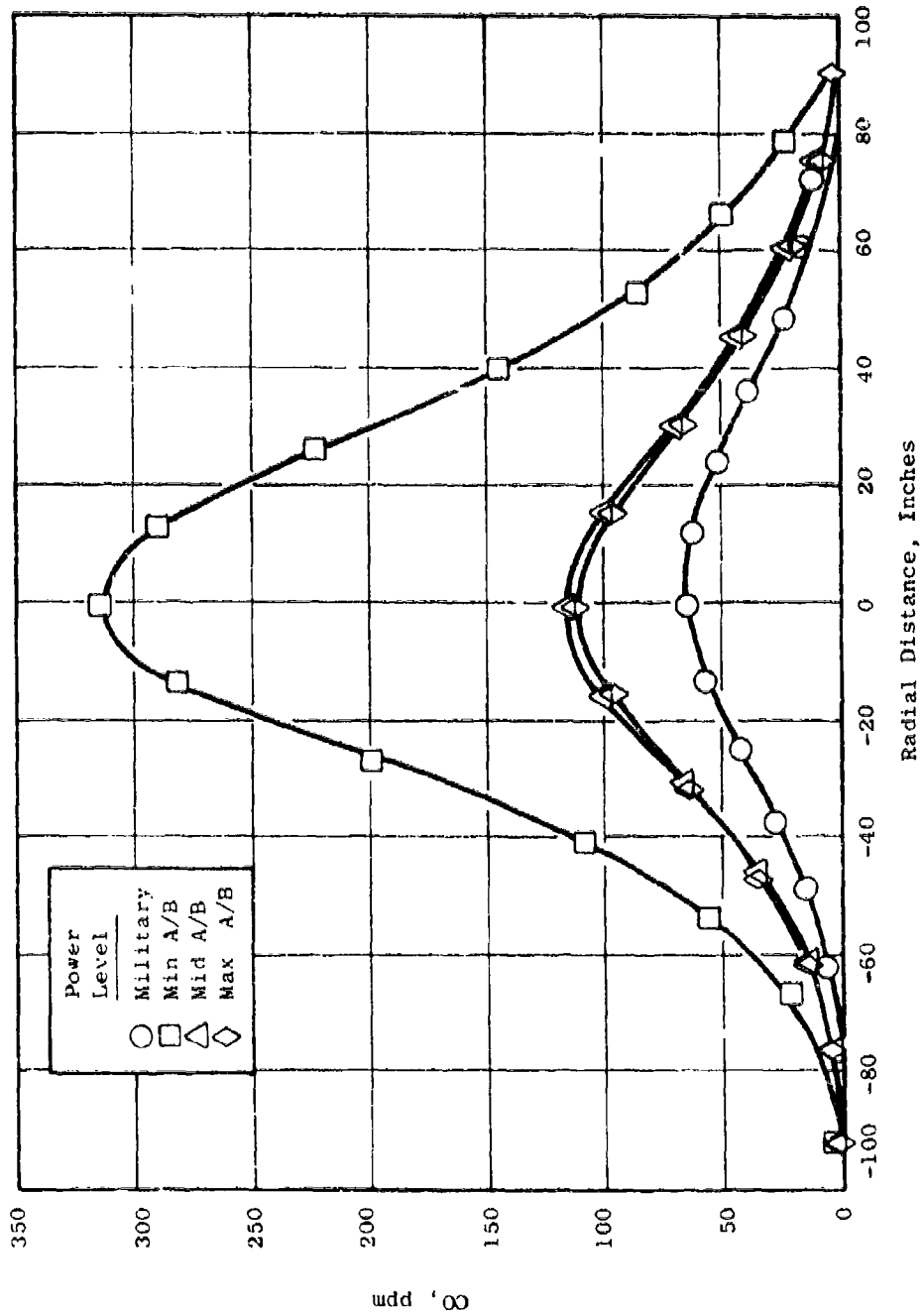


Figure 86. CO Radial Profile for J85-5 Engine, 30 feet Aft of Nozzle for Various Power Levels. Final Data by Far Plume Method.

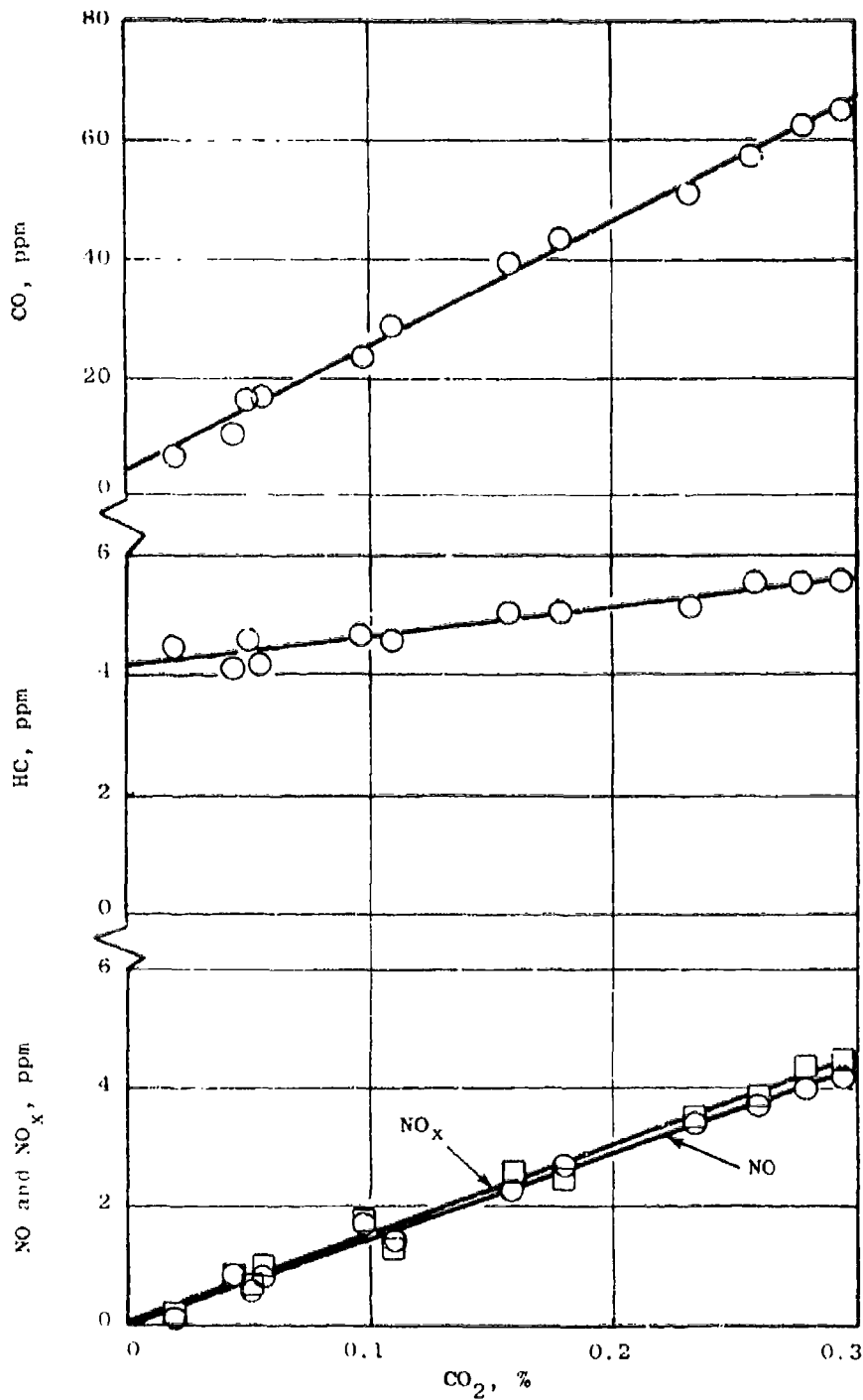


Figure 87. Emissions Concentrations Vs. CO₂ for J85-5 Engine, 30 feet Aft of Exhaust Nozzle, Military Power. Final Data by Far Plume Method.

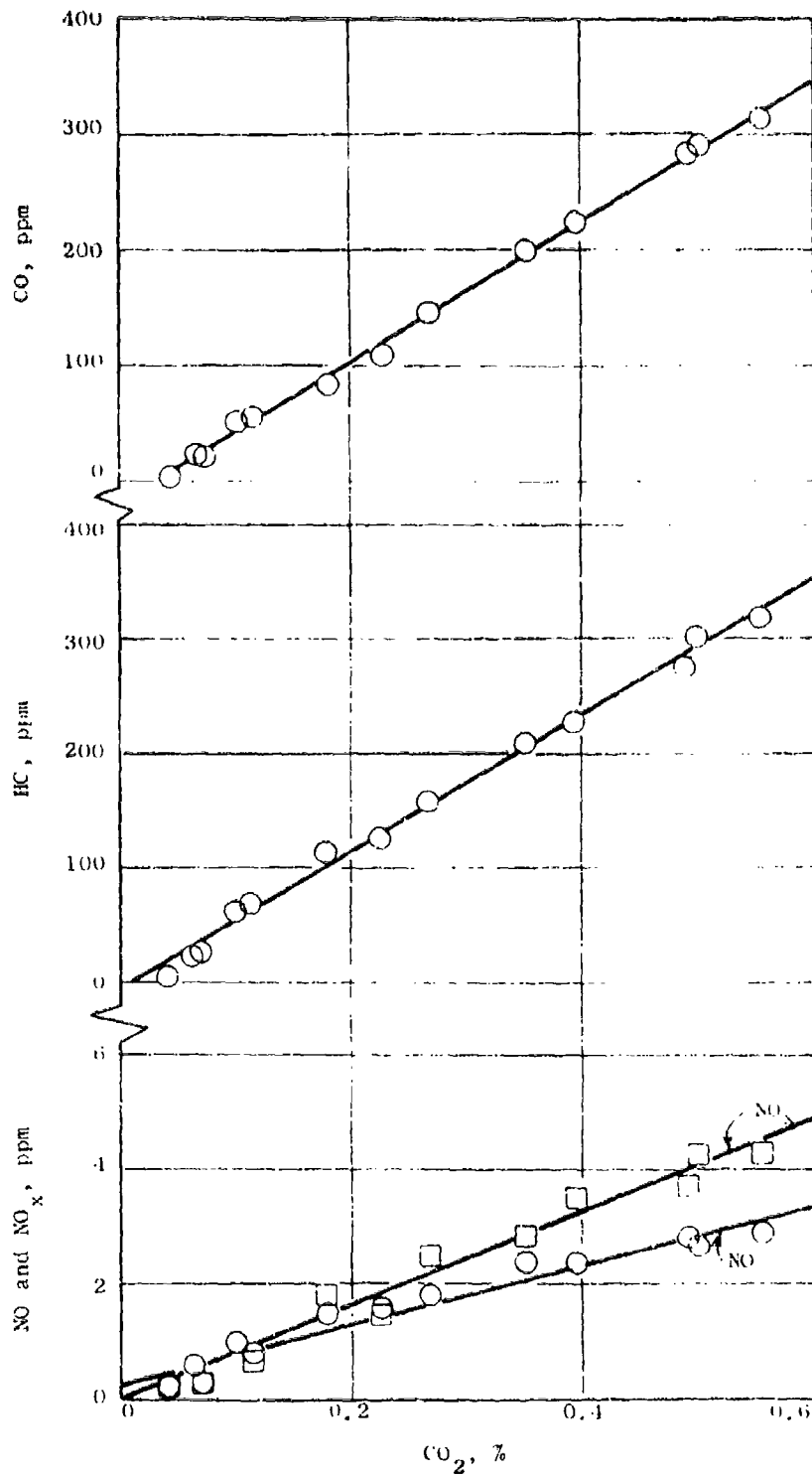


Figure 88. Emissions Concentrations Vs. CO_2 for J85-3 Engine, 30 feet Aft of Exhaust Nozzle, Min. A/B Power. Final Data by Far Plume Method.

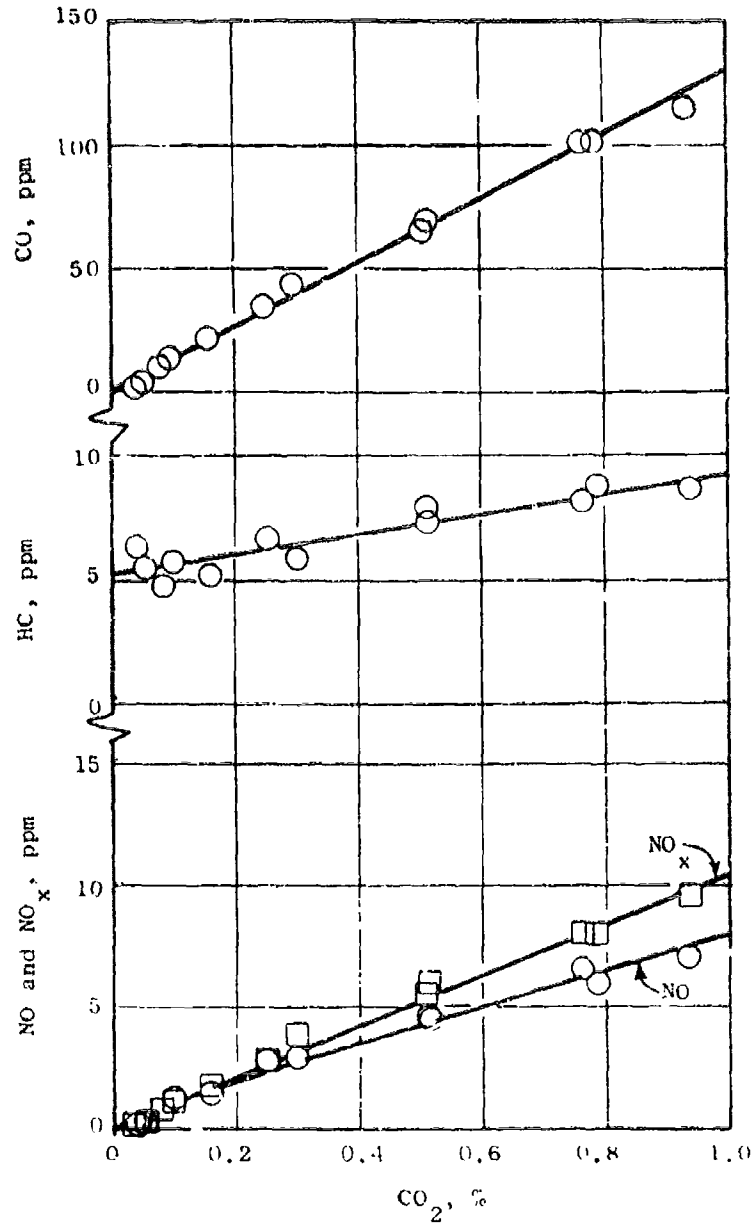


Figure 39. Emissions Concentrations Vs. CO₂ for J85-5 Engine, 30 feet Aft of Exhaust Nozzle at Mid A/B Power. Final Data by Far Plume Method.

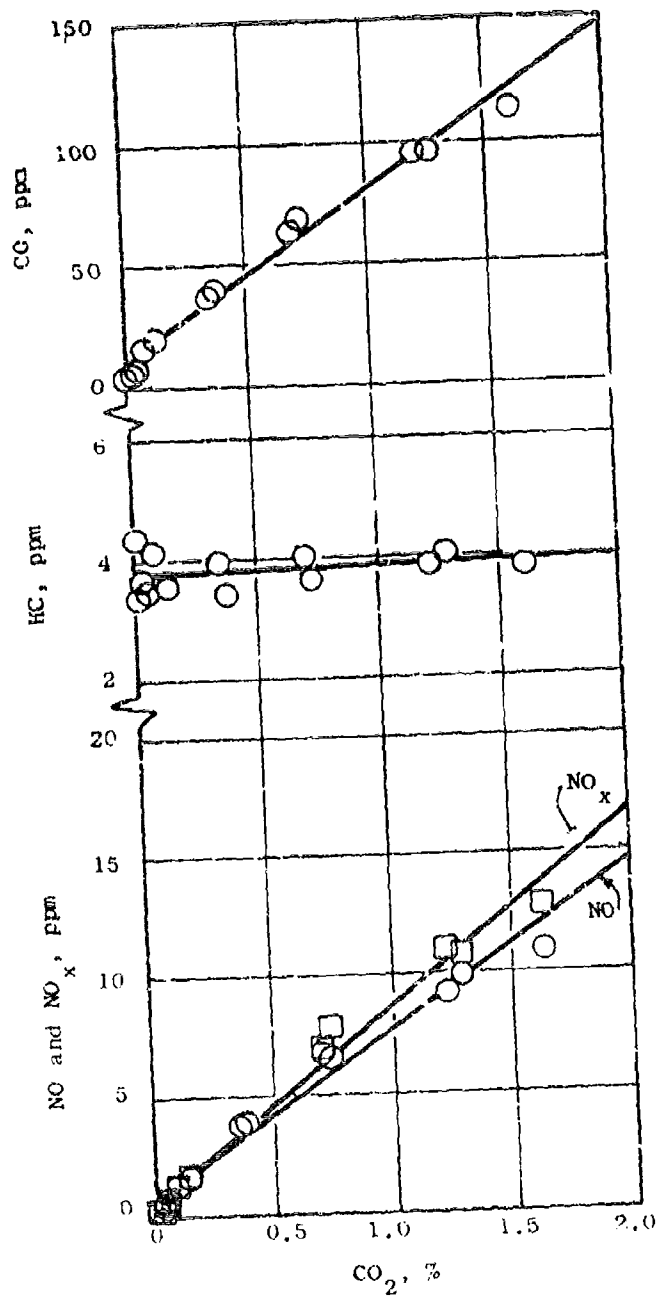


Figure 90. Emissions Concentrations Vs. CO_2 for J85-5 Engine, 30 feet Aft of Exhaust Nozzle, at Max. A/B Power. Final Data by Far Plume Method.

Table 20. Summary of Emissions Data from Final J85-5 Tests.

Near Plume Procedure - Nozzle Exit (Integral Programs)

Power Level	Fuel Flow, pps		% Diff.	Emission Index lb/1000 lb fuel			Flow Rate, pps		
	Meas.	Calc.		CO	HC	NO _x	CO	HC	NO _x
Min	0.706	0.76	- 7.6	33.9	0.3	4.6	.0258	.0003	.0025
Mid A/B	1.167	1.16	- 0.6	95.9	60.3	2.8	.112	.070	.0033
Mid A/B	1.724	1.79	- 3.8	56.3	7.2	2.8	.101	.0130	.0051
Max A/B	2.222	2.30	+ 3.5	144	1.5	2.6	.332	.0031	.0060

Far Plume Procedure - 30-Foot Station (ABE Program)

Power Level	Emission Index, lb/1000 lb fuel			Meas. Fuel Flow Rate, pps	Flow Rate, pps		
	CO	HC	NO _x		CO	HC	NO _x
Min	40.9	0.5	4.7	.731	.0299	.0004	.0034
Mid A/B	10.9	53.3	1.5	1.171	.128	.0624	.0018
Mid A/B	25.3	0.4	2.5	1.722	.0436	.0007	.0043
Max A/B	11.1	0	2.3	2.222	.0313	0	.0051

quantitative measure of its effectiveness was made. This damper was shown earlier in this report (Figure 10).

Table 22 is a summary of the engine operating data for the J79-15 final afterburner emissions tests.

Figures 91 through 94 show radial profiles of fuel-air ratio, CO, HC, and NO_x for the J79-15 at 60 feet aft of the nozzle exit plane. As with the J85 data, these measurements demonstrate good symmetry and sensitivity. The apparent plume centerline is about 10 inches above the projected engine centerline, corresponding to an angular displacement of 0.8 degree. It should be noted that radial locations for the final emissions measurements are uncorrected values (computer program NEWRAD was not used), since the data reduction procedure used (slope method) does not require radial position measurements. Note also that the highest CO and HC levels occurred at mid A/B power level.

Figures 95 through 98 show plots of the emissions concentrations versus CO_2 at the four engine power levels. The linearity of the relationships and the locations of the intercept can be judged on these plots. At military and maximum A/B (Figures 95 and 98), the slope of the HC plot is negative, indicating a negative emission index. This indicates that the engine exhaust was actually lower in HC concentration than was the ambient air.

A summary of the J79-15 emissions data is given in Table 23, which shows results of both the Near and Far Plume measurements. For the Near Plume procedure, excellent agreement between measured and calculated fuel flow may be noted. The data show good internal consistency, and, except for the mid A/B power level, the data are in good agreement with the Phase II test results. At mid A/B power, unusually high concentrations of HC were noted at the nozzle exit location. Examinations of local profiles show considerably higher HC concentrations near the nozzle perimeter than occurred in the previous Phase II tests. HC in this region was not completely consumed in the plume since it tended to mix with the surrounding cooler ambient air. Thus, high HC levels persisted even to the 60-foot station, as shown by the Far Plume measurements. Some conversion of HC to CO apparently occurred in the plume as indicated by the higher CO level at the 60-foot station. Total reactive carbon (carbon as CO + HC) was, however, about 20 percent lower at the 60-foot station than at the nozzle exit.

The basic cause of the higher emissions in these tests at mid A/B power is not apparent. It is clear that the fuel from the annular A/B system was not burning as efficiently as in the previous test, and that this could be related to differences in test conditions such as ambient temperature or pressure, or to some real changes in fuel split between the various A/B fuel systems. This problem indicates that for continuously modulated afterburners, a large number of power settings should be investigated in order to accurately determine the emissions characteristics of the engine.

The NO_2 concentration in the plume was also highest at the mid A/B power level. At military power, essentially 100 percent of the NO_x was NO , while at mid A/B power, only 16 percent of the NO_x was NO .

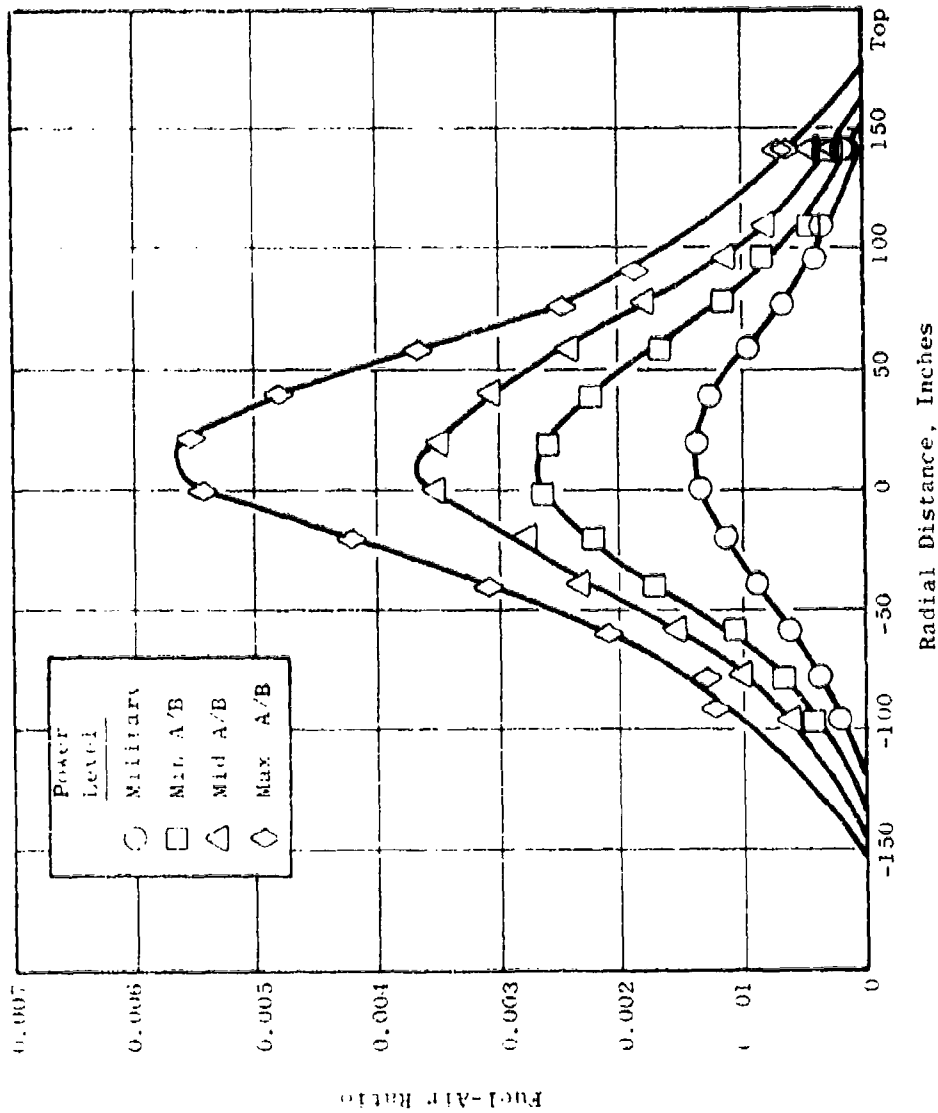


Figure 91. Fuel-Air Ratio Radial Profile for J79-15 Engine at 60 feet Alt of Nozzle for Various Power Levels. Final Data by Far Plume Method.

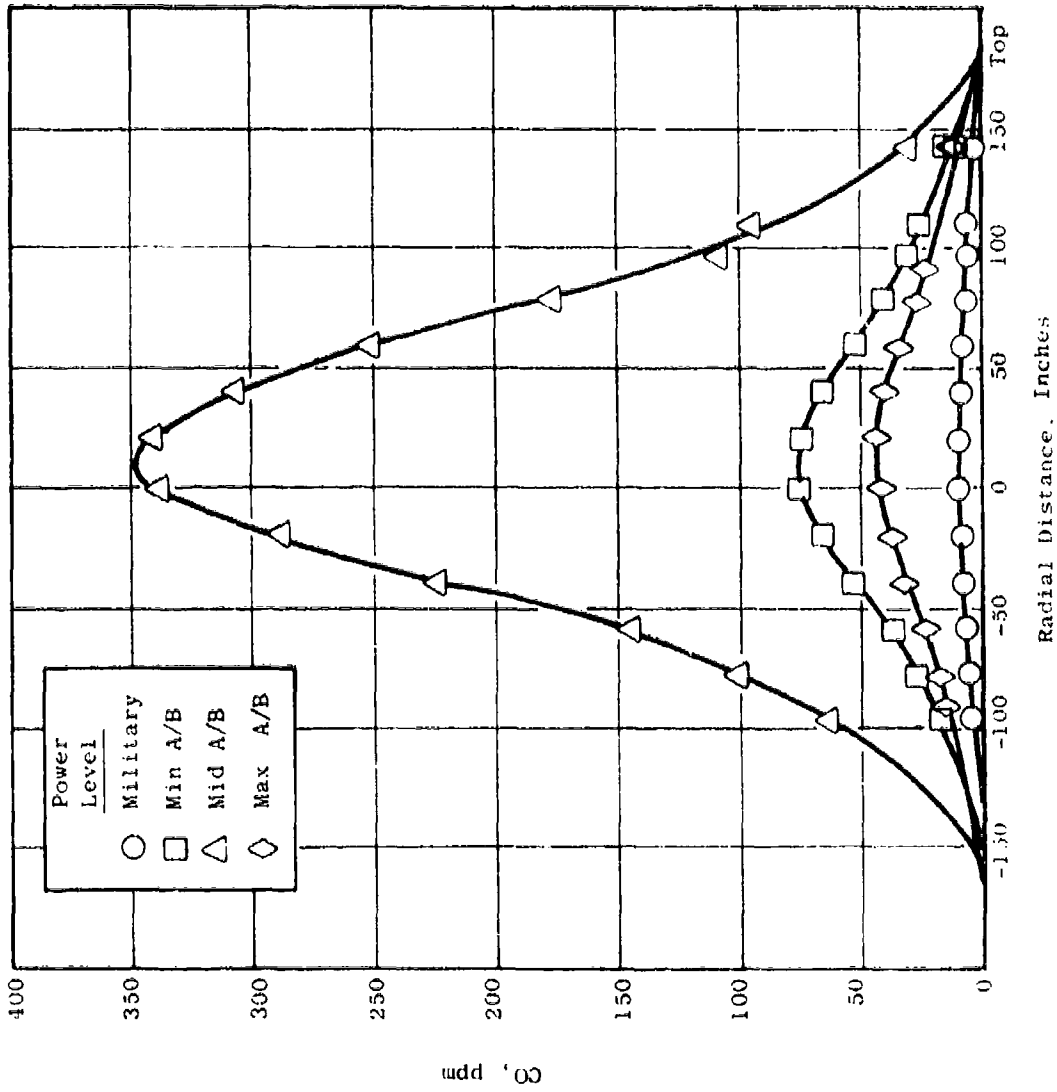


Figure 92. CO Radial Profile for J79-15 Engine at 60 feet Aft of Nozzle for Various Power Levels. Final Data by Far Plume Method.

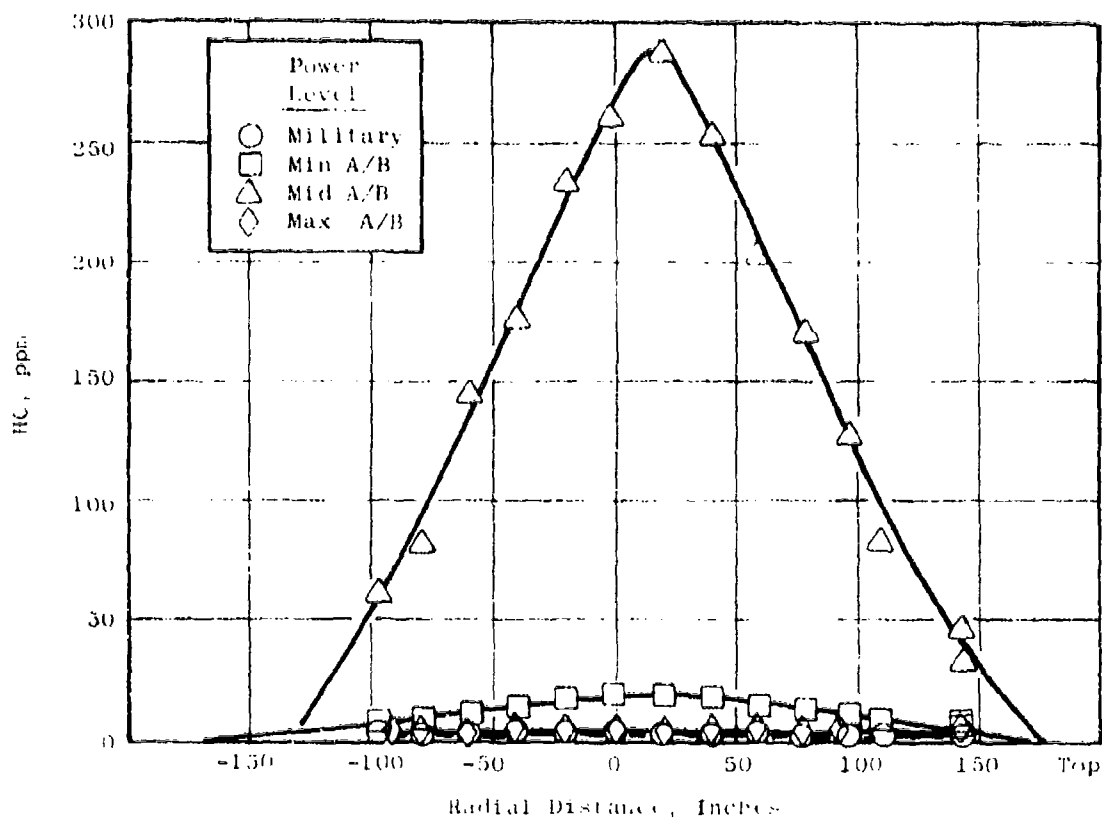


Figure 93. HC Radial Profile for J79-15 Engine at 60 feet Aft of Nozzle for Various Power Levels. Final Data by Far Plume Method.

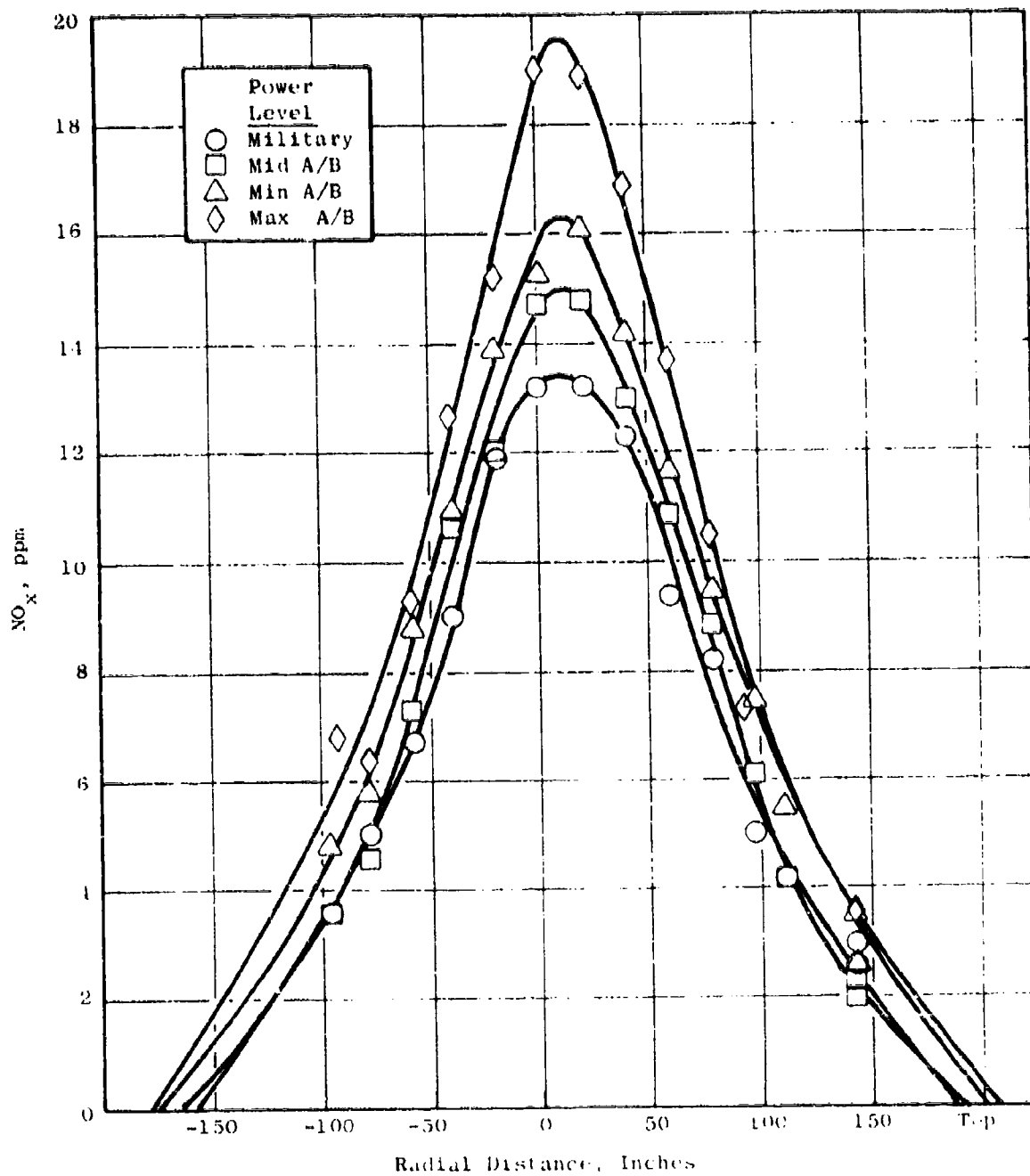


Figure 94. NO_x Radial Profile for J79-15 Engine at 60 feet Alt of Nozzle for Various Power Levels. Final Data by Far Plume Method.

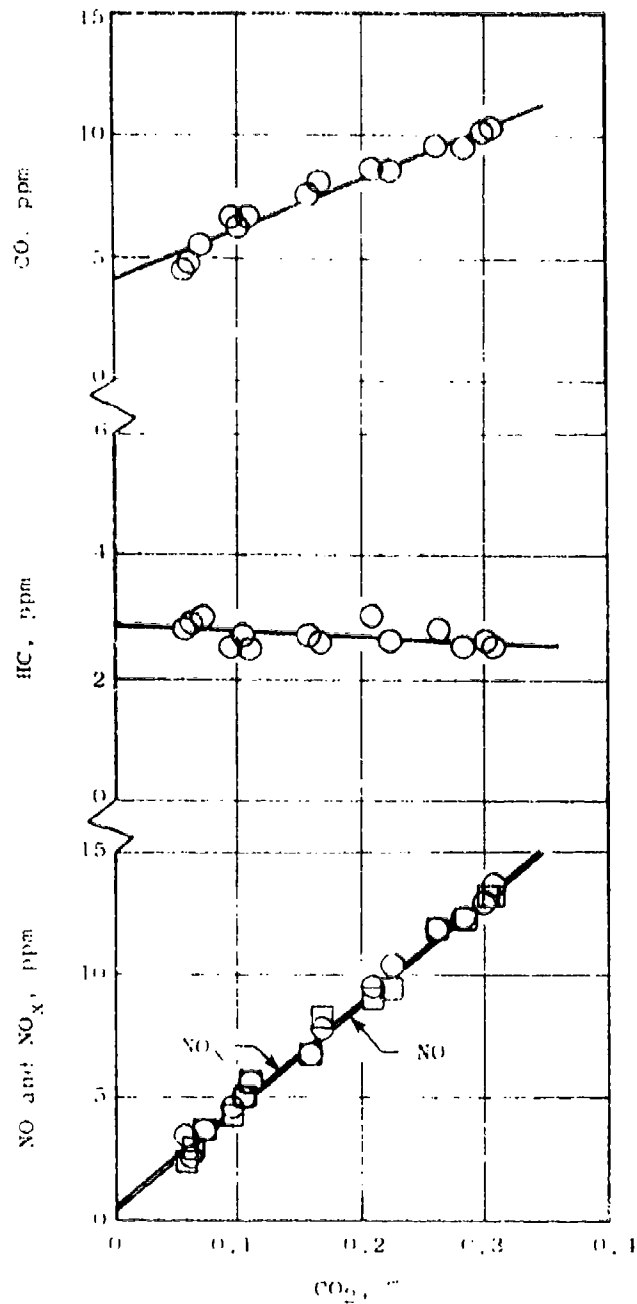


Figure 95. Emissions Concentrations Vs. CO₂ for J79-15 Engine, 60 feet Alt of Exhaust Nozzle, at Military Power Levels. Final Data by Far Plume Method.

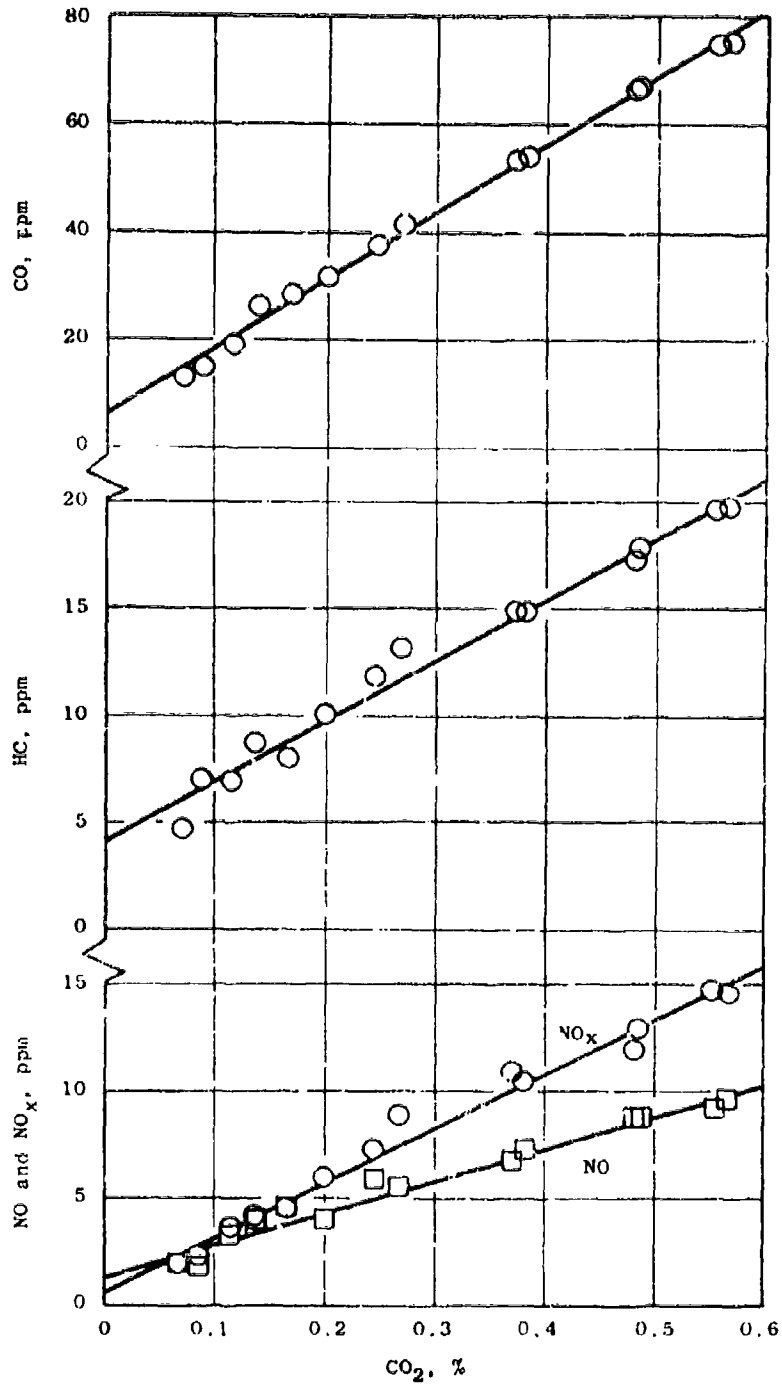


Figure 96. Emissions Concentrations Vs. CO₂ for J79-15 Engine, 60-feet Aft of Exhaust Nozzle, at Min. A/B Power. Final Data by Far Plume Method.

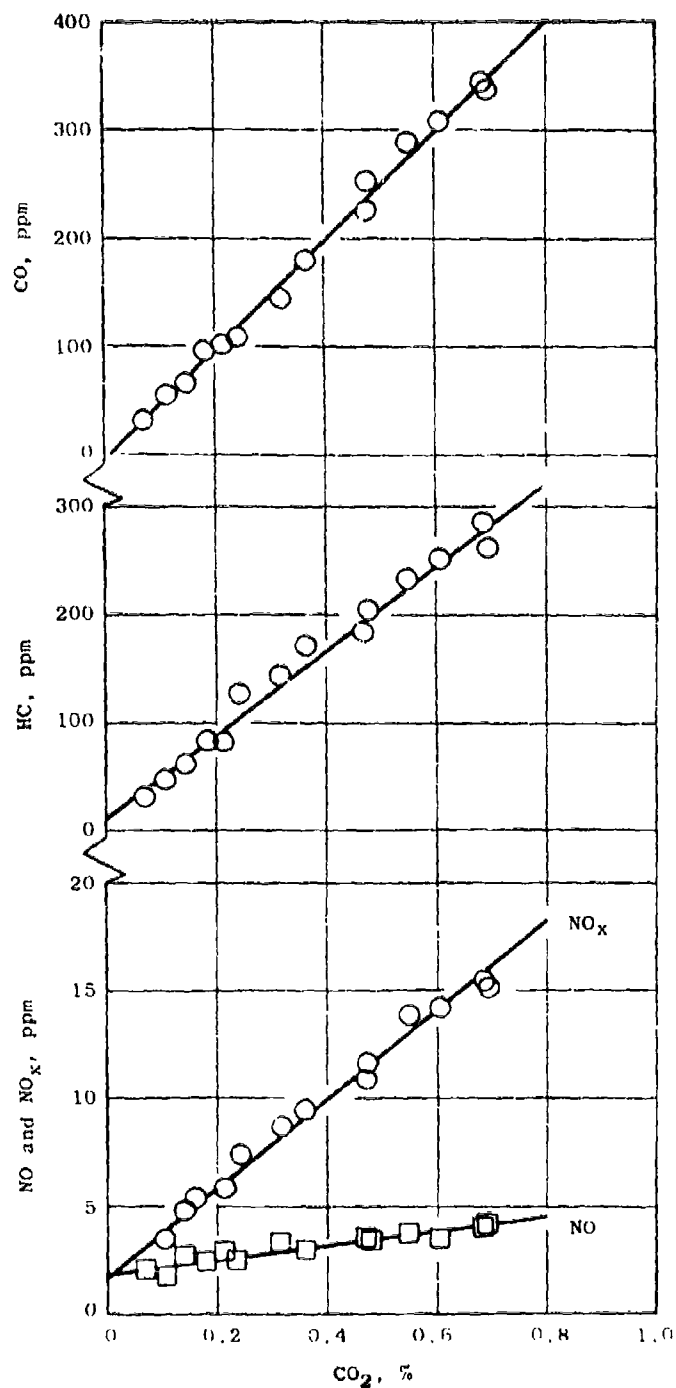


Figure 97. Emissions Concentrations Vs. CO₂ for J79-15 Engine, 60-foot Aft of Exhaust Nozzle, at Mid. A/B Power. Final Data by Far Plume Method.

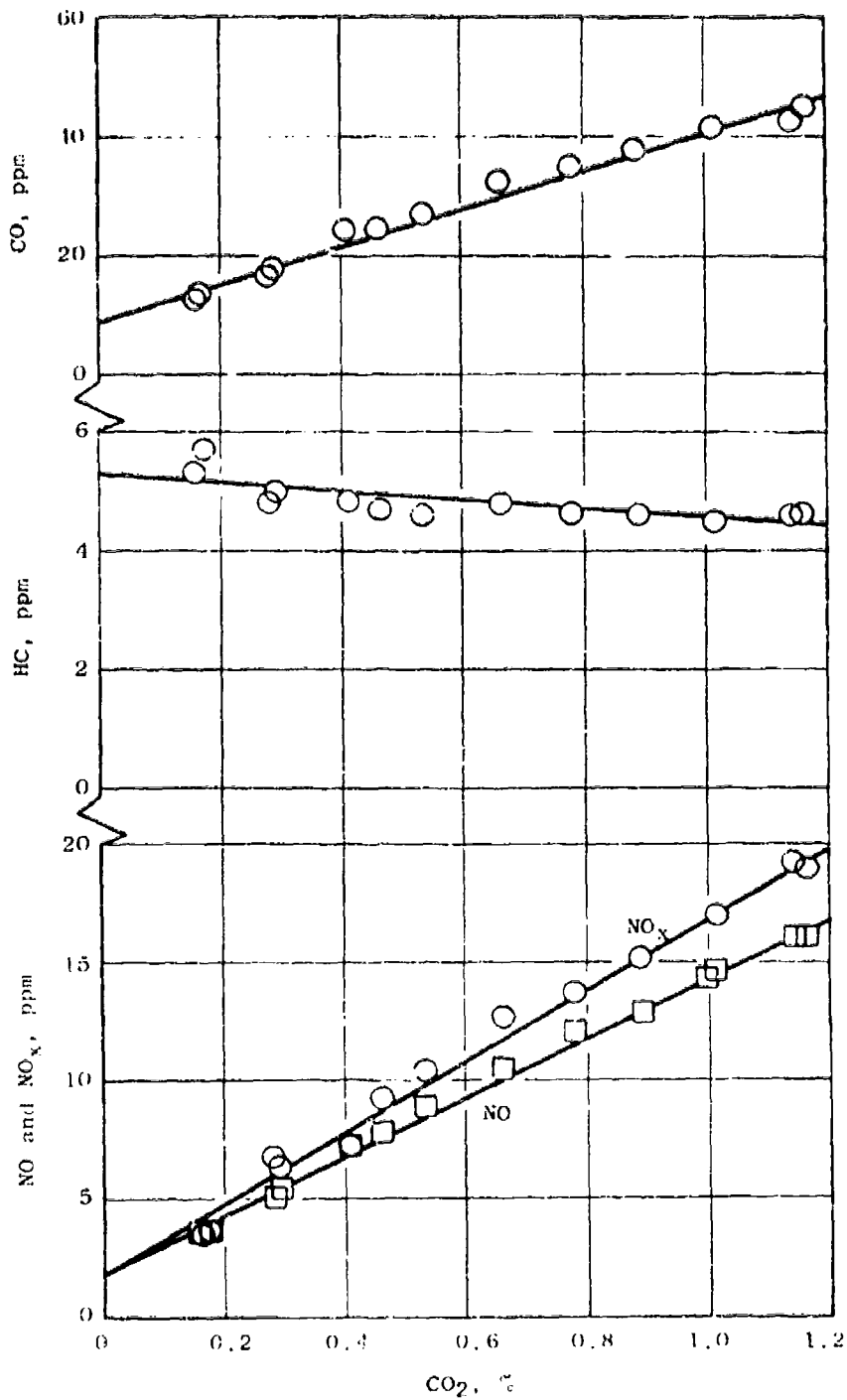


Figure 98. Emissions Concentrations Vs. CO₂ for J79-15 Engine, 60 feet Aft of Exhaust Nozzle, at Max. A/B Power. Final Data by Far Plume Method.

Table 23. Summary of Emissions Data from Final J79-15 Tests.

Near Plume Procedure - Nozzle Exit (Integral Programs)

Power Level	Fuel Flow, pps		% Diff.	Emission Index lb/1000 lb fuel			Flow Rate, pps		
	Meas.	Calc.		CO	HC	NO _x	CO	HC	NO _x
Min	2.450	2.65	+ 8.1	4.0	0.05	12.0	.0106	.0001	.0318
Min A/B	4.128	4.47	+ 0.9	35.4	11.9	7.1	.158	.0532	.0317
Mid A/B	6.094	6.19	- 1.6	76.8	65.8	5.2	.476	.107	.0322
Max A/B	8.328	8.50	- 2.1	73.0	2.8	5.0	.621	.0239	.0421

12
11

Far Plume Procedure - 60-Foot Station (ABE Program)

Power Level	Emission Index, lb/1000 lb fuel		Meas. Fuel Flow Rate, pps	Flow Rate, pps		
	CO	HC		CO	HC	NO _x
Min	4.1	- 0.09	2.535	.0104	-	.0350
Min A/B	24.6	2.8	4.486	.1104	.0126	.0368
Mid A/B	93.3	35.8	6.056	.565	.217	.0382
Max A/B	6.2	- 0.07	8.322	.0516	-	.0341

Table 24 is a summary of statistical parameters from the Far Plume procedure for the final J79 tests. Linear correlation coefficients are generally above 0.98 except for very low slopes (R_1 less than 10).

8.4 COMPARISON OF PHASE II AND PHASE III MEASUREMENTS

A total of seven separate emissions measurements were made at various axial stations, at each of the four power settings, for each of the two engines. There were a total of 56 separate tests. To compare these data, the emission index of each contaminant was plotted against axial distance for each engine and for each power level. These plots are shown in Figures 99 to 104.

For the Phase II tests, at the three axial stations nearest the engine, the data were reduced using the integral computer programs; while at the two stations farthest from the engine, the slope method was used. For the Phase III tests, the Near Plume and Far Plume procedures were followed, in which the integral data reduction programs are used at the nozzle exit location and the slope method at the downstream location. As has been explained previously in this report, the data from the Phase II tests at the two locations farthest from the engine are of questionable accuracy, but they are included here for comparison purposes.

Figure 99 shows CO emission index for the J85 versus axial distance for the various power levels. The solid curves indicate what is judged to be an average or most probable value from the tests. The Phase II data at the farthest downstream locations are generally disregarded for these curves. The dashed curves indicate what appears to be a general change in level between the Phase II and the Phase III tests. The exact reason for this change is not clear. Figure 99 shows constant CO with axial distance at military power level, an initial increase with axial distance at minimum A/B, and rather large consumption of CO in the plume at both mid A/B and maximum A/B. The increase in CO at minimum A/B resulted from the concurrent partial oxidation of HC (Figure 100). Although there may have been some consumption occurring, there was a net production of CO. Changes in CO level apparently ceased after about 3 feet at minimum A/B, 10 feet at mid A/B, and about 18 feet at maximum A/B.

Figure 100 shows HC emission index versus axial distance for the J85. Data from the various tests are fairly consistent in magnitude and show consistent trends with axial distance. HC was most reactive in the plume and was nearly completely consumed at the higher A/B power levels.

Figure 101 shows NO_x emission index versus axial distance for the J85. These data show essentially constant NO_x emission index versus axial distance at all power levels.

The CO data for the J79 are shown in Figure 102. Again, an apparent change in level between the Phase II and Phase III tests is indicated by the dashed curves. In the Phase II tests, net consumption of CO in the plume was indicated at mid A/B power level while in the Phase III tests, net production

Table 21. Summary of Statistical Parameters for J79-15 - Far Plume Method - Final Test Data.

Power Level	CO			HC			NO			NOx		
	BO	BI	r	BO	BI	r	BO	BI	r	BO	BI	r
Mid	4.1	20.4	.979	2.8	-0.9	-0.38	0.4	42.2	.995	0.6	42.1	.996
Min A/B	6.2	125.2	.998	4.2	28.2	.989	1.5	14.5	.983	0.7	25.4	.991
Mid A/B	-5.9	509	.997	11.8	390	.988	1.9	3.3	.944	1.7	20.8	.994
Max A/B	9.3	31.1	.991	5.3	-0.7	-.74	1.9	12.5	.997	1.8	15.0	.995

BO = Intercept

BI = Slope

r = Correlation Coefficient

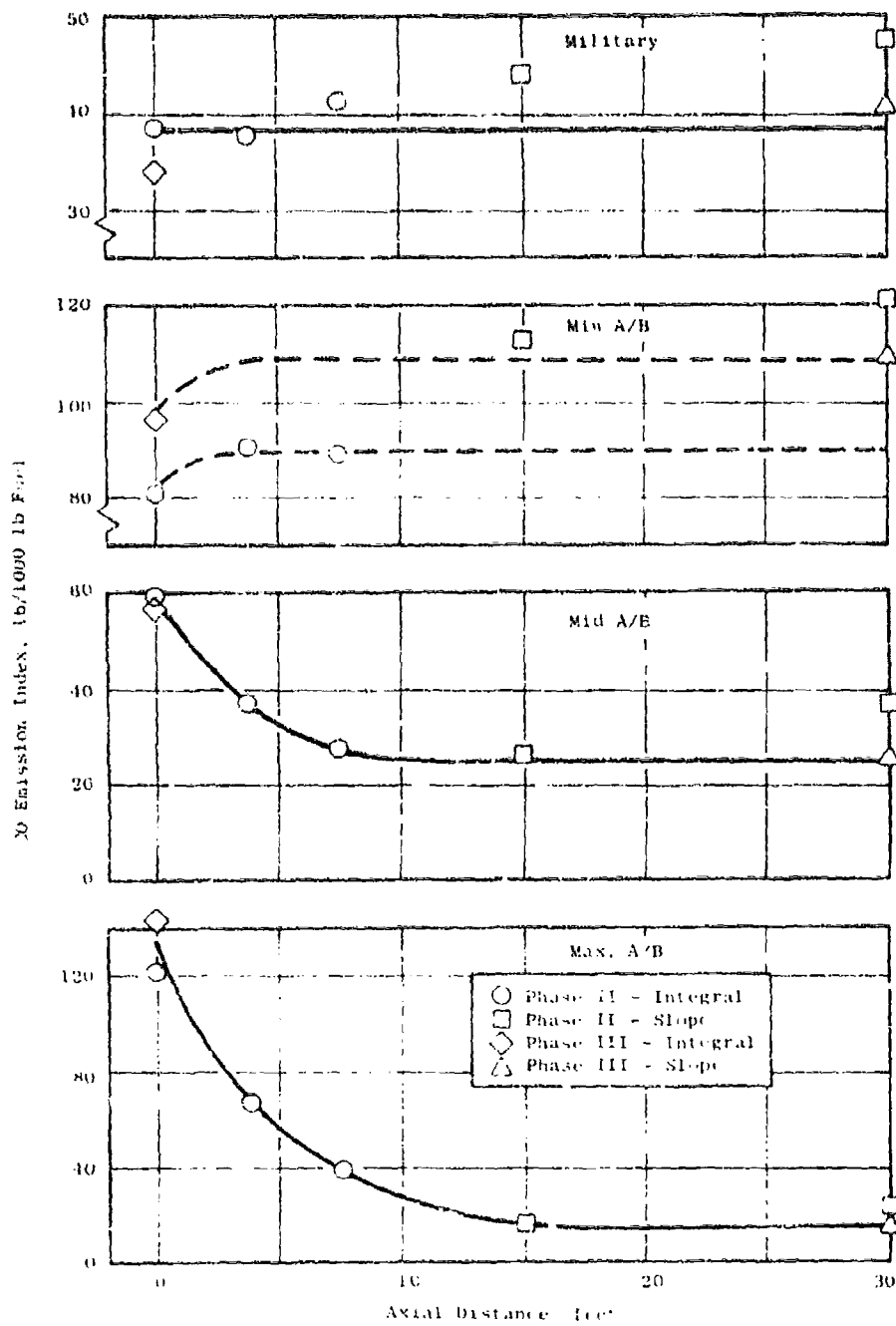


Figure 99. CO Emission Index Vs. Axial Distance for J85-5 Engine at Various Power Levels.

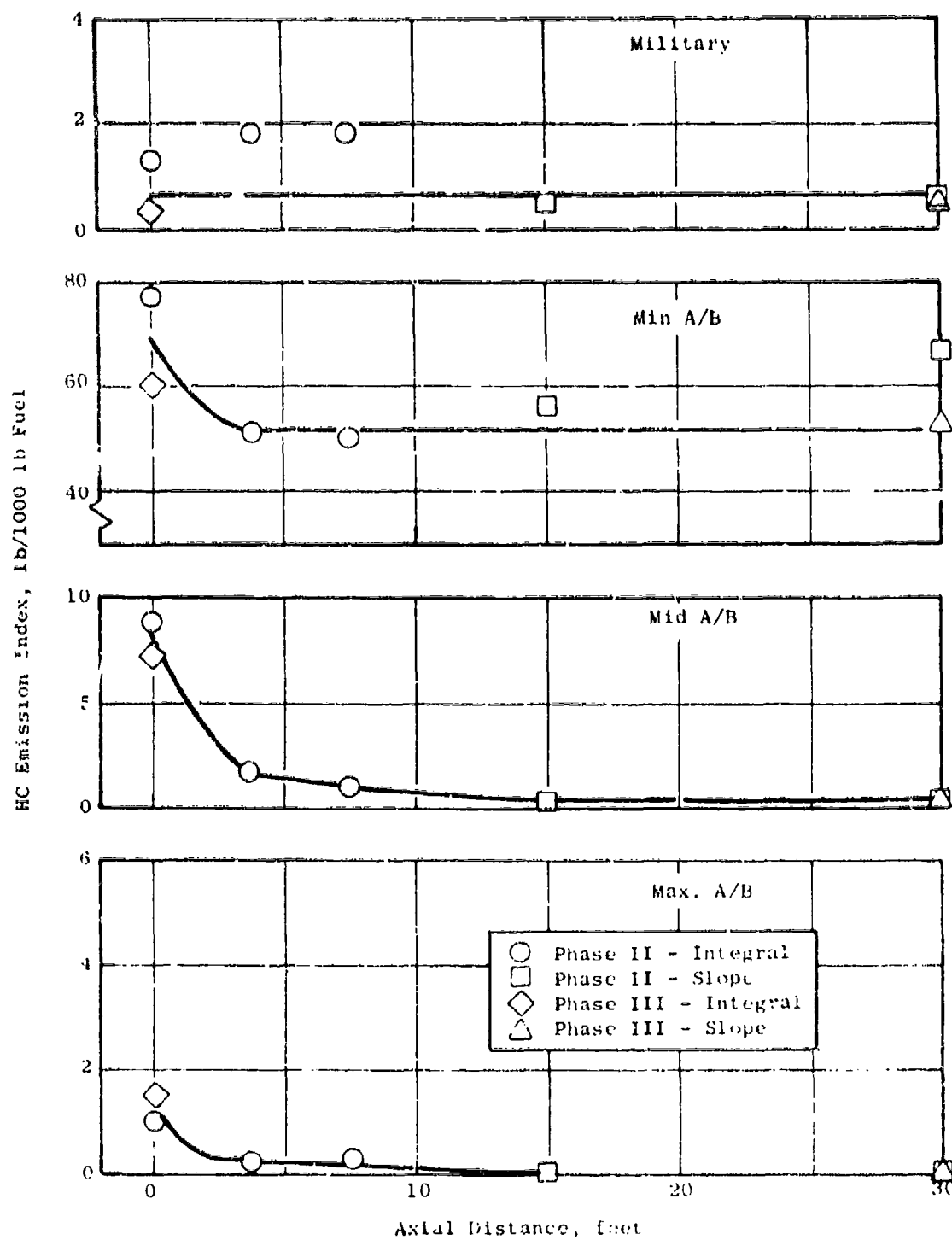


Figure 100. HC Emission Index Vs. Axial Distance for J45-b Engine at Various Power Levels.

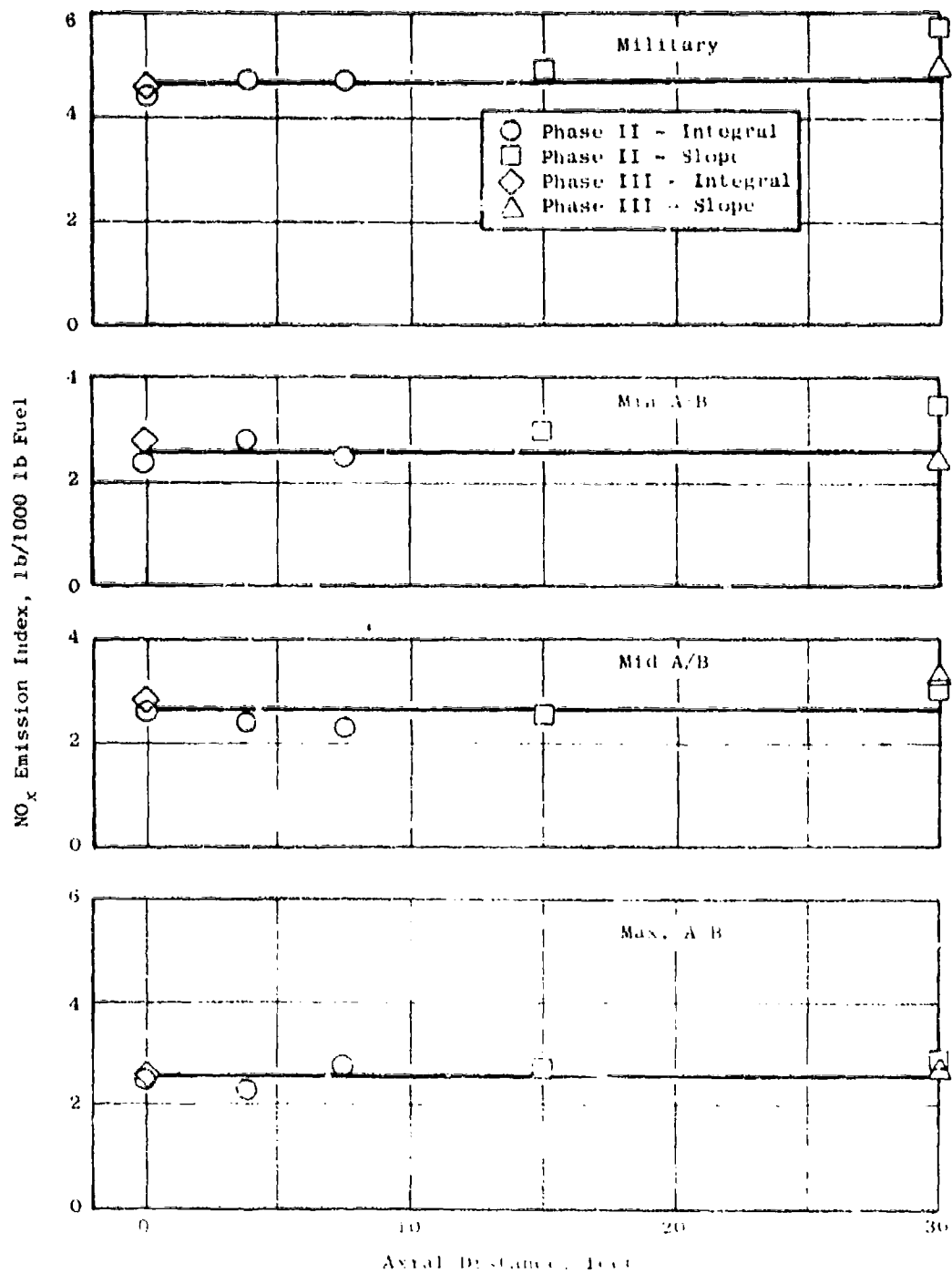


Figure 101. NO_x Emission Index Vs. Axial Distance For J85-a Engine at Various Power Levels.

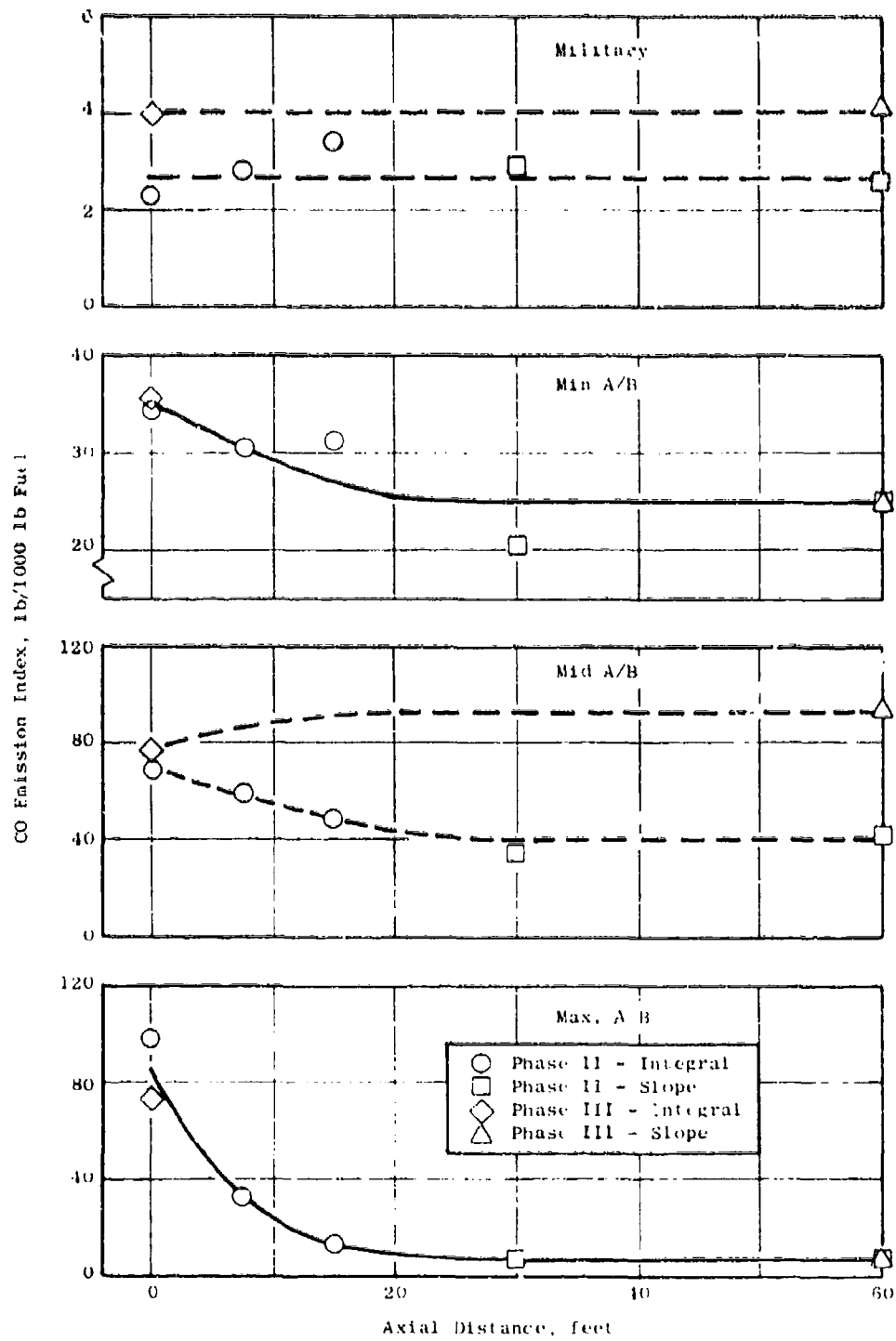


Figure 102. CO Emission Index Vs. Axial Distance for J79-15 Engine at Various Power Levels.

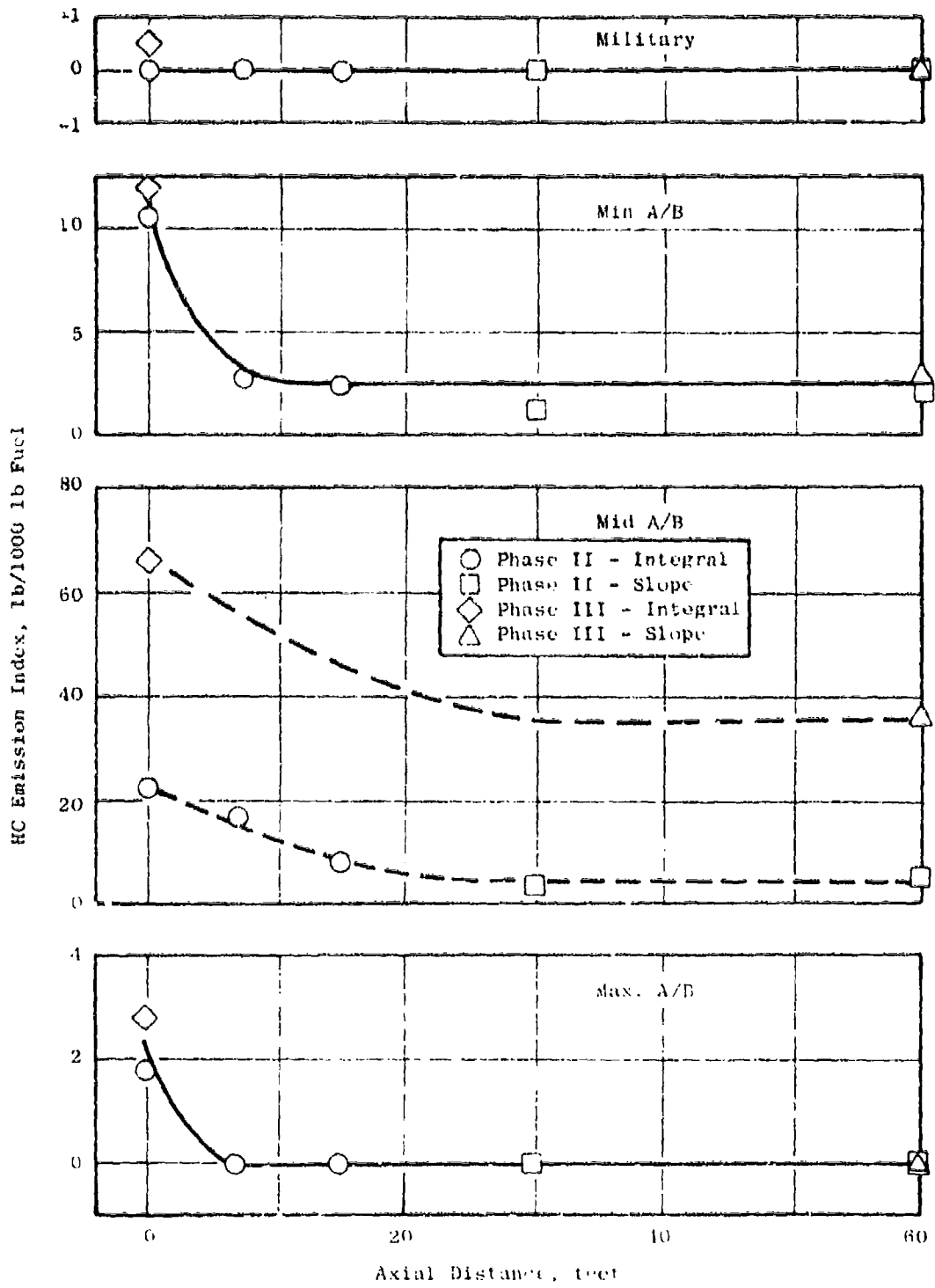


Figure 103. HC Emission Index Vs. Axial Distance for J79-15 Engine, Various Power Levels.

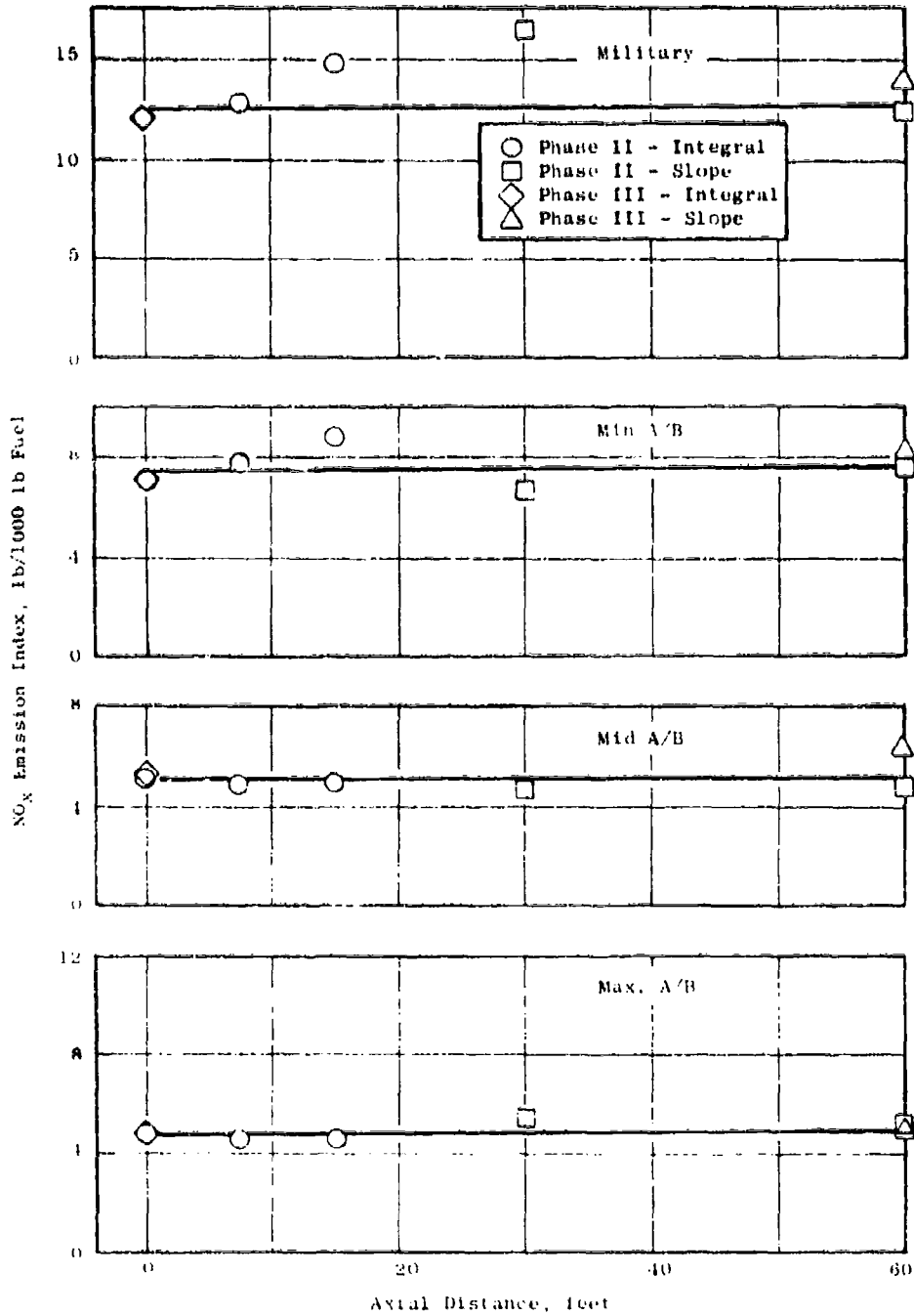


Figure 101. NO_x Emission Index Vs. Axial Distance for J79-15 Engine at Various Power Levels.

of CO was observed. This difference in CO variation with axial distance is attributed to the higher HC concentrations in the Phase III tests (Figure 103).

The HC plume data for the J79 are shown in Figure 103. Except for the Phase III tests at mid A/B power level, very low residual levels of HC existed for the J79. As has been mentioned previously in this report, the high residual HC levels at mid A/B power level for the Phase III tests are attributed to the high initial HC concentration outside of the flame zone, which mixed with low temperature ambient air and was thus not consumed in the plume.

As was observed for the J85, Figure 104 shows no appreciable change in NO_x in the plume at any power level for the J79.

The data shown in Figures 99 to 104 suggest some general observations that can be made regarding the change in total emissions with axial distance in the plume of afterburning engines. Total CO may either increase or decrease in the plume, depending on the overall HC level and the distribution of HC. The increase in CO, if any, must be consistent with concurrent decrease in HC. The total HC generally decreases in the plume at all A/B power levels. No change in total NO_x has been observed in the plume at any power level.

It should be noted that the overall changes referred to here are changes in total flow rate, as indicated by changes in the emission index. If one compares emission indices at different power levels, it must be noted that the fuel flows are different and the emission index of itself is not a good index of the total change. A comparison of flow rates for the various power settings for the Phase III measurements has already been given in Table 20 for the J85 and in Table 23 for the J79.

The overall repeatability of the measurements, as judged by the data of Figures 99 and 104, appears to be fairly good. It is apparent, however, that with high initial levels of HC, the changes in CO and HC in the plume are extremely sensitive to the initial distribution of HC. In addition to the overall precision of the emission measurements, the repeatability of the data is affected by the changes in ambient conditions and by normal engine variability. A quantitative assessment of the effect of each of these factors was not attempted.

8.5 COMPARISON WITH PLUME MODEL

Fuel-air ratio profiles predicted by the plume model were compared with local fuel-air ratios as measured by the Far Plume procedure during the final engine emissions test series (Phase III). Figure 105 shows the plume model predictions plotted against radial distance for the J85-5 at minimum A/B (Figure 105a) and maximum A/B (Figure 105b) power levels. Measured values at the same axial station (30 ft aft) are shown for comparison. These plots indicate local measured fuel-air ratios somewhat lower than the predicted values, as was generally observed in the Phase II engine tests (comparisons presented in Section 6.1). The data from the J79 engine tests showed similar trends.

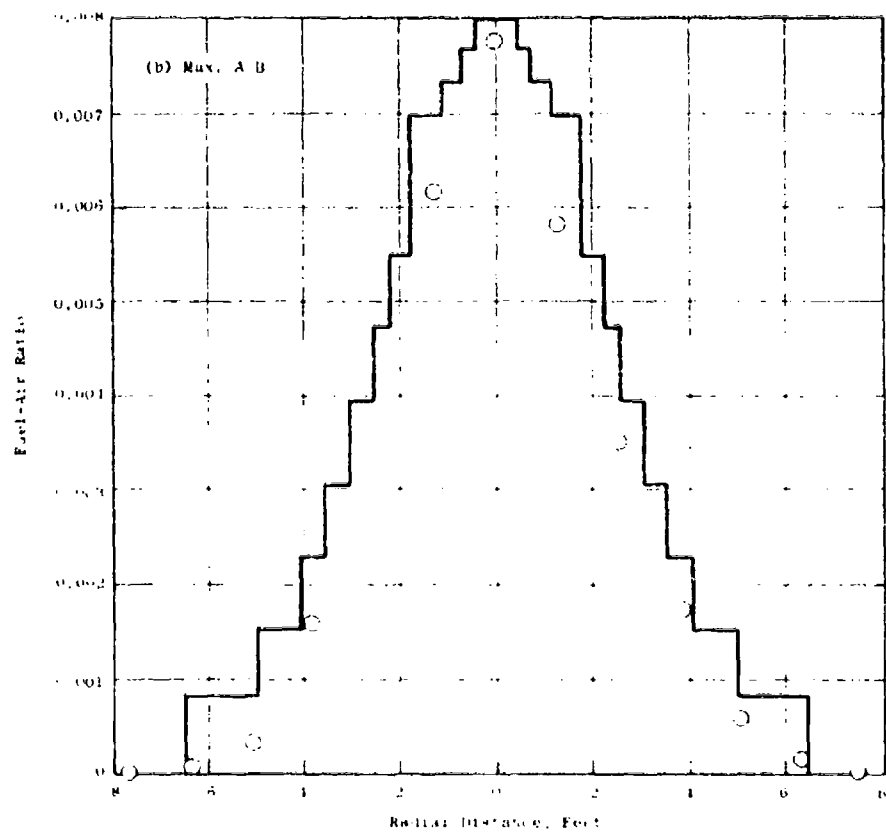
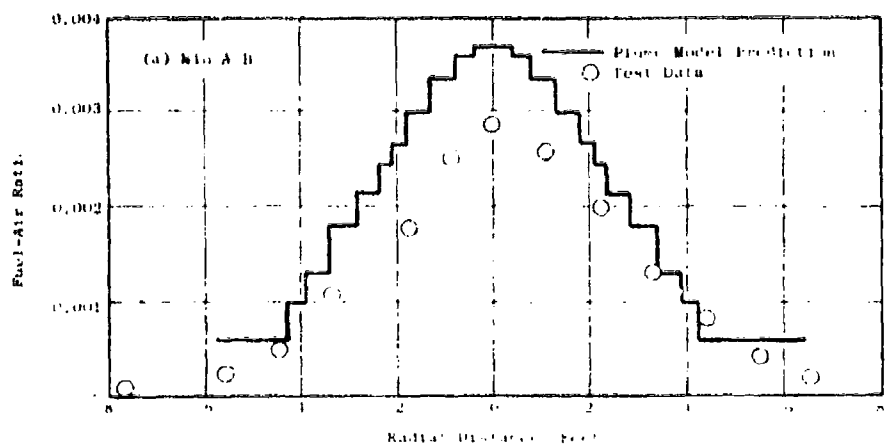


Figure 105. Predicted Fuel-Air Ratio Profile Compared to Final Test Data, J85-5 Engine at Min. A/B and Max. A/B, 30 feet Alt of Exhaust Plane.

Figures 106 through 111 illustrate use of the analytical plume model to predict the subsequent consumption of contaminants measured by the Near Plume procedure as the hot exhaust gases mix with ambient air. Shown for comparison are the emissions indices measured by the Far Plume procedure. These illustrations reveal that the residual emissions measured by the Near Plume procedure and extrapolated by the plume model can, in some cases, differ significantly from the corresponding values measured by the more direct Far Plume procedure. In the case of CO, the extended Near Plume residual can differ from the Far Plume value by as much as a factor of two. In the case of HC, the Near Plume method can yield a small residual where none is measured by the Far Plume method. These observations would suggest that allowable limits of emissions levels for afterburning engines would have to be set lower if the emissions were to be measured by the Near Plume method, than if they were to be measured by the Far Plume method.

It should be noted, however, that the consumption of contaminants in the plume is predicted by the plume model much more accurately than is the residual level, especially when large fractional consumption occurs. For example, if the model predicts consumption of 90% of the initial value, compared to a correct value of 95% of the initial level, quite good agreement (within 5%) in actual consumption is indicated. The same values yield a predicted residual level of 10% of the initial level versus a correct value of 5% of the initial level for an actual discrepancy of 100% of the correct value. It is thus obvious that for accurate prediction of residual levels, extremely accurate values of consumption must be obtained for large overall changes in the plume.

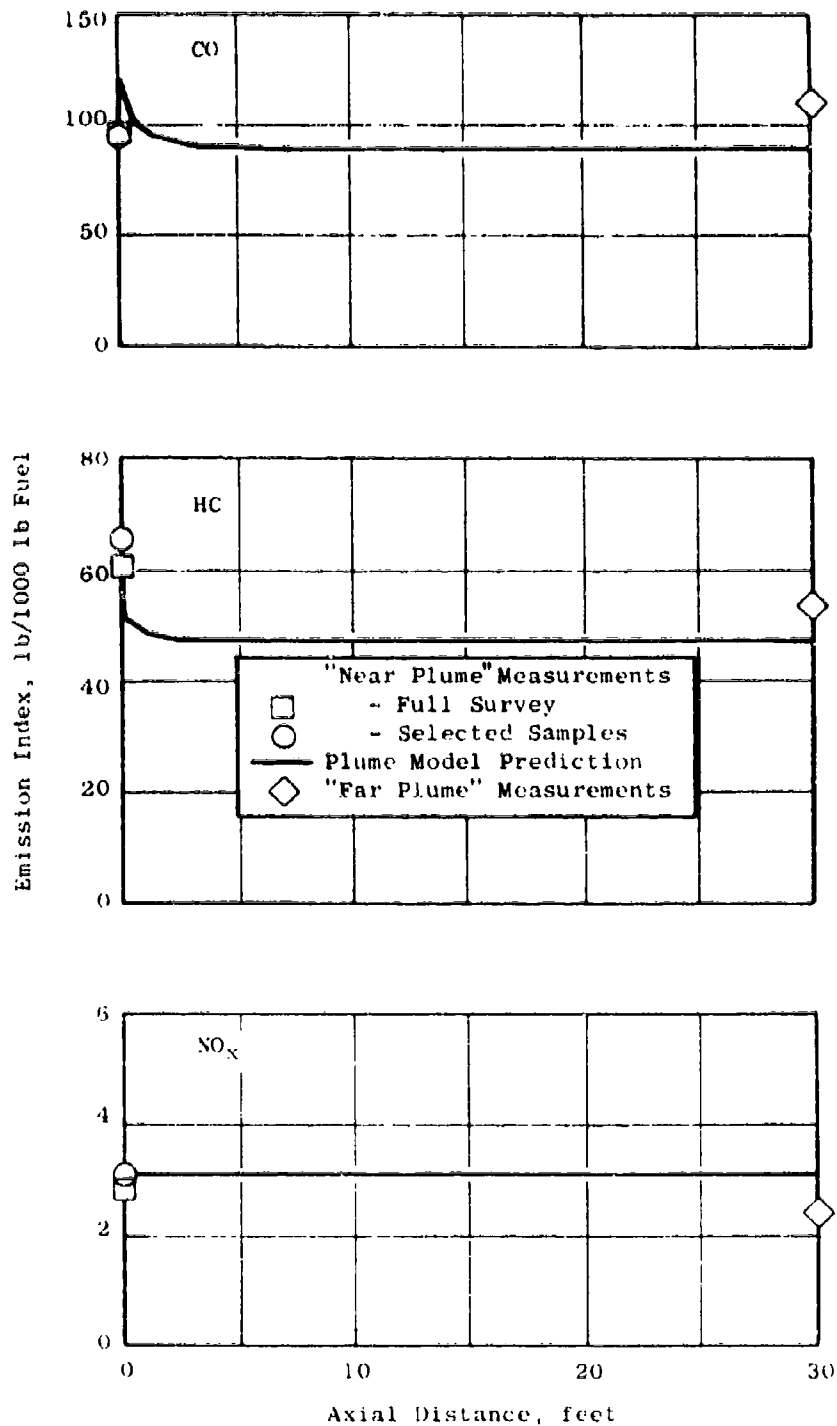


Figure 106. Plume Model Predictions of Overall Emissions Indices Compared with Phase III Test Data - J85-5 Engine, Min. A/B.

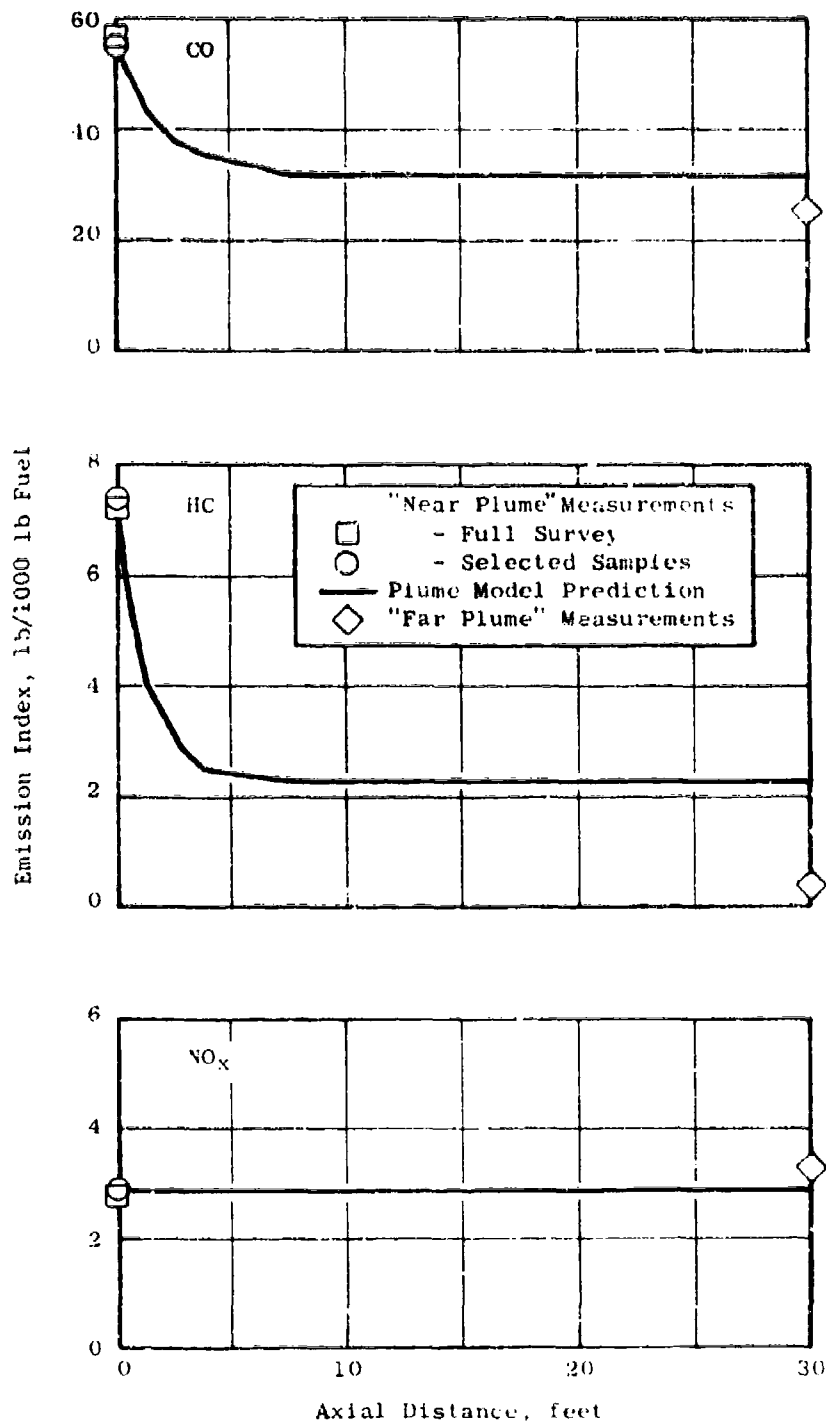


Figure 107. Plume Model Predictions of Overall Emissions Indices Compared with Phase III Test Data - J85-5 Engine, Mid. A/B.

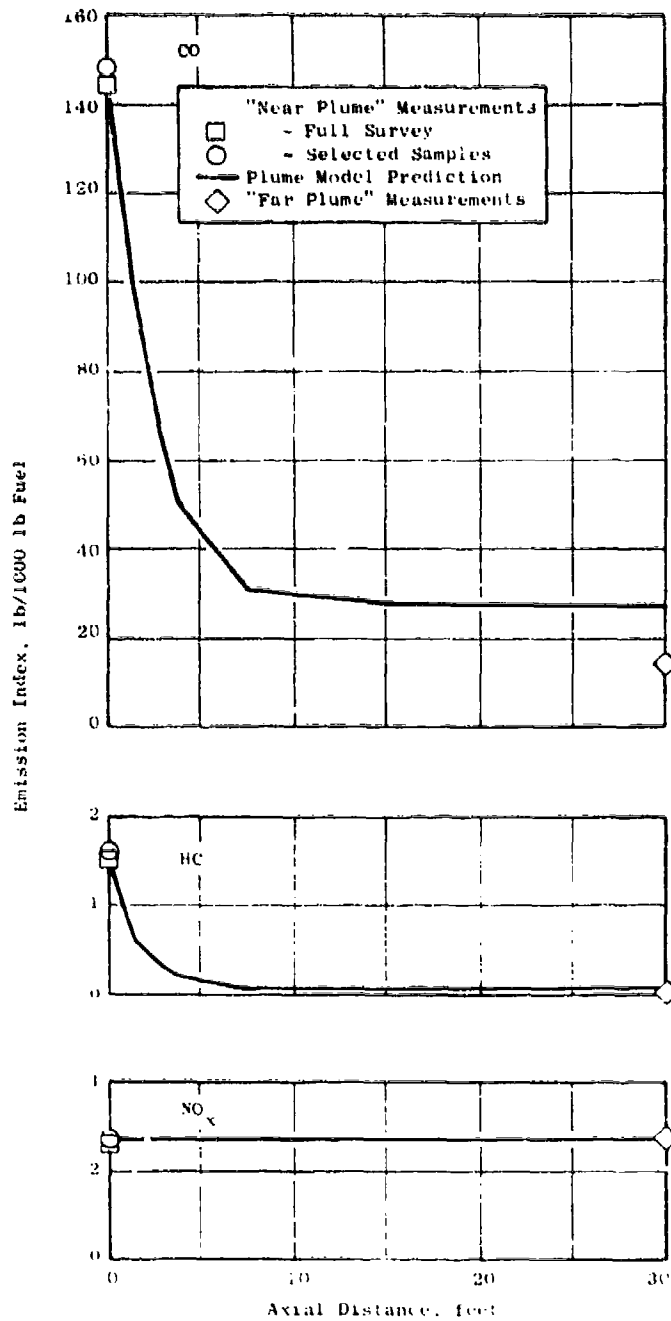


Figure 108. Plume Model Predictions of Overall Emissions Indices Compared with Phase III Test Data - J85-5 Engine, Max. A/B.

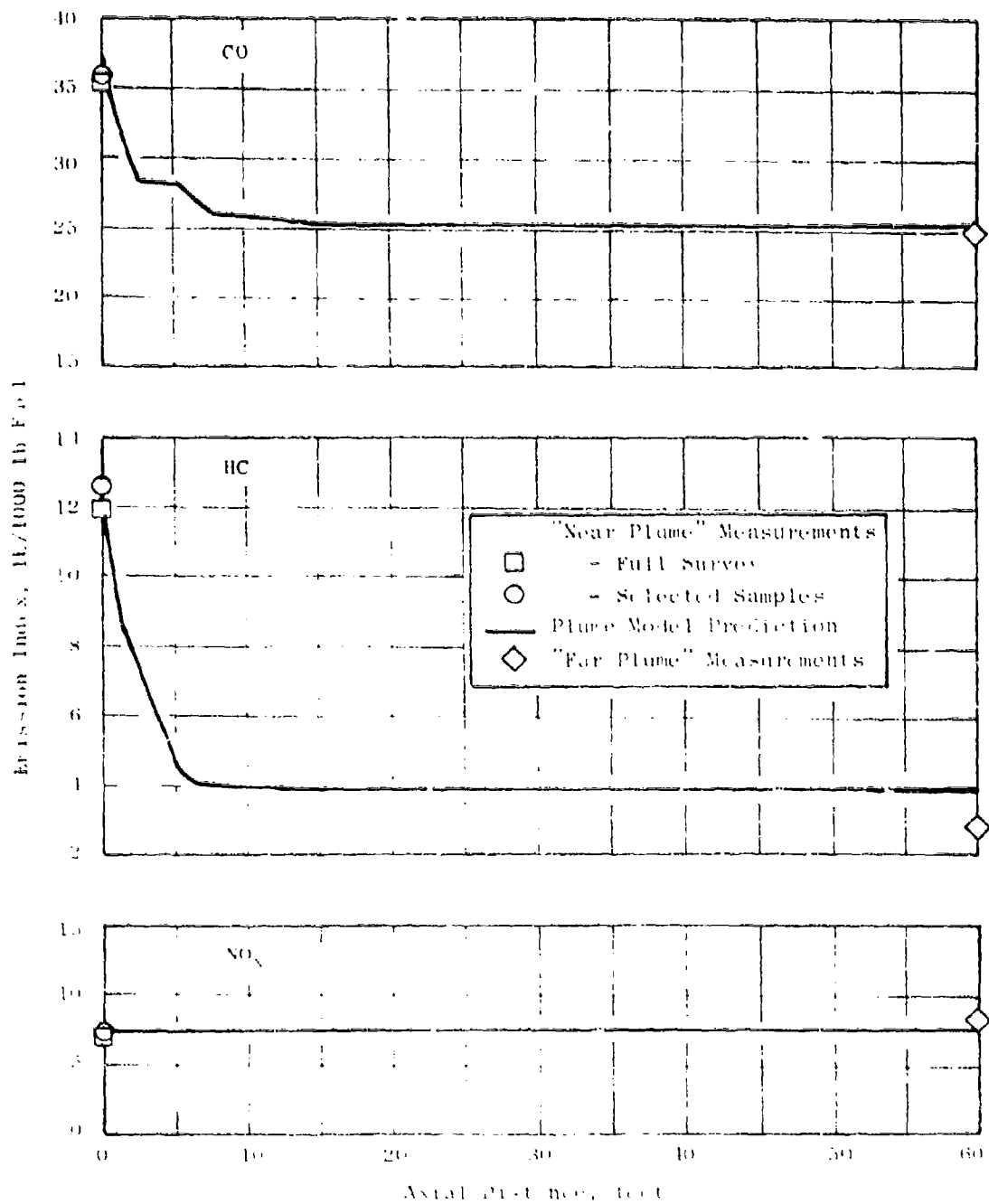


Figure 109. Plume Model Predictions of Overall Emissions Indices Compared with Phase III Test Data - J79-15 Engine, Min. A/B.

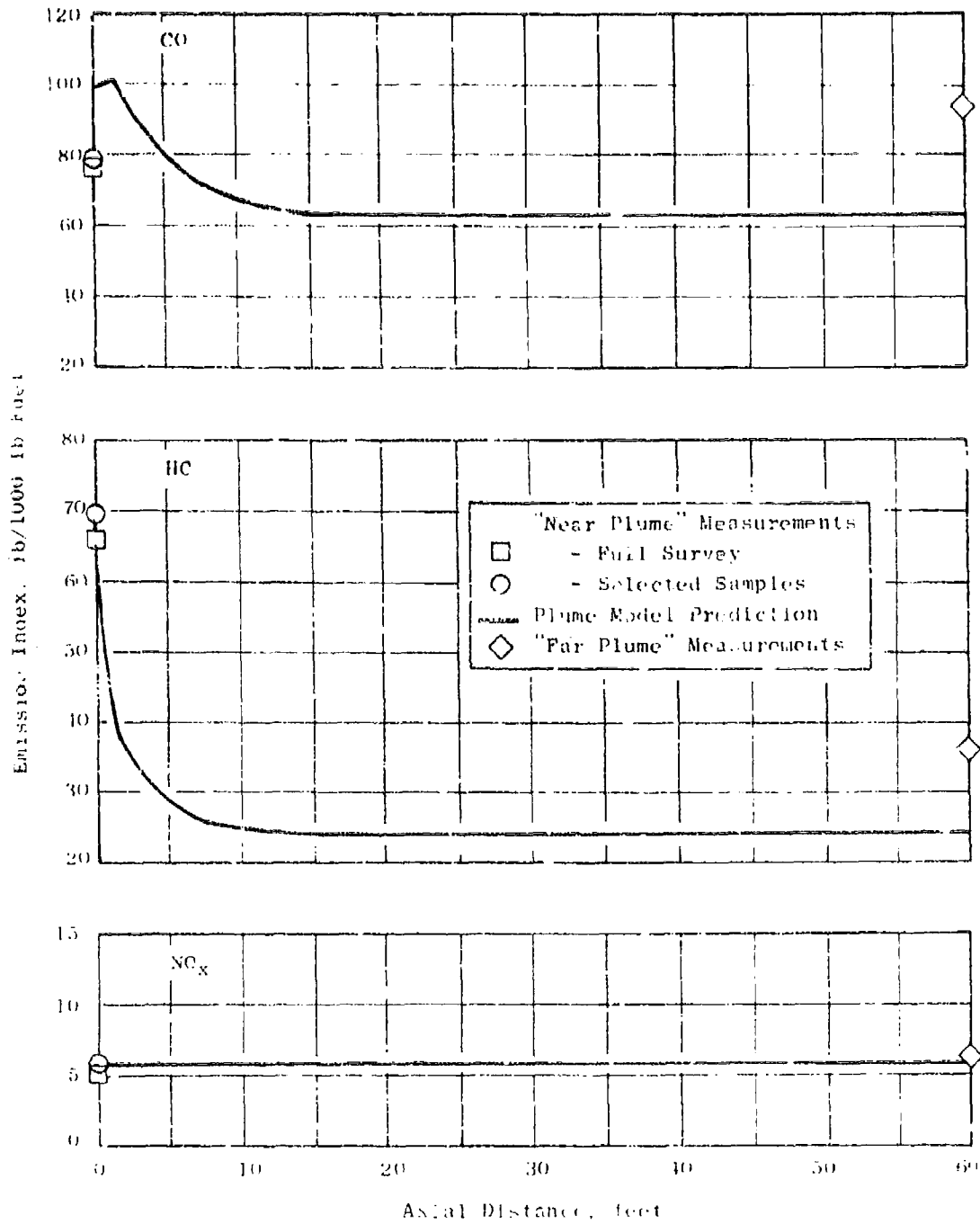


Figure 110. Plume Model Predictions of Overall Emissions Indices Compared with Phase III Test Data - J79-15 Engine, Max. A-3.

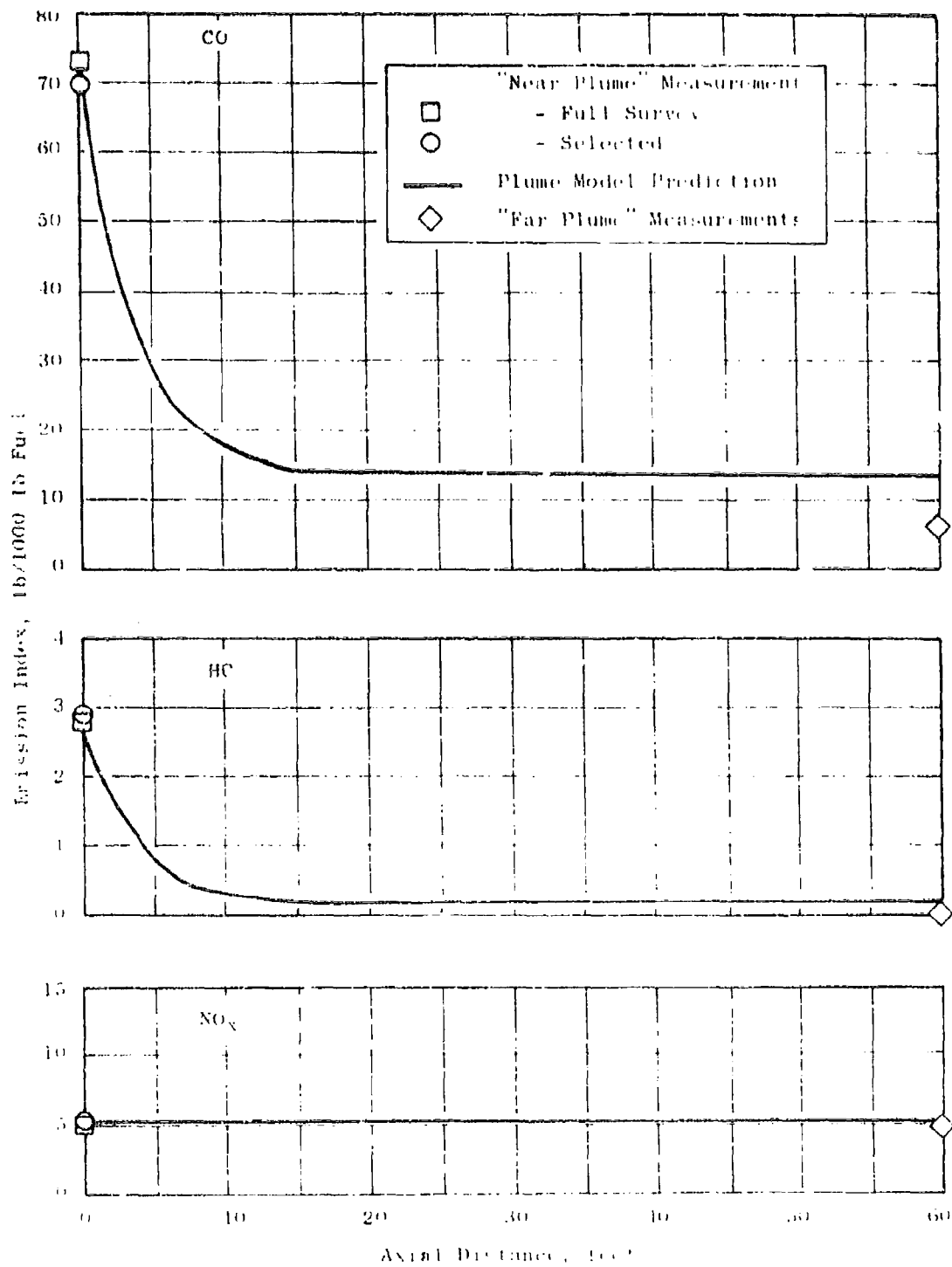


Figure 121. Plume Model Predictions of Overall Emissions Indices Compared with Phase III Test Data - 379-Lb Engine, Max. A/R.

SECTION 9.0

CONCLUSIONS AND RECOMMENDATIONS

9.1 CONCLUSIONS

The principal conclusions resulting from the work conducted under this program are the following:

1. Significant changes in emissions levels can occur in the plumes of afterburning engines. Moderate increases in CO were observed due to partial oxidation of HC at low and intermediate A/B power levels. At the highest power levels (near-stoichiometric fuel-air ratio) large reductions in CO generally were found to occur in the plume. HC was found to be the most reactive contaminant in the plume, and, at the highest A/B power levels, essentially complete consumption of HC occurred. NO_x was found to be the least reactive of the exhaust contaminants. No significant changes in NO_x in the plume were observed at any power level.
2. These plume reactions must be considered in the development of augmentors with reduced CO and HC emissions levels. The plume reactions are dependent upon both the initial (nozzle exit plane) emissions levels and on the radial distribution of the emissions at the exit plane. At low afterburning power levels, obtaining large reductions in residual CO and HC emissions levels involves reducing the amount of contaminants generated in the afterburner, since the consumption of these contaminants in the plume is incomplete. At maximum power levels, CO emissions may be unavoidably high at the exhaust plane due to equilibrium dissociation and local oxygen depletion, but the consumption of both CO and HC in the exhaust plume is nearly complete at sea level. Thus, the residual levels of these emissions at maximum power are quite low.
3. Under certain conditions, NO from the main burner can be partially converted to NO₂ in the afterburner. Since NO₂ is colored, the potential for plume visibility exists for afterburning engines.
4. An analytical plume model has been developed which calculates from nozzle exit plane data, the emissions levels ultimately ejected into the atmosphere. This highly complex and sophisticated model is comprised of:
 - a. Detailed chemical kinetic mechanism equations;
 - b. Features for the treatment of mixing within the potential core, as well as subsequent mixing with ambient air;
 - c. Features for the treatment of mixing of time inhomogeneities.

5. An afterburning engine emissions measurement technique, called the "Far Plume Method," has been developed. With this method, accurate results are obtained from direct measurements of emissions levels at a location far enough removed from the engine that mixing and chemical reactions are complete. A new data reduction approach has been developed for use with this method, which accounts for ambient emissions levels and avoids the need for accurate position measurements and for total and static pressure measurements. This method also simplifies probe design since quenching of the gas samples is not required.
6. An alternative afterburning engine emissions measurement technique, called the "Near Plume Method", has also been developed. This method generally provides less reliable results than the "Far Plume Method." The "Near Plume Method" involves measurements of the emission levels at the nozzle exit plane. Due to the very high temperature, nonuniform, and chemically reactive nature of the exhaust at this location, very carefully designed sampling probes are necessary, and accurate probe position and total pressure measurements are required to properly mass-weight and area-weight the individual samples. To estimate subsequent modifications to the emissions levels due to reactions in the plume, the plume model computer program is required to calculate the quantity of emissions ultimately ejected into the atmosphere.
7. Analytical instruments normally specified for use in gas turbine engine emissions measurements (NDIR's for CO and CO₂, FID for HC, and chemiluminescence for NO and NO_x) can be used, with little modification, for afterburning engine emissions measurements. For measurements at locations far downstream of the exhaust plane, special provisions may be necessary to obtain adequate sensitivity and stability.
8. Smoke measurements made on the J79-15 engine showed a decrease in smoke level with increasing reheat power level. This is to be expected since conditions in the mainburner are more conducive to smoke formation, while the high temperature, low pressure conditions in the afterburner tend to oxidize smoke particles and hence reduce smoke levels.

9.2 RECOMMENDATIONS

Based on the results of this program, the following recommendations are made:

1. The Far Plume Measurement Procedure should be used if a suitable engine test facility is available.
2. The Near Plume Measurement Procedure should be used if measurements must be made in an enclosed test cell.

1. Smoke measurements should not be required for engines at afterburning power levels. The highest smoke levels are likely to occur under non afterburning conditions, and adequate procedures already exist for such measurements (e.g. ARP 1179).
4. Further investigation of NO₂ conversion in afterburners should be made, and criteria for plume visibility due to NO₂ should be developed.

SECRET

ABSTRACTS

1. Souza, A.L., and Rockwell, L.K., "Variability in the Tail Section of the Emission Measurements," EPA-600/3-74-006, January, 1974.
2. Heck, L.H., & Ferguson, D.K., "Experimental Investigation of Turbulent Mixing in Compressible Flows," 33rd Paper, AIAA, January, 1972.
3. Bittker, D.A., & Spalding, D.B., "Aerodynamic and Kinetic Studies of a Program for Static and Flow Tunnel Experiments on Turbulent Mixing and Shock-Tube Kinetics," NASA TR-69-599, January, 1972.
4. Colley, W.G., Ferguson, D.K., Marina, P.G., & Lenwerthe, H.F., "The Technology of Hypersonic Ramjet Combustion Systems," ARAA TR-67-10, December, 1967.
5. Spalding, D.B., "Concentration Fluctuations in a Turbulent Jet," Chemical Engineering Science, Vol. 29, pp. 101-114, 1974.
6. Spalding, D.B., "Mathematical Models of Concentration Fluctuations in Jets of Emissions from Continuous Combustion Systems," Combustion and Flame, Vol. 20, W.G. (Eds.), Plenum Press, 1972.
7. Lauder, B.E., and Spalding, D.B., Mathematical Models of Turbulence, McGraw-Hill Academic Press, 1972.
8. Shapiro, A.H., The Dynamics and Thermodynamics of Compressible Fluid Flow, The Ronald Press Company, 1953.
9. Bradshaw, P., Ferriss, J.H., & Atkinson, H.C., "Calculation of Re-Entrant Turbulence Using the Turbulent Energy Equation," Compressible Fluid Flow, G. K. V. Karasik & W.G. (Eds.), MPI Aer. Report 1217, 1966.
10. Mellor, G.L., "Boundary Layer Methods," Handbook of Heat Transfer, Vol. 2, Turbulent Boundary Layers, ed. by S. Kakota, McGraw-Hill, 1971.
11. Spalding, D.B., Pitomkin, Y.I., and Gurevich, I.V., Flow in Turbulent Jets, Pergamon/Morgan-Grampian, London, 1975.
12. Prandtl, L., "Über die ausgebildete Turbulenz," Z. für angewandte Math. Phys., Nachr. Akad. Wiss. Göttingen, 5, 1905.

13. Glushko, G.S., Turbulent Boundary Layer on a Flat Plate in an Incompressible Fluid, NASA TTF-10, 080 (translation of Izv. Akad. Nauk SSR Mekhanika, 4, p. 13), 1965.
14. Spalding, D.B., et. al., Turbulent Mixing in Combustion Chambers, Northern Research and Engineering Corporation, Report No. 1118-1, 1966.
15. Kolmogorov, A.N., "Equations of the Turbulent Motion of an Incompressible Fluid," Izv. Akad. Nauk SSSR Serv. Phys., 6 (3), 1942.
16. Hinze, J.O., Turbulence, McGraw-Hill, 1959.
17. Rotta, J., Statistical Theory of Non-Homogeneous Turbulence, Part II, NASA TT FF-11, 696, June, 1968.
18. Ollerhead, J.B., On the Prediction of Near Field Noise of Supersonic Jets, NASA CR-857, August, 1967.
19. Eldred, K.M. et. al., Suppression of Jet Noise with Emphasis on the Near Field, ASD-TDR-62-578, February, 1963.
20. Smith, G.D., Numerical Solution of Partial Differential Equations, Oxford University Press, 1965.
21. Becker, H.A., Hottel, H.C., & Williams, G.C., "The Nozzle Fluid Concentration Field of the Round Free Turbulent Jet," Journal of Fluid Mechanics, Vol. 30, Pt. 2, pp. 285-303, 1967.
22. Anderson, L.B., & Meyer, J.W., "High Altitude Jet Plume Chemistry," Aeronomica Acta, 1974.
23. Hammond, D.C., & Mellor, A.M., Analytical Calculations For the Performance and Pollutant Emissions of Gas Turbine Combustors, AIAA Paper 71-711, 1971.
24. Dryer, F., et al., "Temperature Dependence of the Reaction $\text{CO} + \text{OH} = \text{CO}_2 + \text{H}$," Combustion and Flame, Vol. 17, pp. 270-272, 1971.
25. Fenimore, C.P., "Formation of Nitric Oxide in Premixed Hydrocarbon Flames," Thirteenth Symposium (International) on Combustion, The Combustion Institute, Pittsburgh, 1971.
26. Baulch, D.L., Drysdale, D.D., Horne, D.G., & Lloyd, A.C., High Temperature Reaction Rate Data, No. 4, Dept. Phys. Chem., The University, Leeds, England, December, 1969.

27. Brokaw, R.S., & Bittker, D.A., Carbon Monoxide Oxidation Rates Computed for Automobile Exhaust Manifold Reactor Conditions, NASA TN D-7024, December, 1970.
28. Mullins, B.P., "Studies on the Spontaneous Ignition of Fuels Injected Into a Hot Air Stream" V-Ignition Delay Measurements on Hydrocarbons," Fuel, Vol. XXXII, pp. 363-379, 1953.
29. "Procedure for the Continuous Sampling and Measurement of Gaseous Emissions from Aircraft Turbine Engines," ARP 1256, Society of Automotive Engineers, October 1971.
30. Heck, P.H. & Ferguson, D.R., Analytical Solution For Free Turbulent Mixing in Compressible Flows, AIAA Paper No. 71-4, January, 1971.
31. Becker, H.A., Hottel, H.C., & Williams, G.C., "The Nozzle Fluid Concentration Field of the Round Free Turbulent Jet," Journal of Fluid Mechanics, Vol. 30, Pt. 2. pp. 285-303, 1967.
32. Kaskan, W.E., "Excess Radical Concentrations and the Disappearance of Carbon Monoxide in Flame Gases From Some Lean Flames," Combustion and Flame, Vol. 3, p. 49, 1959.
33. German, R.C., High, M.D., & Robinson, C.E., Measurement of Exhaust Emissions From a J85-GE-5B Engine At Simulated High-Altitude, Supersonic, Free-Stream Flight Conditions, Dept. of Transportation Report No. FAA-RD-73-92, June, 1973.
34. Quillevere, A., Briancon, R., and Decoufflet, J., AGARD Conference Proceedings No. 125 on Atmospheric Pollution by Aircraft Engines, AGARD-CP-125, September 1973.
35. Bittker, D.A. & Scullin, V.J., General Chemical Kinetics Computer Program For Static and Flow Reactions, With Application to Combustion and Shock-Tube Kinetics, NASA TN D-6586, January, 1972.
36. McBride, B.J., & Gordon, S., Fortran IV Program For Calculation of Thermodynamic Data, NASA TN D-4097, August, 1967.
37. Powell, H.N., Shaffer, A., & Suciu, S.N. Properties of Combustion Gases System: C_nH_{2n} - Air, McGraw-Hill Book Company, 1956.
38. Anon., JANAF Thermochemical Tables, Dow Chemical Co., Rev. 1969.

39. Jessup, R.S., Mears, T.W., Marantz, S., & Walker, J.A., Net Heat of Combustion of Kerosene - Like Fuels and Its Correlation With Other Properties, National Bureau of Standards, Report 5917. March, 1957.
40. Shapiro, A.H., The Dynamics and Thermodynamics of Compressible Fluid Flow, The Ronald Press Company, 1953.
41. Kreith, F., Principles of Heat Transfer, International Textbook Company, 1961.
42. Burgstad, L., & Wilton, M.L., Transport Properties of Air and Fuel-Air Mixtures, General Electric Company, TIS Report 70AEG403, October, 1970.
43. Society of Automotive Engineers - Aerospace Recommended Practice, ARP 1296, (October 1, 1971).
44. Federal Register Vol. 38, No. 136 (July 17, 1973).
45. Ambrosius, E., Fellows, R., Brickman, A., Mechanical Measurement and Instrumentation. The Ronald Press Company, New York (1966).
46. Beers, Y., Introduction to the Theory of Error. Addison-Wesley Publishing Company, Inc. Cambridge, Mass. (1953).

APPENDIX A

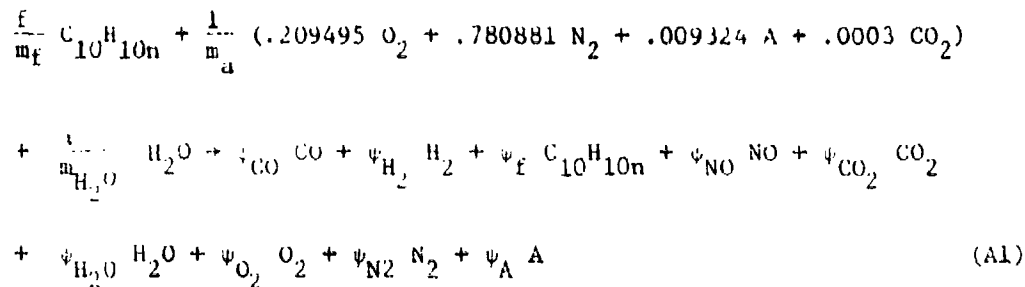
DERIVATION OF MATHEMATICAL RELATIONS USED IN PLUME MODEL DEVELOPMENT

This Appendix is divided into four separate parts. Each part treats a major segment of the mathematical relationships employed in developing the analytical plume model. These parts are the following:

- Part 1. Computation of Sample Fuel-Air Ratio and Emissions Indices from Gas Analysis.
- Part 2. Efficient Calculation of Equilibrium and Pseudo-Equilibrium Composition of Combustion Gases.
- Part 3. Thermodynamic Properties of Combustion Gas Mixtures and Hydro-Carbon Fuels.
- Part 4. Interaction of Probes with Two-Part Heterogeneous Gas Streams.

PART 1. COMPUTATION OF SAMPLE FUEL-AIR RATIO AND EMISSIONS INDICES FROM GAS ANALYSIS

The combustion reaction is written on the basis of one pound of dry air:



From the constituent mass balances, some of the ψ 's can be evaluated:

$$\psi_{CO_2} = \frac{10f}{m_f} + \frac{.0003}{m_a} - \psi_{CO} - 10\psi_f \quad (A2)$$

$$\psi_{H_2O} = \frac{5nf}{m_f} + \frac{a}{m_{H_2O}} - \psi_{H_2} - 5n\psi_f \quad (A3)$$

$$\begin{aligned} \psi_{O_2} &= \frac{.209495 + .0003}{m_f} + \frac{1}{2} \frac{1}{m_{H_2O}} - \frac{1}{2} \psi_{CO} - \frac{1}{2} \psi_{NO} - \psi_{CO_2} - \frac{1}{2} \psi_{H_2O} \\ &= \frac{.209495}{m_a} - (10+2.5n) \frac{f}{m_f} + \frac{1}{2} \psi_{CO} + \frac{1}{2} \psi_{H_2} + (10+2.5n) \psi_f - \frac{1}{2} \psi_{NO} \end{aligned} \quad (A4)$$

$$\psi_{N_2} = \frac{.780881}{m_a} - \frac{1}{2} \psi_{NO} \quad (A5)$$

$$\psi_A = \frac{.009324}{m_a} \quad (A6)$$

The total moles of sample mixture per pound of dry air is

$$\begin{aligned}
 M_T &= \psi_{CO} + \psi_{H_2} + \psi_f + \psi_{NO} + \psi_{CO_2} + \psi_{H_2O} + \psi_{O_2} + \psi_{N_2} + \psi_A \\
 &= \frac{1}{m_a} + \frac{a}{m_{H_2O}} + \frac{2.5nf}{m_f} + \frac{1}{2} \psi_{CO} + \frac{1}{2} \psi_{H_2} + (1-2.5n)\psi_f
 \end{aligned} \tag{A7}$$

The moles of bone-dry sample per pound of air is

$$\begin{aligned}
 M_D &= \psi_{CO} + \psi_{H_2} + \psi_f + \psi_{NO} + \psi_{CO_2} + \psi_{O_2} + \psi_{N_2} + \psi_A \\
 &= \frac{1}{m_a} - \frac{2.5nf}{m_f} + \frac{1}{2} \psi_{CO} + \frac{3}{2} \psi_{H_2} + (1+2.5n)\psi_f
 \end{aligned} \tag{A8}$$

The CAROL analyzer measures NO_x as moles of NO and NO_2 combined per mole gas as-sampled:

$$R_{NO_x} = \frac{\psi_{NO}}{M_T} \tag{A9}$$

Likewise, hydrocarbons are measured as single-carbon-atom molecules on an as-sampled basis:

$$R_{HC} = \frac{10. f}{M_T} \tag{A10}$$

Before measuring CO and CO_2 , the sample is dried to 32° F saturation, where the water content is approximately .006202 moles per mole dry gas. The CO and CO_2 analyzer readings are then

$$R_{CO} = \frac{\psi_{CO}}{1.006202 M_D} \tag{A11}$$

$$R_{CO_2} = \frac{\psi_{CO_2}}{1.006202 M_D} \tag{A12}$$

the H_2 is not measured, but the H_2 "reading" is estimated from R_{CO} using an empirical correlation:

$$R_{H_2} = \frac{R_{CO}}{1.000000} M_P = R_{CO} F(R_{CO}) \quad (A13)$$

$$F(R_{CO}) = 1.000000 e^{-0.0016 R_{CO}} \quad R_{CO} = 0.001022792 \quad (A14a)$$

$$F(R_{CO}) = 1.000000 e^{-0.0016 R_{CO}} \quad R_{CO} = 0.001022792 \quad (A14b)$$

Equations A10, A11, and A13 are combined with A7 to yield

$$\frac{2.5n}{m_f} = \left[1 - \left(\frac{1-2.5n}{10} \right) R_{HC} \right] M_T - .503101 (R_{CO} + R_{H_2}) M_D - \left(\frac{1}{m_a} + \frac{a}{m_{H_2O}} \right) \quad (A15)$$

Equations A10, A11, and A13 are combined with A8 to yield

$$\frac{2.5n}{m_f} = \left(\frac{1+2.5n}{10} \right) R_{HC} M_T + \left[.503101 (R_{CO} + 3R_{H_2}) - 1 \right] M_D + \frac{1}{m_a} \quad (A16)$$

Equations A2, A10, A11, and A13 are combined to yield

$$\frac{2.5n}{m_f} = \frac{1}{10} R_{HC} M_T + .517305n (R_{CO} + R_{H_2}) M_D - \frac{.000075n}{m_f} \quad (A17)$$

Equations A15, A16, and A17 are solved together to yield values for t , M_T , and M_D , after which the emissions indices are readily calculated:

$$E_{HC} = \frac{m_f}{m_a} \left(\frac{m_f}{t} \right) \left(\frac{M_T}{t} \right) \quad (A18)$$

$$E_{CO} = \frac{m_f}{m_a} \left(\frac{1.000000}{t} M_P \right) \quad (A19)$$

$$E_{\text{NO}_x} = R_{\text{NO}_x} m_{\text{NO}_2} \left(\frac{M_{\text{NO}_2}}{M_{\text{NO}_x}} \right) \quad (\text{A20})$$

PART 2. EFFICIENT CALCULATION OF EQUILIBRIUM AND PSEUDO-EQUILIBRIUM COMPOSITION OF COMBUSTION GASES

A specialized procedure is used in the afterburner emissions plume model for computation of equilibrium and pseudo-equilibrium composition of combustion gases. The procedure is computationally efficient and has been found reliable at the temperatures of interest.

Species concentrations are expressed as moles of species per pound of mixture, denoted Z_i . This method is computationally convenient, as will be shown, and the Z 's can readily be converted to mass fractions

$$Y_i = \bar{m}_i Z_i \quad (\text{A21})$$

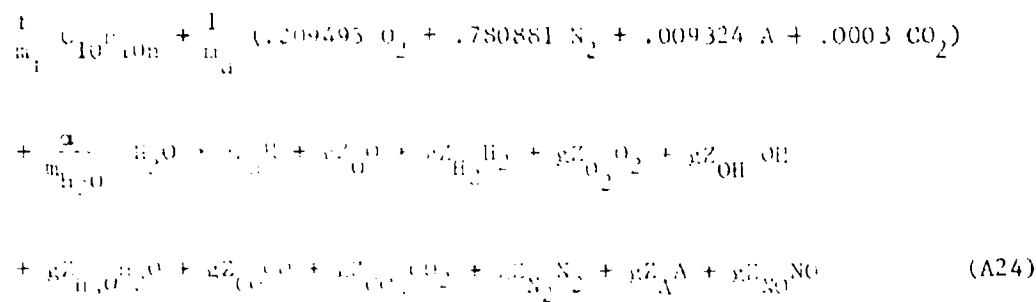
mixture molecular weight

$$\frac{1}{\bar{m}} = \sum_i Z_i \quad (\text{A22})$$

or mole fractions

$$X_i = \bar{m}_i Z_i \quad (\text{A23})$$

The general combustion reaction of one pound of dry air, f pounds of fuel $\text{C}_{10}\text{H}_{10}$, and w pounds of water is:



$$\text{where } g = 1 + f + \alpha \quad (\text{A25})$$

$$\text{and } m_f = 120.1 + 10.08n \quad (\text{A26})$$

Constituent mass balances provide five conservation equations:

$$\begin{aligned} z_H &= z_H + 2z_{H_2} + z_{OH} + 2z_{H_2O} \\ &= \frac{1}{g} \left(\frac{10nf}{m_f} + \frac{2\alpha}{m_{H_2O}} \right) \end{aligned} \quad (\text{A27})$$

$$z_C = z_{CO} + z_{CO_2} = \frac{1}{g} \left(\frac{10f}{m_f} + \frac{.0003}{m_a} \right) \quad (\text{A28})$$

$$\begin{aligned} z_O &= z_O + 2z_{O_2} + z_{OH} + z_{H_2O} + z_{CO} + 2z_{CO_2} + z_{NO} \\ &= \frac{1}{g} \left[\frac{2}{m_a} (.209495 + .0003) + \frac{\alpha}{m_{H_2O}} \right] \end{aligned} \quad (\text{A29})$$

$$z_N = 2z_{N_2} + z_{NO} = \frac{1}{g} \left[\frac{2}{m_a} (.780881) \right] \quad (\text{A30})$$

$$z_A = z_A = \frac{1}{g} \left(\frac{.009324}{m_a} \right) \quad (\text{A31})$$

Equilibration of "two-body" reactions that do not alter molarity and, hence, are independent of pressure, are used to provide five more nonlinear equations:

$$\begin{aligned} H_2 + OH &\rightleftharpoons 2H_2O \\ z_{OH} &= \frac{K_1 z_{H_2} z_{OH}}{z_{H_2O}^2} \end{aligned} \quad (\text{A32})$$

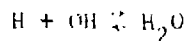
$$\begin{aligned} H_2 + O_2 &\rightleftharpoons 2H_2O \\ z_{O_2} &= \frac{K_2 z_{H_2} z_{O_2}}{z_{H_2O}^2} \end{aligned}$$

$$\text{H}_2 + \text{OH} \rightleftharpoons \text{H}_2\text{O} + \text{H} / z_{\text{H}} = \frac{K_3 z_{\text{H}_2} z_{\text{OH}}}{z_{\text{H}_2\text{O}}} \quad (\text{A34})$$

$$\text{CO}_2 + \text{H}_2 \rightleftharpoons \text{CO} + \text{H}_2\text{O} / z_{\text{CO}} = \frac{K_4 z_{\text{CO}_2} z_{\text{H}_2}}{z_{\text{H}_2\text{O}}} \quad (\text{A35})$$

$$\text{N}_2 + \text{O}_2 \rightleftharpoons 2\text{NO} / z_{\text{NO}} = \sqrt{K_5 z_{\text{N}_2} z_{\text{O}_2}} \quad (\text{A36})$$

The choice of Equation A31 depends upon whether full-equilibrium or pseudo-equilibrium composition is desired. For full chemical equilibrium, Equation A31 is provided by equilibration of a "three-body" pressure-dependent reaction:



$$\frac{z_{\text{H}_2\text{O}}}{z_{\text{H}} z_{\text{OH}} P \frac{1}{m}} = K_6 \quad (\text{A37})$$

In all cases, the equilibrium constants are evaluated from the Gibbs free energies of the species at the specified temperature (Appendix A, Part 3). For example:

$$-\ln K_1 = \frac{1}{R} \left(\frac{G_{\text{OH}}^0}{T} \right) - \left(\frac{G_{\text{H}_2}^0}{RT} \right) - \left(\frac{G_{\text{O}_2}^0}{RT} \right) \quad (\text{A38})$$

For pseudo-equilibrium composition, Equation A31 is provided by the specified mixture molecular weight (Equation A22):

$$\frac{1}{m} = \sum_i \frac{z_i}{M_i}$$

which is normalized by the parameter λ , defined as

$$\left(\frac{\lambda}{m} \right) = \left(\frac{1}{\sum_i \frac{z_i}{M_i}} \right) \quad (\text{A39})$$

where \bar{m}_u is the molecular weight of the "unreacted" mixture (fuel oxidized only to CO and H₂):

$$\frac{1}{\bar{m}_u} = \frac{1}{2} \Sigma_O + \frac{1}{2} \Sigma_C + \frac{1}{2} \Sigma_N + \Sigma_A - \frac{1}{2} (Z'_{CO_2} + Z'_{H_2O}) \quad (A40a)$$

$$Z'_{CO_2} = .0003 \left(\frac{\frac{1}{2} \Sigma_N}{.780881} \right) \quad (A40b)$$

$$Z'_{H_2O} = \frac{m_{H_2O}}{m_{H_2O}} \left(\frac{\frac{1}{2} \Sigma_N}{.780881} \right) \quad (A40c)$$

and \bar{m}_c is the molecular weight of the completely reacted (undissociated) mixture:

$$\frac{1}{\bar{m}_c} = \frac{1}{4} \Sigma_H + \frac{1}{2} \Sigma_N + \frac{1}{2} \Sigma_C + \Sigma_A \quad \phi \leq 1 \quad (A41a)$$

$$\frac{1}{\bar{m}_c} = \frac{1}{2} \Sigma_H + \Sigma_C + \frac{1}{2} \Sigma_N + \Sigma_A \quad \phi > 1 \quad (A41b)$$

where ϕ is the equivalence ratio

$$\phi = f/f_s \quad (A42a)$$

$$f_s = \frac{.209495 m_f}{10 m_a \left(1 + \frac{1}{4} n \right)} \quad (A42b)$$

Options are provided for regarding the CO, the NO, or both as inert species with predetermined concentration. When these options are exercised, Equations A35 and/or A36 are replaced by the predetermined value for Z_{CO} and/or Z_{NO} .

The system of 11 nonlinear algebraic equations is solved by an iterative technique. To initiate the procedure, an inefficient but undissociated mixture composition is computed where

$$Z_H = Z_C = Z_{OH} = 0, \text{ and}$$

$$Z_{CO} = 0, \text{ unless predetermined.}$$

For lean mixtures ($\phi \leq 1$),

$Z_{CO} = 0$, unless predetermined

$$Z_{H_2} = (1 - \beta) \left[\Sigma_C + \frac{1}{2} \Sigma_H - (Z'_{CO_2} + Z'_{H_2O}) \right] - Z_{CO} \quad (A43)$$

and

$$Z_{O_2} = \frac{1}{2} \Sigma_O - \Sigma_C - \frac{1}{4} \Sigma_H + \frac{1}{2} Z_{H_2} + \frac{1}{2} Z_{CO} - \frac{1}{2} Z_{NO} \quad (A44)$$

For rich mixtures ($\phi > 1$),

$$Z_{O_2} = (1 - \beta) \left[\frac{1}{2} \Sigma_O - \frac{1}{2} \Sigma_C - \frac{1}{2} (Z'_{CO_2} + Z'_{H_2O}) \right] - \frac{1}{2} Z_{NO} \quad (A45)$$

If not predetermined, Z_{CO} is initialized as a zero of the equation

$$\begin{aligned} (K_4 - 1) Z_{CO}^2 - \left[(2 \Sigma_C + \frac{1}{2} \Sigma_H - \Sigma_O + 2Z_{O_2} + Z_{NO}) (K_4 - 1) \right. \\ \left. + K_4 \Sigma_C + \frac{1}{2} \Sigma_H \right] Z_{CO} + (2 \Sigma_C + \frac{1}{2} \Sigma_H - \Sigma_O + 2Z_{O_2} \\ \left. + Z_{NO}) K_4 \Sigma_C = 0 \end{aligned} \quad (A46)$$

and

$$Z_{H_2} = 2\Sigma_C + \frac{1}{2} \Sigma_H - \Sigma_O + 2Z_{O_2} - Z_{CO} + Z_{NO} \quad (A47)$$

For both lean and rich mixtures, from Equations A28 and A29,

$$Z_{H_2O} = \Sigma_O - 2 \Sigma_C - 2 Z_{O_2} + Z_{CO} - Z_{NO} \quad (A48)$$

For full-equilibrium compositions, the estimate $\beta = .99$ is used to compute the initial mixture.

The iterative procedure is to estimate concentrations of the "primary" species H_2 , O_2 , and H_2O , compute values for all other species corresponding to the estimated values of the primary species, test for closure, then revise the estimates of the primary species and repeat. First Z_{O_2} , then Z_{H_2} and Z_{H_2O}

are computed directly from Equations A32, A33, and A34. If not predetermined, Z_{CO} is computed from a combination of Equations A28 and A35.

$$Z_{CO} = \frac{K_4 \Sigma C Z_{H_2}}{Z_{H_2O} + K_4 Z_{H_2}} \quad (A49)$$

then Z_{CO_2} is computed from Equation A28. If not predetermined, Z_{NO} is computed from a combination of Equations A30 and A36:

$$Z_{NO} = \sqrt{\frac{1}{4} K_5 Z_{O_2} \left(\frac{1}{4} K_5 Z_{O_2} + 2Z_N \right)} - \frac{1}{4} K_5 Z_{O_2} \quad (A50)$$

then Z_{N_2} is computed from Equation A30 and Z_A from Equation A31.

To test for closure, continuity errors for hydrogen and oxygen are derived from Equations A27 and A29:

$$\Delta \Sigma_H = \Sigma_H - Z_H - 2Z_{H_2} - Z_{OH} - 2Z_{H_2O} \quad (A51)$$

$$\Delta \Sigma_O = \Sigma_O - Z_O - 2Z_{O_2} - Z_{H_2O} - Z_{CO} - 2Z_{CO_2} - Z_{NO} \quad (A52)$$

For pseudo-equilibrium mixtures, a third closure error is derived from Equation A22:

$$\Delta \left(\frac{1}{m} \right) = \left(\frac{1}{m} \right) - \Sigma_i Z_i \quad (A53)$$

For full equilibrium mixtures, the third closure error is derived from Equations A22 and A37:

$$\Delta (\ln PK_6) = \ln(PK_6) - \ln \left(\frac{Z_{H_2O}}{Z_H Z_{OH}} \Sigma_i Z_i \right) \quad (A54)$$

If the magnitude of any closure error exceeds the tolerance, new estimates of Z_{H_2} , Z_{O_2} and Z_{H_2O} are made, and the process is reiterated:

$$(Z_{H_2})_{new} = (Z_{H_2})_{old} + Z_{H_2} \quad (A55)$$

$$(Z_{O_2})_{\text{new}} = (Z_{O_2})_{\text{old}} + \Delta Z_{O_2} \quad (\text{A55b})$$

$$(Z_{H_2O})_{\text{new}} = (Z_{H_2O})_{\text{old}} + \Delta Z_{H_2O} \quad (\text{A55c})$$

The values of the ΔZ 's that will effect the desired corrections indicated by Equations A51 through A54 are derived by differentiation of Equations A27, A29, and A22 or A32:

$$\Delta \Sigma_H = \frac{\partial \Sigma_H}{\partial Z_{H_2}} \Delta Z_{H_2} + \frac{\partial \Sigma_H}{\partial Z_{O_2}} \Delta Z_{O_2} + \frac{\partial \Sigma_H}{\partial Z_{H_2O}} \Delta Z_{H_2O} \quad (\text{A56})$$

$$\Delta \Sigma_O = \frac{\partial \Sigma_O}{\partial Z_{H_2}} \Delta Z_{H_2} + \frac{\partial \Sigma_O}{\partial Z_{O_2}} \Delta Z_{O_2} + \frac{\partial \Sigma_O}{\partial Z_{H_2O}} \Delta Z_{H_2O} \quad (\text{A57})$$

For both pseudo-equilibrium and full-equilibrium mixtures, and

$$\Delta \left(\frac{1}{m} \right) = \frac{\partial}{\partial Z_{H_2}} \left(\frac{1}{m} \right) \Delta Z_{H_2} + \frac{\partial}{\partial Z_{O_2}} \left(\frac{1}{m} \right) \Delta Z_{O_2} + \frac{\partial}{\partial Z_{H_2O}} \left(\frac{1}{m} \right) \Delta Z_{H_2O} \quad (\text{A58})$$

for pseudo-equilibrium mixtures, or

$$\Delta (\ln PK_6) = \frac{\partial}{\partial Z_{H_2}} (\ln PK_6) \Delta Z_{H_2} + \frac{\partial}{\partial Z_{O_2}} (\ln PK_6) \Delta Z_{O_2} + \frac{\partial}{\partial Z_{H_2O}} (\ln PK_6) \Delta Z_{H_2O} \quad (\text{A59})$$

for full equilibrium mixtures. The set of three linear equations provided by Equations A56, A57, and A58 (or A56, A57, and A59) are solved simultaneously for the three Z 's, after first evaluating the partial derivatives. This is done as follows: from Equation A27,

$$\frac{\partial \Sigma_H}{\partial Z_{H_2}} = \frac{\partial Z_{O_2}}{\partial Z_{H_2}} + 2 + \frac{\partial Z_{OH}}{\partial Z_{H_2}} \quad (\text{A60})$$

Rearranging Equation A34,

$$\ln Z_H = \ln K_3 + \ln Z_{H_2} + \ln Z_{OH} - \ln Z_{H_2O} \quad (A61)$$

$$\frac{1}{Z_H} \left(\frac{\partial Z_H}{\partial Z_{H_2}} \right) = \frac{1}{Z_{H_2}} + \frac{1}{Z_{OH}} \left(\frac{\partial Z_{OH}}{\partial Z_{H_2}} \right) \quad (A62)$$

Similarly, from Equation A32

$$\frac{1}{Z_{OH}} \left(\frac{\partial Z_{OH}}{\partial Z_{H_2}} \right) = \frac{1}{2} \left(\frac{1}{Z_{H_2}} \right) \quad (A63)$$

Combining Equations A60, A62, and A63,

$$\frac{\partial Z_H}{\partial Z_{H_2}} = 2 + \frac{3}{2} \left(\frac{Z_H}{Z_{H_2}} \right) + \frac{1}{2} \left(\frac{Z_{OH}}{Z_{H_2}} \right) \quad (A64)$$

The remaining partial derivatives are similarly evaluated:

$$\frac{\partial Z_H}{\partial Z_{O_2}} = \frac{1}{2} \left(\frac{Z_H}{Z_{O_2}} \right) + \frac{1}{2} \left(\frac{Z_{OH}}{Z_{O_2}} \right) \quad (A65)$$

$$\frac{\partial Z_H}{\partial Z_{H_2O}} = 2 - \left(\frac{Z_H}{Z_{H_2O}} \right) \quad (A66)$$

$$\frac{\partial Z_O}{\partial Z_{H_2}} = \left(\frac{Z_O}{Z_{H_2}} \right) + \frac{1}{2} \left(\frac{Z_{OH}}{Z_{H_2}} \right) - \frac{K_4 \cdot Z_{H_2O}}{(Z_{H_2O} + K_4 Z_{H_2})^2} \quad (A67)$$

$$\frac{\partial Z_O}{\partial Z_{O_2}} = 2 + \left(\frac{Z_O}{Z_{O_2}} \right) + \frac{1}{2} \left(\frac{Z_{OH}}{Z_{O_2}} \right) + \frac{1}{2} \left(\frac{K_5 Z_{N_2}}{K_5 Z_{O_2} + Z_{NO}} \right) \quad (A68)$$

$$\frac{[O]}{[Z_{H_2O}]} = 1 - \left(\frac{Z_O}{Z_{H_2O}} \right) + \frac{k_4 [O]_{OH_2}}{(Z_{H_2O} + k_4 Z_{H_2})^2} \quad (A69)$$

$$\frac{d}{dZ_{H_2}} \left(\frac{1}{m} \right) = 1 + \frac{1}{2} \left(\frac{Z_{H_2}}{Z_{H_2}} \right) + \left(\frac{Z_O}{Z_{H_2}} \right) + \frac{1}{2} \left(\frac{Z_{OH}}{Z_{H_2}} \right) \quad (A70)$$

$$\frac{d}{dZ_{O_2}} \left(\frac{1}{m} \right) = 1 + \frac{1}{2} \left(\frac{Z_{H_2}}{Z_{O_2}} \right) + \left(\frac{Z_O}{Z_{O_2}} \right) + \frac{1}{2} \left(\frac{Z_{OH}}{Z_{O_2}} \right) + \frac{1}{2} \left(\frac{k_4 Z_{H_2}}{Z_{O_2} (Z_{H_2O} + k_4 Z_{H_2})} \right) \quad (A71)$$

$$\frac{d}{dZ_{H_2O}} \left(\frac{1}{m} \right) = 1 - \left(\frac{Z_{H_2}}{Z_{H_2O}} \right) - \left(\frac{Z_O}{Z_{H_2O}} \right) \quad (A72)$$

$$\frac{d}{dZ_{H_2}} (\text{cnPK}_b) = \frac{m}{Z_{H_2}} \left(\frac{1}{2} (Z_{H_2} + Z_{O_2}) + \frac{1}{2} (Z_{OH} + \frac{Z}{m}) \right) \quad (A73)$$

$$\frac{d}{dZ_{O_2}} (\text{cnPK}_b) = \frac{m}{Z_{O_2}} \left[1 + \frac{1}{2} \left(\frac{Z_{H_2}}{Z_{O_2}} \right) + \left(\frac{Z_O}{Z_{O_2}} \right) + \frac{1}{2} \left(\frac{Z_{OH}}{Z_{O_2}} \right) + \frac{1}{2} \left(\frac{k_4 Z_{H_2}}{Z_{O_2} (Z_{H_2O} + k_4 Z_{H_2})} \right) \right] \quad (A74)$$

$$\frac{d}{dZ_{H_2O}} (\text{cnPK}_b) = \frac{m}{Z_{H_2O}} \left[1 - \left(\frac{Z_{H_2}}{Z_{H_2O}} \right) - \left(\frac{Z_O}{Z_{H_2O}} \right) \right] \quad (A75)$$

It is clear that the effect of the concentration of the various species on the rate of reaction is dependent on the relative concentrations of the various species. The effect of the concentration of the various species on the rate of reaction is dependent on the relative concentrations of the various species.

The effect of the concentration of the various species on the rate of reaction is dependent on the relative concentrations of the various species. The effect of the concentration of the various species on the rate of reaction is dependent on the relative concentrations of the various species.

PART 3. THERMOSTATIC PROPERTIES OF COMBUSTION GAS MIXTURES AND HYDROCARBON FUELS

The compositions of combustion gas mixtures are described by a hybrid parameter denoted Z_i , which is the pound-moles of species i per pound of mixture. This system is computationally more convenient than mole fractions or mass fractions, and is the system used internally in the NASA General Chemical Kinetics Program (Reference 35), much of which is incorporated in the plume model.

Using this system to describe the gas mixture, the mixture molecular weight is:

$$\frac{1}{\bar{m}} = \sum_i Z_i \quad (A76)$$

Mixture enthalpy, specific heat, and entropy are derived by appropriately averaging the dimensionless enthalpies, specific heats, and Gibbs free energies of the species at the prescribed temperature T :

$$h = R_0 T \sum_i Z_i \left(\frac{H_i}{RT} \right) \quad (A77)$$

$$C_p = R_0 \sum_i Z_i \left(\frac{C_{p_i}}{R} \right) \quad (A78)$$

$$S = R_0 \sum_i Z_i \left[\left(\frac{H_i}{RT} \right) - \left(\frac{G_i}{RT} \right) - \sum_n Z_n \right] - \frac{R_0}{\bar{m}} \sum_n \left(\frac{P_m}{14.696} \right) \quad (A79)$$

Here, $R_0 = 1.98596$ Btu/mole-deg R, and P is the prescribed pressure in pounds per square inch.

Other mixture properties are specific volume (cubic feet per pound):

$$v = \frac{R_0 J T}{144 P \bar{m}} \quad (A80)$$

where $J = 778.2$ ft-lbf/Btu, and sonic velocity (feet per second):

$$a = \sqrt{144 P v \gamma g_c} \quad (A81)$$

where $g_c = 32.174 \text{ ft-lbm/lbf-sec}^2$ and

$$\gamma = \frac{C_p}{C_v} = \frac{C_p}{C_p - \frac{R}{M}} \quad (\text{A82})$$

The dimensionless specific heats, enthalpies, and Gibbs free energies of the pure species are represented as polynomial functions of temperature, a method recommended by McBride and Gordon (Reference 36) and used in the NASA General Chemical Kinetics Program (Reference 35):

$$\frac{C_p}{R} = A_1 + A_2 T + A_3 T^2 + A_4 T^3 + A_5 T^5 \quad (\text{A83})$$

$$\frac{H}{RT} = A_1 + \frac{A_2}{2} T + \frac{A_3}{3} T^2 + \frac{A_4}{4} T^3 + \frac{A_5}{5} T^4 + \frac{A_6}{T} \quad (\text{A84})$$

$$\frac{G}{RT} = A_1 (1 - \ln T) = \frac{A_2}{2} T - \frac{A_3}{6} T^2 - \frac{A_4}{12} T^3 - \frac{A_5}{20} T^4 + \frac{A_6}{T} - A_7 \quad (\text{A85})$$

Values of the seven-polynomial coefficients for each chemical species and two temperature ranges are presented in Table A1. These values are for temperatures in degrees Kelvin. Except for A_6 , the coefficients are the same as those supplied by Dr. Bittker of NASA as part of the GCKP program.

The coefficient A_6 has been adjusted to conform to the General Electric customary enthalpy datum. The enthalpies are absolute enthalpies, equal to the sum of (a) the sensible enthalpy of the compound from its elements in temperature and (b) the heat of formation of the compound from its elements in their standard states at the reference temperature (Reference 37). The NASA data, as received, used a reference temperature of 298° K , whereas General Electric practice is to use absolute zero reference temperature. A correction ΔA_6 was applied to make the computed enthalpies of the five elements in their standard states at $T = 298^\circ \text{ K}$ agree with the JANAF enthalpies (Reference 38) at $T = 298^\circ \text{ K}$ relative to $H = 0$ at $T = 0$. For the elements:

	JANAF H°_{298} [cal/mole]	$\Delta A_6 = \frac{H^\circ_{298}}{R_0}$ [K]
O_2	2075	1044.8768
N_2	2072	11043.36617
H_2	2024	1019.19552
$C(s)$	252	126.89588
A	--	745.37507

The ΔA_6 corrections for the compounds were derived from the ΔA_6 values of the elements in their reference states. For example, for H_2O :

$$(\Delta A_6)_{H_2O} = (\Delta A_6)_{H_2} + \frac{1}{2} (\Delta A_6)_{O_2} \quad (A86)$$

The properties of unburned fuel vapor in the gas mixture are computed somewhat differently from the other species. The specific heat is taken as that of ethylene gas, coefficients for which are given in Table A-1; however, the enthalpy is corrected:

$$\frac{H_f}{RT} = \frac{H_{C_2H_4}}{RT} + \frac{\Delta H_f}{RT} \quad (A87)$$

where

$$\Delta H_f = (LHV)_{\text{jet fuel}} + (\Delta h_{fg})_{\text{jet fuel}} - (LHV)_{C_2H_4} \quad (A88)$$

$$LHV = \text{lower heating value at } 77^\circ \text{ F} \quad (A89)$$

$$\Delta h_{fg} = \text{approximate heat of vaporization of jet fuel at } 77^\circ \text{ F} \quad (A90)$$

This representation of unburned fuel is inexact, as the fuel is not C_2H_4 but an undetermined mixture of heavier hydrocarbon molecules characterized approximately as $C_{10}H_{10n}$; however, the concentration of unburned fuel is usually quite small, so that errors in gas temperature resulting from these approximations should be negligible.

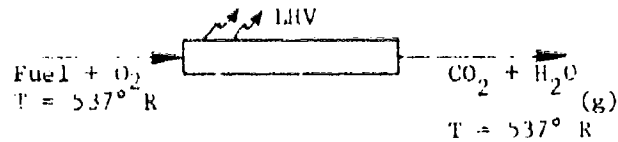
If not specified, the lower heating value of liquid jet fuel is estimated from the hydrogen-to-carbon ratio n , using the empirical relation:

$$LHV = \frac{184686.04 + 37977.7 n}{11.91468 + n} \quad (A91)$$

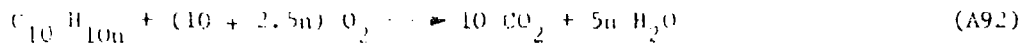
derived from the data and correlations of Jessup et al. (Reference 39).

The absolute enthalpy of the liquid fuel supplied to both main combustor and afterburner is computed from the enthalpies of oxygen, water vapor, and carbon dioxide at room temperature (77° F), and from the lower heating value of the fuel. By definition, the lower heating value is the heat recovered from a constant-pressure, constant-temperature reactor in which one pound of fuel

is burned completely to water vapor and CO₂:



The reaction is:



Writing the heat balance for one pound-mole of fuel:

$$m_F h_{F77} + (10 + 2.5n) H_{O_2} = m_F (LHV) + 10 H_{CO_2} + 5n H_{H_2O} \quad (A93)$$

where h is enthalpy per pound and H is enthalpy per mole. Rearranging, and expressing in terms of the dimensionless species enthalpies used above:

$$h_{F77} = (LHV) + \left[\left(\frac{H_{CO_2}}{RT} \right) + \frac{n}{2} \left(\frac{H_{H_2O}}{RT} \right) - \left(1 + \frac{n}{4} \right) \left(\frac{H_{O_2}}{RT} \right) \right] \left(\frac{10 R_Q T}{m_F} \right) \quad (A94)$$

or, for $T = 537^\circ R$:

$$h_{F77} = LHV = \frac{1066.4605 (158.1830 + 47.0276 n)}{12.01 + 1.008 n} \quad (A95)$$

In general, the fuel is not supplied to the engine at $77^\circ F$, so that

$$h_1 = h_{1n} + \Delta h_f \quad (A96)$$

where Δh_f is the sensible enthalpy of the liquid fuel relative to $77^\circ F$, approximated by:

$$\Delta h_f = 1.43733823 (T_1 - 77) + 3.0451394 (10^{-4}) (T_1 - 77)^2 + 5.7682466 (10^{-7}) (T_1 - 77)^3 + 1.1234368 (10^{-10}) (T_1 - 77)^4 \quad (A97)$$

where $T_1 = T_2 = 77^\circ F$.

PART 4. INTERACTION OF PROBES WITH TWO-PART HETEROGENEOUS GAS STREAMS

The heterogeneous gas stream is modeled analytically as a "marble cake" flow of only two gases, dispersed in each other but unmixed. The two gases, called "hot" and "cold", are assumed to have the same static pressure and, being mechanically interlocked, the same velocity. In the following developments, they will also be assumed to be perfect gases with constant (but not equal) molecular weights and specific heats.

This simple model lends itself to analytical prediction of the response of measurement probes immersed in the heterogeneous flow. The equations derived are those utilized in the plume model.

1. Gas Sample Probe

The gas sample probe, shown schematically in Figure A1, has orifice area A^* and is aspirated strongly enough that the sample flow is choked at all times. The sample flow is assumed to be steady-state as long as the probe is immersed in one or the other of the gases, and the transition period during passage of a boundary is neglected.

During a period when the probe is sampling one of the two gases, a flow function can be defined for the choked orifice (Reference 40):

$$w^* = \frac{w}{P_T A^*} \sqrt{\frac{R_o T_o}{g_c \bar{m}}} = \sqrt{\gamma \left(\frac{2}{\gamma+1}\right)^{\frac{\gamma+1}{\gamma-1}}} \quad (A98)$$

where w is the instantaneous sample flow rate and P_T is the instantaneous probe impact pressure, which depends upon the specific heat ratio γ and the Mach number:

$$\frac{P_T}{P} = \left(1 + \frac{\gamma-1}{2} M^2\right)^{\frac{\gamma}{\gamma-1}} \quad M < 1 \quad (A99)$$

$$\frac{P_T}{P} = \frac{\left(\frac{\gamma+1}{2} M^2\right)^{\frac{\gamma}{\gamma-1}}}{\left(\frac{\gamma+1}{2} M^2 - \frac{\gamma-1}{2}\right)^{\frac{1}{\gamma-1}}} \quad M > 1 \quad (A100)$$

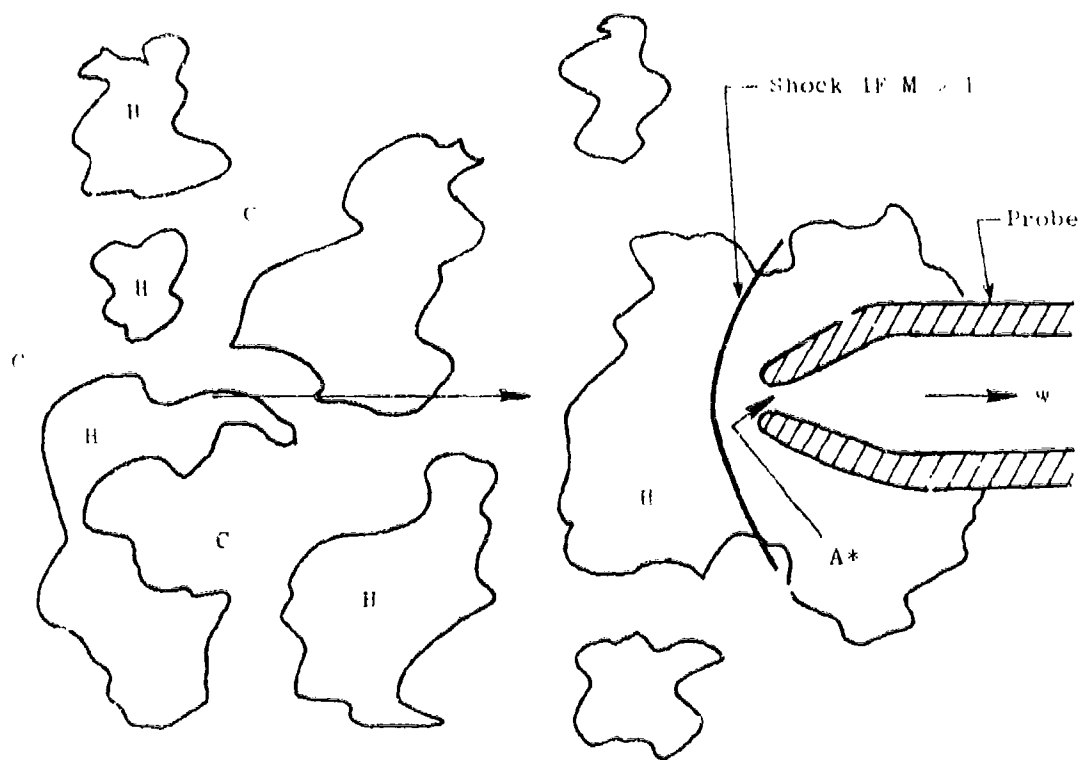


Figure A1. Gas Sample Probe in Two-Part Heterogeneous Stream.

Over an extended period of time, the total mass of gas sampled per unit time will be:

$$\bar{w}_s = w_H \tau + w_c (1 - \tau) \quad (\text{A100})$$

where the subscripts refer to the hot and cold gases, and τ is the fraction of time during which the probe samples hot gas. τ is also equal to the fraction of free volume occupied by hot gas:

$$\tau = y \left(\frac{v_H}{\bar{v}} \right) \quad (\text{A101})$$

where y is the mass fraction of hot gas in the free stream, v is specific volume, and

$$\bar{v} = yv_H + (1 - y) v_c \quad (\text{A102})$$

The mass fraction of hot gas in the sample will be:

$$y_s = \frac{w_H \tau}{\bar{w}_s} \quad (\text{A103})$$

Using Equation A100 to evaluate \bar{w}_s ,

$$\frac{w_H \tau}{y_s} = w_H \tau + w_c (1 - \tau) \quad (\text{A104})$$

Equating τ from Equation A101 and rearranging,

$$\frac{1}{y} = \frac{v_H}{\bar{v}} \left[1 + \frac{w_H}{w_c} \left(\frac{1}{y_s} - 1 \right) \right] \quad (\text{A105})$$

Evaluating \bar{v} from Equation A102 and further rearranging,

$$\frac{1}{y} - 1 = \left(\frac{v_H}{v_c} \right) \left(\frac{w_H}{w_c} \right) \left(\frac{1}{y_s} - 1 \right) \quad (\text{A106})$$

The ratio w_H/w_c can be evaluated from Equation A98:

$$\frac{w_H}{w_c} = \left(\frac{w_H^*}{w_c^*} \right) \frac{(P_T/P)_H}{(P_T/P)_C} \sqrt{\left(\frac{m_H}{m_c} \right) \left(\frac{T_{TC}}{T_{TH}} \right)} \quad (\text{A107})$$

Combining Equations A106 and A107,

$$y = \frac{1}{1 + \left(\frac{v_H}{v_c} \right) \left(\frac{w_H^*}{w_c^*} \right) \frac{(P_T/P)_H}{(P_T/P)_C} \sqrt{\left(\frac{m_H}{m_c} \right) \left(\frac{T_{TC}}{T_{TH}} \right) \left(\frac{1}{y_s} - 1 \right)}} \quad (\text{A108a})$$

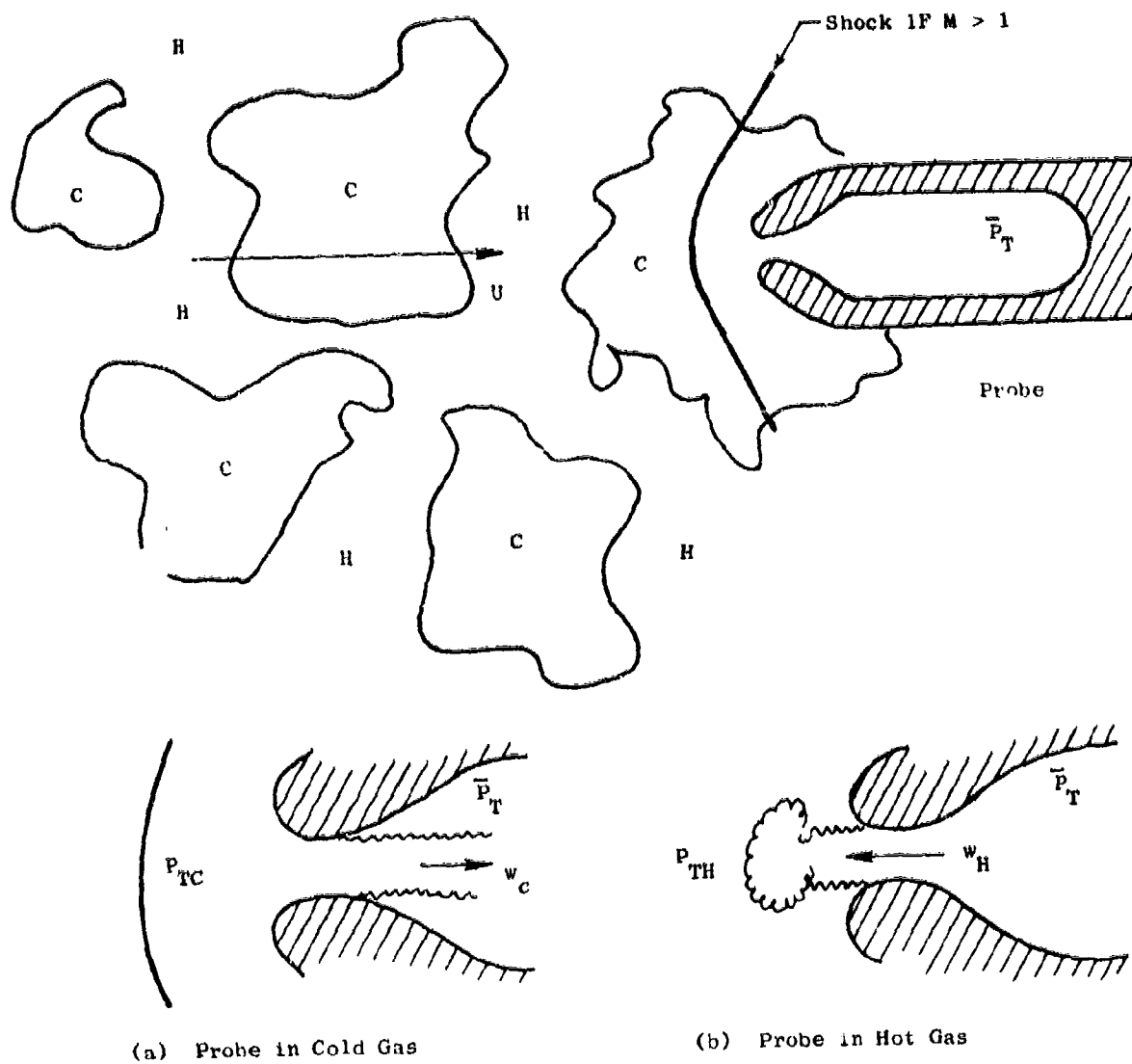
$$y_s = \frac{1}{1 + \left(\frac{v_c}{v_H} \right) \left(\frac{w_c^*}{w_H^*} \right) \frac{(P_T/P)_c}{(P_T/P)_H} \sqrt{\left(\frac{m_c}{m_H} \right) \left(\frac{T_{TH}}{T_{TC}} \right) \left(\frac{1}{y} - 1 \right)}} \quad (\text{A108b})$$

2. Total Pressure Probe

The total pressure probe, Figure A2, is assumed to contain a large, closed chamber behind the probe orifice, which is otherwise similar to the gas sample probe. The pressure in the chamber, \bar{P}_T , is assumed to be steady and of a magnitude between P_{TH} and P_{TC} . Since the hot and cold gases have the same velocity and static pressure, the cold gas will have a higher Mach number, hence a higher impact pressure. During the period when the probe is immersed in cold gas, gas flows into the probe chamber through the orifice. It is assumed that the flow separates at the orifice throat, so that the throat static pressure is \bar{P}_T , and that the pressure differences are low enough that the low-speed approximations apply at the throat:

$$P_{TC} - \bar{P}_T = \frac{U^2}{2g_c v_c} = \frac{v_c}{2g_c} \left(\frac{w_c}{A^*} \right)^2 \quad (\text{A109})$$

Here, w_c is the flow of cold gas into the probe while the probe is exposed to cold gas.



(a) Probe in Cold Gas

(b) Probe in Hot Gas

Figure A2. Total Pressure Probe in Two-Part Heterogeneous Stream.

During the period when the probe is exposed to hot gas, the gas impact pressure is lower than \bar{P}_T , so that cold gas already in the probe chamber flows out into the probe's stagnation region. Using the same assumptions as before,

$$P_{TH} - \bar{P}_T = - \frac{v_c}{2g_c} \left(\frac{w_H}{A^*} \right)^2 \quad (A103)$$

where w_H is the flow of cold gas out of the probe while the probe is exposed to hot gas.

Over an extended period of time, the total flows into and out of the probe chamber must be equal:

$$w_H \tau = w_c (1 - \tau) \quad (A104)$$

where τ is the fraction of time during which the probe is exposed to hot gas, as in Equation A100. Combining Equation A104 with A109 and A103.

$$\left(\frac{w_H}{w_c} \right)^2 = \left(\frac{1 - \tau}{\tau} \right)^2 = - \frac{P_{TH} - \bar{P}_T}{P_{TC} - \bar{P}_T} \quad (A105a)$$

or

$$\bar{P}_T = \frac{\tau^2 P_{TH} + (1 - \tau)^2 P_{TC}}{\tau^2 + (1 - \tau)^2} \quad (A105b)$$

3. Aspirated Thermocouple Probe

The thermocouple probe, Figure A3, resembles the gas sample probe, except that a thermocouple junction is inserted in the throat of the sampling orifice. The probe is assumed to be sufficiently aspirated to choke the flow in the throat at all times. The flow and heat transfer are assumed to be steady-state as long as the probe is immersed in one or the other of the gases, and the transition period during passage of a hot-cold gas boundary is neglected. The thermocouple junction is assumed to be sufficiently massive that its temperature is constant with time.

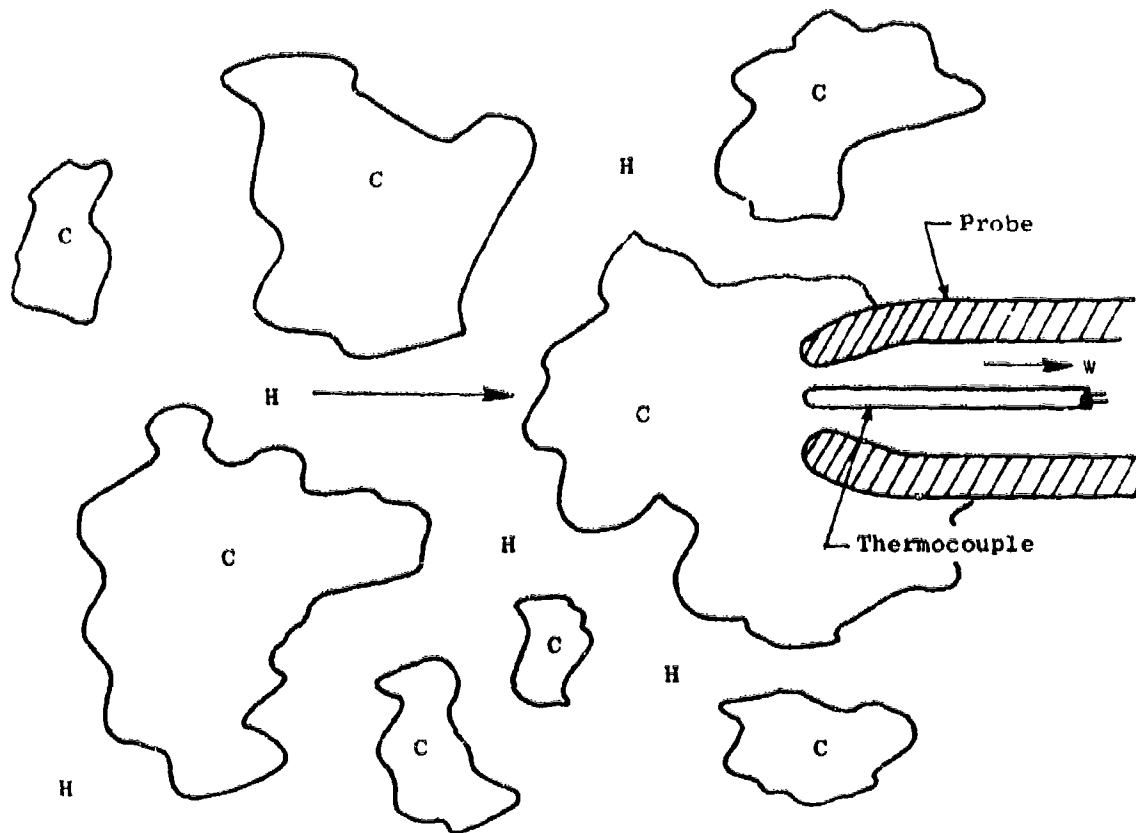


Figure A3. Aspirated Thermocouple Probe in Two-Part Heterogeneous Stream.

While the probe is immersed in one of the gases, the instantaneous rate of heat transfer from the aspirated gas stream to the thermocouple junction is

$$Q = \bar{h}A (T_T - \bar{T}_T) \quad (\text{A106})$$

where A and \bar{T}_T are the surface area and temperature of the thermocouple, T_T is the gas total temperature, and \bar{h} is the mean heat transfer coefficient, which may be approximated by the empirical formula for heat transfer to a sphere of diameter D (Reference 41):

$$\frac{\bar{h}D}{k} = .37 \left(\frac{UD}{\nu\mu} \right)^{.6} \quad (\text{A107})$$

Over an extended period of time, there is no net heat transfer to the thermocouple:

$$Q_H \tau + Q_C (1 - \tau) = 0 \quad (\text{A108})$$

Using Equations A106 and A107, this becomes

$$\tau k_H \mu_H^{-.6} (U^*/\nu^*)_H^{.6} (T_{TH} - \bar{T}_T) + (1-\tau) k_C \mu_C^{-.6} (U^*/\nu^*)_C^{.6} (T_{TC} - \bar{T}_T) = 0 \quad (\text{A109})$$

By continuity,

$$\frac{U^*}{\nu^*} = \frac{w}{\Lambda^*} \quad (\text{A110})$$

so that Equation A109 becomes:

$$\tau \left(\frac{k_H}{k_C} \right) \left(\frac{\mu_C}{\mu_H} \right)^{.6} \left(\frac{w_H}{w_C} \right)^{.6} (T_{TH} - \bar{T}_T) + (1-\tau) (T_{TC} - \bar{T}_T) = 0 \quad (\text{A111})$$

The gas transport properties can be evaluated approximately by observing that, for combustion gases with equilibrium adiabatic temperatures along a fuel addition line from standard day ambient air temperature,

$$\frac{k}{\mu^{.6}} \propto T^{.45} \quad (\text{A112})$$

is a good approximation up to $T = 2500^\circ R$, which is close to the upper limit for base-metal thermocouples (Figure A4). Substituting Equation A112 in A111 and solving for \bar{T}_T ,

$$\bar{T}_T = \frac{\tau \left(\frac{T_{TH}}{T_{TC}} \right)^{.45} \left(\frac{w_H}{w_c} \right)^{.6} T_{TH} + (1-\tau) T_{TC}}{\tau \left(\frac{T_{TH}}{T_{TC}} \right)^{.45} \left(\frac{w_H}{w_c} \right)^{.6} + (1-\tau)} \quad (A113)$$

The ratio of aspirated gas flow rates through the sonic throat of the probe, w_H/w_c , is evaluated by Equation A107, and the fraction of time the probe is exposed to hot gas, τ , is evaluated by Equations A101 and A102.

$$\tau = \frac{y \left(\frac{v_H}{v_c} \right)}{1 + y \left(\frac{v_H}{v_c} - 1 \right)} \quad (A114)$$

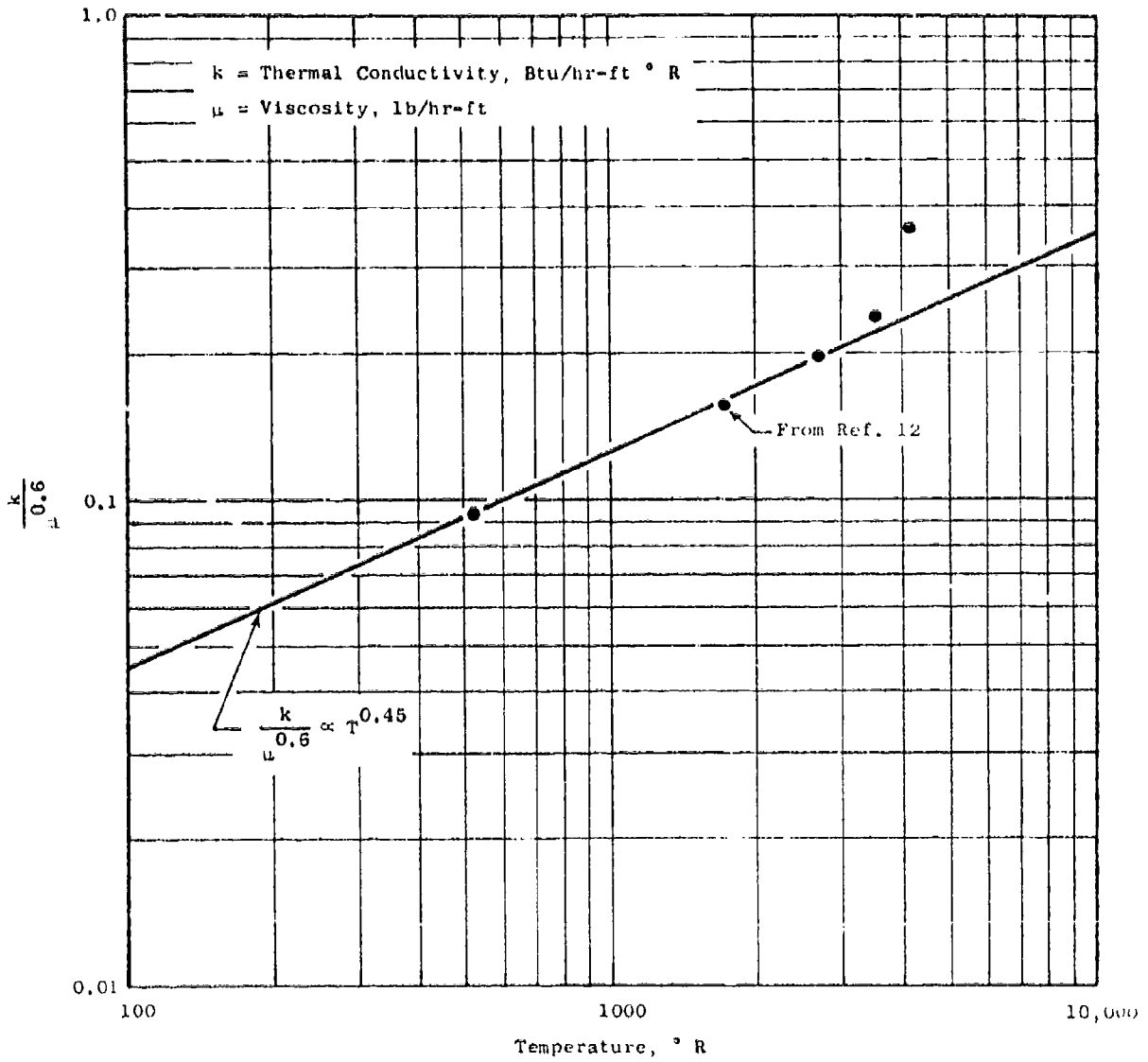


Figure A4. Approximate Relationship Between Thermal Conductivity, Viscosity, and Temperature for Combustion Gases.

APPENDIX B

PROCEDURE FOR MEASUREMENT OF GASEOUS EMISSIONS FROM AFTERBURNING AIRCRAFT GAS TURBINE ENGINES

PURPOSE

This is the recommended procedure for the continuous sampling and analysis of gaseous emissions from afterburning aircraft gas turbine engines and is intended to standardize the emission test procedures and equipment for measuring carbon monoxide, carbon dioxide, nitric oxide, total NO_x , and total hydrocarbon. Due to the reactive nature of the exhaust plume from afterburning engines, special procedures are necessary to assure that the measured emissions levels correspond to those actually emitted into the surrounding atmosphere. This procedure is comprised of two distinct parts. Part A describes the procedure for use when exhaust gas samples are taken at axial stations far removed from the engine exhaust plane. This is the preferred procedure. In case the required test facilities are not available for using this procedure, an alternative procedure is given (Part B) which involves sampling at the nozzle exit plane. The use of the Part B procedure requires calculation of the ultimate emissions levels utilizing a computer program derived from a reactive plume analytical model.

INTRODUCTION

Procedures have been developed and published by the SAE (Reference 43) and EPA (Reference 44) for the measurement of gaseous emissions from aircraft gas turbine engines. Since these procedures are not suitable for afterburning engines, the U.S. Air Force sponsored a program (Contract F33615-73-C-2047) with the General Electric Company to develop emissions measurement techniques applicable to afterburning engines. A complete description of the development of these procedures is given in the final report, AFAP1-TR-75-52.

For non-afterburning turbine engines, temperatures at the exhaust nozzle are typically less than 1200°F . At such temperatures, chemical reactions no longer proceed at an appreciable rate and the measured emission levels correspond to those actually ejected into the atmosphere. In the case of afterburning gas turbine engines, exhaust temperatures can reach 3500°F and chemical reactions can occur for a considerable distance downstream of the exhaust plane. Thus to obtain the true emissions levels for afterburning turbine engines, the plume should be sampled at a location far enough removed from the engine that the gases have been cooled to a temperature where reactions have ceased. Such a technique is described in Part A of this measurement procedure. This procedure, however, requires considerable clear area aft of the engine and thus would generally necessitate an outdoor test facility.

In case no such test facility is available, measurements may be made at the nozzle exit location, as described in Part B of this procedure. The measured emissions levels must then be corrected for plume reactions through utilization of a computer program derived from a reactive plume analytical model.

The Part A procedure (Far Plume Method) is the preferred procedure and normally gives more reliable results, especially at very high afterburner power levels. This procedure, however, involves accurate measurement of extremely low concentrations, which approach ambient levels and special data reduction methods are required. A test for representative sampling is provided by statistical analysis of the data.

The procedure described in Part B for sampling at the nozzle exit plane (Near Plume Method) requires the use of carefully designed probes or rakes which will not only withstand the severe thermal and mechanical stresses but will also provide for rapid quenching of the chemical reactions (quick quench probe). Accurate probe position and total pressure measurements are required so that proper mass and area weighting factors may be applied. A test for representative sampling is provided for by comparing total fuel flow, as calculated from the exhaust gas measurements, with the measured total engine fuel flow.

SECTIONS

This procedure is divided into the following sections:

PART A - FAR PLUME METHOD

- A1. Definitions of Terms
- A2. Analysis Equipment
- A3. Sampling Equipment
- A4. Equipment Layout
- A5. Instrument Routines
- A6. Reference Gases
- A7. Test Procedure
- A8. Minimum Information to be Recorded
- A9. Calculation of Results

PART B - NEAR PLUME METHOD

- B1. Definitions of Terms
- B2. Analysis Equipment
- B3. Sampling Equipment
- B4. Equipment Layout
- B5. Instrument Routines
- B6. Reference Gases
- B7. Test Procedure
- B8. Minimum Information to be Recorded
- B9. Calculation of Results

PART A. FAR PLUME METHOD (MEASUREMENT PROCEDURE FOR SAMPLING AT AXIAL STATIONS FAR REMOVED FROM NOZZLE EXIT PLANE).

AJ. DEFINITIONS

- A1.1 Aircraft Gas Turbine Engine: A turboprop, turbofan, or turbojet aircraft engine.
- A1.2 Engine Exhaust: Flow of material from an engine as a result of the combustion of fuel and air.
- A1.3 Exhaust Emissions: Substances ejected into the atmosphere from the exhaust discharge nozzle of an aircraft engine.
- A1.4 Particulates: Solid exhaust emissions.
- A1.5 Smoke: Matter in exhaust emissions which obscures light transmission.
- A1.6 Augmentor: A device or method used to obtain thrust in addition to that provided by normal operation of the main engine.
- A1.7 Afterburning Gas Turbine Engine: A gas turbine engine in which thrust augmentation is provided by injection and combustion of additional fuel in an afterburner. The afterburner is located between the turbine and the exhaust nozzle. The term "afterburner" generally applies to a turbojet engine. If the engine is a turbofan type, thrust augmentation may be obtained by burning in the fan stream (fanburner or duct-burner) or in the combined core stream and fan stream (mixed-flow augmentor).
- A1.8 Pollutant: Objectionable exhaust emission.
- A1.9 Plume: Region downstream of engine exhaust plane where exhaust gases mix with the ambient air.
- A1.10 Total Hydrocarbons (abbreviated HC): The total of hydrocarbons of all classes and molecular weights in the engine exhaust.
- A1.11 Oxides of Nitrogen (abbreviated NO_x): The total of oxides of nitrogen in the engine exhaust. The total NO_x value is calculated as equivalent NO₂.

- A1.12 Flame Ionization Detector: A hydrogen-air diffusion flame detector that produces a signal nominally proportional to the mass flow rate of hydrocarbons entering the flame per unit of time, generally assumed responsive to the number of carbon atoms entering the flame.
- A1.13 Nondispersive Infrared Analyzer: An instrument that selectively measures specific components by absorption of infrared energy.
- A1.14 Chemiluminescence Analyzer: An instrument in which the intensity of light produced by the chemiluminescence of the reaction of nitric oxide with ozone is proportional to the concentration of nitric oxide. Conversion of NO₂ to NO prior to entering the analyzer permits the determination of both species.
- A1.15 Interference: Instrument response due to components other than the gas that is to be measured.
- A1.16 Calibrating Gas: Gas of known concentration used to establish instrument response.
- A1.17 Span Gas: A calibrating gas used routinely to check instrument response.
- A1.18 Zero Gas: A calibrating gas used routinely to check instrument zero.
- A1.19 Concentration: The volume fraction of the component of interest in the gas mixture, expressed as volume percentage or as parts per million.

A2. ANALYSIS EQUIPMENT

A2.1 NDIR Instruments: Nondispersive infrared (NDIR) analyzer shall be used for the continuous monitoring of carbon monoxide (CO) and carbon dioxide (CO₂) in the turbine exhaust.

The NDIR instruments operate on the principle of differential energy absorption from parallel beams of infrared energy. The energy is transmitted to a differential detector through parallel cells, one containing a reference gas, and the other, sample gas. The detector, charged with the component to be measured, transduces the optical signal to an electric signal. The electrical signal thus generated is amplified and continuously recorded.

A2.1.1 Instrument Performance Specifications:

Response Time (electrical) - 90% full scale response in 0.5 second or less.
Zero Drift - Less than $\pm 0.5\%$ of full scale in 1 hour on most sensitive range.
Span Drift - Less than $\pm 0.5\%$ of full scale in 1 hour on most sensitive range.
Repeatability - Within $\pm 0.5\%$ of full scale.
Noise - Less than $\pm 1.0\%$ of full scale on most sensitive range.
Sample Cell Temperature - Minimum 50°C (122°F) maintained within $\pm 2^{\circ}\text{C}$ (3.6°F).

A2.1.2 Range And Accuracy:

	<u>Range</u>	<u>Accuracy Excluding Interferences</u>
Carbon	0 to 100 ppm	$\pm 2\%$ of full scale
Monoxide	0 to 500 ppm	$\pm 1\%$ of full scale
	0 to 1,000 ppm	$\pm 1\%$ of full scale
Carbon	0 to 1%	$\pm 1\%$ of full scale
Dioxide	0 to 2%	$\pm 1\%$ of full scale
	0 to 5%	$\pm 1\%$ of full scale

A2.1.3 Sensitivity:

CO Sensitivity (on most Sensitive range) - 0.3 ppm
CO₂ Sensitivity (on most Sensitive range) - 0.005%

A2.1.4 NDIR Cells: All NDIR instruments shall be equipped with cells of suitable length to measure concentrations within the above ranges to the indicated accuracy. Range changes may be accomplished by use of stacked sample cells and/or changes in the electronic circuitry.

A2.1.5 Interference: Interferences from water vapor, carbon dioxide, and carbon monoxide shall be determined on the most sensitive instrument range. Response of CO instruments shall be less than 5% of full scale for 2.5% CO₂ or 4% water vapor. Optical filters are the preferred method of discrimination. In some cases a cold trap or drying agent may be necessary to reduce water content below the level at which its interference is acceptable.

A2.2 Total Hydrocarbon Analyzer: The measurement of total hydrocarbon is made by an analyzer using a flame ionization detector (FID). With this type detector an ionization current, proportional to the mass rate of hydrocarbon entering a hydrogen flame is established between two electrodes. This ionization current is measured using an electrometer amplifier and is continuously recorded.

A2.2.1 General Design Specifications: The analyzer shall be fitted with a constant temperature oven housing the detector and sample-handling components. It shall maintain temperature within $\pm 2^\circ \text{C}$ of the set point, which shall be within the range 155 to 165°C (311 - 329°F).

The detector and sample handling components shall be suitable for continuous operation at temperatures to 200°C (392°F).

A2.2.2 Instrument Performance Specifications:

Response Time (electrical) - 90% of full scale in 0.5 second or less.

Noise - Less than $\pm 1.0\%$ of full scale on most sensitive range.

Repeatability - Within $\pm 1.0\%$ of full scale.

Zero Drift - Less than $\pm 1\%$ of full scale in 4 hours on all ranges.

Span Drift - Less than $\pm 1\%$ of full scale in 2 hours.

Linearity - Response with propane in air shall be linear within $\pm 2\%$ over the range of 0 to 500 ppmC.

A2.2.3 Range and Accuracy

<u>Range</u>	<u>Accuracy</u>
0 to 10 ppmC	$\pm 5\%$ of full scale with propane calibration gas.
0 to 100 ppmC	$\pm 2\%$ of full scale with propane calibration gas.
0 to 500 ppmC	$\pm 1\%$ of full scale with propane calibration gas.

A2.2.4 Sensitivity

HC Sensitivity (on most sensitive range) - 0.1 ppm

A2.3 Chemiluminescence Analyzer

A2.3.1 General Instrument Description: A chemiluminescence analyzer with thermal converter shall be used for measuring nitric oxide (NO) and total oxides of nitrogen (NO_x). The chemiluminescence method utilizes the principle that NO reacts with ozone (O_3) to give nitrogen dioxide (NO_2) and oxygen (O_2). Approximately 10 percent of the NO_2 is electronically excited. The transition of excited NO_2 to the ground state yields a light emission (600-2600 nanometer region) at low pressures. The detectable region of this emission depends on the PM-tube/optical filter being used in the detector. The intensity of this emission is proportional to the mass flow rate of NO into the reactor. The light emission can be measured utilizing a photomultiplier tube and associated electronics.

The method also utilizes the principle that NO_2 thermally decomposes to NO ($2\text{NO}_2 \rightarrow 2\text{NO} + \text{O}_2$). A thermal converter unit designed to provide essentially complete conversion of NO_2 to NO is included as a part of the chemiluminescence analyzer package. If the sample is passed through the converter prior to entering the chemiluminescence analyzer, an NO_x reading ($\text{NO} + \text{NO}_2$) is obtained. If the converter is bypassed, only the NO portion is indicated.

A2.3.2 Instrument Performance Specifications

Response time (electrical) - 90% of full scale in 0.5 second or less.

Noise - Less than 1% of full scale.

Repeatability - $\pm 1\%$ of full scale.

Zero drift - Less than $\pm 1\%$ of full scale in 2 hours.

Span drift - Less than $\pm 1\%$ of full scale in 2 hours.

Linearity - Linear to within $\pm 2\%$ of full scale on all ranges.

Accuracy - $\pm 1\%$ of full scale on all ranges.

A2.3.3 Range and Accuracy

<u>Range</u>	<u>Accuracy</u>
0 to 10 ppm	$\pm 5\%$ of full scale
0 to 100 ppm	$\pm 2\%$ of full scale

A2.3.4 Sensitivity

NO sensitivity (on most sensitive range) - 0.1 ppm

A3 SAMPLING EQUIPMENT

A3.1 Sampling Probe:

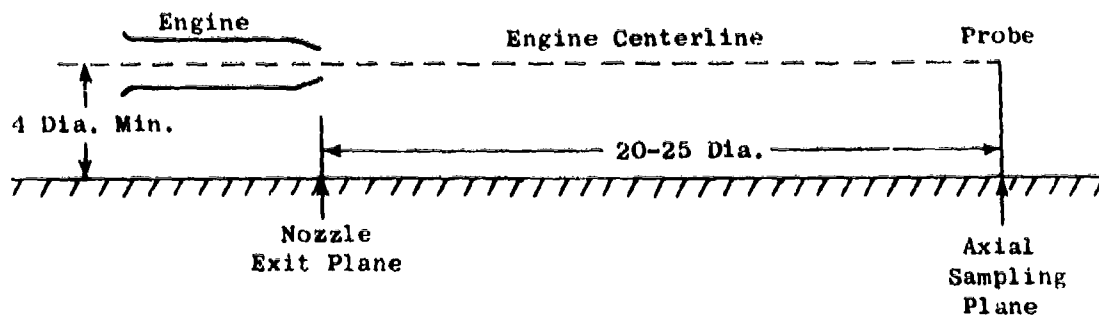
A3.1.1 Design Concept: The sampling probe shall be constructed so that individual samples may be withdrawn at various locations across a diameter of the plume. Mixed samples are not permitted. Either a single-element movable probe or a multielement rake may be used.

A3.1.2 Probe Material: The parts of the probe wetted by the sample gas shall be of stainless steel. Other materials may be used in contact with the sample gas if it is demonstrated that the material does not alter the composition of the sample.

A3.1.3 Probe Temperatures: The sample line within the probe shall be maintained at a temperature between 160 and 327° F.

A3.2 Sampling Locations. Both radial and axial sampling locations depend upon the size of the engine. In order to arrive at a common dimension, referred to the particular engine to be tested, there is herein defined a nozzle exit diameter, and all sampling locations are referred to this dimension. The nozzle exit diameter is for the maximum engine power condition and either may be obtained by actual measurement or may be calculated from engine operating conditions. The calculated nozzle exit diameter is obtained by complete expansion of the total engine flow to ambient pressure at the maximum power condition.

A3.2.1 Axial Sampling Station. The axial sampling plane shall be no less than 20 nor more than 25 nozzle exit diameters from the nozzle exit plane as shown below. At this sampling plane, there shall be an unobstructed area at least four nozzle exit diameters in radial distance about the projected engine centerline. (See sketch below.)



A3.2.2 Radial Sampling Locations. A minimum of 11 sampling points shall be used. These sampling points should be approximately equally spaced across the plume diameter, with one sample located on the plume centerline. If the sampling system is such that the sampling points cannot lie in a straight line (across a diameter), then a minimum of five samples shall be taken in each of two opposite sampling quadrants, with one sample taken at the plume centerline.

The outermost sampling points shall be at least four but no more than five exit nozzle diameters from the plume centerline. The sample at the center of the plume shall be taken at a distance no greater than 0.6 exit nozzle diameters from the true projected engine centerline.

A3.3 Sample Transfer. The sample shall be transferred from the probe to the analytical instruments through a heated sample line of either stainless steel or Teflon of 0.18 to 0.32-inch ID. The sample line shall be maintained at a temperature of $300 \pm 27^\circ \text{F}$.

Sample line length should be as short as possible, consistent with the test setup. Suitable noncontaminating sample pumps are required to maintain the proper sample flow rate and to provide adequate sample pressure at the instruments. The total sample flow rate shall be such that the sample gas is transported from the probe inlet to the analyzer inlet in less than 10 seconds.

A4. EQUIPMENT LAYOUT

A schematic diagram of the emissions measuring system is shown in Figure B1. Additional components such as instruments, thermocouples, valves, solenoids, pumps, and switches may be used to provide additional information and coordinate the functions of the component systems. Parallel installation of CO and CO₂ analyzers is an acceptable alternative. No desiccants, dryers, water traps or related equipment may be used to treat the sample flowing to the NO_x analyzer. The NO_x instrument configuration must be such that water condensation is avoided throughout the instrument.

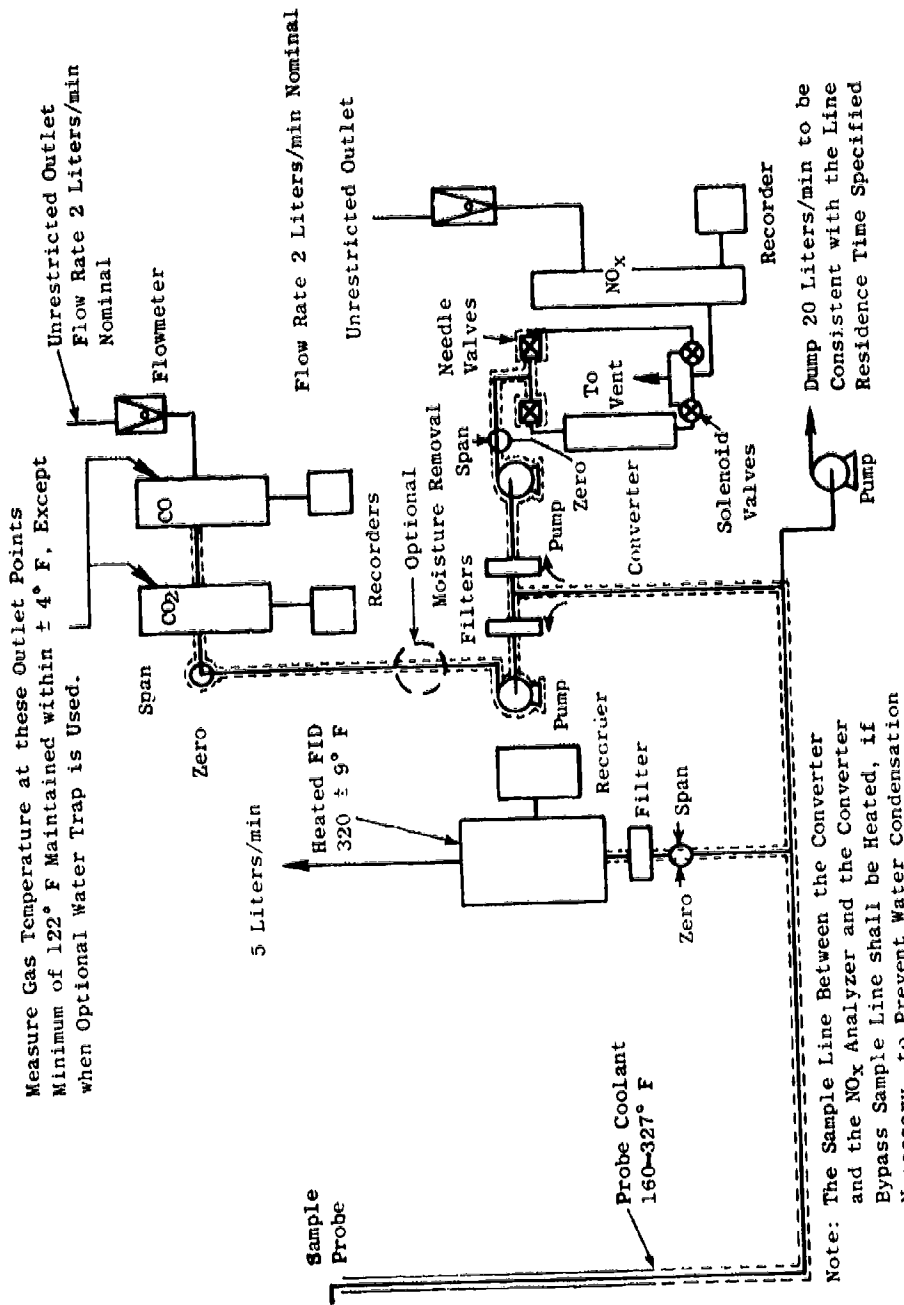


Figure B1. Sampling System Schematic.

A5. INSTRUMENT ROUTINES

A5.1 NDIR Instruments: Following the instrument manufacturer's instructions for startup of instruments, the following minimum requirements shall be adhered to:

A5.1.1 Monthly Routine:

- (1) Check detector tuning, following manufacturer's prescribed routine.
- (2) Set instrument zero using dry nitrogen.
- (3) Using previous gain setting check calibration curves using calibration gas with nominal concentrations of 30, 60, and 90% of each range used. Use the same gas flow rate through instruments during calibration as when sampling exhaust. Any response value differing from the previous value by more than $\pm 3\%$ of the previous value at the same gain setting may reflect some problem in the instrument system, and a thorough instrument check should be made. Confirm or reestablish calibration curves for each range. Log gain reading.
- (4) Check response of interference gases as called out in A2.1.4. If unacceptable, determine cause and correct -- detector replacement may be indicated.
- (5) Prior to each testing period, a check of the instrument zero and span drift, repeatability and noise level shall be made on the most sensitive instrument range to insure that it conforms with the instrument performance specifications.

A5.1.2 Daily Routine:

- (1) If analyzer power is not left on continuously, allow 2 hours for warmup. (If daily use is anticipated, it is recommended that analyzer be left on continuously.)
- (2) Replace or clean filters.
- (3) Check system for leaks.
- (4) Check detector tuning and record reading. If the reading changes by more than $\pm 3\%$ from the previous value, instrument readjustment is indicated. For the following tests the temperature of zero and span gas in the instrument cells shall be within $\pm 2^\circ \text{C}$ ($\pm 3.6^\circ \text{F}$) of typical sample gas temperature

measured at the outlet of the sample cell, and gas flow rate through the instruments shall be the same for zero and span gas as for sample gas.

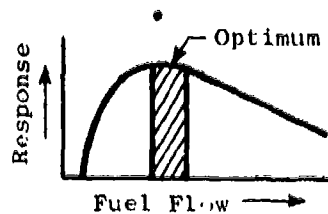
- (5) Zero the instrument on dry nitrogen. If there is a significant change in setting of Zero control, determine the cause and correct.
- (6) Using span gas to give 75 to 90% full-scale deflection, check the response of the instrument on each range using the gain setting from the previous use. If the reading differs from the previous value by more than 3%, an instrument problem may be indicated. Check and correct as necessary. If instrument reading is within $\pm 3\%$ of previous value, adjust gain control to produce proper instrument output. Log gain setting at final adjustment.
- (7) Check zero with dry nitrogen and repeat step 6 if necessary.
- (8) Zero and span shall be checked before and after each test, and at approximately one-hour intervals during the test.

A5.2 Total Hydrocarbon Analyzer

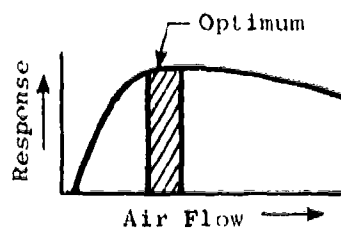
A5.2.1 Initial Alignment:

A5.2.1.1 Optimization of Detector Response:

- (1) Follow manufacturer's instructions for instrument startup and basic operating adjustment. Fuel shall be 60% helium, 40% hydrogen containing less than 0.1 ppmC hydrocarbon. Air shall be "hydrocarbon-free" grade containing less than 0.1 ppmC.
- (2) Set oven temperature at $160^{\circ} \text{C} \pm 5^{\circ} \text{C}$ ($320^{\circ} \text{F} \pm 9^{\circ} \text{F}$) and allow at least one-half hour after oven reaches temperature for the system to equilibrate. The temperature is to be maintained at set point $\pm 2^{\circ} \text{C}$ ($\pm 3.6^{\circ} \text{F}$).
- (3) Introduce a mixture of propane in air at a propane concentration of about 500 ppmC. Vary the fuel flow to burner and determine the peak response. A change in zero may result from a change in fuel flow; therefore, the instrument zero should be checked at each fuel flow rate. Select an operating flow rate that will give near maximum response and the least variation in response with minor fuel flow variations.



- (4) To determine the optimum airflow, use fuel flow setting determined above and vary airflow. A typical curve for response versus airflow is shown below:



After the optimum flow settings have been determined, these flows are to be measured and recorded for future reference.

A5.2.1.2 Oxygen Effect: Check the response of the detector with varied concentrations of oxygen in the sample following steps outlined below; this test shall be made with oven temperature at the set point and with gas flow to the detector at optimum conditions, as determined in A5.2.1.1.

- (1) Introduce nitrogen (N_2) zero gas and zero analyzer; check zero using hydrocarbon-free air; the zero should be the same.
- (2) The following blends of propane shall be used to determine the effect of oxygen (O_2) in the sample:

Propane in N_2

Propane in 90% N_2 + 10% O_2

Propane in air

The volume concentration of propane in the mixture reaching the detector should be about 500 ppmC, and the concentration of both the O_2 and hydrocarbon should be known within $\pm 1\%$ of the absolute value. The zero should be checked after each mixture is measured. If the zero has changed, then the test shall be repeated.

The response to propane in air shall not differ by more than 3% from the response to propane in the 10%-O₂/90%-N₂ mixture, nor differ by more than 5% from the response to propane in nitrogen.

If these specifications cannot be met by changing the sample flow rate or burner parameters, such as airflow and/or fuel flow rate, it is recommended that the detector be replaced.

A5.2.1.3 Linearity and Relative Response:

- (1) With analyzer optimized per A5.2.1.1, the instrument linearity shall be checked for the range 0 to 100 and 0 to 500 ppmC in air at nominal concentrations of 50 and 95% full scale of each range. The deviation of a best fit curve from a least-squares best-fit straight line should not exceed 2% of the value at any point. If this specification is met, concentration values may be calculated by use of a single calibration factor. If the deviation exceeds 2% at any point, concentration values shall be read from a calibration curve prepared during this alignment procedure.
- (2) A comparison of response to the different classes of compounds shall be made using (individually) propylene, toluene, and n-hexane, each at 20 to 50 ppmC concentration in nitrogen. If the response to any one differs by more than 5% from the average of the three, check instrument operating parameters. Reducing sample flow rate improves uniformity of response.

A5.2.2 Routine At Three-Month Intervals: These checks are to be made at three-month intervals or more frequently should there be any question regarding the accuracy of the hydrocarbon measurements:

- (1) Check for and correct any leaks in system.
- (2) Check and optimize burner flows (air, fuel, and sample) as required by criteria of A5.2.1.1.
- (3) Check O₂ effect as outlined in A5.2.1.2.
- (4) Check response of propylene, toluene, and n-hexane as outlined in A5.2.1.3.
- (5) Check linearity as outlined in A5.2.1.3.

- (6) Prior to each testing period, a check of the instrument zero and span drift, repeatability, and noise level shall be made on the most sensitive instrument range to insure that it conforms with the instrument performance specifications. Zero instability may be caused by HC condensation in the zero gas cylinder. A molecular sieve trap has been found effective in removing HC from the zero gas.

A5.2.3 Daily Routine

- (1) Clean or replace filters.
- (2) Check instrument for leaks.
- (3) Check instrument temperatures.
- (4) Ascertain that all flows to detector are correct.
- (5) Check zero with zero gas.
- (6) The response using blends of propane in air shall be checked on each range:

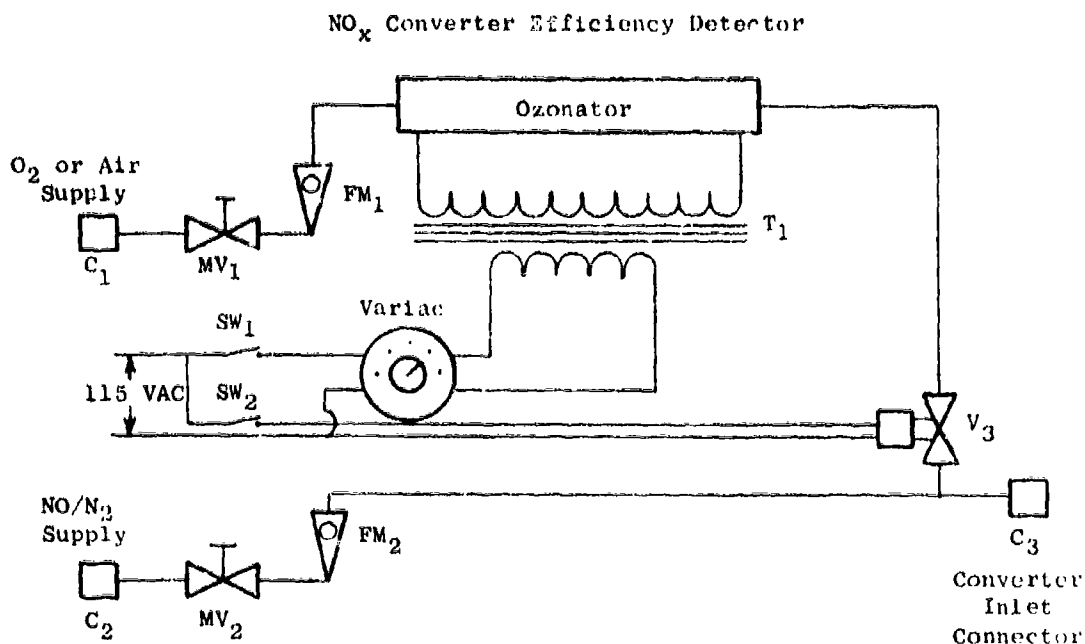
<u>For range</u>	<u>Use</u>
0 to 10 ppmC	7 to 10 ppmC propane in air
0 to 100 ppmC	70 to 100 ppmC propane in air
0 to 500 ppmC	350 to 500 ppmC propane in air

If the response differs from the last previous check value by more than 3% of the value logged during the last prior day's use, an instrument problem may be indicated.

A zero and span gas check shall be made before and after each test and at approximately one-hour intervals during the test. If the cumulative changes exceed 3% during the day, an instrument problem may be indicated.

A5.3 Chemiluminescence Analyzer: Follow the instrument manufacturer's instructions for startup of instrument.

A5.3.1 Thermal Converter Efficiency Check: Check the NO_x to NO converter efficiency by the following procedure. Use the apparatus described and illustrated below:



- (a) Attach the NO/N_2 supply (75-100 ppm) at C_2 , the O_2 supply at C_1 , and the analyzer inlet connection to the efficiency detector at C_3 . If lower concentrations of NO are used, air may be used in place of O_2 to facilitate better control of the NO_2 generated during step (d).
- (b) With the efficiency detector variac off, place the NO_x converter in bypass mode and close valve V_3 . Open valve MV_2 until sufficient flow and stable readings are obtained at the analyzer. Zero and span the analyzer output to indicate the value of the NO concentration being used. Record this concentration.
- (c) Open valve V_3 (on/off flow control solenoid valve for O_2) and adjust valve MV_1 (O_2 supply metering valve) to blend enough O_2 to lower the NO concentration (b) about 10%. Record this concentration.

- (d) Turn on the ozonator and increase its supply voltage until the NO concentration of (c) is reduced to about 20% of (b). NO₂ is now being formed from the NO+O₃ reaction. There must always be at least 10% unreacted NO at this point. Record this concentration.
- (e) When a stable reading has been obtained from (d), place the NO_x converter in the convert mode. The analyzer will now indicate the total NO_x concentration. Record this concentration.
- (f) Turn off the ozonator and allow the analyzer reading to stabilize. The mixture NO+O₂ is still passing through the converter. This reading is the total NO_x concentration of the dilute NO span gas used at step (c). Record this concentration.
- (g) Close valve V3. The NO concentration should be equal to or greater than the reading of (d) indicating whether the NO contains any NO₂.

Calculate the efficiency of the NO_x converter by substituting the concentrations obtained during the test into the following equation.

$$\% \text{ Eff.} = \frac{(e) - (d)}{(f) - (d)} \times 100\%$$

The efficiency of the converter should be greater than 90 percent. Adjusting the converter temperature may be needed to maximize the efficiency.

- (h) If the converter efficiency is not greater than 90 percent, the cause of the inefficiency shall be determined and corrected before the instrument is used.
- (i) The converter efficiency shall be checked at least monthly.

A5.3.2 Monthly Routine

- (1) Adjust analyzer to optimize performance.
- (2) Set instrument zero using zero grade nitrogen.
- (3) Calibrate the NO_x analyzer with nitric oxide (nitrogen diluent) gases having nominal concentrations of 50 and 95% of full scale on each range used. Use the same gas flow rate through the instrument during calibration as when sampling exhaust. Log zero and gain settings.

- (4) Prior to each testing period, a check of the instrument zero and span drift, repeatability, and noise level shall be made on the most sensitive instrument range to insure that it conforms with the instrument performance specifications.

A5.3.3 Daily Routine

- (1) If analyzer power is not left on continuously, allow two hours for warmup.
- (2) Clean or replace filters.
- (3) Check system for leaks.
- (4) Ascertain that flow to detector is correct.
- (5) Check zero with zero-grade nitrogen.
- (6) Zero and span shall be checked before and after each test and also at approximately one-hour intervals during the test.

A6. REFERENCE GASES

A6.1 Mixture Composition: Reference gases for carbon monoxide and carbon dioxide shall be prepared using nitrogen as the diluent. They may be blended singly or as dual component mixtures. Nitric oxide reference gas shall be blended in nitrogen. Hydrocarbon reference gas shall be propane in air. Zero gas shall be nitrogen, or optionally high purity air as specified in A6.4.

A6.2 Calibration Gases: Calibration gases shall be certified by the vendor as accurate within $\pm 1\%$.

A6.3 Span Gases: Span gases shall be supplied by the vendor to a stated accuracy within $\pm 2\%$.

A6.4 Zero Gas: Nitrogen zero gas shall be minimum 99.998% N₂ with less than 1 ppm CO. This gas shall be used to zero the CO, CO₂ and NO analyzer.

Zero-grade air shall not exceed 0.1 ppm hydrocarbon. This gas shall be used to zero the HC analyzer. Zero-grade air includes artificial air consisting of a blend of N₂ and O₂ with O₂ concentration between 18 and 21 mole percent.

A7. TEST PROCEDURE

A7.1 Test Layout: Set up engine, sampling equipment, and analysis equipment as specified in Sections A3 and A4.

A7.2 Fuel: The fuel used shall be as specified by the engine manufacturer. The carbon-to-hydrogen ratio shall be determined; this parameter is required in the calculation of results (Section A9). The emissions levels determined by this procedure may be a function of the type of fuel used, and, therefore, the type of fuel shall be included as an integral part of the test data, as specified in Section A8.

A7.3 Ambient Conditions

A7.3.1 Ambient Temperature, Pressure, and Humidity. Changes in ambient temperature, pressure, and humidity can cause changes in emissions levels both through direct changes in combustor conditions and through changes in engine operating parameters. Since generally accepted methods are not currently available for correcting test data to standard conditions, extremes of ambient conditions should be avoided. Ambient temperature, pressure, and humidity shall be measured for the test record (Section A8), but these data are not required for calculation purposes.

A7.3.2 Wind Velocity and Direction. The wind velocity and direction shall be recorded, and the crosswind and tailwind components shall be calculated. The crosswind velocity component shall not exceed 5 mph during the test. The tailwind component shall not exceed 1 mph.

A7.3.3 Ambient Air Composition. Unusually high concentrations of CO, HC, and CO₂ in the ambient air should be avoided since high values can adversely effect data accuracy. For comparison purposes, standard air contains 300 ppm CO₂, and the EPA ambient air quality standards are 9 ppm, 0.24 ppm, and 0.05 ppm for CO, HC, and NO₂ respectively. Unusually high concentrations may indicate abnormal conditions such as exhaust gas reingestion, fuel spillage, or additional sources of these emissions in the test area. It is suggested that an ambient air sample be obtained with the engine running before obtaining emissions data at each power setting.

A7.4 Instrument Calibration. Calibrate exhaust analysis instruments before and after each test period using daily procedures given in Section A5.

A7.5 Test Sequence

- (a) Start engine and adjust to desired power setting, allow adequate time for stabilization.
- (b) Measure concentrations of CO, CO₂, HC, NO, and NO_x at 11 radial sampling locations as specified in Section A3.2.2.
- (c) The engine may then be stabilized at another power setting and measurements made as in (b) above. Repeat until test series is complete.

A8 MINIMUM INFORMATION TO BE RECORDED.

The following information, as applicable, shall form a part of the permanent record for each test.

A8.1 General:

- (a) Facility performing test and location.
- (b) Individual responsible for conduct of test.
- (c) Test number, reading number, etc.
- (d) Date.
- (e) Time.
- (f) Fuel type, fuel specification, additives, H/C ratio and method of determination.
- (g) Ambient Conditions: temperature, pressure, humidity, wind velocity, and direction.
- (h) Engine mounting position and height.
- (i) Test procedure designation.
- (j) Exceptions, if any, to this procedure.

A8.2 Engine Description

- (a) Manufacturer
- (b) Model number, serial number

- (c) Time since overhaul and other pertinent maintenance information.
- (d) Nozzle exit diameter (per Section A3.2) and method of determination.

A8.3 Engine Operating Data:

- (a) Nominal power setting, throttle angle.
- (b) Rotational speed: N_1 , N_2 .
- (c) Fuel flow (main engine and afterburner).
- (d) Airflow and method of determination.
- (e) Compressor discharge temperature and method of determination.
- (f) Compressor discharge pressure or EPR.
- (g) Exhaust nozzle position.
- (h) Thrust.

A8.4 Exhaust Sampling Data:

- (a) Axial sampling location.
- (b) Radial sampling location (distance from projected engine centerline).
- (c) Concentrations of CO, CO₂, HC, NO, and NO_x at each sampling location.
- (d) Sample line temperature.
- (e) Probe coolant temperature.

A9 CALCULATION OF RESULTS

A9.1 General Calculations Procedure. Calculation of results involves the following steps:

- (a) Correction of measured concentrations to actual or wet concentrations of CO, CO₂, HC, NO, and NO_x.
- (b) Calculation of the slope of a linear fit, by the method of least squares, of the concentration of each pollutant plotted against the concentration of CO₂.
- (c) Calculation of emission indices (lb per 1000 lb of fuel) for CO, HC, NO, and NO_x from the slopes found in (b) above.
- (d) Calculation of emission flow rate (lb per hr) from emission indices found in (c) above and the total engine fuel flow rate.

A9.2 Symbols

- (CO) = Actual (wet) concentration of CO in exhaust, ppm.
- (CO₂) = Actual (wet) concentration of CO₂ in exhaust, %.
- (HC) = Actual (wet) concentration of hydrocarbon in exhaust, expressed as ppm equivalent methane.
- (NO) = Actual (wet) concentration of NO in exhaust, ppm.
- (NO_x) = Actual (wet) concentration of NO_x in exhaust, ppm.
- (CO)_d, (CO₂)_d, etc. = Dry concentration of CO, CO₂, etc.
- (CO)_{sd}, (CO₂)_{sd}, etc. = Semi-dry (0.602% moisture) concentrations of CO, CO₂, etc.
- a, b = Constants in linear curve fit relationship.
- y, x = Variables in linear curve fit relationship;
y represents pollutant concentrations (wet) in ppm;
x represents CO₂ concentration (wet) in %.
- Y_i, X_i = Actual (wet) concentration of pollutant (Y_i) and CO₂ (X_i) at each sampling point.
- m = Total number of sampling points (i = 1 to m).
- r = Correlation coefficient.

WFE = Total engine (mainburner plus afterburner) fuel flow rate, lb per hr.

EI_Z = Emission index of pollutant Z, lb per 1000 lb fuel

W_Z = Emission flow rate of pollutant Z, lb per hour

n = hydrogen to carbon atomic ratio of fuel

K_d = Correction factor for water of combustion

K_w = Correction factor for water of combustion and water vapor in the inlet air

h = Water content (humidity) of inlet air (% by volume)

M_C = Atomic weight of carbon

M_H = Atomic weight of hydrogen

σ_y = Standard deviation of y variable

σ_a = Standard deviation of a

σ_b = Standard deviation of b

A9.3 Correction for Moisture. All measured concentrations shall be corrected for moisture, as required, in order to form a consistent basis for further calculations. The calculation procedure presented here is for conversion to actual or wet concentration, although any reference moisture level may be used as long as it is consistent for all species in an equation.

The correction factor K_d corrects measured concentrations for water of combustion. The factor K_w corrects measured concentrations for water of combustion and for moisture in the inlet air. The values of K_d and K_w depend on the moisture removal devices in the analysis system. Note that no moisture removal device is permitted in the NO_x or HC analyzer sample lines so that HC and NO_x are always measured on a wet basis. If an ice trap (32° F) is used to partially dry the CO and CO₂ analyzer samples, then the CO and CO₂ samples are semidry and contain 0.602% moisture. Factors for converting CO and CO₂ concentrations to appropriate wet values are:

$$K_d = \frac{100}{100 + \frac{1.006 n}{2} \left(\frac{(CO)_{sd}}{10^4} + (CO_2)_{sd} \right)} \quad (B1)$$

$$K_w = K_d \frac{200 - h(1 + n/2)}{200 - h + \frac{K_d hn}{2} \left(1 - \frac{1.006 (CO)_{sd}}{10^6}\right)} \quad (B2)$$

where $(CO)_{sd}$ and $(CO_2)_{sd}$ are the measured semi-dry concentrations. Then,
 Concentration (wet) = $K_w \times 1.006 \times$ Concentration (semi-dry).

A9.4 Calculation of the Slope of Emissions vs. CO₂ by the Method of Least Squares

At a given engine power setting, the linearity of CO, HC, NO, and NO_x with respect to CO₂ shall be determined, by analysis of the measurements collected at the various probe sampling locations, in the following manner.

(a) Using the method of least squares, a polynomial of the form:

$$y = a + b x \quad (B3)$$

shall be fitted to each pollutant (CO, HC, NO, NO_x), in turn, where y represents the wet concentration (ppm) of the pollutant being analyzed, and x is the wet concentration (%) of CO₂. The constants a and b are determined by the well-known least square relationships (Reference 45):

$$a = \frac{\sum X_1 \sum Y_1 - \sum Y_1 \sum X_1}{(\sum X_1)^2 - m \sum X_1^2} \quad (B4)$$

$$b = \frac{\sum X_1 \sum Y_1 - m \sum X_1 Y_1}{(\sum X_1)^2 - m \sum X_1^2} \quad (B5)$$

X_1 and Y_1 represent the concentrations of X and Y at the ith sampling location of the particular test point, and the summations are over the total number (m) of sampling locations at which gas samples were extracted.

The slope, b, of the linear fit is proportional to the emission index. The intercepts are related to the ambient concentrations. Note that the Y intercept, a, should be no greater than the ambient pollutant level, and the x intercept, $-a/b$, should be no greater than the ambient CO₂ level. Ambient level is taken to be concentrations in the local air with which the engine exhaust mixes.

(b) The appropriateness of the linear fit of each constituent versus CO_2 shall be determined by calculation of the correlation coefficient (r) for each constituent, defined by the equation (Reference 45):

$$r = \frac{m\sum X_1 Y_1 - \sum X_1 \sum Y_1}{\sqrt{[m\sum X_1^2 - (\sum X_1)^2][m\sum Y_1^2 - (\sum Y_1)^2]}} \quad (\text{B6})$$

Values of r near 1.00 indicate good data consistency over the plume diameter, that plume reactions have ceased, and that plume mixing is complete. If the slope, b , is greater than about 10, then r should be greater than 0.99 if measurements are carefully made. For smaller values of b , r is influenced by instrument sensitivity, and low values may result.

Low values of r may be an indication that plume reactions are not complete. If b is greater than 10 and r is less than 0.95, the measurements shall be repeated at a sampling station farther downstream from the engine. The new sampling station shall be at a distance from the engine exhaust plane 1.3 to 1.4 times the distance of the previous measurements.

(c) The following standard deviations shall be computed and reported for each pollutant as a statistical measure of the degree of error associated with each term in the curve fit (Reference 46):

$$\sigma_y = \sqrt{\frac{\sum (Y_1 - a - bX_1)^2}{m-1}} \quad (\text{B7})$$

$$\sigma_a = \sigma_y \sqrt{\frac{m\sum X_1^2}{(m-1)[m\sum X_1^2 - (\sum X_1)^2]}} \quad (\text{B8})$$

$$\sigma_b = \sigma_y \sqrt{\frac{m}{(m-1)[m\sum X_1^2 - (\sum X_1)^2]}} \quad (\text{B9})$$

A9.5 Calculation of the Emission Indices of CO, HC, NO, NO_x

The emissions indices (lb/1000 lb fuel) of CO, HC, NO and NO_x at a given test condition shall be determined from the values of b (Section A9.4a, Equation B3) obtained for each pollutant using the following equations:

$$EI_{\text{CO}} = \frac{2.801 (b_{\text{CO}})}{(M_C + nM_H) \left(1 + \frac{b_{\text{CO}} + b_{\text{HC}}}{10^4} \right)} \quad (\text{B10})$$

$$EI_{HC} = \frac{0.100 (b_{HC})}{1 + \frac{b_{CO} + b_{HC}}{10^4}} \quad (B11)$$

$$EI_{NO} = \frac{4.601 (b_{NO})}{(M_C + nM_H) \left(1 + \frac{b_{CO} + b_{HC}}{10^4} \right)} \quad (B12)$$

$$EI_{NO_x} = \frac{4.601 (b_{NO_x})}{(M_C + nM_H) \left(1 + \frac{b_{CO} + b_{HC}}{10^4} \right)} \quad (B13)$$

A9.6 Calculation of Emissions Flow Rates for CO, HC, NO, NO_x

The emissions flow rates (lb/hr) of CO, HC, NO, NO_x shall be determined from the equation:

$$W_z = .001 (EI_z) (WFE) \quad (B14)$$

where z represents CO, HC, NO, and NO_x.

PART B. NEAR PLUME METHOD (MEASUREMENT PROCEDURE FOR SAMPLING AT NOZZLE EXIT PLANE)

B1. DEFINITIONS

- B1.1 Aircraft Gas Turbine Engine: A turboprop, turbofan, or turbojet aircraft engine.
- B1.2 Engine Exhaust: Flow of material from an engine as a result of the combustion of fuel and oxidizer.
- B1.3 Exhaust Emissions: Substances ejected into the atmosphere from the exhaust discharge nozzle of an aircraft engine.
- B1.4 Particulates: Solid exhaust emissions.
- B1.5 Smoke: Matter in exhaust emissions which obscures light transmission.
- B1.6 Augmentor: A device or method used to obtain thrust in addition to that provided by normal operation of the main engine.
- B1.7 Afterburning Gas Turbine Engine: A gas turbine engine in which thrust augmentation is provided by injection and combustion of additional fuel in an afterburner. The afterburner is located between the turbine and the exhaust nozzle. The term "afterburner" generally applies to a turbojet engine. If the engine is a turbofan type, thrust augmentation may be obtained by burning in the fan stream (fanburner or ductburner) or in the combined core stream and fan stream (mixed-flow augmentor).
- B1.8 Pollutant: Objectionable exhaust emission.
- B1.9 Plume: Total external engine exhaust including ambient air with which the exhaust mixes.
- B1.10 Total Hydrocarbons (abbreviated HC): The total of hydrocarbons of all classes and molecular weights in the engine exhaust.
- B1.11 Oxides of Nitrogen (abbreviated NO_x): The total of oxides of nitrogen in the engine exhaust. The total NO_x value is calculated as equivalent NO_2 .
- B1.12 Flame Ionization Detector: A hydrogen-air diffusion flame detector that produces a signal nominally proportional to the mass flow rate of hydrocarbons entering the flame per unit of time, generally assumed responsive to the number of carbon atoms entering the flame.

- B1.13 Nondispersive Infrared Analyzer: An instrument that selectively measures specific components by absorption of infrared energy.
- B1.14 Chemiluminescence Analyzer: An instrument in which the intensity of light produced by the chemiluminescence of the reaction of nitric oxide with ozone is proportional to the concentration of nitric oxide. Conversion of NO₂ to NO prior to entering the analyzer permits the determination of both species.
- B1.15 Interference: Instrument response due to components other than the gas that is to be measured.
- B1.16 Calibrating Gas: Gas of known concentration used to establish instrument response.
- B1.17 Span Gas: A calibrating gas used routinely to check instrument response.
- B1.18 Zero Gas: A calibrating gas used routinely to check instrument zero.
- B1.19 Concentration: The volume fraction of the component of interest in the gas mixture, expressed as volume percentage or as parts per million.

B2. ANALYSIS EQUIPMENT

- B2.1 NDIR Instruments: Nondispersive infrared (NDIR) analyzers shall be used for the continuous monitoring of carbon monoxide (CO) and carbon dioxide (CO₂) in the turbine exhaust.

The NDIR instruments operate on the principle of differential energy absorption from parallel beams of infrared energy. The energy is transmitted to a differential detector through parallel cells, one containing a reference gas, and the other, sample gas. The detector, charged with the component to be measured, transduces the optical signal to an electric signal. The electrical signal thus generated is amplified and continuously recorded.

B2.1.1 Instrument Performance Specifications:

- Response Time (electrical) - 90% full scale response in 0.5 second or less.
- Zero Drift - Less than $\pm 1\%$ of full scale in 2 hours on most sensitive range.
- Span Drift - Less than $\pm 1\%$ of full scale in 2 hours on most sensitive range.
- Repeatability - Within $\pm 1.0\%$ of full scale.

Noise - Less than $\pm 1.0\%$ of full scale on most sensitive range.
Sample Cell Temperature - Minimum 50°C (122°F) maintained within $\pm 2^{\circ}\text{C}$ (3.6°F).

B2.1.2 Range and Accuracy

	<u>Range</u>	<u>Accuracy Excluding Interferences</u>
Carbon	0 to 100 ppm	$\pm 2\%$ of full scale
Monoxide	0 to 500 ppm	$\pm 1\%$ of full scale
	0 to 2,500 ppm	$\pm 1\%$ of full scale
	0 to 20,000 ppm	$\pm 1\%$ of full scale
Carbon	0 to 2%	$\pm 1\%$ of full scale
Dioxide	0 to 5%	$\pm 1\%$ of full scale
	0 to 15%	$\pm 1\%$ of full scale

B2.1.3 NDIR Cells: All NDIR instruments shall be equipped with cells of suitable length to measure concentrations within the above ranges to the indicated accuracy. Range changes may be accomplished by use of stacked sample cells and/or changes in the electronic circuitry.

B2.1.4 Interferences: Interferences from water vapor, carbon dioxide, and carbon monoxide shall be determined on the most sensitive instrument range. Response of CO instruments shall be less than 5% of full scale for 2.5% CO_2 , or 4% water vapor. Optical filters are the preferred method of discrimination. In some cases a cold trap or drying agent may be necessary to reduce water content below the level at which its interference is acceptable.

B2.2 Total Hydrocarbon Analyzer: The measurement of total hydrocarbon is made by an analyzer using a flame ionization detector (FID). With this type detector an ionization current, proportional to the mass rate of hydrocarbon entering a hydrogen flame is established between two electrodes. This ionization current is measured using an electrometer amplifier and is continuously recorded.

B2.2.1 General Design Specifications: The analyzer shall be fitted with a constant temperature oven housing the detector and sample-handling components. It shall maintain temperature within $\pm 2^{\circ}\text{C}$ of the set point, which shall be within the range 155 to 165°C (311 - 329°F).

The detector and sample handling components shall be suitable for continuous operation at temperatures to 200°C (392°F).

B2.2.2 Instrument Performance Specifications:

Response Time (electrical) - 90% of full scale in 0.5 second or less.
Noise - Less than $\pm 1.0\%$ of full scale on most sensitive range.
Repeatability - Within $\pm 1.0\%$ of full scale.
Zero Drift - Less than $\pm 1\%$ of full scale in 4 hours on all ranges.
Span Drift - Less than $\pm 1\%$ of full scale in 2 hours.
Linearity - Response with propane in air shall be linear within $\pm 2\%$ over the range of 0 to 2,000 ppmC.

B2.2.3 Range and Accuracy

<u>Range</u>	<u>Accuracy</u>
0 to 10 ppmC:	$\pm 5\%$ of full scale with propane calibration gas.
0 to 100 ppmC:	$\pm 2\%$ of full scale with propane calibration gas.
0 to 1,000 ppmC:	$\pm 1\%$ of full scale with propane calibration gas.
0 to 10,000 ppmC:	$\pm 1\%$ of full scale with propane calibration gas.

B2.3 Chemiluminescence Analyzer

B2.3.1 General Instrument Description: A chemiluminescence analyzer with thermal converter shall be used for measuring nitric oxide (NO) and total oxides of nitrogen (NO_x). The chemiluminescence method utilizes the principle that NO reacts with ozone (O_3) to give nitrogen dioxide (NO_2) and oxygen (O_2). Approximately 10 percent of the NO_2 is electronically excited. The transition of excited NO_2 to the ground state yields a light emission (600-2600 nanometer region) at low pressures. The detectable region of this emission depends on the PM-tube/optical filter being used in the detector. The intensity of this emission is proportional to the mass flow rate of NO into the reactor. The light emission can be measured utilizing a photomultiplier tube and associated electronics.

The method also utilizes the principle that NO_2 thermally decomposes to NO ($2\text{NO}_2 \rightarrow 2\text{NO} + \text{O}_2$). A thermal converter unit designed to provide essentially complete conversion of NO_2 to NO is included as a part of the chemiluminescence analyzer package. If the sample is passed through the converter prior to entering the chemiluminescence analyzer, an NO_x reading ($\text{NO} + \text{NO}_2$) is obtained. If the converter is bypassed, only the NO portion is indicated.

B2.3.2 Instrument Performance Specifications

Response time (electrical) - 90% of full scale in 0.5 second or less.
Noise - Less than 1% of full scale.
Repeatability - $\pm 1\%$ of full scale.
Zero drift - Less than $\pm 1\%$ of full scale in 2 hours.
Span drift - Less than $\pm 1\%$ of full scale in 2 hours.
Linearity - Linear to within $\pm 2\%$ of full scale on all ranges.
Accuracy - $\pm 1\%$ of full scale on all ranges.

B3. SAMPLING EQUIPMENT

B3.1 Sampling Probe:

B3.1.1 Design Concept: Local exhaust gas temperature at the nozzle exit plane of afterburning engines may be as high as 3500° F with corresponding total pressures 30 to 40 psia. Extremely careful design of the probe coolant passages is required to remove the heat resulting from impingement of the hot gases on the probe surface. The coolant must have good heat transfer properties (water is preferred), and high coolant velocities must be maintained, especially at the probe leading edge.

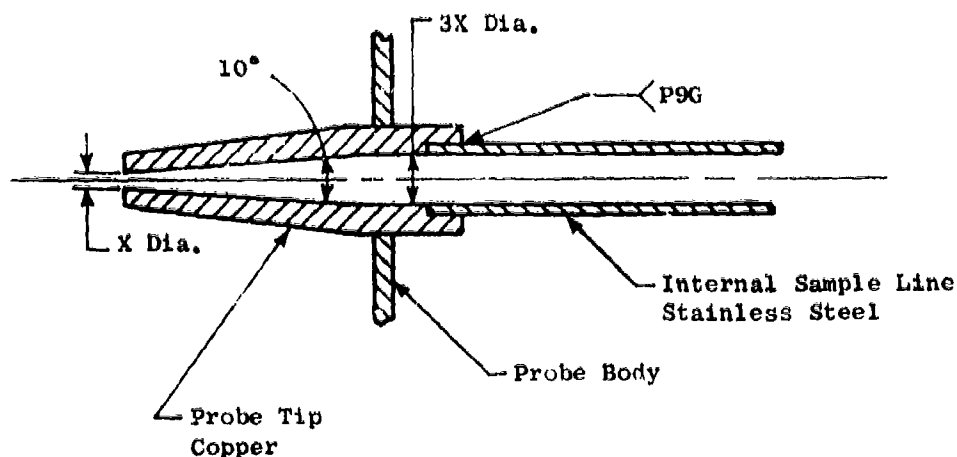
In order to prevent continued chemical reaction within the probe, a quenching-type probe is required. Quenching of the reactions is accomplished by adequate cooling of the tip and by expansion of the gas flow across the orifice.

In order to properly mass weight the various samples, impact pressure must be measured at the sampling point. Local mass flow is subsequently calculated from the local impact pressure, static (ambient) pressure, and total temperature (calculated from the gas composition). The mass weighting implies that individual samples must be taken. Due to potential nonhomogeneities in the exhaust stream, both radially and circumferentially, a relatively large number of samples are required. Either a movable probe (single element) or a fixed rake (multiple element) may be used. In either case, accurate positioning of the probe is required.

B3.1.2 Probe Material: The parts of the probe wetted by the sample gas, except for the probe tip, should be of stainless steel. Other material may be used in contact with the sample gas, if it is demonstrated that the material does not alter the composition of the sample. To assure adequate cooling, the probe tip shall be of copper (AMS 4500).

B3.1.3 Probe Temperature: The sample line within the probe shall be maintained at a temperature between 130 and 327° F.

B3.1.4 Probe Tip Design: The probe tip orifice shall be sized so as to give adequate sample flow under critical flow conditions. A short expansion section directly following shall enlarge the flow passage to a minimum diameter of three times the orifice diameter. A typical probe tip design is shown below:



B3.1.5 Total Pressure Measurement: Total pressure shall be measured within 0.2 inch of the sampling location. This permits a combination probe tip design in which separate orifices are provided for the gas sample and impact pressure measurements. Alternatively, both pressure measurement and gas sample may be obtained from a single orifice, in which case the measurements cannot be made simultaneously.

B3.2 Sampling Locations

B3.2.1 Axial Sampling Plane: The axial sampling plane shall be within eight inches of the plane at which the exhaust is completely expanded. Care should be taken so that adequate clearance exists between the sampling probe and exhaust nozzle for every position of the exhaust nozzle during the test.

B3.2.2 Radial Sampling Locations: A minimum of 22 sampling points shall be used for each test condition. A minimum of five sampling points shall be located in each of four quadrants, with two sampling points located

near the engine centerline. Sampling points in adjacent quadrants shall be separated by at least 60 degrees angular displacement.

Adjacent sampling points along each diameter should be equally spaced. In order to accurately locate the edge of the exhaust stream, the impact pressure at the outermost sampling point shall be between $1.05 P_{amb}$ and $1.10 P_{amb}$, where P_{amb} is the ambient pressure.

B3.3 Sample Transfer: The sample shall be transferred from the probe to the analytical instruments through a heated sample line of either stainless steel or teflon of 0.18 to 0.32-inch ID. The sample lines shall be maintained at a temperature of $300 \pm 27^\circ$ F from the probe to each analytical instrument.

Sample line length should be as short as possible, consistent with the test setup. Suitable noncontaminating sample pumps shall be used to maintain a partial vacuum within the probe so that the pressure ratio across the probe orifice is no less than five. The total sample flow rate shall be such that the sample gas is transported from the probe inlet to the analyzer inlet in less than ten seconds.

B4. EQUIPMENT LAYOUT

A schematic diagram of the emissions measuring system is shown in Figure B2. Additional components such as instruments, thermocouples, valves, solenoids, pumps, and switches may be used to provide additional information and coordinate the functions of the component systems. Parallel installation of CO and CO₂ analyzers is an acceptable alternative. No desiccants, dryers, water traps or related equipment may be used to treat the sample flowing to the NO_x analyzer. The NO_x instrument configuration must be such that water condensation is avoided throughout the instrument.

B5. INSTRUMENT ROUTINES

B5.1 NDIR Instruments: Following the instrument manufacturer's instructions for startup of instruments, the following minimum requirements shall be adhered to:

B5.1.1 Monthly Routine:

- (1) Check detector tuning, following manufacturer's prescribed routine.
- (2) Set instrument zero using dry nitrogen.

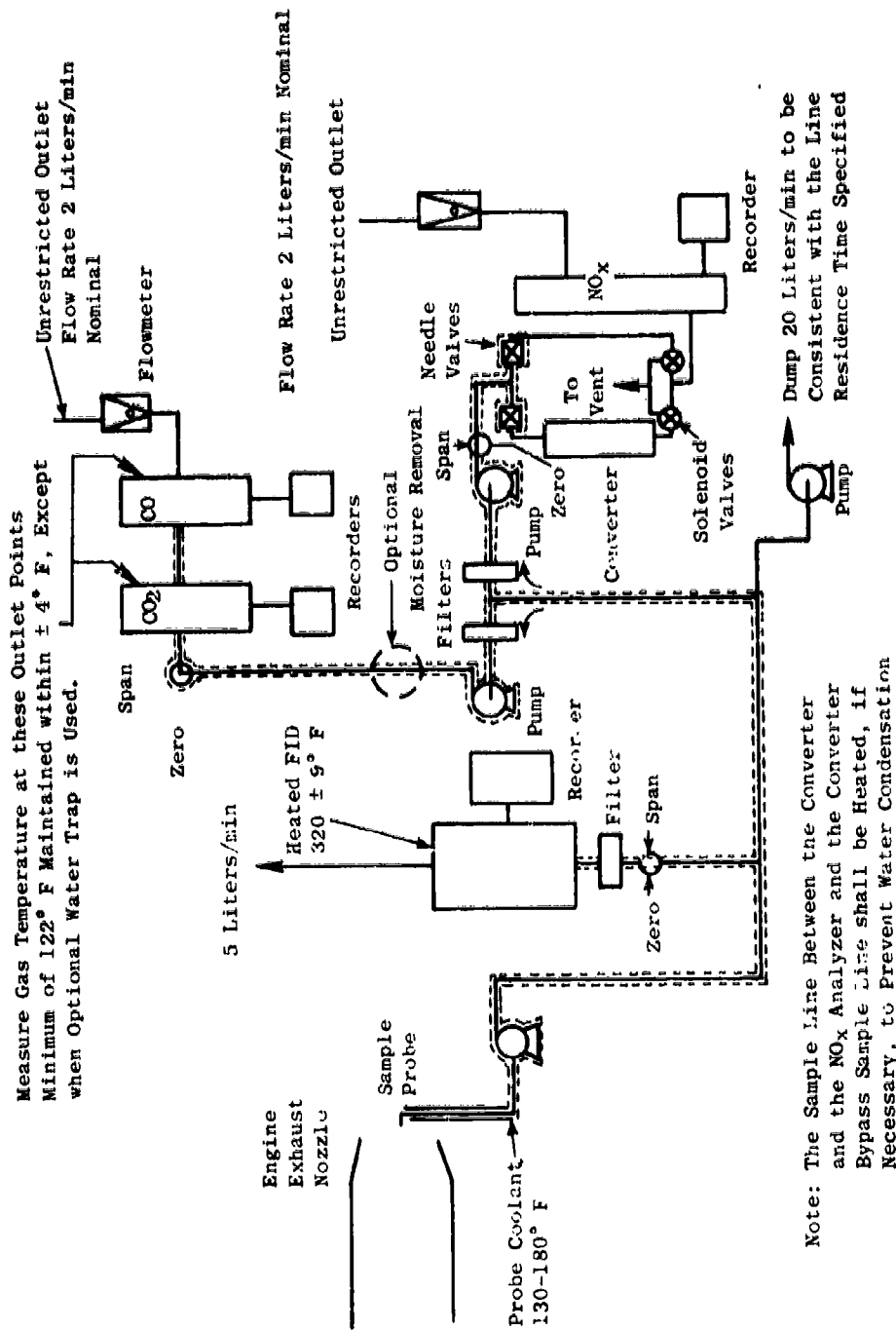


Figure B2. Sampling System Schematic. Instrument Layout is the Same as in Figure B1. Major Difference is the Probe Pump.

- (3) Using previous gain setting check calibration curves using calibration gas with nominal concentrations of 30, 60, and 90% of each range used. Use the same gas flow rate through instruments during calibration as when sampling exhaust. Any response value differing from the previous value by more than $\pm 3\%$ of the previous value at the same gain setting may reflect some problem in the instrument system, and a thorough instrument check should be made. Confirm or reestablish calibration curves for each range. Log gain reading.
- (4) Check response of interference gases as called out in B2.1.4. If unacceptable, determine cause and correct -- detector replacement may be indicated.

B5.1.2 Daily Routine:

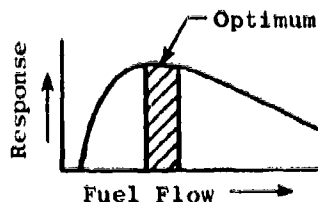
- (1) If analyzer power is not left on continuously, allow 2 hours for warmup. (If daily use is anticipated, it is recommended that analyzer be left on continuously.)
- (2) Replace or clean filters.
- (3) Check system for leaks.
- (4) Check detector tuning and record reading. If the reading changes by more than $\pm 3\%$ from the previous value, instrument readjustment is indicated. For the following tests the temperature of zero and span gas in the instrument cells shall be within $\pm 2^\circ \text{C}$ ($\pm 3.6^\circ \text{F}$) of typical sample gas temperature measured at the outlet of the sample cell, and gas flow rate through the instruments shall be the same for zero and span gas as for sample gas.
- (5) Zero the instrument on dry nitrogen. If there is a significant change in setting of Zero control, determine the cause and correct.
- (6) Using span gas to give 75 to 90% full-scale deflection, check the response of the instrument on each range using the gain setting from the previous use. If the reading differs from the previous value by more than 3%, an instrument problem may be indicated. Check and correct as necessary. If instrument reading is within $\pm 3\%$ of previous value, adjust gain control to produce proper instrument output. Log gain setting at final adjustment.
- (7) Check zero with dry nitrogen and repeat step 6 if necessary.
- (8) Zero and span shall be checked before and after each test, and at approximately one-hour intervals during the test.

B5.2 Total Hydrocarbon Analyzer

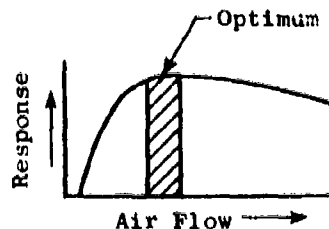
B5.2.1 Initial Alignment:

B5.2.1.1 Optimization of Detector Response:

- (1) Follow manufacturer's instructions for instrument startup and basic operating adjustment. Fuel shall be 60% helium, 40% hydrogen containing less than 0.1 ppmC hydrocarbon. Air shall be "hydrocarbon-free" grade containing less than 0.1 ppmC.
- (2) Set oven temperature at $160^{\circ}\text{C} \pm 5^{\circ}\text{C}$ ($320^{\circ}\text{F} \pm 9^{\circ}\text{F}$) and allow at least one-half hour after oven reaches temperature for the system to equilibrate. The temperature is to be maintained at set point $\pm 2^{\circ}\text{C}$ ($\pm 3.6^{\circ}\text{F}$).
- (3) Introduce a mixture of propane in air at a propane concentration of about 500 ppmC. Vary the fuel flow to burner and determine the peak response. A change in zero may result from a change in fuel flow; therefore, the instrument zero should be checked at each fuel flow rate. Select an operating flow rate that will give near maximum response and the least variation in response with minor fuel flow variations.



- (4) To determine the optimum airflow, use fuel flow setting determined above and vary airflow. A typical curve for response versus airflow is shown below:



After the optimum flow settings have been determined, these flows are to be measured and recorded for future reference.

B5.2.1.2 Oxygen Effect: Check the response of the detector with varied concentrations of oxygen in the sample following steps outlined below; this test shall be made with oven temperature at the set point and with gas flow to the detector at optimum conditions, as determined in B5.2.1.1.

- (1) Introduce nitrogen (N_2) zero gas and zero analyzer; check zero using hydrocarbon-free air; the zero should be the same.
- (2) The following blends of propane shall be used to determine the effect of oxygen (O_2) in the sample:

Propane in N_2

Propane in 90% N_2 + 10% O_2

Propane in air

The volume concentration of propane in the mixture reaching the detector should be about 500 ppmC, and the concentration of both the O_2 and the hydrocarbon should be known within $\pm 1\%$ of the absolute value. The zero should be checked after each mixture is measured. If the zero has changed, then the test shall be repeated.

The response to propane in air shall not differ by more than 3% from the response to propane in the 10%- O_2 /90%- N_2 mixture, nor differ by more than 5% from the response to propane in nitrogen.

If these specifications cannot be met by changing the sample flow rate or burner parameters, such as airflow and/or fuel flow rate, it is recommended that the detector be replaced.

B5.2.1.3 Linearity and Relative Response:

- (1) With analyzer optimized per B5.2.1.1, the instrument linearity shall be checked for the range 0 to 1,000 and 0 to 10,000 ppmC in air at nominal concentrations of 50 and 95% full scale of each range. The deviation of a best fit curve from a least-squares best-fit straight line should not exceed 2% of the value at any point. If this specification is met, concentration values may be calculated by use of a single calibration factor. If the deviation exceeds 2% at any point, concentration values shall be read from a calibration curve prepared during this alignment procedure.

- (2) A comparison of response to the different classes of compounds shall be made using (individually) propylene, toluene, and n-hexane, each at 20 to 50 ppmC concentration in nitrogen. If the response to any one differs by more than 5% from the average of the three, check instrument operating parameters. Reducing sample flow rate improves uniformity of response.

B5.2.2 Routine At Three-Month Intervals: These checks are to be made at three-month intervals or more frequently should there be any question regarding the accuracy of the hydrocarbon measurements:

- (1) Check for and correct any leaks in system.
- (2) Check and optimize burner flows (air, fuel, and sample) as required by criteria of B5.2.1.1.
- (3) Check O₂ effect as outlined in B5.2.1.2.
- (4) Check response of propylene, toluene, and n-hexane as outlined in B5.2.1.3.
- (5) Check linearity as outlined in B5.2.1.3.

B5.2.3 Daily Routine

- (1) Clean or replace filters.
- (2) Check instrument for leaks.
- (3) Check instrument temperatures.
- (4) Ascertain that all flows to detector are correct.
- (5) Check zero with zero gas.
- (6) The response using blends of propane in air shall be checked on each range:

<u>For range</u>	<u>Use</u>
0 to 10 ppmC	7 to 10 ppmC propane in air
0 to 100 ppmC	70 to 100 ppmC propane in air
0 to 1,000 ppmC	700 to 1,000 ppmC propane in air

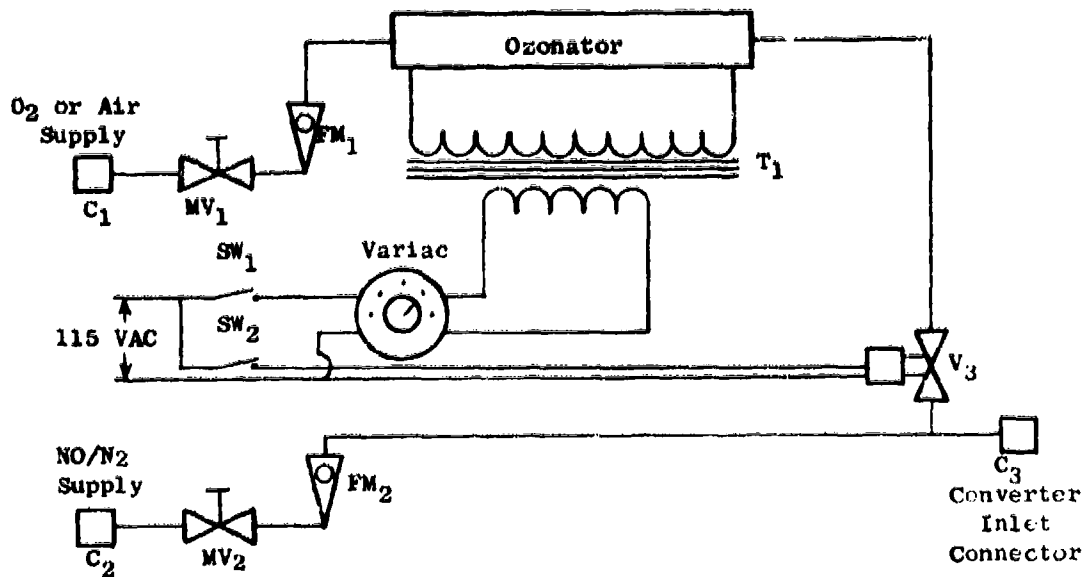
If the response differs from the last previous check value by more than 3% of the value logged during the last prior day's use, an instrument problem may be indicated.

A zero and span gas check shall be made before and after each test and at approximately one-hour intervals during the test. If the cumulative changes exceed 3% during the day, an instrument problem may be indicated.

B5.3 Chemiluminescence Analyzer: Follow the instrument manufacturer's instructions for startup of instrument.

B5.3.1 Thermal Converter Efficiency Check: Check the NO_x to NO converter efficiency by the following procedure. Use the apparatus described and illustrated below:

NO_x Converter Efficiency Detector



- (a) Attach the NO/N₂ supply (150-250 ppm) at C₂, the O₂ supply at C₁, and the analyzer inlet connection to the efficiency detector at C₃. If lower concentrations of NO are used, air may be used in place of O₂ to facilitate better control of the NO₂ generated during step (d).
- (b) With the efficiency detector variac off, place the NO_x converter in bypass mode and close valve V₃. Open valve MV₂ until sufficient flow and stable readings are obtained at the analyzer. Zero and span the analyzer output to indicate the value of the NO concentration being used. Record this concentration.

- (c) Open valve V3 (on/off flow control solenoid valve for O₂) and adjust valve MV1 (O₂ supply metering valve) to blend enough O₂ to lower the NO concentration (b) about 10%. Record this concentration.
- (d) Turn on the ozonator and increase its supply voltage until the NO concentration of (c) is reduced to about 20% of (b). NO₂ is now being formed from the NO+O₃ reaction. There must always be at least 10% unreacted NO at this point. Record this concentration.
- (e) When a stable reading has been obtained from (d), place the NO_x converter in the convert mode. The analyzer will now indicate the total NO_x concentration. Record this concentration.
- (f) Turn off the ozonator and allow the analyzer reading to stabilize. The mixture NO+O₂ is still passing through the converter. This reading is the total NO_x concentration of the dilute NO span gas used at step (c). Record this concentration.
- (g) Close valve V3. The NO concentration should be equal to or greater than the reading of (d) indicating whether the NO contains any NO₂.

Calculate the efficiency of the NO_x converter by substituting the concentrations obtained during the test into the following equation.

$$\% \text{ Eff.} = \frac{(e) - (d)}{(f) - (d)} \times 100\%$$

The efficiency of the converter should be greater than 90 percent. Adjusting the converter temperature may be needed to maximize the efficiency.

- (h) If the converter efficiency is not greater than 90 percent, the cause of the inefficiency shall be determined and corrected before the instrument is used.
- (i) The converter efficiency shall be checked at least monthly.

B5.3.2 Monthly Routine

- (1) Adjust analyzer to optimize performance.
- (2) Set instrument zero using zero grade nitrogen.

- (3) Calibrate the NO_x analyzer with nitric oxide (nitrogen diluent) gases having nominal concentrations of 50 and 95% of full scale on each range used. Use the same gas flow rate through the instrument during calibration as when sampling exhaust. Log zero and gain settings.

B5.3.3 Daily Routine

- (1) If analyzer power is not left on continuously, allow two hours for warmup.
- (2) Clean or replace filters.
- (3) Check system for leaks.
- (4) Ascertain that flow to detector is correct.
- (5) Check zero with zero grade nitrogen.
- (6) Zero and span shall be checked before and after each test and also at approximately one-hour intervals during the test.

B6. REFERENCE GASES

B6.1 Mixture Composition: Reference gases for carbon monoxide and carbon dioxide shall be prepared using nitrogen as the diluent. They may be blended singly or as dual component mixtures. Nitric oxide reference gas shall be blended in nitrogen. Hydrocarbon reference gas shall be propane in air. Zero gas shall be nitrogen, or optionally high purity air as specified in B6.4.

B6.2 Calibration Gases: Calibration gases shall be certified by the vendor as accurate within $\pm 1\%$.

B6.3 Span Gases: Span gases shall be supplied by the vendor to a stated accuracy within $\pm 2\%$.

B6.4 Zero Gas: Nitrogen zero gas shall be minimum 99.998% N₂ with less than 1 ppm CO. This gas shall be used to zero the CO, CO₂ and NO analyzer.

Zero-grade air shall not exceed 0.1 ppmC hydrocarbon. This gas shall be used to zero the HC analyzer. Zero-grade air includes artificial air consisting of a blend of N₂ and O₂ with O₂ concentration between 18 and 21 mole percent.

B7. TEST PROCEDURE

B7.1 Test Layout: Set up engine, sampling equipment, and analysis equipment as specified in Sections B3 and B4.

B7.2 Fuel: The fuel used shall be as specified by the engine manufacturer. The carbon-to-hydrogen ratio shall be determined and this parameter is required in the calculation of results (Section B9). The emissions determined by this procedure may be a function of the type of fuel used and so the type of fuel shall be included as an integral part of the test data, as specified in Section B8.

B7.3 Ambient Conditions: Changes in ambient temperature, pressure, and humidity can cause changes in emissions levels both through direct changes in combustor conditions and through changes in engine operating parameters. Since generally accepted methods are not currently available for correcting test data to standard conditions, extremes of ambient conditions should be avoided. Ambient temperature, pressure, and humidity shall be measured for the test records (Section B8).

B7.4 Instrument Calibration: Calibrate exhaust analysis instruments before and after each test period using daily procedures given in Section B5.

B7.5 Test Sequence:

- (a) Start engine and adjust to desired power setting. Allow adequate time for stabilization.
- (b) Measure concentrations of CO, CO₂, HC, NO, NO_x, and impact pressure on a minimum of 22 radial sampling locations as specified in Section B3.2.2.
- (c) The engine may then be stabilized at another power setting and measurements made as in (b) above. Repeat until test series is complete.

B8. MINIMUM INFORMATION TO BE RECORDED

The following information, as applicable, shall form a part of the permanent record for each test.

B8.1 General

- (a) Facility performing test and location.
- (b) Individual responsible for conduct of test.

- (c) Test number, reading number, etc.
- (d) Date
- (e) Time
- (f) Fuel type, fuel specification, additives, HC ratio, and method of determination.
- (g) Ambient Conditions: Temperature, pressure, humidity.
- (h) Test procedure designation.
- (i) Exceptions, if any, to this procedure.

B8.2 Engine Description

- (a) Manufacturer
- (b) Model number, serial number.
- (c) Time since overhaul and other pertinent maintenance information.

B8.3 Engine Operating Data

- (a) Nominal power setting, throttle angle.
- (b) Rotational speed; N_1 , N_2 .
- (c) Fuel flow (main engine and afterburner).
- (d) Airflow and method of determination.
- (e) Compressor discharge temperature and method of determination.
- (f) Compressor discharge pressure or EPR.
- (g) Exhaust nozzle position.
- (h) Thrust.
- (i) Fuel temperature.
- (j) Engine bypass ratio.
- (k) Engine inlet (ram) total temperature.

B8.4 Exhaust Sampling Data

- (a) Axial sampling location.
- (b) Radial sampling location (distance from projected engine centerline).
- (c) Concentrations of CO, CO₂, HC, NO and NO_x at each sampling location.
- (d) Probe impact pressure at each sampling location.
- (e) Sample line temperature.
- (f) Sample line pressure within probe.
- (g) Probe coolant temperatures.

B9. CALCULATION OF RESULTS

For afterburning engines, chemical reactions can continue in the exhaust plumes downstream of the nozzle exit plane. The higher the exhaust temperature at the exit plane, the greater is the extent of subsequent reactions. The composition of the exhaust at the nozzle exit plane is thus not representative of the actual levels of pollutants ejected into the surrounding atmosphere, the actual levels being generally less than the levels at the nozzle exit plane. The measured emissions levels must thus be corrected for plume reactions through the use of a computer program derived from a reactive plume analytical model.

B9.1 Plume Model Input Data

The plume model computer program computes mixing and reactions along a maximum of 11 stream tubes in the plume, but the measurements are made at 22 radial probe positions. The 22 separate measurements must be reduced to 11 values before insertion into the plume model. To accomplish this, the impact pressure measurements are first plotted against radial position, as shown in Figure B3, and a smooth, averaged curve is drawn through the data. The outer radius (R_0) of the exhaust jet is taken as that radial location at which the impact pressure equals the ambient pressure.

Similarly, the CO and CO₂ concentration data are plotted against radial position (Figure B4) and smooth, average curves shall be drawn through each set of data. The plume model computer program requires that input CO and CO₂ composition data be on a semi-dry basis; that is, with 0.602% moisture in the sample. In case the samples were not partially dried (with an ice trap) to this level, then appropriate correction factors shall be applied. Suitable correction factors are given in Section A9.3 of this procedure.

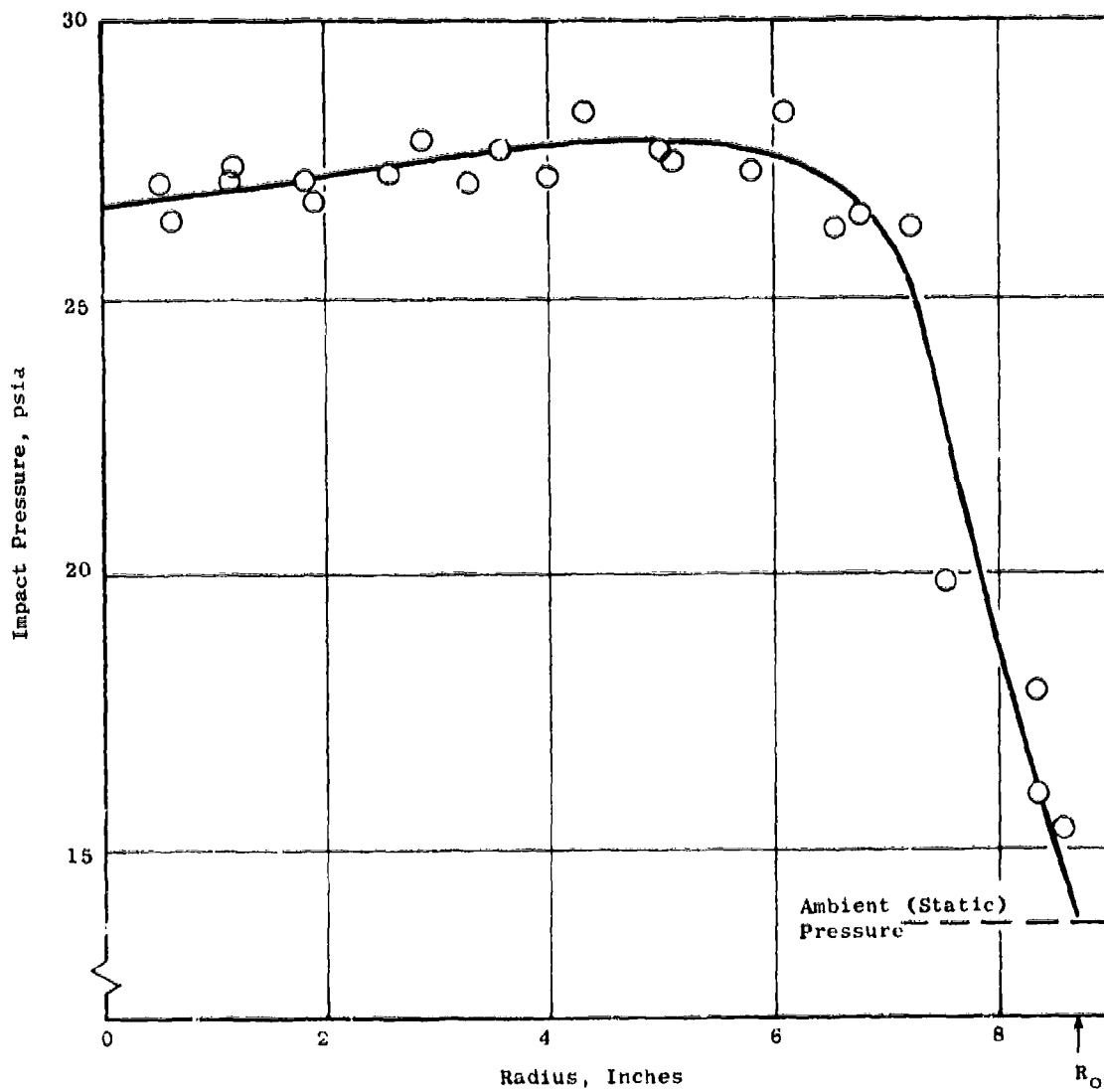


Figure B3. Impact Pressure Vs. Radial Position at Max. A/B Power Level. R_0 is Outer Radius of Exhaust.

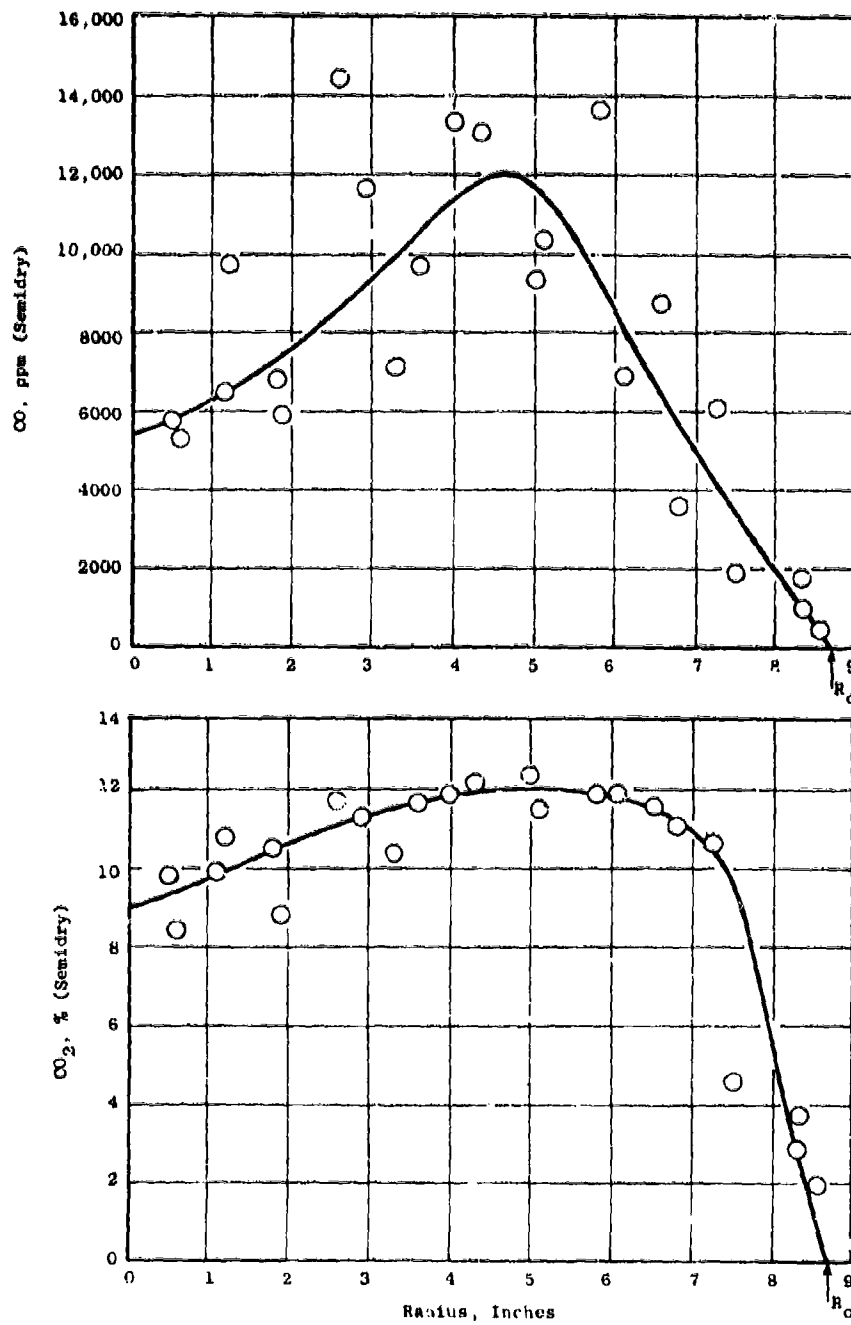


Figure B4. CO₂ and CO Concentrations Vs. Radial Position at Max. A/B Power Level. R_o is Outer Radius of Exhaust.

Finally, the HC and NO_x concentration data shall be plotted against radial position, as shown in Figure B5. If large variations in HC concentrations are noted across the stream, then the HC data shall be plotted on semilogarithmic coordinate paper, as in Figure B5.

The exhaust area, as determined by R₀, shall be divided into 11 equal areas by defining

$$g = \frac{\pi R_0^2}{11} \quad (B15)$$

The 11 radial locations, R_i, are then selected to be in the center of each of 11 equal areas. Thus,

$$\pi R_i^2 = \frac{(2i-1)}{2} g \quad (B16)$$

where i = 1, 2, ---, 11.

This equation can be simplified to yield

$$R_i = 0.2132 R_0 \sqrt{(2i-1)} \quad (B17)$$

where i = 1, 2, ---, 11.

The complete list of input data required for the plume model computer program is given in Table B1 along with a brief description of each variable. Note that Item 5, RADJ, is equal to R₀ expressed in feet. Similarly, Item 13, RADII, is equal to R_i expressed in feet.

The local gas composition at the 11 selected radial locations (Item 12, CAROL) must be expressed either in mole fraction, parts per million, or some unit proportional to mole fractions. Note that mixed units (e.g., ppm and %) cannot be entered. Item 19, SF, is the scale factor appropriate to the units used.

The emissions indices for NO_x (LIN02C) and for CO (EIC0C) at the afterburner inlet are also required for inputs to the plume model. These values are normally obtained from previous measurements on the engine at military power.

For mixed flow augmentors, in which afterburning fuel is injected into the mixed stream consisting of core engine exhaust and fan air, the overall engine bypass ratio (BETA) may be obtained from engine cycle data. The local bypass ratio (BL0C) at each probe location is generally obtained from emissions measurements at military power condition.

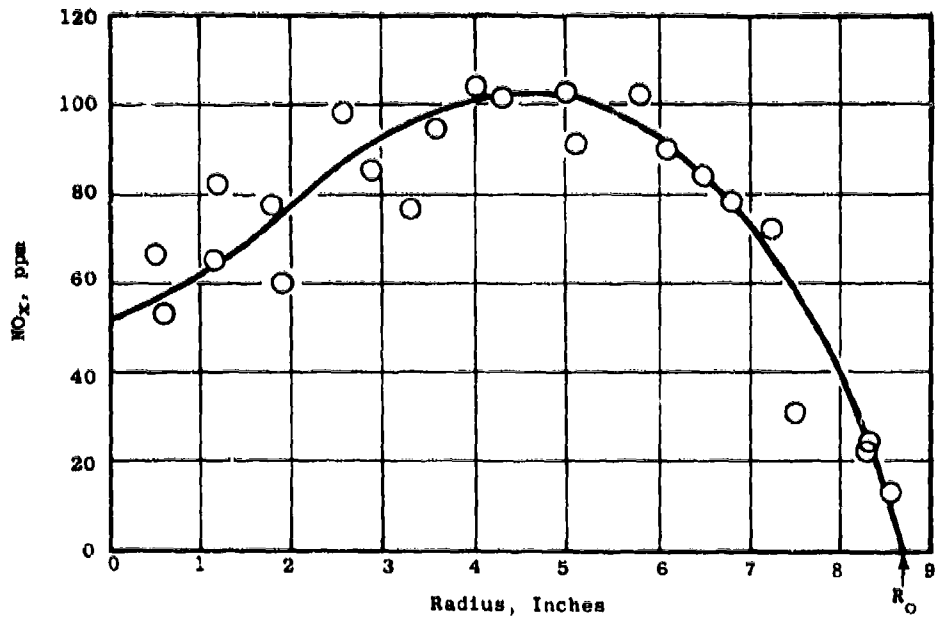
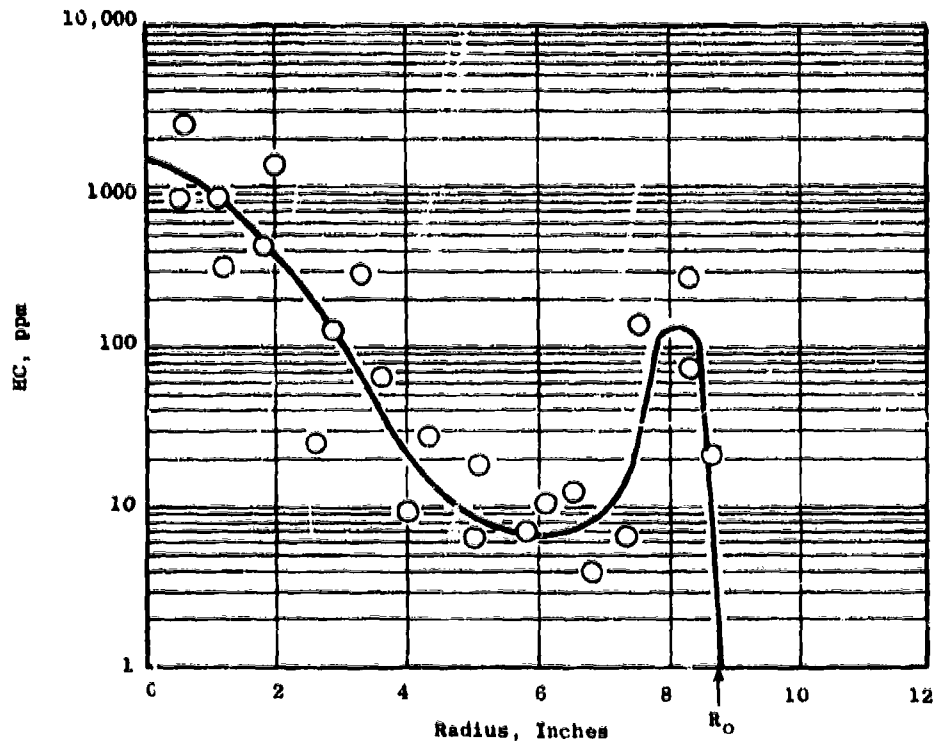


Figure B5. HC and NO_x Concentrations Vs. Radial Position at Max. A/B Power Level. R_0 is Outer Radius of Exhaust.

Table B1. Input Data to Plume Model Computer Program.

Item Number	Variable Name	Dimension	Initial Value	Default Value	Description
1	PO	1	14.696	-	Ambient air static pressure, psia
2	TO	1	518.69	-	Ambient air static temperature, ° R.
3	HCM	1	.00531	-	Specific humidity of ambient air, lb H ₂ O/lb dry air.
4	VO	1	0.0	-	Flight speed, ft/sec.
5	RADJ	1	1.0	-	Outer radius of exhaust jet, ft.
6	TZ	1	518.69	-	Engine inlet (rain) total temperature, ° R.
7	FARS	1	0.02	-	Turbine exit fuel-air ratio, lb fuel/lb dry air.
8	EINE2C	1	20.0	-	Main combustor NO _x emission index, lb NO ₂ /1000 lb fuel.
9	BETA	1	0.0	-	Engine bypass ratio, lb fan air/lb core air.
10	T25	1	518.69	-	Bypass air (fan discharge) temperature, ° R.
11	FUEL	3	2.0 537.0 BITS	-	Hydrogen - carbon atom ratio of fuel. Fuel temperature, ° R. Lower heating value of fuel, Btu/lb.
12	CAROL	4, 11	BITS	-	Local gas composition CO, CO ₂ , HC, NO _x .
13	RADII	11	BITS	-	Radial locations of probe measurements, ft.
14	PT	11	BITS	-	Probe impact pressure, psia.
15	PS	11	BITS	PO	Static pressure at probe locations, psia.
16	BLOC	11	BITS	BETA	Local bypass ratio at each probe location.
17	ELIOW	11	BITS	0.0	Main combustor CO emission index, lb CO/1000 lb fuel.
18	ITITLE	0	Blank	-	Output page heading information
19	SF	1	1.0	-	Scale factor for CAROL data (leave 1.0 if composition in mole fraction - set 1E-6 if in ppm, etc.)
20	PRINT	30	BITS	0.1*RADJ .0*RADJ BITS	Axial stations (feet) at which output is to be printed.

Data Item No. 20 (PRINT) contains the axial stations at which the output is to be printed. Data shall be calculated and reported for at least three axial stations as follows: (1) nozzle exit plane (zero feet aft), (2) 35 times RADJ, and (3) 50 times RADJ. Data may be calculated for additional axial stations in order to follow the course of reactions within the plume. Reactions are substantially completed at 35 times RADJ.

The Computer Program User's Manual should be consulted for additional information and for the complete description of the plume model computer program. The User's Manual has been published as Supplement 2 to AFAPL-TR-75-52.

B9.2 Plume Model Output

At each axial station, as designated in the input data, the plume model computer program calculates various quantities related to mixing and reactions in the plume along the 11 stream tubes initially selected. In addition, at each station, the following overall or integrated values are calculated, and shall be reported:

Total Flow, pps:	Gas Mixture, Fuel
Emission Indices, lb/1000 lb fuel:	CO, HC, NO _x
Contaminant Flow, pps:	CO, HC, NO _x

The overall values shall be examined for internal consistency. The following criteria shall apply:

- (a) Calculated fuel flow shall agree within $\pm 15\%$ with the metered total engine fuel flow. If the agreement is not within 15%, then the plume model input data shall be reassessed. In particular, the curves of concentration versus radial location shall be examined to determine that the composition of the samples is representative of the actual local composition.
- (b) Emission indices and contaminant flows at axial station 50 times RADJ shall be within 5% of the value calculated for axial stations 35 times RADJ. If such is not the case, the computer program shall be rerun for an axial station of 70 times RADJ.